

**Identification and analysis of the  
signalling networks that regulate Ciz1  
levels in normal and cancer cell lines**

**PhD Biomedical and Life Sciences**

**By Teklè Paužaitė**

**Lancaster University**

**A Thesis submitted in fulfilment of requirement for the degree  
of Doctor of Philosophy**

**March 2019**

## Declaration

This dissertation is the result of my own work and includes nothing, which is the outcome of work done in collaboration except where specifically indicated in the text. It has not been previously submitted, in part or whole, to any university or institution for any degree, diploma, or other qualification.

Signed: Teklé Paužaité

A handwritten signature in black ink, consisting of several fluid, overlapping strokes that form a cursive representation of the name Teklé Paužaité.

Date: 01 07 2019

## Dedication

*This thesis is dedicated to the strongest, most caring and extraordinary person I know, my mother Eglė Paužienė.*

## **Abstract**

Ciz1 is a nuclear protein that associates with cyclin A – cyclin dependent kinase 2 (CDK2) and facilitates the initiation of DNA replication. Ciz1 overexpression has been linked to common cancer types, including breast, colon, prostate, lung, and liver cancers. This suggests that identification of mechanisms that regulate Ciz1 levels may represent potential drug targets in cancer.

This work identifies that CDK2 and DDK activity are required to maintain Ciz1 levels. Chemical or genetic inhibition of CDK2 or DDK (Cdc7-Dbf4) activity in murine fibroblasts reduced Ciz1 levels. Further analysis demonstrated that CDK and DDK activity promotes Ciz1 accumulation in G1 phase by reducing ubiquitin proteasome system (UPS) mediated degradation. Furthermore, Ciz1 levels are actively controlled by the proteasome, as inhibition of protein translation rapidly reduced Ciz1 levels, and this is reversed by proteasomal inhibition. The data suggest a model where Ciz1 is regulated by opposing kinase and UPS activities, leading to Ciz1 accumulation in response to rising kinase activity in G1 phase, and its degradation later in the cell cycle.

Significantly, human prostate adenocarcinoma (PC3) and oestrogen receptor positive breast cancer (MCF7) cell lines require Ciz1 for efficient proliferation. The data demonstrate that Ciz1 levels can be reduced with CDK2/ DDK inhibitors via proteasomally mediated degradation in human cancer cell lines similarly to normal fibroblasts. In PC3 and MCF7 cell lines, repurposing small molecule CDK2 inhibitors efficiently reduce Ciz1 levels, decrease E2F mediated transcription and proliferation. The targeted depletion of Ciz1 via CDK2/ DDK inhibition and UPS mediated

degradation requires a functional E3 ligase to be effective. As a first step towards identifying the regulatory E3 ligase(s), a biochemical fractionation and mass spectrometry approach revealed three putative E3 ligases: UBR5, FBXO8 and UBE2O, which require further characterisation.

Taken together, this work suggests that deregulation of CDK activity or inactivation of UPS signalling may promote Ciz1 overexpression in specific cancers. Importantly, Ciz1 is required for proliferation of some cancer cell lines, suggesting that approaches, which reduce Ciz1 levels may be of clinical benefit. Therefore, the identification of the regulatory mechanisms that control Ciz1 levels, represent potential targets in Ciz1 dependent cancers.

## **Acknowledgements**

I would like to thank my supervisor Nikki A. Copeland for his patience and guidance through the research and writing experience.

I would like to thank my extraordinary friends in the lab and outside. Special thanks to James Tollitt for his friendship and support in every step of the way. Without his cooperation and positivity, the A27 lab experience would not have been so effective and wonderful. Thank you for keeping me sane and caffeinated! I would like to thank Urvi Thacker for teaching me and answering every silly question I could think of, and Daria Kania for always being there for me professionally and personally.

I would like to express gratitude to our collaborators Dr Jason Parsons and Jonny Hughes for teaching me invaluable protein biochemistry techniques. Also, huge thanks to my co-supervisor Dr Sarah Allinson for her advice and support.

All of this would not have been possible without my brilliant and outstanding mother Eglė Paužienė and sister Urtė Paužaitė, and obviously without my beloved partner Ben Rowan. Thank you for coping with me throughout these long years and many to come! Finally, would like to thank my crazy dogs, Archie and Copper, for keeping me active!

## List of contents

Abstract	IV
Acknowledgements	VI
List of figures	XVI
List of tables	XXI
Abbreviations	XXII
<b>1. Introduction</b>	<b>2</b>
1.1. Mammalian cell cycle is driven by cyclin – CDKs	5
1.1.1. Critical analysis of quantitative model of kinase activity driving the cell cycle	6
1.2. Definition of the restriction point	9
1.3. DNA replication	11
1.4. Ubiquitin proteasome system	15
1.5. CDK and UPS activities temporally control cell cycle events	19
1.6. The deregulation in CDK and UPS in tumourigenesis	22
1.7. The Cip1-interacting zinc-finger protein 1 (Ciz1) aids the initiation of DNA replication	24
1.7.1. Ciz1 discovery and structure	24

1.7.2.	Ciz1 function in initiation of DNA replication	25
1.7.3.	Role of Ciz1 in tumourigenesis	26
1.7.4.	Association of Ciz1 in other disorders	30
1.8.	Aims	31
<b>2.</b>	<b>Materials and methods</b>	<b>35</b>
2.1.	Tissue culture	35
2.1.1.	Culturing transformed 3T3 fibroblasts	35
2.1.2.	Culturing cancer cell lines	35
2.2.	Immunofluorescence	36
2.3.	RNA extraction and RT-qPCR	36
2.4.	Drug treatments	37
2.5.	Protein harvesting and western blotting	38
2.6.	Nucleofection of cell lines	41
2.7.	Site directed mutagenesis using whole plasmid mutagenesis	41
2.8.	Translational inhibition with Cycloheximide	43
2.9.	CRISPR-Cas9 protocol	43
2.10.	MTT assays	46
2.11.	Flow cytometry	47

2.12. Apoptosis assay	47
2.13. E-Ciz1-His6x purification	48
2.13.1. E-Ciz1-His6x cloning into pET-28a vector	48
2.13.2. E-Ciz1-His6x expression	49
2.13.3. E-Ciz1-His6x purification with Ni-NTA resin	50
2.13.4. E-Ciz1-His6x purification via anion exchange chromatography	51
2.14. N471-Ciz1 purification	51
2.15. Biochemical identification of E3 ligases and phosphatases	52
2.15.1. <i>In vitro</i> ubiquitylation assay	52
2.15.2. <i>In vitro</i> phosphatase assay	53
2.15.3. Ion exchange column (20ml)	54
2.15.4. Size exclusion chromatography (SEC)	54
2.15.5. Analytical ion exchange column (1 ml)	55
2.16. Methods for LC-MS analysis of FPLC fractions	55
2.16.1. Sample preparation	55
2.16.2. LC-MS/MS analysis	56
2.17. Statistical analysis	57
2.18. Immunoprecipitation experiments	57

<b>3.</b>	<b>Identification of the networks that regulate Ciz1 levels during G1 phase</b>	<b>59</b>
3.1.	Evaluation of Ciz1 expression levels in synchronised populations of 3T3 cells	60
3.2.	Defining the restriction point in post-quiescent 3T3 cells	61
3.3.	Ciz1 protein expression and mRNA transcription	63
3.4.	Ciz1 is destabilised by kinase inhibition in asynchronous 3T3 population	64
3.5.	A model of Ciz1 phosphorylation and accumulation analysis using small molecule kinase inhibitors	66
3.6.	Phosphorylation of Ciz1 promotes its accumulation in pre-restriction point cells	68
3.7.	CDK2 and DDK inhibition destabilises Ciz1 levels post-restriction point	70
3.8.	Ciz1 is stabilised by phosphorylation after the entry to S phase	72
3.9.	Genetic depletion of G1 – S regulators reduces S phase entry	73
3.10.	Ciz1 is destabilised by G1 – S regulator depletion	75
3.11.	Ciz1 is regulated by the proteasome in asynchronous and synchronised 3T3 cells	77
3.12.	Proteasomal inhibition recovers Ciz1 levels after genetic cyclin A depletion	80

3.13.	Ciz1 is ubiquitylated <i>in vivo</i>	82
3.14.	Discussion	83
<b>4.</b>	<b>Evaluation of the role of CDK mediated phosphorylation for Ciz1 stability</b>	<b>88</b>
4.1.	Introduction	89
4.2.	CRISPR-Cas9 and homology directed repair (HDR) for introducing point mutations in genomic Ciz1 DNA	90
4.3.	Screening for CDK site specific point mutations in Ciz1 gene	92
4.4.	DNA sequencing of mutated sites after CRISPR-Cas9 and HDR	96
4.5.	Endogenous Ciz1 stability after translational inhibition	99
4.6.	Evaluation of the role of phosphorylation at 4 CDK sites within Ciz1	101
4.7.	Analysis of GFP – E-Ciz1/ S331A/ S331D stability	103
4.8.	Phospho-mutant stability after translational inhibition	104
4.9.	Discussion	106
<b>5.</b>	<b>Characterisation of the differential activities of Cdc7-Dbf4 (DDK) inhibitors XL-413 and PHA-767491</b>	<b>110</b>
5.1.	PHA-767491 and XL-413 display different effects on cell cycle progression	112

5.2.	PHA-767491 and XL-413 efficiently reduce DDK activity, but only PHA-767491 reduces CDK2 activity	114
5.3.	PHA-767491 is a potent DDK and CDK2 inhibitor	117
5.4.	PHA-767491 displays a similar inhibitory activity to classical CDK2 inhibitors Roscovitine and CVT-313	118
5.5.	PHA-767491 inhibits E2F-Rb mediated transcription consistent with off target CDK2 inhibition	120
5.6.	The effect on E2F-Rb transcription is not due inhibition of CDK9 - RNA Polymerase II transcriptional activity	123
5.7.	Genetic depletion of Cdc7-Dbf4 does not inhibit E2F transcription	125
5.8.	Discussion	127
<b>6.</b>	<b>Enhancing UPS mediated degradation of Ciz1 with small molecule DDK and CDK2 inhibitors</b>	<b>131</b>
6.1.	Introduction	132
6.2.	Kinase inhibition reduced Ciz1 levels in cancer cell lines	135
6.3.	Ciz1 is degraded by the UPS after CDK2 or DDK inhibition in PC3 and SW480 cancer cell lines	138
6.4.	CDK2 inhibitors reduced E2F transcription in cancer cell lines	141
6.5.	CDK or DDK inhibition does not affect Ciz1 transcription in PC3 and SW480 cancer cell lines	144

6.6.	CDK2 or DDK inhibition reduces cellular proliferation and S phase entry in Rb positive cancer cells	145
6.7.	PHA-767491, Roscovitine and CVT-313 reduce proliferation in PC3, SW480 and SW620 cancer cell lines	146
6.8.	Identification of Ciz1 dependent cancer cell lines	148
6.9.	Ciz1 depletion shows differential effects in Luminal A cancer cell lines T47D and MCF7	152
6.10.	Ciz1 depletion reduced proliferation in MCF7 breast cancer cell line	154
6.11.	Ciz1 depletion reduces proliferation without inducing cell death	155
6.12.	Discussion	157
<b>7.</b>	<b>Ciz1 is regulated by ubiquitin proteasome system (UPS) and kinase/phosphatase activities</b>	<b>162</b>
7.1.	Identification of putative E3 ligases that regulate Ciz1 accumulation	165
7.1.1.	Overexpression and purification of E-Ciz1-His <sub>6</sub>	167
7.1.2.	<i>In vitro</i> ubiquitylation assay of Ciz1	170
7.1.3.	Phosphocellulose fractionation of HeLa extracts identified that Ciz1 is poly-ubiquitylated <i>in vitro</i>	171
7.1.4.	Fractionation of high salt extracts using cation exchange chromatography	172

7.1.5.	Potential E3 ligase identification via LC-MS/MS analysis	176
7.2.	Identification of phosphatases opposing Ciz1 regulating CDK2 activity	178
7.2.1.	Overexpression and purification of GST-Ciz1-N471	178
7.2.2.	Validation of the phosphospecific pT293 antibody	180
7.2.3.	Developing a strategy to identify phosphatase activity using <i>in vitro</i> phosphatase assays and cellular fraction	182
7.2.4.	Fractionation of low salt extracts exhibiting phosphatase activity using anion exchange chromatography	183
7.2.5.	Identification of putative regulatory phosphatases by LC-MS/MS	187
7.3.	Discussion	192
<b>8.</b>	<b>General discussion</b>	<b>198</b>
8.1.	Ciz1 level is upregulated by kinase phosphorylation in G1 phase	199
8.2.	Genetic depletion of cyclins and DDK suggests kinase activity is required for Ciz1 accumulation	202
8.3.	Ciz1 de-phosphorylation by phosphatases	203
8.4.	Ciz1 is downregulated by ubiquitin proteasome system in G1 phase	206
8.5.	Ciz1 expression and regulation in cancers	211
8.6.	Future perspectives/ Future work	214
<b>9.</b>	<b>References</b>	<b>216</b>

**Appendices**

**263**

Appendix 1

259

## List of figures

1.1.	Cell cycle is driven by the sequentially expressed cyclins and rising kinase activity	6
1.2.	Quantitative model of rising kinase activity driving the cell cycle	7
1.3.	Formation of replication complex	13
1.4.	The chain of enzymatic reactions involved in substrate ubiquitylation	18
1.5.	The cell cycle is driven by kinase and UPS activities	21
1.6.	Schematic of Ciz1 gene translated regions and protein structure	25
3.1.	Cell cycle synchronisation of 3T3 cells from G1 into S phase	61
3.2.	Determination of the restriction point	62
3.3.	Ciz1 protein accumulation and transcription	63
3.4.	Ciz1 levels are reduced by inhibition of CDK2 (Roscovitine) and DDK (PHA-767491)	65
3.5.	The model of active kinase complexes and Ciz1 accumulation in G1 – S transition and experimental overview	67
3.6.	Inhibition of CDK or DDK activity reduces Ciz1 protein levels, but not Ciz1 transcription, in pre-restriction point cells	69
3.7.	Ciz1 levels are reduced by inhibition of CDK2 or DDK in post-restriction point murine fibroblasts	71

3.8.	CDK2 phosphorylation stabilises Ciz1 in S phase	73
3.9.	Genetic depletion of G1 – S transition regulators reduce S phase entry	74
3.10.	Ciz1 is destabilised by G1 – S regulator depletion	76
3.11.	MG132 recovers Ciz1 levels destabilised by kinase inhibitors in asynchronous population	77
3.12.	Proteasomal inhibition recovers Ciz1 levels after kinase inhibition	79
3.13.	MG132 recovers Ciz1 levels in S phase after reduction by CDK2 inhibitors	80
3.14.	MG132 recovers Ciz1 after genetic cyclin A depletion	81
3.15.	Ciz1 is ubiquitylated <i>in vivo</i>	82
4.1.	Introduction of the point mutation (PM) by homology directed repair (HDR) pathway	91
4.2.	The type II CRISPR-Cas system	92
4.3.	ssODN knock-in screening using point mutation specific restriction enzymes	94
4.4.	The representative sequences of Ciz1 phospho- sites point mutations	97
4.5.	Ciz1 is a labile protein rapidly degraded after translational inhibition	100
4.6.	GFP – E-Ciz1/ -AAAA/ -DDDD overexpression profile	102
4.7.	Both GFP-E-Ciz1-S331A and -S331D reduced protein degradation	104

4.8.	GFP – E-Ciz1 is more prone to degradation than GFP – E-Ciz1 –AAAA or – DDDD	105
5.1.	Different effect of PHA-767491 and XL-413 on cell cycle progression	113
5.2.	Distinct PHA-767491 and XL-413 activities in Rb phosphorylation	115
5.3.	PHA-767491 is a potent DDK and CDK2 inhibitor	118
5.4.	PHA-767491 inhibits Rb phosphorylation and cyclin A expression consistent with inhibition of CDK2	119
5.5.	PHA-767491 is a potent E2F-Rb transcriptional pathway inhibitor	121
5.6.	PHA-767491 affected E2F transcription by inhibiting CDK2 rather than CDK9	124
5.7.	Cdc7-Dbf4 co-depletion does not reduce E2F transcription	126
6.1.	Model of opposing regulation of Ciz1 protein levels by CDK and DDK kinase activity and UPS mediated degradation	134
6.2.	Kinase inhibition reduces Ciz1 levels in PC3 and SW480 cancer cells	137
6.3.	Ciz1 recovery with MG132 in PC3 and SW480 cancer cell lines	139
6.4.	Roscovitine, CVT-313 and PHA-767491 inhibit E2F transcription in cancer cells	141
6.5.	PHA-767491, Roscovitine, and CVT-313 inhibit E2F - Rb axis transcription in cancer cell lines	143

6.6.	Ciz1 transcription is unaffected by CDK2 or DDK inhibition	144
6.7.	CDK2 kinase inhibition prevents S phase entry of Rb positive cancers	146
6.8.	PHA-767491 resembles CDK2 inhibitors in cancer cell lines	147
6.9.	Ciz1 depletion in cancer cell lines	149
6.10.	Ciz1 requirement for PC3 and SW480 proliferation	151
6.11.	Flow cytometry analysis of MCF7 and T47D showing cell cycle progression after Ciz1 depletion	153
6.12.	Ciz1 depletion reduces proliferation in MCF7	155
6.13.	Quantitation of apoptotic and necrotic cells after Ciz1 depletion in PC3, MCF7, and T47D cell lines	156
7.1.	Recombinant E-Ciz1-His6x cloning	166
7.2.	E-Ciz1-His <sub>6</sub> purification with Ni-NTA resin	168
7.3.	Ciz1 purification with Resource Q 1 ml column	169
7.4.	The diagram of chromatography steps and <i>in vitro</i> ubiquitylation reaction involved in identification of E3 ligase	170
7.5.	Ciz1 ubiquitylation by phosphocellulose column fractions	172
7.6.	Ciz1 ubiquitylation by fractions after Mono S cation exchange chromatography column	173
7.7.	Ciz1 ubiquitylation with fractions after SEC	174

7.8.	Ciz1 ubiquitylation by MonoS 1ml fractions	175
7.9.	The chromatogram of LC-MS/MS analysis	176
7.10.	GST-Ciz1 (N471) purification	180
7.11.	The T293 antibody is specific for pCiz1	181
7.12.	Strategic overview for the identification of phosphatase activity	183
7.13.	p-Ciz1-N471 is de-phosphorylate by phosphocellulose P150 fraction	184
7.14.	Phosphatase activity assays of anion exchange fractions	185
7.15.	Phosphatase assays of SEC fractions showing phosphatase active fractions	186
7.16.	Phosphatase assays of MonoQ fractions	187
7.17.	The chromatogram of LC-MS/MS analysis	188
7.18.	The diagram of the structure of serine/threonine protein phosphatases PP1 and PP2A	189
7.19.	Model of Ciz1 protein level regulation by opposing activities of kinases vs UPS and kinases vs phosphatases	192
8.1.	Model of Ciz1 phosphorylation/dephosphorylation in G1 – S transition	205

## List of Tables

2.1.	Summary of small molecule inhibitors used in this study	38
2.2.	List of antibodies	40
2.3.	Side directed mutagenesis primers	42
2.4.	The list of synthesised single strand guide sequences (Eurofins)	44
2.5.	The list of single strand ODN sequences with point mutations	44
2.6.	The list of the restriction enzymes used for identification of specific point mutations introduced via CRISPR-Cas9 and HDR	46
4.1.	Summary of point mutation introduced by homology directed repair	98
5.1.	Statistical analysis of PHA-767491, XL-413, Roscovitine, and CVT-313 in reducing E2F regulated transcription	122
6.1.	Quantitation of RT-qPCR analysis of cyclin E1, E2, A2 after kinase inhibitors	142
6.2.	The statistical analysis of the difference between GAPDH mRNA and 18S rRNA	143
6.3.	The quantitation of cell fate after Ciz1 depletion in PC3, MCF7, and T47D	157
7.1.	The potential E3 ligases revealed after LC-MS/MS analysis	177
7.2.	The serine/threonine protein phosphatases identified by LC-MS/MS	190



## Abbreviations

AML	Acute myeloid leukaemia
AMP	Adenosine monophosphate
APC/C	Anaphase promoting complex/ cyclosome
APS	Ammonium persulfate
ATM	Serine/threonine protein kinase - Ataxia Telangiectasia Mutated
ATP	Adenosine triphosphate
BSA	Bovine serum albumin
CAPS	3-(Cyclohexylamino)-1-propanesulfonic acid
CD4	Cluster of differentiation 4
CDC20	WD-40 domain – cell division cycle protein 20 of APC/C
Cdc25	Cell division cycle 25 phosphatase
Cdc45	Cell division cycle 45
Cdc6	Cell division cycle 6
CDH1	WD-40 domain substrate adaptor protein of the APC/C
CDK	Cyclin dependent kinase
Cdt1	Chromatin Licensing and DNA Replication Factor 1
CHK	Serine/threonine protein kinase – Checkpoint kinase
Ciz1	Cip1-interacting zinc finger protein
CLL	Chronic lymphocytic leukaemia
CMG	Cdc45, Mcm2-7, GINS replicative DNA helicase complex
CNS	Central nervous system
CRISPR-Cas9	Clustered regularly interspaced short palindromic repeats – CRISPR associated proteins
CRL4 – CDT2	Cullin-RING E3 ubiquitin ligase - Cdc10-dependent transcript 2
CTGF	Connective tissue growth factor
DAPI	4',6-diamidino-2-phenylindole
DDK	Dbf4 dependent kinase (Cdc7 - Dbf4)

DLC1	Dynein light chain 1
DMEM	Dulbecco's modified Eagles Media
DNA	Deoxyribonucleic acid
DPBS	Dulbecco's Phosphate-Buffered Saline
DTT	Dithiothreitol
E1	Ubiquitin activating enzyme
E2	Ubiquitin conjugating enzyme
E2F	E2 factor family of transcription factors
E3	Ubiquitin ligase
EDTA	Ethylenediaminetetraacetic acid
EdU	Ethynyl deoxyuridine
EGFR	Epidermal growth factor receptor
EM1	Early mitotic inhibitor 1
ER	Oestrogen receptor
ERK	Serine/threonine protein kinase - Extracellular signal regulated kinase
FBS	Foetal calf serum
GFP	Green fluorescent protein
GIN5	from the Japanese go-ichi-ni-san meaning 5-1-2-3, after the four related subunits of the complex Sld5, Psf1, Psf2 and Psf3
HDR	Homology directed repair
HECT E3	Homologous to the E6AP carboxyl terminus ubiquitin ligase
HEPES	4-(2-hydroxyethyl)-1-piperazineethanesulfonic acid
HER2	Human epidermal growth factor receptor 2
IMAC	Immobilized metal affinity chromatography
IP	Immunoprecipitation
LB	Lysogeny broth
LC-MS/MS	Liquid chromatography–mass spectrometry
MCM2-7	Minichromosome Maintenance Proteins 2-7
Mono Q	Anion exchange chromatography

Mono S	Cation exchange chromatography
MTT	3-(4,5-Dimethylthiazol-2-yl)-2,5-diphenyltetrazolium bromide for
NLS	Nuclear localisation sequence
ORC	Origin recognition complex
PAM	Protospacer adjacent motif
PCNA	Proliferating cell nuclear antigen
PCR	Polymerase chain reaction
PFA	Paraformaldehyde
PMSF	Phenylmethane sulfonyl fluoride
PP1	Serine/threonine protein phosphatase 1
PP2A	Serine/threonine protein phosphatase 2
PPi	Pyrophosphate
PR	Progesterone receptor
Pre-IC	Pre-initiation complex
Pre-RC	Pre-replication complex
PVDF	Polyvinylidene fluoride
Rb	Retinoblastoma protein
RBR E3	RING between RING ubiquitin ligase
RING E3	Really Interesting New Gene ubiquitin ligase
RKO	Rectal carcinoma cell line
RNA	Ribonucleic acid
RP	Restriction Point
RS-1	RAD51 stimulatory compound 1
RTK	Receptor tyrosine kinase
SCF – CDC4	Cell division control protein 4
SCF	Skp, Cullin, F-box containing complex
SCR-7	DNA ligase IV inhibitor
SDS	Sodium dodecyl sulfate

SDS-PAGE	Sodium dodecyl sulfate polyacrylamide gel electrophoresis
SEC	Size exclusion chromatography/ gel filtration chromatography
siRNA	Short interfering ribonucleic acid
SKP1/2	S-phase kinase-associated protein 1/2
ssODN	Single stranded oligodeoxynucleotide
TCF4	Transcription factor 4
TEMED	Tetramethylethylenediamine
UPS	Ubiquitin proteasome system
Xist RNA	X-inactive specific transcript RNA
YAP	Yes-associated protein 1 transcription factor

# Chapter 1

## Introduction

## **1. Introduction**

The mammalian cell cycle is divided into 4 phases, namely, growth phase 1 (G1), DNA replication phase (S), growth phase 2 (G2), and mitotic phase (M) (Bajar et al., 2016). Majority of mammalian cells can exit the cell cycle and enter the reversible dormant state, called quiescence (G0 phase), which is important for maintaining stem cell populations, tissue repair and regeneration, and homeostasis (Cheung and Rando, 2013; Gérard and Goldbeter, 2012; Yao, 2014; Zetterberg and Larsson, 1985).

The cell cycle is driven by sequential cyclin expression that in turn activates cyclin dependent kinases (CDK) required for cell cycle progression (Lim and Kaldis, 2013; Morgan, 1995). Starting from G1 phase, the cyclin D is expressed in response to mitogenic signalling (Klein and Assoian, 2008), it activates CDK4/6 and phosphorylates retinoblastoma protein (Rb) (VanArsdale et al., 2015). This leads to E2F release for cyclin E and cyclin A transcription that further phosphorylate Rb (Bertoli et al., 2013a; Weinberg, 1995). The hyperphosphorylation of Rb drives cell passage through the restriction point (RP) where cell growth becomes independent from mitogenic signalling. Second major event in the cell cycle is the entry to mitosis that is driven by cyclin B – CDK1. Cyclin B is expressed and accumulated in G2 phase (Figure 1.1), it binds and activates its catalytic partner CDK1 for nuclear import and generation of the mitotic spindle, chromosome condensation, and nuclear envelope breakdown (Gavet and Pines, 2010).

The ubiquitin proteasome system (UPS) is another controlling mechanism of the cell cycle (Frescas and Pagano, 2008; Zhu and Mao, 2015). Both systems tightly regulate protein expression, activation and accumulation that is required for cell cycle

progression. During the cycle progression the irreversible transitions are enforced by collaborating CDK and UPS mediated signalling. These activities produce the oscillations in kinase activity required to maintain the unidirectionality of the cell cycle. Kinase activity rises in G1 phase, which leads to APC/C-CDH1 inactivation and further increase in kinase activity in S phase. This is followed by the maximal CDK activity in prophase and metaphase of the mitosis, which in turn phosphorylates and activates APC/C-CDC20 resulting in cyclin destruction and a drop in kinase activity in anaphase of mitosis, leading to APC/C-CDH1 re-activation (Frescas and Pagano, 2008; Wang et al., 2015).

The tight control of cyclin – CDK activity and UPS is crucial for faithful cell cycle progression and DNA replication (Canavese et al., 2012; Frescas and Pagano, 2008; Kitagawa et al., 2009). The upregulation and overexpression of kinases or downregulation and mutation in UPS can lead to deregulated cell cycle, which can result in deregulation of protein levels and function, DNA replication stress, and DNA damage that pinpoint tumourigenesis (Benanti, 2012; Lim and Kaldis, 2013; Pal et al., 2014; Trovesi et al., 2013; Zeman and Cimprich, 2014).

The replication stress is defined as transient slowing or staling of replication forks in response to endogenous or exogenous stress. The intrinsic replication fork obstacles include transcribing RNA polymerases, unusual DNA structures, and oncogene activation. The replication stress response is essential for DNA replication machinery to overcome the obstacles in order to faithfully replicate genomic information (Berti and Vindigni, 2016). Importantly, cancer cells display increased DNA damage and rely heavily on replication stress responses in order to proliferate, introduce new

mutations, and overcome DNA damaging chemotherapy treatments (Zeman and Cimprich, 2014).

Cancer biology is defined by 6 main hallmarks of cancer: increased proliferation, inhibition of tumour suppressors, evasion of apoptotic cell death, acquired immortality, stimulated angiogenesis, other tissue invasion and metastasis (Hanahan et al., 2000). Additional cancer characteristics have been proposed later, including changes in metabolism, immunosuppression, cancer promoting inflammation and genome instability (Hanahan and Weinberg, 2011). Overall, cancer development is a multistep process, and dysregulation of cyclin – CDK and UPS activities may drive a number of changes stimulating cancer progression. Therefore, this chapter is going to focus on the control of the cell cycle and DNA replication by cyclin – CDKs complexes and the UPS. Additionally, the consequences of deregulation in cyclin - CDKs and UPS activities will be discussed briefly.

The primary focus of this work is to identify and understand the regulatory networks that control Cip1-interacting zinc finger protein (Ciz1) function. Ciz1 is a nuclear matrix protein that facilitates DNA replication initiation (Ainscough et al., 2007; Copeland et al., 2010; Copeland et al., 2015; Coverley et al., 2005). Deregulation of Ciz1 levels is linked to a number of cancers (Den Hollander and Kumar, 2006; Lei et al., 2016; Liu et al., 2016; Pauzaite et al., 2017; Wang et al., 2018; Wu et al., 2016; Yin et al., 2013; Zhang et al., 2015). However, the molecular pathway or pathways that control Ciz1 levels have not been determined yet. Understanding how Ciz1 is regulated will provide insight into the regulation of Ciz1 activity in normal cells and

potentially provide an understanding of mechanisms that promote Ciz1 over-expression and accumulation in cancer cells.

### **1.1. Mammalian cell cycle is driven by cyclin - CDKs**

Cyclins are expressed sequentially, starting from cyclin D in early G1 phase, then cyclin E in mid- G1, cyclin A in G1 - S transition, and cyclin B in G2 - M phase (Figure 1.1) (Hochegger et al., 2008; Pines, 1999). Each cyclin associates with their cognate CDK to activate their catalytic kinase activity. This way the total kinase activity rises temporally organising cell cycle events.

In human cells there is 20 different CDKs and 30 Cyclins (Malumbres, 2014; Wood and Endicott, 2018). Cyclins recognise either RxL motif or LxCxE motif, in case of cyclin D1, and associate with CDKs via strong hydrophobic interactions (Topacio et al., 2018; Wallace and Ball, 2004; Wood and Endicott, 2018). Cyclin – CDK binding results in physical conformational change in CDK, opening the catalytic site (Malumbres, 2014). In case of CDK1 and CDK2 activation, this is further stabilised by threonine (T160) phosphorylation by CDK activating kinase (CAK) (Lolli and Johnson, 2005), which allows for optimal ATP and substrate binding by the enzyme (Donzelli and Draetta, 2003; Nurse, 1997). The final CDK activation step is dephosphorylation of inhibitory threonine (T14) and tyrosine (Y15) by Cdc25 family phosphatases (Boutros et al., 2007).

Cyclins display preference for specific CDK enzymes; however, they are not completely restricted and can bind other CDKs when their partner pools are depleted, under stress conditions, or *in vitro* (Merrick et al., 2008). For instance, cyclin B1 can rescue the S phase progression in cyclin A2 depleted *Xenopus laevis*

(Moore et al., 2003). Different classes of CDKs perform distinct functions, such as driving cell cycle and transcriptional regulation (Wood and Endicott, 2018). Cyclin - CDK complexes are serine/threonine kinases that specifically phosphorylate the S/T-P-X-K/R consensus sequence, where positively charged proline (+1) fits into the negatively charged pocket next to the catalytic site in CDK (Lo and Uhlmann, 2011).

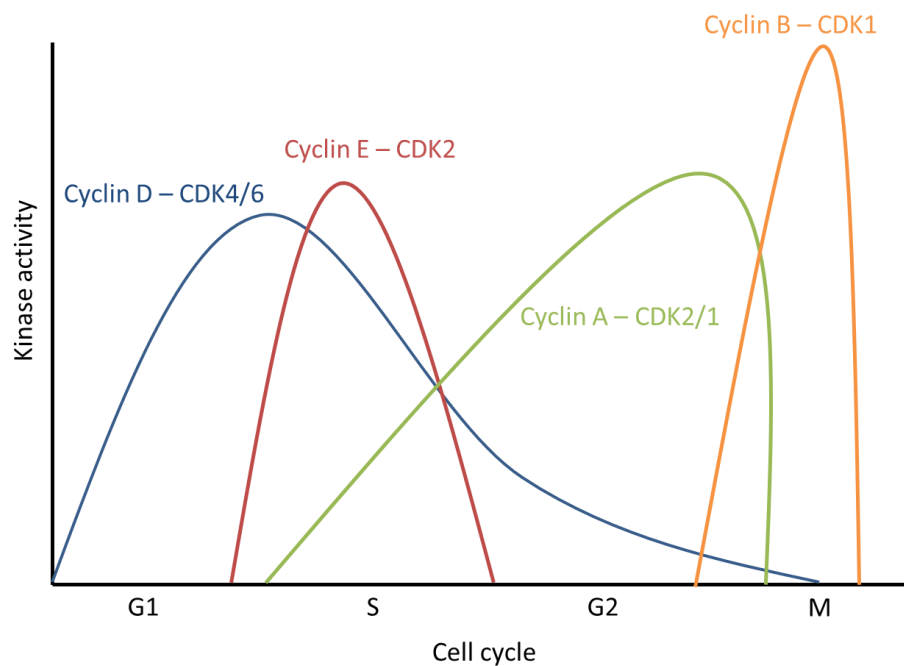


**Figure 1.1. Cell cycle is driven by the sequentially expressed cyclins and rising kinase activity.** In early G1 phase, Cyclin D is expressed and activates CDK4/6 (blue). In mid- G1, Cyclin E is expressed and activates CDK2 (red), raising total kinase activity and driving cell entry to S phase. In late G1 – early S phase, Cyclin A is expressed activating CDK2 and then CDK1 in G2 phase (green). In late G2 phase, cyclin B is expressed activating CDK1 (orange), further increasing total kinase activity and driving cell entry to mitosis (Hochegger et al., 2008; Lo and Uhlmann, 2011; Pines, 1999).

### 1.1.1. Critical analysis of quantitative model of kinase activity driving the cell cycle

The quantitative kinase activity model states that such rigorous cyclin expression and their specific kinase activation are not necessary to drive the cell cycle (Berthet et al., 2003; Coudreuse and Nurse, 2010a; Hochegger et al., 2007; Hochegger et al., 2008;

Lo and Uhlmann, 2011; Malumbres, 2014; Santamaria et al., 2007). For example, the minimal M phase cyclin – CDK (Cdc13 – Cdc2) complex is able to drive G1 – S and G2 – M transition in fission yeast (Coudreuse and Nurse, 2010a). Multiple cyclin - CDK depletion and knockout experiments have provided large amount of evidence stating that mitotic cyclin - CDK is sufficient to drive the cell cycle. The data propose that the entry to S phase requires moderate total kinase activity, and the entry to M phase demands for high kinase activity (Figure 1.2). Both phases have their permissive kinase activity window and are blocked by either lower or higher activity range (Coudreuse and Nurse, 2010a). However, even though cyclin B alone is able to drive G1 – S transition in mammalian cells, it provokes early mitotic entry, thus could not replace other cyclins *in vivo* (Aleem et al., 2004; Moore et al., 2003). Therefore, mitotic cyclin – CDK alone can drive DNA replication and mitosis in mammalian cells; however, it cannot support a complete and regulated cell cycle in mammalian cells.

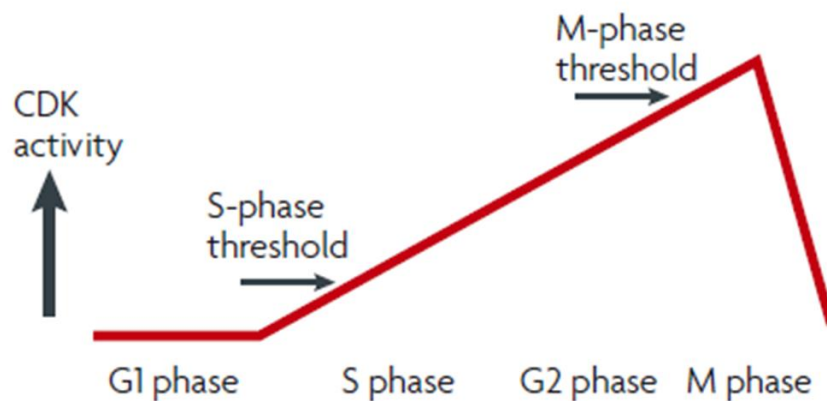


**Figure 1.2. Quantitative model of rising kinase activity driving the cell cycle.** Cell cycle is driven by rising kinase activity, when kinase activity is low to moderate, the DNA replication initiates and cell enters the S phase, and when the kinase activity is high, the cell enters mitosis (M phase) (Hochegger et al., 2008; Lo and Uhlmann, 2011; Pisu et al., 2015).

Additionally, this model fails to uphold in quiescent cells re-entering the cell cycle. The reason might be the residual kinase activity that is maintained in cycling cells (Moser et al., 2018; Spencer et al., 2013). Nonetheless, it has been shown that post-quiescent cells depend of specific cyclin expression for initiation of DNA replication and the entry to S phase (Coverley et al., 2002; Thacker, 2017). This may suggest the reason why many of cyclin – CDK knockout mice failed to expand stem cell populations and were infertile (Brandeis et al., 1998; Geng et al., 2003; Geng et al., 2007; Kalaszczynska et al., 2009; Kozar et al., 2004; Lo and Uhlmann, 2011; Santamaria et al., 2007).

Finally, the quantitative kinase activity model does not explain why kinases prefer S phase substrates prior to M phase substrates (Lo and Uhlmann, 2011). This may be explained by the ratio of kinases and phosphatases during the cell cycle progression, also the affinity of specific substrate for kinase and phosphatase. For instance, Cdc25 phosphatase is required to activate kinases, making phosphatase an important player in cell cycle progression and raising kinase activity (Boutros et al., 2007; Donzelli and Draetta, 2003). Additionally, the PP2A phosphatase was shown to dephosphorylate CDK substrates with high efficiency in interphase and its activity is downregulated in mitosis (Mochida et al., 2009). This way it may provide an additional layer of cell cycle progression control that cannot be attributed to increase in kinase activity alone. Finally, early in the cell cycle of budding yeast, PP2A actively counteracts CDK phosphorylation of their late substrates, and by preferring threonine residues, impose temporal separation of serine and threonine phosphorylation throughout the cell cycle (Cundell et al., 2016; Godfrey et al., 2017). These examples illustrate the

importance of phosphatases in the cell cycle that cannot be explained by quantitative kinase activity model alone.

## **1.2. Definition of the restriction point**

This work is going to focus on G1 – S phase progression and the events underpinning this transition. A key regulatory event in G1 phase is the restriction point (Pardee, 1974). It is described as a 'point of no return', when cells become independent from mitogenic signalling and fully commit to complete the cell cycle. The main regulator of the restriction point is the tumour suppressor retinoblastoma protein (Rb) (Blagosklonny and Pardee, 2002). The Rb protein either directly binds and inhibits transactivation domain of E2F-1 or uses E2F to bind DNA and actively suppresses transcription of proteins required for nucleotide metabolism and DNA synthesis in G1 phase (Bertoli et al., 2013b; Burke et al., 2010; Harbour and Dean, 2000; Zheng and Lee, 2001). The transcriptional repression is alleviated by initial phosphorylation by cyclin D – CDK4/6 (Kato et al., 1993; Klein and Assoian, 2008; Mittnacht, 1998; Ortiz et al., 2017), leading to cyclin E expression and priming of Rb for further phosphorylation by cyclin E – CDK2 (Kelly et al., 1998; Ohtani et al., 1995; VanArsdale et al., 2015). The collaboration of cyclin D - CDK4/6 and cyclin E - CDK2 leads to hyper-phosphorylation of Rb that weakens interactions with the E2F 1-3 family of transcriptions factors enabling transcription of target genes. This is the key event in surpassing the restriction point (Blagosklonny and Pardee, 2002; Heldt et al., 2018a; Mittnacht, 1998; Shen et al., 2004).

However, more recent data show that cells may possess more than one 'restriction point' or the point when cells decide whether they will enter the cell cycle or enter

the quiescent state (Coller, 2007). This decision may depend on cell density, mitogenic signalling, kinase activity levels, or DNA damage (Barr et al., 2016; Barr et al., 2017; Heldt et al., 2018a; Moser et al., 2018; Spencer et al., 2013). The research used a fluorescent-CDK2 activity sensor that enabled analysis of single cells and demonstrated that cells bifurcate into two populations after mitotic anaphase (Moser et al., 2018; Spencer et al., 2013). Cells with low CDK2 activity exit mitosis into a pre-restriction state and are dependent on mitogenic signalling and are regulated by the restriction point in late G1. However, the cells with moderate CDK2 activity can complete the cell cycle with no external stimuli and have a reduced length of G1 phase (Spencer et al., 2013). This decision depends on the levels of p21 in mother cells that partition into daughter cells and determine their intrinsic CDK2 activity (Moser et al., 2018). Similarly, the accumulation of p21 after the DNA damage in G1 phase can promote the cell cycle exit in quiescent like state that is inheritable by daughter cells (Barr et al., 2016; Barr et al., 2017; Heldt et al., 2018a).

Quiescent cells have low kinase activity (Spencer et al., 2013), high levels of E3 ligases targeting cyclin, such as Skp2 (Heldt et al., 2018a; Kossatz et al., 2004; Wang et al., 2011), and high levels of kinase inhibitors p21 and p27 (Barr et al., 2016; Barr et al., 2017; Cheng, 2000; Ladha et al., 1998). In order to re-enter the cell cycle, quiescent cells rely on external stimuli to drive the synthesis of G1 phase regulators (Gerard and Goldbeter, 2009; Gérard and Goldbeter, 2012). Therefore, the G0 cells take longer to reach RP and exit G1 phase by initiation of DNA replication in S phase. Post-quiescent cells require sustained mitogenic signalling to promote sequential cyclin expression and specific cyclin - CDK activation to bypass restriction point and enter the S phase.

### 1.3. DNA replication

The interplay between kinase phosphorylation and ubiquitin mediated protein degradation is important for the temporal regulation of DNA replication. DNA replication can be divided in four specific phases, namely origin specification by the origin recognition complex (ORC), pre-replication complex (pre-RC) assembly, helicase activation, and replisome formation (Leonard and Me, 2013; Riera et al., 2017; Tanaka and Araki, 2013; Yeeles et al., 2017). DNA replication licencing is accomplished by pre-RC assembly on the origins of replication in G1 phase (Prioleau and MacAlpine, 2016). It is followed by pre-initiation complex (pre-IC) formation, double stranded DNA unwinding, DNA replication initiation, and finally by replisome firing (Boos et al., 2013; Chowdhury et al., 2010; Kumagai et al., 2011; Parker et al., 2017; Pauzaite et al., 2017; Yeeles et al., 2015; Yeeles et al., 2017).

The proteins required for origin firing and replisome activation have been identified and the recapitulation of DNA replication licensing, helicase activation and processive DNA replication have been achieved *in vitro* (Deegan and Diffley, 2016; Deegan et al., 2016; Riera et al., 2017; Yeeles et al., 2015; Yeeles et al., 2017). Replication licencing starts from ORC binding to origin of replication still in G2 – M phase (Hoggard et al., 2013; Leonard and Me, 2013). In early G1 phase, the ORC is directly bound by Cell Division Cycle 6 (Cdc6), and Chromatin Licensing and DNA Replication Factor 1 (Cdt1) facilitates loading of Minichromosome Maintenance 2-7 (MCM2-7) complex to putative replication origins (Deegan and Diffley, 2016; Duzdevich et al., 2015). This step requires ATP to promote MCM2-7 helicase loading onto DNA using Cdc6 and ORC ATPase activity (Figure 1.3).

Following the pre-RC assembly, helicase loading and activation are regulated by CDK2 and Dbf4 - Cdc7 (Dbf4-dependent kinase, abbreviated as DDK) activities. Cyclin E – CDK2, in association with Cdc6 and Cdt1, is responsible for MCM2 helicase loading to origins of replication (Blow and Hodgson, 2002; Copeland et al., 2010; Coverley et al., 2002; Donovan et al., 1997). It is followed by DDK phosphorylation of MCM2 leading to Cell Division Cycle 45 (Cdc45) loading (Deegan and Diffley, 2016; Deegan et al., 2016; Francis et al., 2009; Montagnoli et al., 2006; Montagnoli et al., 2010; Takeda and Dutta, 2005), and finally CDK2 aided go-ichi-ni-san (GINS) (Sld5, Psf1, Psf2, and Psf3) association results in active helicase (CMG complex) assembly (Figure 1.3) (MacNeill, 2010). Interestingly, the CDK activity in S phase promotes MCM2 activation, but prevents the loading of new MCM2-7 complexes (Deegan and Diffley, 2016; Siddiqui et al., 2013; Tanaka and Araki, 2013); this way preventing DNA re-replication.

The Ciz1 protein associates to nuclear matrix via its C – terminal and directly binds Cdc6 (Ainscough et al., 2007; Copeland et al., 2010; Copeland et al., 2015). This potentially contributes to the regulation of the initiation phase of DNA replication, as Ciz1 binds to cyclin E - CDK2 and then to cyclin A - CDK2 to recruit CDK2 to its targets at pre-IC (Copeland et al., 2010; Copeland et al., 2015; Coverley et al., 2005) (Figure 1.3).

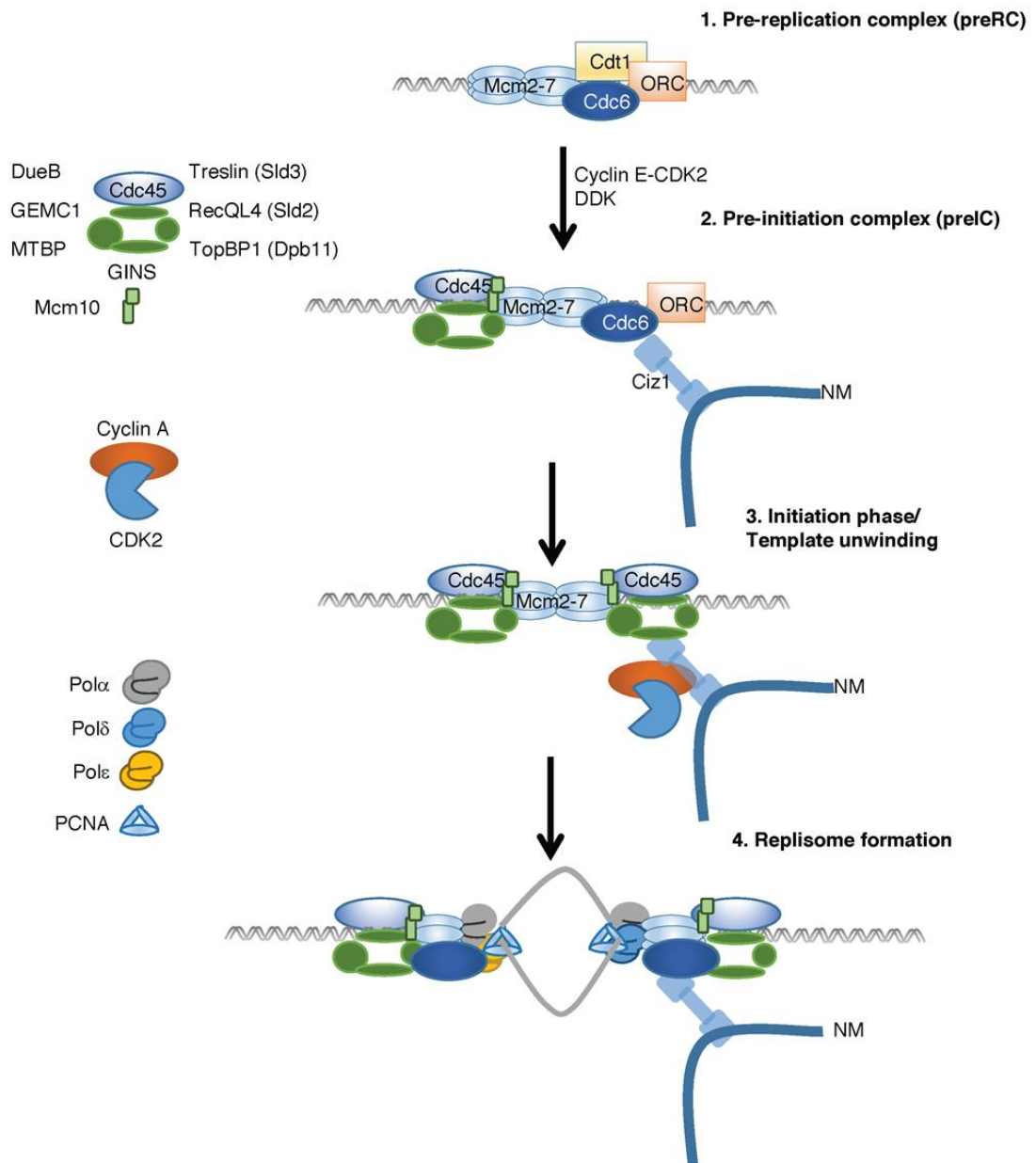


**Figure 1.3. Formation of replication complex.** The origin recognition complex (ORC) binds to origin of replication, Cdc6 directly binds the origin and Cdt1 brings MCM2-7 complex to form pre-replication complex. Cooperating cyclin E – CDK2 and DDK promote Cdc45, MCM2-7, and GINS (CMG) loading this way activating MCM2 helicase activity and forming DNA replication initiation complex. The polymerases and PCNA loading completes the replisome assembly that is activated by kinase phosphorylation (Deegan et al., 2016; Pauzaite et al., 2017; Riera et al., 2017; Yeeles et al., 2015; Yeeles et al., 2017). Ciz1 is a nuclear matrix protein binding to Cdc6 and facilitating cyclin E – CDK2 then cyclin A – CDK2 recruitment to replication complex (Copeland et al., 2010; Copeland et al., 2015; Coverley et al., 2005).

The final step in CDK - dependent replisome activation is the loading of proliferating cell nuclear antigen (PCNA) and DNA polymerases: Polymerase  $\alpha$  priming the DNA synthesis, Polymerase  $\epsilon$  for leading-strand, and Polymerase  $\delta$  for lagging-strand synthesis (Leman and Noguchi, 2013). The mammalian DNA replication involves plethora of accessory proteins aiding DNA replication that are not covered here.

During replication complex assembly, the pre-RC is disassembled as origins are activated and pre-replication complex assembly is inhibited in order to prevent re-replication (Truong and Wu, 2011). The prevention of DNA re-replication involves tight collaboration between kinase phosphorylation and UPS. First, sequential dissociation of Cdc6 and Cdt1 from chromatin leads to the first MCM2-7 complex loading, it is followed by the second Cdc6, Cdt1 and ORC dissociation facilitating the second MCM2-7 ring closure (Riera et al., 2017; Ticaú et al., 2015; Ticaú et al., 2017). The Cdc6 protein is phosphorylated by Cyclin E – CDK2 then by Cyclin A – CDK2 that leads to either exclusion from the nucleus or ubiquitylation by SCF-CDC4 in order to prevent re-replication (Hwang et al., 2014). In addition, Cdt1 is phosphorylated by Cyclin A – CDK2, leading to its dissociation from ORC and polyubiquitylation by SCF-SKP2 and CRL4-CDT2 E3 ligases and UPS mediated degradation (Kim and Kipreos, 2007; Kim et al., 2008; Liu et al., 2004). The ORC is phosphorylated by cyclin A – CDK2 that promotes its dissociation from the chromatin (Lee et al., 2012). Phosphorylation of ORC stimulates ubiquitylation by SCF-SKP2 and consequential degradation by the proteasome (Mendez et al., 2002).

These data suggest that temporal separation of the events leading to origin licencing and firing is tightly regulated by kinase activity and ubiquitin proteasome system.

Both systems collaborate in timely protein loading onto the chromatin and their dissociation in order to prevent re-replication. Additionally, the kinases and UPS regulate each other in order to reach S phase permissive kinase activity after the origin licencing has been completed.

#### **1.4. Ubiquitin proteasome system**

To ensure temporal control of cell cycle progression the ubiquitin proteasome system (UPS) is another crucial cell cycle regulator. Indeed, the oscillation of cyclins during the cell cycle progression would be impossible without cyclin degradation by UPS (Benanti, 2012). The UPS is composed of 2 main parts: specific substrate recognition that promotes ubiquitylation of lysine within the substrate using an ATP dependent enzymatic cascade, and indiscriminate degradation of polyubiquitylated substrates by the 26S proteasome core (Bard et al., 2018; Myung et al., 2001). Ubiquitin is a highly conserved protein consisting of 76 amino acids (Akutsu et al., 2016; Swatek and Komander, 2016; Wagner et al., 2011; Weber et al., 1987). The complexity and specificity of ubiquitylation signal comes from eight linkages ubiquitin can form on itself with its 7 lysine residues (K6, K11, K27, K29, K33, K48, and K63) and its N – terminal (Grice et al., 2015). Each type of linkage forms different binding surfaces providing diverse functions. Further complexity is dictated by the formation of poly-ubiquitin chains, ubiquitin can be linked through either the same lysines that is called homotypic chains, or different lysine residues, which further can form mixed or branched structures that are called heterotypic chains (Akutsu et al., 2016; Meyer and Rape, 2014; Sadowski et al., 2012).

The covalent attachment of the ubiquitin leads to various outcomes of ubiquitylation, such as protein degradation, transcriptional activation, cell signalling, endocytosis, and cell death (Pickart, 2001; Swatek and Komander, 2016). The ubiquitin chain length and branchiness define the regulatory role of ubiquitylation (Meyer and Rape, 2014; Swatek and Komander, 2016). The main outcome of poly-ubiquitylation via K11 and K48 is proteolytic degradation in 26S proteasome (Chau et al., 1989; Jin et al., 2008; Meyer and Rape, 2014; Nathan et al., 2013; Yau et al., 2017). The mono-ubiquitylation and polyubiquitylation of M1 and K63 are linked with assembly of signalling complexes, endocytic trafficking, inflammation, translation and DNA repair (Spence et al., 1995; Tokunaga et al., 2009; Wang et al., 2001; Yau and Rape, 2016). Recently, the APC/C specific K11/K48-branched chains were described as a main quality control mechanism of aggregation prone proteins (Yau et al., 2017). These K11/K48-branched chains lead to rapid degradation in the 26S proteasome.

The general function of 26S proteasome is protein homeostasis and stress response (Bard et al., 2018). The proteasome is composed of the 20S core particle and the 19S regulatory particle (Bedford et al., 2010). The 19S regulatory part recognises ubiquitylated proteins and catalyses the de-ubiquitylation, thus ubiquitin recycling. The active peptidase site resides in chamber of the barrel-shaped 20S core particle that degrades the protein into short peptide sequences that are further digested into amino acids by cellular peptidases, and recycled as building blocks for new protein synthesis.

The first reaction in the ubiquitylation is the ubiquitin activation by the ubiquitin activating enzyme (E1) (Figure 1.4). This process requires the hydrolysis of ATP to AMP and P<sub>Pi</sub> in order to link glycine-76 of ubiquitin and cysteine residue of the E1 enzyme via high energy thioester bond (Schulman and Wade Harper, 2009). The second step of the chain reaction is to transfer the ubiquitin from E1 enzyme to the ubiquitin conjugating enzyme E2 via transthioylation reaction (Stewart et al., 2016). The E2 enzyme has previously been considered to be a simple ubiquitin carrier; however, an increasing amount of evidence suggests that N and C terminal regions, flanking the cysteine residue in the active site, contribute to the binding of specific E3 enzymes, substrate selection and specificity (Burroughs et al., 2008; Pickart, 2001; Van Wijk et al., 2009). The third step of the ubiquitylation reaction is the linkage of ubiquitin protein to the specific substrate. The reaction is catalysed by ubiquitin protein ligase E3 that aids in ubiquitin transfer from E2 enzyme onto specific substrate (Myung et al., 2001). In many cases, such as HECT and RBR E3s, the transfer involves ubiquitin binding to E3 by thiol linkage and subsequent generation of amide isopeptide bond between glycine-76 of ubiquitin and  $\epsilon$  (epsilon) amino group of lysine residue of the substrate (Morreale and Walden, 2016; Van Wijk et al., 2009). Nonetheless, in RING E3s, the ubiquitin protein is transferred directly from E2 to the substrate and is only catalysed by E3 ligase (Morreale and Walden, 2016; Myung et al., 2001; Pickart, 2001).

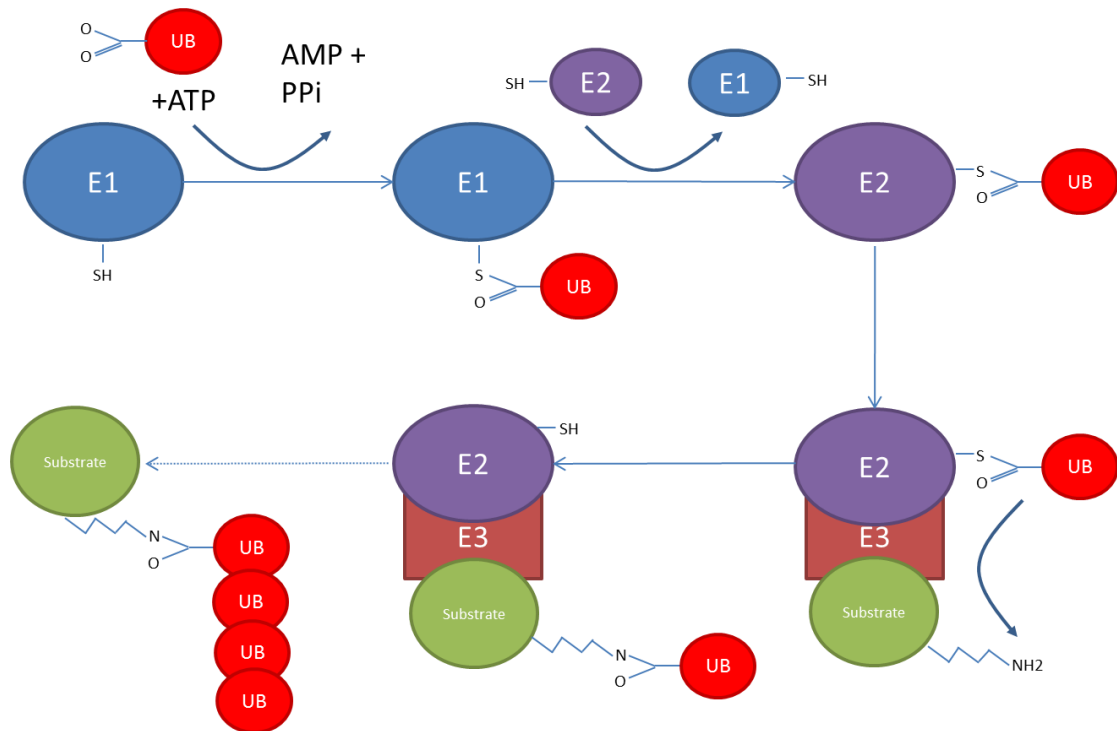


**Figure 1.4. The chain of enzymatic reactions involved in substrate ubiquitylation.** The E1 (ubiquitin activating enzyme) generates high energy thioester bond between E1 and ubiquitin. The ubiquitin is transferred onto E2 (ubiquitin conjugating enzyme). The E2 binds E3 (ubiquitin protein ligase) and the specific substrate. The ubiquitin is transferred either directly from E2 to the substrate, or to E3 and then to the substrate. The reaction can be repeated in order to generate poly-ubiquitin chain.

There are 8 different E1 enzymes (Schulman and Wade Harper, 2009), 40 of E2 conjugating enzymes (Stewart et al., 2016), and approximately 600 - 700 of E3 ligases identified in humans so far (Morreale and Walden, 2016). The substrate specificity is defined by collaborating E2s and E3s. Typically, the UPS is classified according to their E3 ligases. The E3 complexes are separated into three different classes, namely RING E3s that have RING (Really Interesting New Gene) or U-box domain, HECT E3s that have HECT (homologous to the E6AP carboxyl terminus) domain, and RBR E3s that have two RING domains separated by another in between RING domain (Morreale and Walden, 2016).

### **1.5. CDK and UPS activities temporally control cell cycle events**

The cell cycle is driven by sequentially expressed cyclins and oscillating kinase activity (Figures 1.1 and 1.2). However, the temporal separation of cyclin expression and rising kinase activity would not be possible without UPS (Bassermann et al., 2014). For instance, the timely degradation of the cyclins, such as cyclin B upon the mitotic exit, and cyclin dependent kinase inhibitors, such as p21 and p27 in G1 to S progression, is key in the successful cell cycle progression (Figure 1.5) (Bassermann et al., 2014; Skaar and Pagano, 2009).

The main UPS complexes, involved in the cell cycle regulation, are SCF (SKP/CUL1/F-box) and APC/C (anaphase promoting complex or cyclosome) that are multi-subunit cullin RING E3 ligases (Skaar and Pagano, 2009). The SCF complex is composed of CUL1 scaffold, which binds to RING finger protein RBX1, this way creating platform to bind E2s and SKP1/2 adaptor protein that in turn binds F-box protein that recognises the phosphorylated substrate (Nakayama and Nakayama, 2006; Skaar and Pagano, 2009; Skaar et al., 2013). Out of 70 identified F box proteins, three groups FBXW $\beta$  (TRCP1/2), FBXL (SKP1/2), and FBXO target cell cycle controllers, thus, have been linked with the cell cycle control (Zheng et al., 2016). F-box proteins have plethora of targets driving cell cycle, such as FBXW $\beta$  targets Emi1, Cdc25A/B, Wee1, and Cyclin D; FBXL targets p21, p27, p57, cyclin D, cyclin A, cyclin E, Cdh1; and FBXO targets cyclin B, cyclin D, p53, Chk1 (Davis et al., 2014; Frescas and Pagano, 2008; Nakayama and Nakayama, 2006; Pal et al., 2014; Skaar and Pagano, 2009; Wang et al., 2011; Zheng et al., 2016). Therefore, either mutations or overexpression in F-box protein family may lead to deregulated cell cycle that is a hallmark of cancer.

The APC/C is structurally related to SCF consisting of RING finger protein APC11, CUL1 related scaffold protein APC2, another 11 subunits with no clearly identified functions, and the activator that is responsible for substrate specificity (Arnold et al., 2015; He et al., 2013; Nakayama and Nakayama, 2006; Skaar and Pagano, 2009). The key cell cycle associated regulators of APC/C are CDC20 and CDH1 (Da Fonseca et al., 2011; Hein and Nilsson, 2016; Huang et al., 2001; Lee et al., 2015). The CDC20 is active in metaphase to anaphase of mitosis, is responsible for spindle assembly checkpoint, and degrades S and M phase cyclins for M phase exit (Wang et al., 2015). Similarly, CDH1 is active from late mitosis to late G1 phase, targets M phase cyclins for mitotic exit, and maintains low CDK activity in G1 phase by degradation of S phase and M phase cyclins (Arnold et al., 2015; Huang et al., 2001) (Figure 1.5).

SCF and APC/C have distinct activities and their activity oscillates during the cell cycle. SCF is active from late G1 phase up to early mitosis (Bassermann et al., 2014; Nakayama and Nakayama, 2006). However, the activity of APC/C is restricted to M – G1 phase, CDC20 being mainly responsible for mitotic exit and CDH1 for maintenance of G1 phase (Benanti, 2012; Vodermaier, 2004).

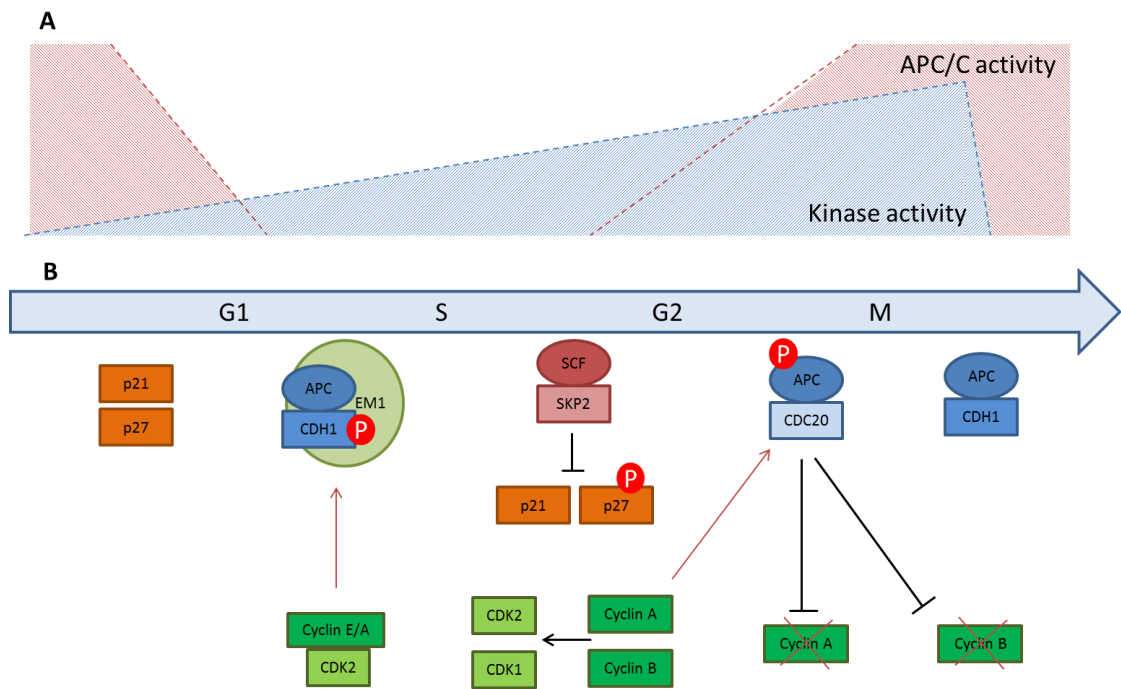


**Figure 1.5. The cell cycle is driven by kinase and UPS activities. A)** DNA replication events are temporally controlled by rising kinase activity and decreasing APC/C activity, and mitotic exit is driven by rapid degradation of cyclins and CDK, and recovery in APC/C activity (Nakayama and Nakayama, 2006; Vodermaier, 2004; Zhu and Mao, 2015). **B)** In M - G1 phase APC/C-CDH1 is active, it degrades SCF-SKP2, this way p21 and p27 accumulates and inhibits Cyclin A – CDK1/2, Cyclin B – CDK2 activity. In G1 – S transition, CDH1 is phosphorylated, APC/C-CDH1 is inhibited by EM1, SCF-SKP2 accumulates, and degrades p21 and p27 phosphorylated by Cyclin E – CDK2, kinase activity rises (Bornstein et al., 2003; Huang et al., 2001; Lu and Hunter, 2010). In G2 – M, APC/C-CDC20 is phosphorylated and activated by Cyclin A – CDK1/2 and Cyclin B – CDK1, it degrades Cyclin A, APC/C-CDH1 activity is recovered, it further degrades Cyclin A and Cyclin B, kinase activity drops in the end of mitosis, and cell cycle is reset (Arnold et al., 2015; Frescas and Pagano, 2008; Hein and Nilsson, 2016; Huang et al., 2001; Wang et al., 2015).

The interplay between the kinase activity and ubiquitin proteasome system drives the cell cycle (Figure 1.5). The transitions in the cell cycle are promoted by CDK activity that also drives transitions in the activities of the UPS that promotes cyclin degradation to maintain directionality in the cell cycle. APC/C-CDH1 targets cyclin A, cyclin B, and SCF-SKP2 in early G1. Cyclin E – CDK2 phosphorylates CDH1 leading to Emi1 binding that inactivates APC/C-CDH1 at the G1 – S transition (Cappell et al.,

2018) followed by the degradation of CDH1 by the SCF-SKP2 complex (Vodermaier, 2004). This induces the rising CDK activity due to inactivation of APC-CDH1 and phosphorylation of p21 and p27 leading to SCF-SKP2 mediated degradation (Bassermann et al., 2014). As cyclin - CDK activity rises in G1 phase, CDH1 is phosphorylated at the G1/S transition that facilitates further accumulation of cyclin A. Phosphorylated CDH1 is a substrate for SCF-SKP2 that promotes degradation of CDH1 and contributes to the transition from G1 phase into S phase (Arnold et al., 2015; Benanti, 2012; Hein and Nilsson, 2016; Vodermaier, 2004). The quantitative increase in CDK activity in G1 phase is mediated by destruction of the CDK inhibitor proteins p21 and p27, which are phosphorylated by cyclin E – CDK2 in order to be targeted by SKP2 (Bornstein et al., 2003; Lu and Hunter, 2010).

Later in the cell cycle rising activity of cyclin A – CDK1/2 and cyclin B – CDK1 leads to APC/C-CDC20 phosphorylation and activation (Qiao et al., 2016). APC/C-CDC20 degrades cyclin A that leads to de-phosphorylation and reactivation of APC/C-CDH1 (Robbins and Cross, 2010). APC/C-CDH1 further degrades cyclin A and cyclin B, re-setting low kinase activity for the second round of DNA replication initiation (Simpson-Lavy et al., 2015).

### **1.6. The deregulation in CDK and UPS in tumourigenesis**

CDK and UPS activities coordinate tempo-spatial regulation and ensure precise orchestration of the cell cycle progression (Bassermann et al., 2014; Nakayama and Nakayama, 2006; Rizzardi and Cook, 2012). Therefore, deregulation either in CDK activity or ubiquitin mediated protein degradation can lead to dysregulation of cell cycle control. Inactivation or hyper-activation of both CDK and UPS activities are

commonly associated with deregulation of cell cycle and uncontrolled cell proliferation in cancer.

Any modification in cyclin – CDK pathway, such as overexpression of cyclin, downregulation of CDK inhibitors, mutations that render CDK to become insensitive to inhibition, and downregulation of cyclin degradation may lead to a loss of normal cell cycle control, increased cellular proliferation and promote tumorigenesis (Canavese et al., 2012; Deshpande et al., 2005; Santamaria and Ortega, 2006). For instance, a number of major cancers, such as breast, lung, cervix, endometrial, pancreatic, and colon, have been linked to cyclin E overexpression and SCF-Fbw7 loss-of-function mutations that targets cyclin E for degradation (Davis et al., 2014; Hwang and Clurman, 2005; Kitagawa et al., 2009; Welcker and Clurman, 2008). A plethora of molecular pathways are involved in cyclin E and Fbw7 driven tumourigenesis, but it is known that deregulation in both causes chromosomal instability and tumorigenesis (Welcker and Clurman, 2008).

The overexpression of SKP2 E3 ligase leads to downregulation of CDK inhibitors in G1 – S transition (Kitagawa et al., 2009; Nakayama and Nakayama, 2006; Wang et al., 2011). However, mitotic and G1 UPS regulators APC/C-CDH1 and –CDC20 display a more complex phenotype. Both CDC20 and CDH1 can be either overexpressed or inactivated by mutation/ deletion in different tumour types (Bassermann et al., 2014; Benanti, 2012; Huang et al., 2001; Lee et al., 2015; Nakayama and Nakayama, 2006; Skaar and Pagano, 2009). These data illustrate the importance of individual cancer type analysis and specification down to a molecular and proteomic level.

## **1.7. The Cip1-interacting zinc-finger protein 1 (Ciz1) aids the initiation of DNA replication**

### **1.7.1. Ciz1 discovery and structure**

The Cip1-interacting zinc-finger protein 1 (Ciz1) was first discovered and cloned from human B cells with modified yeast two hybrid system using cyclin E – p21 (Cip1/Waf1) as a bait (Mitsui et al., 1999). Additionally, it was cloned and characterised independently for the second time in human medulloblastoma (Warder and Keherly, 2003). Both pieces of research provided evidence for tissue specific expression of Ciz1, namely in the kidney, testis, pancreas and brain; nonetheless, the protein is expressed abundantly in various tissues and cell types (Mitsui et al., 1999; Warder and Keherly, 2003).

Human Ciz1 shares 70 % identity with murine Ciz1 and much of the characterisation work has been performed in murine and human systems (Ainscough et al., 2007; Copeland et al., 2010; Copeland et al., 2015; Coverley et al., 2005; Mitsui et al., 1999; Warder and Keherly, 2003). Ciz1 is only conserved in vertebrates and mammalia and is composed of two glutamine-rich domains, three zinc finger domains, the acidic domain, and MH3 domain homologous to nuclear matrix protein Matrin 3 (Coverley et al., 2005; Mitsui et al., 1999; Warder and Keherly, 2003). Matrin 3 has matrin 3 type zinc finger (MH3 domain) that has been linked with pre-mRNA splicing and DNA binding (Ainscough et al., 2007). Ciz1 is conserved between human and mouse by more than 80% in its N - and C – terminal regions. However, the conservation between human, mouse, reptilian and bird is mainly conserved in N – terminal and zinc finger domains (Coverley et al., 2005). Ciz1 was shown to bind DNA directly via

consensus sequence. However, Ciz1 also associates with the nuclear matrix fraction and is not released from the chromatin fraction after DNase I digestion (Ainscough et al., 2007; Warder and Keherly, 2003). Nuclear matrix is a dynamic structure maintaining shape of the nucleus and the spatial organization of chromatin (Barboro et al., 2012; Wilson and Coverley, 2013). Nuclear matrix associates with the chromatin and its composition depends on cell type, cell cycle phase and level of differentiation. Proteins in nuclear matrix regulate DNA replication and repair, gene expression, RNA transport, cell signalling and differentiation, cell cycle regulation, apoptosis and carcinogenesis.

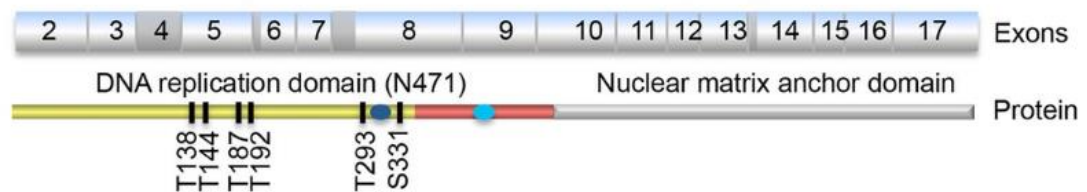


**Figure 1.6. Schematic of Ciz1 gene translated regions and protein structure.** Diagram shows murine Ciz1 translated exons (numbered), reported splicing events (exons 4, 6, 8, and 14) are shaded in grey (Dahmcke et al., 2008; Greaves et al., 2012; Higgins et al., 2012; Rahman et al., 2007). DNA replication domain (N471) is labelled in yellow and red (exons 2-9 and part of 10) (Copeland et al., 2010; Copeland et al., 2015), nuclear matrix binding domain in grey (exon 10-17) (Ainscough et al., 2007). CDK phosphorylation sites in replicatory domain of Ciz1 are labelled in black (T138, T144, T187, T192, T293, S331) (Copeland et al., 2015). Cyclin binding domains are labelled in blue ovals, dark blue binds cyclin E and cyclin A and is required for Ciz1 DNA replication initiation activity, light blue binds cyclin A (Copeland et al., 2015).

### 1.7.2. Ciz1 function in initiation of DNA replication

Ciz1 is a nuclear protein that co-localises with nascent DNA replication sites and associates with the nuclear matrix fraction (Ainscough et al., 2007; Coverley et al., 2005; Mitsui et al., 1999; Warder and Keherly, 2003). Ciz1 was found to bind detergent resistant nuclear fraction, that resists extraction with high salt and

nuclease treatments, consistent with the nuclear matrix association (Ainscough et al., 2007). Analysis of the domain structure of Ciz1 identified that the C terminal domain anchors Ciz1 to the nuclear matrix (Ainscough et al., 2007). The N terminal of Ciz1 was shown to promote DNA replication initiation, but cannot bind the nuclear matrix (Copeland et al., 2010; Coverley et al., 2005).

The working model suggests that Ciz1 promotes the initiation of DNA replication by directly binding to Cdc6 this way coming in close proximity to origins of replication and pre-replication complex (Copeland et al., 2015; Pauzaite et al., 2017). Ciz1 interacts with cyclin E in mid G1 phase and is displaced by cyclin A at the G1 – S transition. It was therefore proposed that Ciz1 contributes to timely and efficient delivery of cyclin – CDK2 complexes to the origins of replication (Copeland et al., 2015). The activity of Ciz1 is regulated by CDK mediated phosphorylation of Ciz1. The full length murine Ciz1 has 14 CDK phosphorylation sites, and the minimal N terminal fragment (N471), that maintains replication activity, has 6 CDK sites (Copeland et al., 2015). Three CDK sites have been shown to regulate Ciz1 DNA replication function (T144, T192 and T293). Their inhibitory activity is additive, with phosphomimetic mutations within Ciz1, preventing cyclin A - CDK2 binding and its replicative function. The model proposes that Ciz1 responds to increasing CDK activity by acquiring phosphorylation at multiple sites, preventing its DNA replication activity. It has been proposed that it contributes to prevention of DNA re-replication in high CDK activity contexts (Copeland et al., 2015).

### **1.7.3. Role of Ciz1 in tumourigenesis**

Ciz1 overexpression and alternative splicing is associated with common tumour types that include four most common cancers: breast, colorectal, prostate and lung cancers. There is an increasing amount of evidence on how alternative splicing or overexpression of Ciz1 can lead to cancer. For instance, the alternative splicing of exon 4 has been identified in Ewing tumour (Rahman et al., 2007; Rahman et al., 2010). Additionally, the alternative splicing at junction between exon 14 and 15 has been found in small cell and non-small cell lung cancers, and has been termed Ciz1 b-variant. Ciz1 b-variant has been identified as a potential biomarker for lung cancer and targeting of this cancer specific splice variant reduces tumour size in xenograft models (Coverley et al., 2017; Higgins et al., 2012). Finally, the alternative splicing in exons 8-12 has been identified as a signature in early stage solid tumours of breast and colon cancers (Swarts et al., 2018).

Although overexpression and differential splicing of Ciz1 is associated with tumorigenesis, the precise molecular mechanisms that mediate increased proliferation is yet to be determined. In addition, the signalling networks that regulate Ciz1 accumulation remain to be fully elucidated. There are distinct mechanisms proposed in specific cancers, but as yet there is no consensus for the mechanism whereby Ciz1 contributes to tumour growth. However, there is a common observation that Ciz1 is required for the proliferation of liver, prostate, gallbladder, colorectal, lung, and breast cancers (Den Hollander and Kumar, 2006; Den Hollander et al., 2006; Higgins et al., 2012; Lei et al., 2016; Liu et al., 2015; Liu et al., 2016; Wu et al., 2016; Yin et al., 2013; Zhang et al., 2015).

In breast cancers, Ciz1 protein has two distinct activities that promote proliferation. Ciz1 interacts with Dynein Light Chain 1 (DLC1), and facilitates sequestering of p21 from the nucleus, potentially increasing CDK2 activity that promotes cell cycle progression. In addition, Ciz1 enhances oestrogen receptor (ER) transactivation activity by aiding ER recruitment to the target genes, while being upregulated by ER signalling itself (Den Hollander and Kumar, 2006; Den Hollander et al., 2006). Therefore, overexpression of Ciz1 induces oestrogen hypersensitivity in breast cancers, that forms a positive feedback loop increasing Ciz1 expression (Den Hollander and Kumar, 2006; Den Hollander et al., 2006).

Additionally, Ciz1 overexpression has been shown to promote hepatocellular cancer (HCC) growth, migration and metastasis *in vitro* and *in vivo*. Ciz1 interacts with transcriptional factor YAP (Hippo-Yes-Associated Protein), and Ciz1 overexpression leads to increased interaction between YAP/TEAD and increased signalling of YAP/TAZ transcription factors. This transcriptional network promotes expression of cyclin E and connective tissue growth factor (CTGF) enhancing cell proliferation and tumour growth (Lei et al., 2016; Wu et al., 2016).

Further, Ciz1 overexpression has been correlated with prognosis of colorectal cancer (Wang et al., 2014; Yin et al., 2013). In colorectal tumours Ciz1 was present at higher levels in tumour when compared with adjacent normal tissues. In this context, Ciz1 levels were a prognostic marker for survival (Wang et al., 2014). The depletion of Ciz1, in Ciz1 overexpressing colon cancer cell line (RKO), leads to inhibition of cell proliferation and colony formation, and the increase in apoptosis.

Moreover, the level of Ciz1 has been shown to be elevated in gallbladder cancers (GBC) when compared with adjacent tissues (Zhang et al., 2015). Ciz1 interacts with the T cell factor (TCF4) and activates  $\beta$ -catenin/TCF expression of c-Myc, Snail, and Cyclin D, promoting tumour growth and migration *in vitro* and *in vivo*. In prostate carcinoma, Ciz1 levels directly correlate with the aggressiveness of the tumour (Liu et al., 2015). The depletion of Ciz1 reduces cell proliferation by inhibiting cells in G1 phase, decreases colony formation *in vitro* and tumour growth *in vivo*.

Finally, most recent data have identified Ciz1 as a contributor to angiogenesis. Overexpression of Ciz1 in vascular cells of lung squamous cell carcinoma (Zhou et al., 2018) and haemangioma of the tongue (Wang et al., 2018) has been correlated with cancer growth and migration.

In regards to hallmarks of cancer (Hanahan and Weinberg, 2011; Hanahan et al., 2000), Ciz1 contributes to a number of cancer driving characteristics. Ciz1 has been shown to increase cellular proliferation (Coverley et al., 2017; Den Hollander and Kumar, 2006; Den Hollander et al., 2006; Higgins et al., 2012; Lei et al., 2016; Liu et al., 2015; Wu et al., 2016; Yin et al., 2013; Zhang et al., 2015). Ciz1 may aid in evasion of tumour suppressors by either activating oncogene expression and activity (Den Hollander et al., 2006) or sequestering them from their targets (Den Hollander and Kumar, 2006; Mitsui et al., 1999). Ciz1 has been demonstrated to contribute to cancer cell migration *in vitro* and invasiveness *in vivo* (Liu et al., 2016; Wang et al., 2014; Wang et al., 2018; Yin et al., 2013; Zhang et al., 2015; Zhou et al., 2018). Ciz1 aids tumour vascularisation in case of lung squamous cell carcinoma (Zhou et al., 2018) and haemangioma of the tongue (Wang et al., 2018). The depletion of Ciz1 in

cancer cells increased apoptosis showing that Ciz1 overexpression may inhibit cancer cell death (Higgins et al., 2012; Wang et al., 2014; Yin et al., 2013).

In summary, either the deregulation of Ciz1 function by alternative splicing or overexpression of Ciz1 may contribute to deregulation of the cell cycle progression - a common early event in tumorigenesis (Coverley et al., 2017; Den Hollander and Kumar, 2006; Den Hollander et al., 2006; Higgins et al., 2012; Lei et al., 2016; Liu et al., 2016; Pauzaite et al., 2017; Rahman et al., 2007; Rahman et al., 2010; Swarts et al., 2018; Wang et al., 2014; Wu et al., 2016; Yin et al., 2013; Zhang et al., 2015; Zhou et al., 2018). Multiple pathways of Ciz1 contribution to tumorigenesis have been identified suggesting that Ciz1 aids deregulation of transcriptional pathways regulated by ER and YAP/TAZ transcription factors that are associated with tumorigenesis (Den Hollander and Kumar, 2006; Den Hollander et al., 2006; Lei et al., 2016). In addition, there is evidence that Ciz1 may also contribute to dysregulation of the cell cycle via p21 sequestration and activation of CDK2 activity.

#### **1.7.4. Association of Ciz1 with other disorders**

In addition to its association with promotion of tumorigenesis, Ciz1 has been implicated in neurodegenerative disorders (Khan et al., 2018; Xiao et al., 2016; Xiao et al., 2018), X chromosome inactivation (Ridings-Figueroa et al., 2017; Sunwoo et al., 2017; Yamada et al., 2015) and cardiac repair mechanisms (Bageghni et al., 2017).

The alternative splicing of exon 8 of Ciz1 has been linked to Alzheimer's disease (Dahmcke et al., 2008); however, as yet there is no further study of Ciz1 in Alzheimer's disease. This may be explained by the recent observation that Ciz1<sup>(-/-)</sup> mice expressed profound oxidative damage in the brain, which is known as one of

the main drivers of neurodegenerative disorders (Khan et al., 2018). In Ciz1 null murine model, loss of Ciz1 was associated with mild motor dysfunction, cell cycle abnormalities and genetic stress, but no severe effects on development or fertility have been observed (Xiao et al., 2016; Xiao et al., 2018). This may be explained by the change in protein expression in Ciz1<sup>(-/-)</sup> cells that potentially rescue the normal phenotype. However, more profound effect has been observed in aged Ciz1 null mice (Khan et al., 2018). The Ciz1<sup>(-/-)</sup> mice had motor and cognitive deficits, extensive DNA and oxidative damage, vascular impairment, inflammation, and cell death in brain tissues. The embryonic fibroblasts of Ciz1 null mice presented with hypersensitivity to  $\gamma$ -irradiation, high DNA damage, deregulation of cell cycle, and increased apoptosis (Khan et al., 2018). These data suggest that Ciz1 has a profound effect on a number of cell functions, and that any deviation from normal Ciz1 levels may lead to a range of pathologies.

In addition, Ciz1 has been shown to interact with X inactive specific transcript (Xist) RNA via its E repeats in order to facilitate its localisation on X chromosome and X chromosome silencing in female cells (Ridings-Figueroa et al., 2017; Sunwoo et al., 2017). The ablation of Ciz1 in female mice leads to abnormalities and enlargement of lymphoid tissues, such as spleen and lymph nodes, as well as hyper-proliferation of B and T lymphocytes (Ridings-Figueroa et al., 2017). This phenotype resembles non-Hodgkin follicular type lymphoma supporting the notion that normal levels of Ciz1 can act as a tumour suppressor (Nishibe et al., 2013). These data demonstrate that Ciz1 may contribute to various pathways in cell proliferation and development, and again emphasise that normal Ciz1 levels are important in orderly cell cycle and tissue homeostasis.

## 1.8. Aims

Normal Ciz1 levels play key role in orderly cell cycle progression, DNA replication initiation and prevention from re-replication, DNA repair, and normal organ and tissue development. Various pathways of Ciz1 involvement in the cell cycle and pathology development have been proposed. Majority of researchers agree that overexpression or depletion in Ciz1 leads to abnormalities. However, there is no data available on the regulation of Ciz1 levels in the cell so far. Therefore, this work aims to identify the molecular pathway or pathways that regulate Ciz1 levels.

- The phosphorylation of Ciz1 has been shown to contribute to Ciz1 activation and inactivation (Copeland et al., 2010; Copeland et al., 2015). However, the role for CDK mediated phosphorylation of Ciz1 in regulation of Ciz1 accumulation has not been determined. Therefore, a temporal analysis of Ciz1 phosphorylation will be performed and the role of CDK mediated phosphorylation for Ciz1 accumulation will be determined.
- Further, previous data have linked Ciz1 deregulation with cancer development. In this work, cancer cell lines are going to be screened for Ciz1 dependency and Ciz1 stability is going to be assessed in these cancer cell lines.
- Cancer cell lines that are capable in reducing Ciz1 levels after kinase inhibitors would have to possess functional ubiquitin – proteasome mediated protein degradation mechanism. Therefore, using an *in vitro* ubiquitylation assay, the putative E3 ligase(s) activity that may target Ciz1 for degradation will be identified.

- Finally, as CDK activity contributes to accumulation and upregulation of Ciz1 levels, phosphatase activity that removes CDK mediated phosphorylation of Ciz1 may contribute to Ciz1 down-regulation. Therefore, the phosphatases responsible for Ciz1 de-phosphorylation will be identified.

Knowing that normal Ciz1 levels are essential in normal cell cycle and development, it is important to determine the molecular pathway of Ciz1 level regulation. These data may provide new opportunities in cancer therapies, for instance, targeting kinases, E3 ligases or phosphatases that are responsible for Ciz1 levels. Additionally, establishing Ciz1 regulatory mechanism may provide some insight whether certain therapies would be effective in certain tumours.

# Chapter 2

## Materials and Methods

## **2. Materials and methods**

### **2.1. Tissue culture**

#### **2.1.1. Culturing transformed 3T3 fibroblasts**

NIH-3T3 and D-3T3 cells were grown in the Dulbecco's modified Eagles Media (D-MEM) (Gibco) medium with 10% foetal calf serum (FBS) (Labtech) and 1% penicillin-streptomycin-glutamine (Gibco) in 37 °C incubator with 4% CO<sub>2</sub>, and were dissociated for passaging with 0.1% of Trypsin in 1x Dulbecco's Phosphate-Buffered Saline (DPBS) (both Gibco) for 1 minute at 37 °C.

Mouse embryonic fibroblasts (3T3) were cultured at 50 – 70 % confluency and passaged every 24 – 48 hours. To produce synchronised 3T3 cells, contact inhibition and serum starvation was used. Cells were maintained at approximately 30 – 50 % in confluence, media changed and left for 48 hours to reach 100 % confluence. Media was then replaced and cells were cultured for a further 48 hours (Ainscough et al., 2007; Copeland et al., 2010; Copeland et al., 2015; Coverley et al., 2005). The cells were then released into fresh medium at lower density in order to stimulate cell cycle re-entry (Holley and Kiernan, 1968).

#### **2.1.2. Culturing cancer cell lines**

Cancer cell lines, PC3 (human prostate cancer cell line), SW480, and SW620 (primary and metastatic human colorectal carcinoma cell line, respectively) were kept at 50-70% confluency in D-MEM with 10% foetal calf serum (FBS) (Labtech) and 1% penicillin-streptomycin-glutamine (Gibco) (Hole, 2006; Ma et al., 2014; Tai et al., 2011). The breast cancer cell lines MCF7 and T47D were kept at 80-90% confluency in

RPMI 1640 medium (Gibco) with 10% foetal calf serum (FBS) (Labtech) and 1% penicillin-streptomycin-glutamine (Gibco) (Azizi et al., 2010). Where indicated, cancer cell lines were synchronised in S phase using a double thymidine protocol. Cells were treated for 24 hours with 2.5 mM thymidine (Sigma Aldrich), released for 8 hours into fresh media and a second thymidine incubation for 16 hours (Chen and Deng, 2018). To synchronise cells at the early M phase cells were treated with 2.5 mM thymidine for 24 hours, released into fresh medium for 3 hours, followed by a 10 hour nocodazole (100 ng/ml) treatment (Knehr et al., 1995).

## **2.2. Immunofluorescence**

To determine cell synchrony, cells were pulse labelled with ethynyl deoxyuridine (EdU) (Invitrogen) thymidine analogue and fluorescently labelled using the Click-it reaction adding Alexa Fluor 555 Azide. Click-iT™ EdU Cell Proliferation Assay Cocktail (Invitrogen) was used, which provides the tool for visualising cells that entered S phase and are actively replicating the DNA, and Click-IT reactions were performed according to manufacturer's instructions. The pulse label length was 30 minutes for quantitation by fluorescence microscopy and 1 hour for flow cytometry experiments (Section 2.11). Visualisation of DAPI (Vector Laboratories) and EdU labelled cells was performed using either fluorescence microscopy (Zeiss Scope.A1) or confocal microscopy (Zeiss LSM880).

## **2.3. RNA extraction and RT-qPCR**

Total RNA was purified from cells using PureLink® RNA Mini Kit (Ambion) according to manufacturer's instructions. The quantitation of transcript abundance was performed using ONE STEP qPCR kit (Invitrogen) using 25 ng of total RNA and

Taqman primer pairs (Thermo Fisher Scientific) for Ciz1 (Mm00503766, Hs00967155), cyclin E1 (Mm00432367, Hs01026536), cyclin E2 (Mm00438077, Hs00180319), cyclin A2 (Mm00438063, Hs00996788), Dbf4 (Mm01324087), Cdc7 (Mm00438122), GAPDH (Mm03302249, Hs02758991), and 18S (Mm03928990, Hs03003631) using a FX96 Touch™ Real-Time PCR Detection System (BIO-Rad). Program used: cDNA production at 50.0°C - 15min, DNA polymerase activation at 95.0°C - 2min, 40 cycles of 95.0°C - 15s, 60.0°C - 30s, and dissociation at 95°C – 60s.

#### **2.4. Drug treatments**

The asynchronous cell population, 50-70% in confluency, were treated with small molecule inhibitors (Table 2.1) 4 hours prior to cell harvesting. Synchronous cells were treated for 4 and 8 hours as indicated in the figures. The cells were synchronised with thymidine (2.5 mM) and nocodazole (100 ng/ml) at 50 % in confluency. The cells were treated with 50 µg/ml of cycloheximide for endogenous Ciz1 stability experiments, and with 100 µg/ml of cycloheximide for GFP – Ciz1 stability experiments for the time intervals indicated in the figures.

Drug	Target	IC50 in cell-free assays	Concentration	Provider
<b>Palbociclib (PD0332991) Isethionate</b>	CDK4 CDK6	11nM 16nM	10µM	Sigma Aldrich
<b>PHA-767491 dihydrochloride</b>	Cdc7	10nM	10µM	Sigma Aldrich
<b>XL-413 hydrochloride</b>	Cdc7	3.4nM	10µM	Selleckchem
<b>Roscovitine</b>	CDK2	0.7µM	30µM	Sigma Aldrich; Selleckchem
<b>CVT-313</b>	CDK2	0.5µM	10µM	Santa Cruz Biotechnology
<b>MG132</b>	Proteasomal Inhibitor	1.2µM	10µM	Sigma Aldrich
<b>Cyclohexamide</b>	Eukaryotic protein translation inhibitor		50 - 100 µg/ml (175 – 350 µM)	Sigma Aldrich
<b>Thymidine</b>	G1-S synchrony		2.5 mM	Sigma Aldrich
<b>Nocodazole</b>	M synchrony	0.21- 0.65µM	100 ng/mL (0.33 µM)	Sigma Aldrich

**Table 2.1. Summary of small molecule inhibitors used in this study.** The table indicates the drugs used in the experiments, their main targets, activity expressed as IC50, concentration used in the experiments, and supplier.

## 2.5. Protein harvesting and western blotting

Cells were scrape-harvested in 1 x PBS with 1 mM DTT, 1 mM PMSF protease inhibitor, and total phosphatase inhibitor cocktail Set V (Calbiochem). Samples were dissolved in 4X SDS loading dye with bromophenol blue, and resolved on 4 – 15% gradient gels (Bio-Rad) or hand poured 10 % SDS-PAGE gels using the Bio-Rad mini-protean system. 10 % gels were run at 150 V constant voltage and precast gels were run at 200 V constant voltage. Protein were transferred onto nitrocellulose membrane using semi-dry transfer (10 % ethanol, 0.3 M Tris-Base, 10 mM CAPS, 0.02

% SDS). Eight sheets of blotting paper, nitrocellulose membrane, and protein gel were soaked in transfer buffer. The nitrocellulose membrane and protein gel were sandwiched between four sheets of blotting paper, and run for 90 minutes at constant current of 1 mA per 1 cm<sup>2</sup>. The membrane was probed with specific antibodies (Table 2.2) in 1 x TBS, 1 % BSA buffer with 0.1 % Tween, 4 °C overnight.

Protein was quantified against its actin load control using Bio-Rad Image Lab Software. The band intensity on western blot was converted into relative number, the protein number was divided by actin number giving relative quantity. The control was then equalised to 1, every sample was divided by the relative control number showing relative variation from control.

<b>Antibody</b>	<b>Concentration</b>	<b>Provider</b>
<b>Ciz1-N471</b>	1:1000	Covalabs
<b>pCiz1-T293</b>	1:500	Covalabs
<b>pCiz1-S331</b>	1:250	Covalabs
<b>Cyclin E (HE12)</b>	1:500	Abcam
<b>Cyclin A (CY-1A)</b>	1:500	Sigma Aldrich
<b>Dbf4 ab116613</b>	1:500	Abcam
<b>MCM2 (BM28)</b>	1:500	BD Transduction Lab
<b>pMCM2-ser53 A300-756A</b>	1:500	Bioscience Bethyl Laboratories
<b>pMCM2-ser40/41 ab70371</b>	1:500	Abcam
<b>Actin (AC15)</b>	1:2500	Sigma Aldrich
<b>RB ab181616</b>	1:500	Abcam
<b>pRB-ser811 ab109399</b>	1:500	Abcam
<b>pRB-ser780 (D59B7)</b>	1:250	Cell Signalling Technologies
<b>RB (XZ55)</b>	1:250	BD Pharmingen
<b>Cdc7 (DCS-341)</b>	1:200	Invitrogen
<b>His 6x (4E3D10H2 / E3)</b>	1:2500	Invitrogen
<b>HRP anti-mouse secondary</b>	1:5000	Sigma Aldrich
<b>HRP anti-rabbit secondary</b>	1:5000	Sigma Aldrich
<b>HRP anti-goat secondary</b>	1:5000	Sigma Aldrich
<b>Alexafluor 680nm goat anti-rabbit IgG secondary</b>	1:5000	Invitrogen
<b>IR dye 800nm goat anti- mouse IgG secondary</b>	1:5000	Li-Cor

**Table 2.2. List of antibodies.** The table includes antibodies used in the experiments, their clone numbers, the concentration used, and supplier.

## **2.6. Nucleofection of cell lines**

Mouse fibroblasts were synchronised in G0 by serum starvation and contact inhibition. Synchronised cells were transfected at the time of release with anti-cyclin A2 siRNA (s63506), co-transfected with anti-cyclin E1 siRNA (s63521) and anti-cyclin E2 siRNA (s63524), or co-transfected using anti-Cdc7 siRNA (s63747) and anti-Dbf4 siRNA (s77567) (Ambion) in Cell Line Nucleofector® Solution R for NIH3T3 (Amaxa® Cell Line Nucleofector® Kit R; Lonza protocol). The cells were transfected with Nucleofector® program U-030 for NIH3T3. The cells were harvested at 20 hours after the transfection with Cyclin E1,2 and Cdc7-Dbf4 siRNA, and 24 hours after transfection with cyclin A2 siRNA. Asynchronous 3T3 cells 50-70% in confluence were transfected with 1 µg of plasmid for protein overexpression.

The thymidine synchronised human cancer cell lines were transfected with anti-Ciz1 siRNA (s24488) (Ambion) upon the release from thymidine block. The Cell Line Nucleofector® Solution V was used for PC3 (program T-013), SW480 (L-024), MCF7 (P-020), and T47D (X-005) (Amaxa® Cell Line Nucleofector® Kit V; Lonza protocol). The cells were harvested after 24 hours for protein and RNA analysis, and 24, 48, and 72 hours for flow cytometry analysis as indicated in the figures.

## **2.7. Site directed mutagenesis using whole plasmid mutagenesis**

Whole plasmid mutagenesis was used to perform alanine and aspartic acid substitutions in Ciz1 at CDK2 phosphorylation sites T144, T192, T293, and S331 of Ciz1 (Appendix 1). Mutagenesis was performed using 100 ng of pEGFPC1-Ciz1 and primers in Table 2.3.

The Pfu Ultra II (Stratagene) was used for PCR reaction using the following program: initial denature at 94°C – 5 min, followed by 30 cycles of 94 °C – 15 s, 55 °C – 30 s, 68 °C – 5 min, and the final extension at 72 °C for 7 min. The PCR product was treated with 1 µl of Dpn1 (NEB) for 1 hour at 37 °C, transformed into Top10 competent cells, and grown on LB plates with 50 µg/mL of Kanamycin. The single colonies were expanded, plasmid purified using GeneJET Plasmid Miniprep Kit (Thermo Fisher Scientific), and confirmed by sequencing (Eurofins).

CDK2 site	Point mutation	Primer	Sequence
T144	Alanine	Forward	CCACCCCAGATGGTCgCCCCAAATCTGCAGC
		Reverse	GCTGCAGATTTGGGGcGACCATCTGGGGTGG
	Aspartic acid	Forward	CCACCCCAGATGGTCgaCCCCAAATCTGCAGC
		Reverse	GCTGCAGATTTGGGtcGACCATCTGGGGTGG
T192	Alanine	Forward	CCCTCTTCCACCgCCCCAATCGCAAG
		Reverse	CTTGCGATTGGGGGcGGTGGGAAGAGGG
	Aspartic acid	Forward	CCCTCTTCCACCgaCCCCAATCGCAAG
		Reverse	CTTGCGATTGGGGtcGGTGGGAAGAGGG
T293	Alanine	Forward	CCAAAGCAGACACAGgCCCCGGATCGGCTGCCT
		Reverse	AGGCAGCCGATCCGGGGcCTGTGTCTGCTTTGG
	Aspartic acid	Forward	CCAAAGCAGACACAGgaCCCCGGATCGGCTGCCT
		Reverse	AGGCAGCCGATCCGGGtcCTGTGTCTGCTTTGG
S331	Alanine	Forward	GCACAGACACAGACCgTCCAGAGCACTTAGCG
		Reverse	CGCTAAGTGCTCTGGAGcGGTCTGTGTCTGTGC
	Aspartic acid	Forward	GCACAGACACAGACCgaTCCAGAGCACTTAGCG
		Reverse	CGCTAAGTGCTCTGGAtcGGTCTGTGTCTGTGC

**Table 2.3. Side directed mutagenesis primers.** Primers used in whole plasmid mutagenesis in order to introduce alanine or aspartic acid point mutations in CDK2 phosphorylation sites of Ciz1. The lower case indicates nucleotide substitutions introduced via whole plasmid mutagenesis leading to the change in amino acid.

## **2.8. Translational inhibition with Cycloheximide**

In order to determine endogenous Ciz1 stability, the inhibitor of translocation step in elongation - cycloheximide (Schneider-Poetsch et al., 2010) was used at concentration of 50 µg/ml in asynchronous 3T3 cells at 50-70% in confluence. The cells were incubated with cycloheximide 0 – 8 hours and harvested every 2 hours as indicated in the figures. For analysis of stability of the overexpressed exogenous GFP-Ciz1, GFP-Ciz1-AAAA/DDDD, and GFP-Ciz1-S331A/D, the cells were treated with 100 µg/ml of cycloheximide 8/ 24 hours after transfection with 1 µg of GFP plasmid. Cells were incubated with cycloheximide for 0 – 8 hours and harvested every 2 hours as indicated in the figures.

## **2.9. CRISPR-Cas9 protocol**

The guide sequences (Table 2.4) were introduced in Linearized GeneArt® CRISPR Nuclease Vector containing Cas9 and CD4 reporter according to manufacturer's instruction (Invitrogen). One Shot® TOP10 chemically competent *E. coli* were transformed with the plasmid and guide sequence verified by DNA sequencing using U6 Forward Primer (Eurofins). To produce the requisite mutations within the Ciz1 gene, single strand oligonucleotide directed mutagenesis was performed using approximately 100 base pair single stranded oligodeoxynucleotide (ssODN) sequences (Table 2.5) that contained point mutations (lower case) that were complementary to the region surrounding the PAM site to enable homologous recombination.

CDK site	Direction	Guide sequence
T192	Forward	5'-ACTCACCTTGCGATTGGGGGgtttt-3'
	Reverse	5'-CCCCAATCGCAAGGTGAGTcggtg-3'
T293	Forward	5'-ACCAAAGCAGACACAGACCCgtttt-3'
	Reverse	5'-GGGTCTGTGTCTGCTTTGGTcggtg-3'
S331	Forward	5'-AGACCCAGCCAAAGCTGCTGgtttt-3'
	Reverse	5'-CAGCAGCTTTGGCTGGGTCTcggtg-3'

**Table 2.4. The list of synthesised single strand guide sequences (Eurofins).** Approximately 20 nucleotide complementary sequences next to NGG PAM site were synthesised with -gtttt-3' and -cggtg-3' overhangs for ligation to Linearized GeneArt® CRISPR Nuclease Vector. The PAM sequence (NGG) is not involved in the guide sequence.

CDK site	Mutation	ssODN
T192	Alanine	CCACTCAGGGAGGAACACCCAGAAACAGGCCAGAgCCCCgCTg CCgCCgCCCCAATCGCAAGGTGAGTAGTGCTTTGAGTGGAACA GCTCAGCAGG
	Aspartate	CCACTCAGGGAGGAACACCCAGAAACAGGCCAGAgCCCCgaTg aCgaCgaCCCCAATCGCAAGGTGAGTAGTGCTTTGAGTGGAACA GCTCAGCAGG
T293	Alanine	GCAAGGGTCCAGCCTCAGACCCAGATGACAGCACCAAAGCAGA CACAGgCCCCGGATCGGCTGCCTGAGCCACCAGAAGTCCAAATG CTGC
	Aspartate	GCAAGGGTCCAGCCTCAGACCCAGATGACAGCACCAAAGCAGA CACAGgaCCCCGGATCGGCTGCCTGAGCCACCAGAAGTCCAAATG CTGC
S331	Alanine	GCAGATCCAGACCCAGCCAAAGCTGCTGAGGCAGGCACAGACA CAGACCgCTCCAGAGCACTTAGCGCCCCAGCAGGATCAGGTAGA GCCACAGGTAC
	Aspartate	GCAGATCCAGACCCAGCCAAAGCTGCTGAGGCAGGCACAGACA CAGACCgaTCCcGAGCACTTAGCGCCCCAGCAGGATCAGGTAGA GCCACAGGTAC

**Table 2.5. The list of single strand ODN sequences with point mutations.** Approximately 100 nucleotide single strand ODN sequences were synthesised (Eurofins). The nucleotide substitutions are labelled in lower case leading to changes in amino acid sequence when translated.

The Cas9 endonuclease cuts double strand genomic DNA and CRISPR-Cas9 system utilises single strand ODN sequence as a template for homology directed repair of the DNA break (Cong et al., 2013; Paquet et al., 2016; Prykhozhij et al., 2017). Site directed mutagenesis was performed using 1 µg of CRISPR-Cas9 expression vector and 2.5 µL of 50 µM ssODN. They were co-transfected into 3T3 embryonic mice fibroblast cells using 100 µl of transfection reagent Kit-R (Lonza), via electroporation using Nucleofector™ program U-030 (Lonza). The cells transfected with the GeneArt® CRISPR Nuclease (CD4 Reporter) Vector were enriched using Dynabeads® CD4 magnetic beads (Invitrogen), and were plated in 96 well plate using limited serial dilution method that each well contained single cell.

Wells containing single cell colonies were identified after two weeks, expanded and the genomic DNA was extracted using 50 µl of QuickExtract™ DNA Extraction Solution (Epicentre – Lucigen). The sequences of interest were PCR amplified using One Taq Quick-Load 2x Master Mix (New England BioLabs), 94°C- 30s, 30 cycles of 94°C - 30s, 68°C - 30s, 68°C - 60s, final extension of 68°C - 5min. The primers for PCR amplification were For1 CCCTGGATAAGAGGGTCCCCTC and Rev1 GGGTATGGCTAAAGTCACATTGAGACC for T192 region, and For2 GGAAGTGGTCAAAGGCCTCTGGG and Rev2 CTGGGCCTGCTTCTGTGACTGCGT for T293 and S331 regions. The restriction enzymes were selected using NEBcutter V2.0 ([www.neb.com](http://www.neb.com)) in order to determine the locations of cutting sites in amplified region and the specificity for point mutations. The sequences were screened by digestion with restriction enzymes that identified desired mutations Bsp1286I for T192A, Hpy99I for T192D, Eco0109I for T293A, PpuMI for T293D, BsrBI for S331A, and BsoBI for S331D (Table 2.6). Restriction digests were performed according to

manufacturer's instructions. Products were analysed by electrophoresis using 1% Agarose Gel, and clones that showed efficient digestion were inserted into the TOPO10 Blunt cloning vector (Zero Blunt® TOPO® PCR Cloning Kit – Thermo Fisher Scientific). DNA was sequenced from multiple clones using M13 For/Rev primers by Eurofins Scientific.

Site of the point mutation	Point mutation specific restriction enzyme	Fragment size (base pairs)	
		WT	
T192	Bsp1286I	WT	$59 + 513 = 572$
		Alanine	$59 + 271 + 242 = 572$
	Hpy99I	WT	572
		Aspartic acid	$338 + 234 = 572$
T293	Eco0109I	WT	$247 + 316 = 591$
		Alanine	$247 + 68 + 276 = 591$
	PpuMI	WT	591
		Aspartic acid	$318 + 273 = 591$
S331	BsrBI	WT	591
		Alanine	$430 + 161 = 591$
	BsoBI	WT	591
		Aspartic acid	$443 + 158 = 591$

**Table 2.6. The list of the restriction enzymes used for identification of specific point mutations introduced via CRISPR-Cas9 and HDR.** The table identifies the CDK phosphorylation sites of Ciz1 that were targeted by CRISPR-Cas9, point mutation specific restriction enzymes that were selected for identification of point mutations, and the fragment size that was expected in case of wild type or successful point mutation.

### 2.10. MTT assay

Cells were seeded in 96 well plates, 5000 cells/ well in 200 µl of D-MEM. After 24 hr, the D-MEM was replaced with 100 µl of phenol red free D-MEM (Gibco) with 10 % of MTT prepared in 1 x PBS from Vybrant™ MTT Cell Proliferation Assay Kit (Invitrogen). The cells were incubated for 4 hr at 37°C, then insoluble purple formazan was dissolved with 50 µl of DMSO (Sigma), and absorbance value for 0 hr

control was read at 540 nm using Tecan Absorbance Reader. The same procedure was repeated at indicated time points after Ciz1 depletions.

### **2.11. Flow cytometry**

Cells were pulse labelled with 10  $\mu$ M EdU (Invitrogen) for 1 hour prior to harvesting by trypsinisation. EdU labelled cell pellets were washed 3 x with 500  $\mu$ l 1 % BSA in 1 x PBS, fixed with 4 % PFA for 15 min, washed 3 x, permeabilised with 0.5 % Triton X-100 for 20 minutes, and washed 2 x with 1 % BSA. Cells were protected from light and incubated for 30 minutes on ice with Click-iT™ EdU Cell Proliferation Assay Cocktail (Invitrogen) containing Alexa Fluor 488 Azide. Cells were washed 2 x with 1 % BSA and 1 x with PBS, and stained with 100  $\mu$ g/ml of Propidium Iodide in 0.1 % Triton x-100 in PBS. Cells were analysed with Beckman Coulter CytoFLEX using FITC (525/40) and PE (585/42) channels.

### **2.12. Apoptosis assay**

One million cells, determined via counting using haemocytometer and bright field microscopy, were harvested and washed in 1 x PBS, and in 1 x annexin-binding buffer (FITC Annexin V/Dead Cell Apoptosis Kit, Thermo Fisher Scientific). The cells were incubated with 5  $\mu$ l of FITC annexin V in 195  $\mu$ l of binding buffer at the room temperature for 15 min. The samples were washed with binding buffer, and stained with 20  $\mu$ g/ml of propidium iodide (PI) in binding buffer. The samples were analysed with CytoFLEX using FITC (525/40) channel for apoptotic cells and PE (585/42) channel for necrotic cells.

## **2.13. E-Ciz1-His6x purification**

### **2.13.1. E-Ciz1-His6x cloning into pET-28a vector**

pGEX-6P-3 plasmid with E-Ciz1 insert was amplified with forward primer For 5' GGCCCCATGGgcATGCTGCAAAGAGCTTTGCTCC 3' containing a GGCC clamp, the NcoI restriction site (CCATGG) and 2 nucleotides to maintain frame; and reverse primer Rev 5' GGCCGTCGACGGTTTTGAGGCGTGTGAGCG 3' with Sall restriction endonuclease site (GTCGAC). The PCR reactions were performed using the following conditions: 10 s – 98°C, 30 cycles of 1 s – 98°C, 5 s – 69°C, 15 s – 72°C, and 1 min – 72°C, using Phusion Flash II DNA Polymerase 2 x Master Mix, 1 µM of each primer, and 1 µg of plasmid template. This produced a PCR product for ECiz1 flanked by restriction sites to aid insertion into the expression vector.

The PCR product was gel purified (GeneJET Gel Extraction Kit). The PCR product and pET-28a plasmid were both digested with 1 µl NcoI and Sall restriction enzymes (NEB), using 1 µg of PCR product or plasmid and 1 x Cut Smart buffer (NEB), and 1 µl of SAP (Shrimp Alkaline Phosphatase) in order to prevent re-ligation of linearized plasmid for 1 hour, at 37°C.

The digests were gel purified and used in ligation reaction (Rapid DNA Ligation Kit, Thermo Scientific) in 1:3 molar ratio using the following approach: Vector size was 5000 bp = 3,250,000 g/mol, thus  $5.07 \times 10^{-6}$  mol, and E-Ciz1 size was 2400 bp = 1,560,000 g/mol, thus  $5.13 \times 10^{-6}$  mol, therefore 1:3 volume ratio was used.

In order to confirm that the plasmid contained Ciz1 with His<sub>6</sub> tag on C terminal, the Top 10 (DE3) Competent Cells were transformed with 1 µl of ligation reaction, 30

minutes on ice, 40 s in 42°C, 5 minutes on ice, and expanded in 200 µl of SOC growth medium (0.5% Yeast Extract; 2% Tryptone; 10 mM NaCl; 2.5 mM KCl; 10 mM MgCl<sub>2</sub>; 10 mM MgSO<sub>4</sub>; 20 mM Glucose) for 1 hour in 37 °C incubator with shaking at 200 rpm. 50 µl of medium was plated on LB agar plates containing 30 ng/ml of Kanamycin. The individual colonies were picked cultured in 5 ml LB broth with 30 ng/ml of Kanamycin and incubated at 37 °C with shaking at 200 rpm overnight. The cultures were centrifuged 4000 rpm, and plasmids were purified from the pellets using GeneJET Plasmid Miniprep Kit (Thermo Fisher Scientific), and DNA sequencing was performed using T7 Forward and T7 Reverse primers (Eurofins).

### **2.13.2. E-Ciz1-His6x expression**

The Rosetta™ (DE3) Competent Cells were transformed with 1 µl of sequence verified pET-28s-ECiz1 plasmid by incubating for 30 minutes on ice, 40 seconds at 42 °C, and 5 minutes on ice. Subsequently, 200 µl of SOC growth medium (0.5% Yeast Extract; 2% Tryptone; 10 mM NaCl; 2.5 mM KCl; 10 mM MgCl<sub>2</sub>; 10 mM MgSO<sub>4</sub>; 20 mM Glucose) was added and cells were incubated for 1 hour in 37°C incubator with shaking at 200 rpm. The 50 µl of medium was then plated on LB agar plates containing 30 ng/ml of Kanamycin and 34 ng/ml of Chloramphenicol.

The colonies were then transferred into 5 ml LB broth with 30 ng/ml of Kanamycin and 34 ng/ml of Chloramphenicol, and incubated at 37 °C with shaking at 200 rpm overnight. The culture was then transferred into 75 ml LB broth with 30 ng/ml of Kanamycin and 34 ng/ml of Chloramphenicol, and incubated at 37 °C with shaking at 160 rpm overnight. The medium was then transferred to 750 ml of auto-induction medium (7.5 g Tryptone, 3.75 g Yeast extract, 1 mM MgSO<sub>4</sub>, 1 mM ZnSO<sub>4</sub> (Ciz1 is a

zinc finger protein), 1 x 5052, 1 x NPS, 1 x trace metals, 30 ng/ml of Kanamycin and 34 ng/ml of Chloramphenicol). 20 x NPS was composed of 0.5 M  $(\text{NH}_4)_2\text{SO}_4$ , 1 M  $\text{KH}_2\text{PO}_4$ , 1 M  $\text{Na}_2\text{HPO}_4$ . 50 x 5052 had 0.5% glycerol, 0.05% glucose, 0.2% alpha-lactose w/v, 1000 x trace metals (0.1 M  $\text{FeCl}_3 \cdot 6\text{H}_2\text{O}$ , 1 M  $\text{CaCl}_2$ , 1 M  $\text{MnCl}_2 \cdot 4\text{H}_2\text{O}$ , 1 M  $\text{ZnSO}_4 \cdot 7\text{H}_2\text{O}$ , 0.2 M  $\text{CoCl}_2 \cdot 6\text{H}_2\text{O}$ , 0.1 M  $\text{CuCl}_2 \cdot 2\text{H}_2\text{O}$ , 0.2 M  $\text{NiCl}_2 \cdot 6\text{H}_2\text{O}$ , 0.1 M  $\text{Na}_2\text{MoO}_4 \cdot 2\text{H}_2\text{O}$ , 0.1 M  $\text{Na}_2\text{SeO}_3 \cdot 5\text{H}_2\text{O}$ , 0.1 M  $\text{H}_3\text{BO}_3$ ). The culture was incubated at 20 °C, with shaking at 120 rpm, overnight.

### **2.13.3. E-Ciz1-His6x purification with Ni-NTA resin**

The culture was centrifuged at 4500 rpm for 15 minutes using JLA 8.1000 rotor (Beckman Coulter Avanti J-26 XP centrifuge). The bacterial cell pellet was resuspended in 10 ml of Ni<sub>2</sub>-NTA Buffer A (50 mM  $\text{NaH}_2\text{PO}_4$ , 1 M  $\text{NaCl}$ , 10 mM Imidazole, protease inhibitors (cOmplete, EDTA-free, Roche), 1mM PMSF), sonicated 4 x 15 seconds at 25 - 30 microns peak to peak using probe of 1 cm in diameter in an ice slurry to control temperature of the cells. The lysate was centrifuged at 20,000 rpm for 30 min using JA 25.50 rotor, and the supernatant was incubated with 250  $\mu\text{l}$  of Ni<sub>2</sub>-NTA beads (Amintra Protein Purification Tools) for 30 min at 4 °C. The supernatant was removed and beads were resuspended and incubated for 1 hour at 4 °C in 5 ml of Buffer A with 5 mM of ATP in order to unfold the protein and remove Hsp70 (Clare and Saibil, 2013). The beads were applied to gravity column (Thermo Scientific) and washed with 4 ml of Buffer A, 4 ml of 95 % of Buffer A + 5 % of Buffer B (50 mM  $\text{NaH}_2\text{PO}_4$ , 1 M  $\text{NaCl}$ , 250 mM Imidazole, protease inhibitors, 1mM PMSF), and protein was eluted with 2 ml of Buffer B.

#### **2.13.4. E-Ciz1-His<sub>6</sub>x purification via anion exchange chromatography**

The eluted protein was then diluted down to 50 mM salt concentration with no salt buffer (50 mM NaH<sub>2</sub>PO<sub>4</sub>, 10 mM imidazole, protease inhibitors, 1 mM PMSF, 1mM DTT) in preparation for purification by FPLC using 1 ml Resource Q column (GE Healthcare Life Sciences). The protein was purified using an increasing salt gradient from low salt buffer (50 mM Tris-HCl pH 8.0, 1 mM EDTA, 50 mM KCl, 5 % glycerol, 1 mM DTT, 0.1 mM PMSF) to a high salt buffer (50 mM Tris-HCl pH 8.0, 1 mM EDTA, 1 M KCl, 5% glycerol, 1 mM DTT, 0.1 mM PMSF) using a linear gradient of 20 column volumes. Fractions were collected every 0.5 ml, flow rate 1 ml/min, 4°C, AKTA purifier (GE Healthcare Life Sciences). The fractions were analysed by SDS-PAGE and western blotting with Ciz1-N471 (Covalabs) and anti-His<sub>6</sub>x (Invitrogen, MA1-135) antibodies and snap frozen in 20 µl beads in liquid nitrogen. The concentration of the protein was determined using BCA assay (Pierce™ BCA Protein Assay Kit, Thermo Fisher Scientific) at 562 nm according to manufacturer's instructions.

#### **2.14. N471-Ciz1 purification**

The pGEX-6P-3-Ciz1-N471 plasmid was confirmed by sequencing with pGEX forward and reverse primers and it was transformed into BL-21 *E. coli* competent cells. The cells were grown on LB agar containing 100 µg/ml of Ampicillin and a single colony picked and cultured in LB medium (10 hours in 5 ml then 24 hours in 75 ml) for inoculation of ZY media for protein expression. The culture was centrifuged at 4500 rpm for 15 minutes and the pellet was resuspended in wash buffer HBS (50mM HEPES pH7.8, 135 mM NaCl, 3 mM EDTA, 1mM DTT, protease inhibitors (Roche) and 1mM PMSF). The suspension was sonicated, centrifuged (section 2.13.2), and the

lysate was bound to the Glutathione Sepharose 4B beads (GE life sciences) for 1 hour at 4 °C. The beads were washed with 10 ml of HBS buffer for 5 times, and with 5 ml of 3C cleavage buffer (50 mM Tris HCl pH 7.0, 150 mM NaCl, 2 mM DTT) for 3 times. The beads were incubated with 10 µl of 3C prescission protease (Sigma Aldrich) in 1.5 ml of 3C cleavage buffer over night at 4 °C with rotation. After digestion, the GST tag remains bound to the Glutathione beads and cleaved Ciz1-N471 protein was eluted from a microcentrifuge filter column. The purity was evaluated using SDS-PAGE and coomassie staining. Finally, the concentration was determined by the BCA assay. The protein beads were snap frozen in liquid nitrogen.

## **2.15. Biochemical identification of E3 ligases and phosphatases**

### **2.15.1. *In vitro* ubiquitylation assay**

*In vitro* ubiquitylation assays were performed using 200 ng of Ciz1 protein, 0.1 µg E1, 0.04 µg 9 x E2 (UbcH2, His-UbcH3, UbcH5a, UbcH5b, UbcH5c, His-UbcH6, UbcH7, UbcH8, His-UbcH10) (a gift from Dr Jason Parsons, University of Liverpool), and recombinant His<sub>6x</sub>-ubiquitin. Reactions were performed using 1 x ubiquitylation buffer (25 mM TrisHCl pH 8.0, 5 mM MgCl<sub>2</sub>, 200 µM CaCl<sub>2</sub>, 1 mM DTT, 10 µM MG132), 4 mM ATP, 5 µg Ubiquitin wild type (Ub WT) dissolved in JPDB buffer (50 mM TrisHCl pH 8.0, 50 mM NaCl, 1 mM EDTA, 10% Glycerol). The E3 activity was mediated using 0 - 8 µg HeLa whole cell extract (WCE), Phosphocellulose column flow through (P150), or Phosphocellulose column binding fraction (P1000). The 15 µl reactions were incubated for 1 hour at 37 °C with shaking at 800 rpm. The proteins were separated on 10% SDS-PAGE gel, TGS buffer, 2 hours, 125 V (Thermo Fisher), transferred onto PVDF membrane (1 x TG buffer (2.5 mM Tris, 19.2 mM glycine, pH

8.3), 20% methanol), 1 hour, 20 V, and blocked in 50% Odyssey blocking buffer in PBS. The membrane was probed with Ciz1-N471 1:1000 (Covalabs) and His6x 1:1000 (Invitrogen, MA1-135) in Odyssey blocking buffer in PBS with 0.1% Tween. Active fractions were determined by analysis of western blotting showing Ciz1 polyubiquitylation levels. Where Ciz1 showed higher molecular weight species, fractions were further purified by sequential chromatography steps.

### **2.15.2. In vitro phosphatase assay**

The recombinant Ciz1-N471 protein was *in vitro* phosphorylated using the recombinant cyclin A – CDK2 added in 1:10 ratio (2  $\mu$ M of Ciz1 – N471 and 0.2  $\mu$ M of cyclin A – CDK2). The phosphorylation reaction (50mM HEPES pH = 7.8, 20 mM  $MgCl_2$ , 10 mM ATP, 1 mM DTT) was incubated for 30 min at 37 °C, 500 rpm.

The 200 ng of the phosphorylated pCiz1-N471 was added to reactions in phosphatase buffer (25 mM TrisHCl pH 8.0, 5 mM  $MgCl_2$ , 200  $\mu$ M  $CaCl_2$ , 1 mM DTT, 10  $\mu$ M MG132, 4 mM ATP, 90  $\mu$ M Roscovitine) with 0-8  $\mu$ g HeLa whole cell extract (WCE), Phosphocellulose column flow through (P150), or Phosphocellulose column binding fraction (P1000) (as in section 2.15.1). Active fractions were determined by analysis of phospho-T293-Ciz1 levels. Where phospho-T293 Ciz1 levels were reduced, fractions were further purified by sequential chromatography steps.

### **2.15.3. Ion exchange column (20 ml)**

The 50 ml P1000 fraction for E3 ligase identification and P150 fraction for phosphatase assay of 1 M KCl were dialysed in 4 litres of low salt buffer (50 mM KCl, 50 mM TrisHCl, 1 mM EDTA, 5% Glycerol, 1 mM DTT) overnight at 4°C. The fraction was run through Mono S column (SP Sepharose HP) (E3 ligase assay) of 20 ml bed volume (poured by Jason Parsons), and Mono Q (phosphatase assay) flow rate 1 ml/min, 80 fractions of 4 ml, salt gradient from 50 mM KCl to 1 M KCl. The 500 µl of each even fraction was concentrated down to 50 µl (20 min, 14,000 g) and 2 µl of each concentrated fraction was used in *in vitro* ubiquitylation/phosphatase assay and analysed by western blotting as described before. The rest of Mono S/Q fractions were stored in -80°C.

### **2.15.4. Size exclusion chromatography (SEC)**

The 3 x 4 ml active fractions (Mono S – ubiquitylation, Mono Q – phosphatase) were thawed, protein fractions were pulled and concentrated down to 500 µl at 10,000 rpm. They were run through Superdex 200 10/300 GL 20ml size exclusion chromatography column (GE Healthcare Life Sciences) using SEC buffer (50 mM TrisHCl pH 8.0, 50 mM KCl, 1 mM EDTA, 5% Glycerol, 1 mM DTT, 0.1 mM PMSF), 0.5 ml/min flow rate, 40 x 0.5 ml fractions. The activity of even fractions (2 µl) was tested in *in vitro* ubiquitylation/phosphatase assay and western blotting, and the rest was stored in -80°C.

### **2.15.5. Analytical ion exchange column (1 ml)**

The 500  $\mu$ l fractions were pulled together and diluted 1:2 with no salt buffer (50 mM TrisHCl pH 8.0, 1 mM EDTA, 5% Glycerol, 1 mM DTT, 0.1 mM PMSF) in order to achieve 50 mM salt concentration. The 5 ml of sample was loaded onto 1 ml Mono S 5/50 GL (E3 ligase identification experiments) and Mono Q 5/50 GL (phosphatase identification assays) (GE Healthcare Life Sciences), and eluted using 50 mM to 1 M salt gradient over 40 x 0.5 fractions, 0.3 ml/min flow rate. Each fraction (2  $\mu$ l) was tested in ubiquitylation/phosphatase reaction, and two active fractions expressing ubiquitylation activity (after MonoS) and phosphatase activity (after MonoQ) were selected for Mass Spec analysis.

## **2.16. Methods for LC-MS analysis of FPLC fractions**

### **2.16.1. Sample preparation**

10  $\mu$ l of Strataclean bead slurry was added to each sample and vortexed for 1 min. A low speed 2,000 x g centrifugation for 2 min pelleted the beads and the protein-depleted supernatant was carefully removed. The beads were re-suspended in 1 mL of wash buffer (25 mM ammonium bicarbonate (ambic)) and the centrifugation step repeated. The wash step was repeated twice and the beads then re-suspended in 80  $\mu$ l of 25 mM ambic. 5  $\mu$ l of 1 % (w/v) Rapigest (Waters) in 25 mM ambic was added and samples heated at 80 °C for 10 minutes. DTT (5  $\mu$ l of 9.2 mg/mL in 25 mM ambic) was added and samples heated at 60 °C for 10 min. Iodoacetamide (5  $\mu$ l of 33 mg/mL in 25 mM ambic) was added and the samples incubated in the dark at RT for 30 min. 5  $\mu$ l of 0.2 mg/mL trypsin in 50 mM acetic acid added and samples incubated at 37°C overnight.

The following day the digests were acidified by the addition of 0.5  $\mu\text{l}$  of TFA and incubated for 45 min at 37 °C (to hydrolyse Rapigest). Samples were centrifuged at 17,200 x g for 30 min and the clarified digests transferred to total recovery vials for LC-MS analysis.

### **2.16.2. LC-MS/MS analysis**

Data-dependent LC-MSMS analyses were conducted on a QExactive quadrupole-Orbitrap mass spectrometer coupled to a Dionex Ultimate 3000 RSLC nano-liquid chromatograph (Hemel Hempstead, UK). Sample digest (2-6  $\mu\text{l}$ ) was loaded onto a trapping column (Acclaim PepMap 100 C18, 75  $\mu\text{m}$  x 2 cm, 3  $\mu\text{m}$  packing material, 100 Å) using a loading buffer of 0.1% (v/v) TFA, 2% (v/v) acetonitrile in water for 7 min at a flow rate of 9  $\mu\text{L}/\text{min}$ . The trapping column was then set in-line with an analytical column (EASY-Spray PepMap RSLC C18, 75  $\mu\text{m}$  x 50 cm, 2  $\mu\text{m}$  packing material, 100 Å) and the peptides eluted using a linear gradient of 96.2% A (0.1% [v/v] formic acid): 3.8% B (0.1% formic acid in water: acetonitrile [80:20] [v/v]) to 50% A: 50% B over 30 min at a flow rate of 300 nL/ min, followed by washing at 1% A: 99% B for 5 min and re-equilibration of the column to starting conditions. The column was maintained at 40°C, and the effluent introduced directly into the integrated nano-electrospray ionisation source operating in positive ion mode. The mass spectrometer was operated in DDA mode with survey scans between m/z 300-2000 acquired at a mass resolution of 70,000 (FWHM) at m/z 200. The maximum injection time was 250 ms, and the automatic gain control was set to 1e6. The 10 most intense precursor ions with charges states of between 2+ and 5+ were selected for MS/MS with an isolation window of 2 m/z units. The maximum injection time

was 10 ms, and the automatic gain control was set to 1e5. Fragmentation of the peptides was by higher-energy collisional dissociation using normalised collision energy of 30%. Dynamic exclusion of m/z values to prevent repeated fragmentation of the same peptide was used with an exclusion time of 20 sec.

### **2.17. Statistical analysis**

The significance of the results was measured by either the paired sample two-tailed t-test using Microsoft Excel 2010 or the one-way post-hoc Tukey ANOVA using IBM SPSS Statistics 24 as indicated in each figure. The results were considered statistically significant when p-value was  $\leq 0.05$ . The significance value  $p \leq 0.05$  was labelled as \* in the graphs and tables,  $p \leq 0.01$  as \*\*, and  $p \leq 0.005$  as \*\*\*. Each figure presents at least 3 experimental repeats and graphs show the mean  $\pm$  Standard Deviation (S.D.).

### **2.18. Immunoprecipitation experiments**

NIH-3T3 cells were transfected by electroporation with 1  $\mu$ g of His-ubiquitin and HA-ubiquitin plasmids (present from Dr Jason Parsons). For His6-Ubiquitin and Ni<sup>2+</sup>-NTA immobilisation (IMAC), cells were scraped harvested in lysis/wash buffer (1 x PBS pH 7.4 (Sigma Aldrich), 1 x complete protease inhibitors, 100 mM NaCl, and 10 mM imidazole), 24 hours after transfection +/- 4 hour treatment with 10  $\mu$ M MG132. Sample was incubated with 0.5 % Triton X-100 for 5 min on ice and centrifuged at 10,000 rpm for 5 min. 30  $\mu$ l of Ni<sup>2+</sup>-NTA resin was washed with 500  $\mu$ l of wash buffer for 3 times in the spin column, column was closed, the supernatant (soluble protein) made up to 400  $\mu$ l with wash buffer was added to the column, and incubated at 4 °C with rotation for 1 hour. The resin was washed with 500  $\mu$ l of wash buffer by centrifuging at 1,000 g for 1 min for 4 times. The columns were closed, 60  $\mu$ l of 4 x

SDS loading buffer was added to the beads, boiled at 95 °C for 10 minutes, column plug removed and bound fraction collected. The Ciz1-Ubiquitin was analysed by western blotting using Ciz1 antibody. For HA-Ubiquitin Anti-HA Agarose (Thermo Scientific) immunoprecipitation, cells were scraped harvested in lysis/ wash buffer (1 x PBS, 1 x complete protease inhibitors, 1 mM DTT), and protein containing extract was prepared with Triton X-100. 20 µl of Anti-HA Agarose was washed 3 times, and cell extracts were incubated with agarose for 1 hour. Sample was washed 3 times with wash buffer, boiled in 60 µl of 4 x SDS loading buffer and collected (bound fraction).

# **Chapter 3**

## **Identification of the networks that regulate Ciz1 accumulation during G1 phase**

### **3.1. Evaluation of Ciz1 expression levels in synchronised populations of 3T3 cells**

Ciz1 abundance has been shown to be important in cell cycle progression (Coverley et al., 2005), as well as in tumourigenesis, radiation sensitivity, X chromosome silencing, and maintenance of epigenetics (Den Hollander et al., 2006; Higgins et al., 2012; Pauzaite et al., 2017; Stewart et al., 2019; Sunwoo et al., 2017; Yamada et al., 2015; Yin et al., 2013; Zhou et al., 2018). In order to investigate the mechanisms that regulate Ciz1 protein accumulation and stability, a murine model was used. With respect to cell cycle, regulation and functional analysis of Ciz1 in the 3T3 murine embryonic fibroblasts have been most extensively studied (Ainscough et al., 2007; Copeland et al., 2010; Copeland et al., 2015; Coverley et al., 2002; Coverley et al., 2005; Ridings-Figueroa et al., 2017; Stewart et al., 2019). This system enables cell cycle synchronisation by contact inhibition and serum starvation (Holley and Kiernan, 1968; Zetterberg and Larsson, 1985). The use of contact inhibition enables dissection of events from G1 to S phase without perturbing the system with chemical cell cycle inhibitors that can induce stress responses (Copeland et al., 2010; Coverley et al., 2002; Coverley et al., 2005). The initial aim was to use synchronised 3T3 cells to determine whether Ciz1 expression is cell cycle regulated.

In order to analyse the cells in G1 – S transition, 3T3 cells were synchronised in G0 phase and released in fresh medium. Progression through cell cycle was monitored by EdU, a thymidine analogue that enables detection of nascent DNA using CLICK-IT chemistry (Figure 3.1). The EdU positive cells were quantified by determination of all nuclei (DAPI, blue) and the percentage of S phase cells (EdU, red) (Figure 3.1: B). To confirm the EdU profile, the flow cytometry analysis of cells pulse labelled with EdU

and counterstained with propidium iodide (PI) was performed (Figure 3.1: C). Figure 3.1 shows that cells enter S phase at around 14-16 hours after release from G0 phase with 40-45 % of cells being in S phase at 24 hours after release.

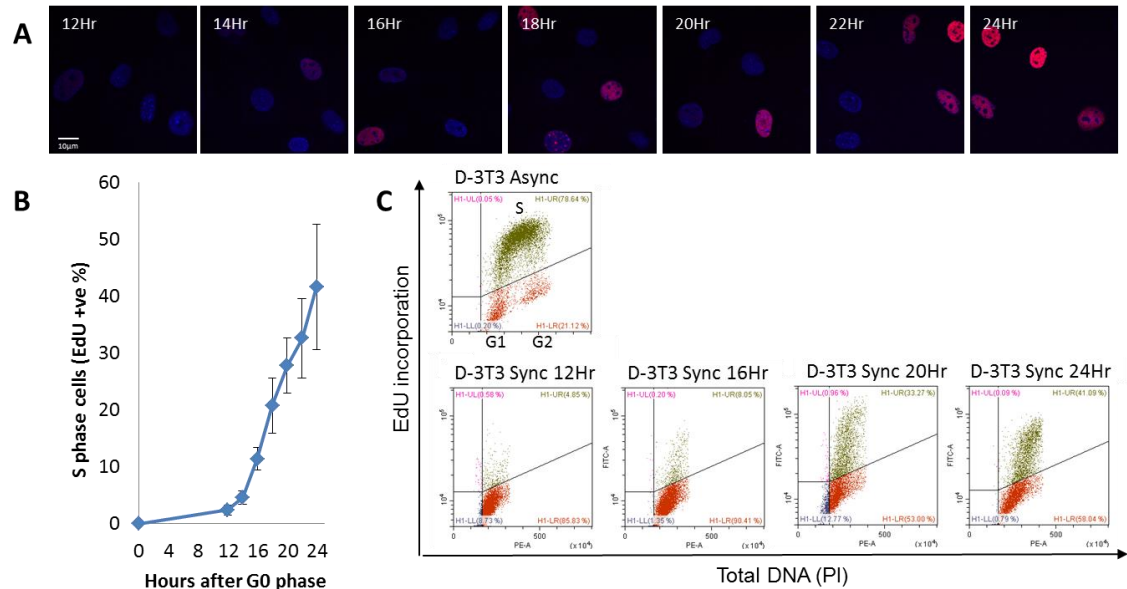


**Figure 3.1. Cell cycle synchronisation of 3T3 cells from G1 into S phase. A)** Contact inhibited 3T3 cells were released from quiescence and followed into S phase by EdU incorporation. Representative confocal microscope images show merged EdU (555nm) and DAPI (405nm) fields between 12 - 24 hour after release from G0 phase. Scale bar indicates 10 μm. **B)** Quantitation of EdU positive cells (S phase) in relation to total DAPI stained nuclei (%). Error bars represent mean ± S.D., n=6. **C)** Multiparameter flow cytometry dot plot showing EdU intensity (y-axis) vs total DNA (x-axis) for asynchronous cell and synchronous cells 12, 16, 20 and 24 hours after release from quiescence. G1 (2N), S phase, and G2 (4N) populations are indicated on the asynchronous dot plot.

### 3.2. Defining the restriction point in post-quiescent 3T3 cells

G1 phase can be separated into 2 distinct stages. In early G1 phase cells respond to mitogen stimulation to grow and in late G1 phase cells no longer require mitogenic stimulation to progress through the cell cycle. The point in G1 where cells no longer require mitogens is referred to as the restriction point (RP) (Pardee, 1974; Zetterberg and Larsson, 1985). Recent evidence suggests that mammalian cells have two

possible exit-to-quiescence points that depend on residual CDK2 activity. If the cells have low p21 and moderate CDK2 activity upon mitotic exit, they enter the G1 phase and pass through the cell cycle independently from mitogenic signalling (Spencer et al., 2013). However, if the cells have high p21 levels, they enter a G0-like state with low CDK2 activity and hypo-phosphorylated Rb. These cells become dependent on mitogenic signalling and the restriction point that is more commonly described.

Quiescent 3T3 murine fibroblasts re-enter the cell cycle with low CDK2 activity and hypo-phosphorylated Rb (Barr et al., 2017; Heldt et al., 2018b; Moser et al., 2018). In order to identify the timing of the restriction point, cells were released from G0 into serum supplemented medium (Figure 3.2). 30 minutes prior to each time point, cells were placed in serum free medium containing EdU. This revealed that the cells became serum independent for replication after 14-15 hours after G0 release, which is consistent with other studies (Coverley et al., 2002).

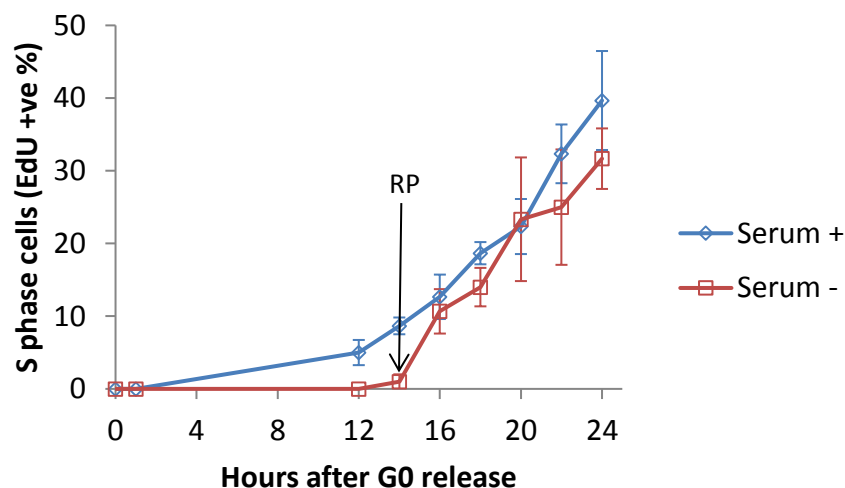


**Figure 3.2. Determination of the restriction point.** The 3T3 cells were inhibited in G0 phase by contact inhibition and nutrient starvation, the cells were released into fresh medium with serum (blue line) and then placed into serum free medium 30 minutes prior each time point (red line). The cells were pulse labelled with EdU and EdU positive nuclei quantified (%). The arrow indicates the approximate timing of the restriction point (RP). Error bars represent mean  $\pm$  S.D., n=3.

### 3.3. Ciz1 protein expression and mRNA transcription

Ciz1 promotes DNA replication initiation *in vitro* and *in vivo* (Copeland et al., 2010; Copeland et al., 2015; Coverley et al., 2005). The DNA replication function is dependent on Ciz1 protein levels and is regulated by CDK mediated phosphorylation (Copeland et al., 2015). Ciz1 is phosphorylated at multiple residues and phospho-specific antibodies are available for 2 CDK sites (consensus motif S/TPXK/R), phospho-threonine (pT293, TPNR) and phospho-serine (pS331, SPEH). To determine the kinetics of Ciz1 expression and site specific phosphorylation, a synchronised population of cells was monitored from G0 to S phase (Figure 3.3: A).

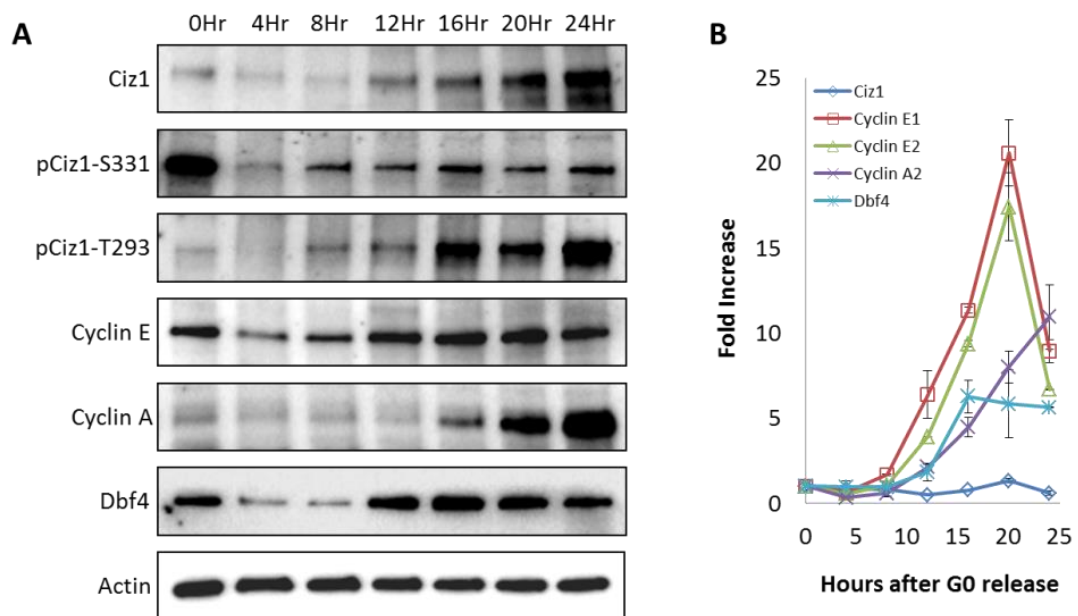


**Figure 3.3. Ciz1 protein accumulation and transcription.** **A)** The 3T3 cells were synchronised, samples were analysed at indicated time points after release from quiescence (0 – 24 hours) and probed with Ciz1, pCiz1-S331, pCiz1-T293, Cyclin E, Cyclin A, Dbf4 specific antibodies. Actin was used as a loading control. **B)** Total RNA was extracted and quantified by RT-qPCR using gene specific primers (Section 2.3). The mRNA levels are shown relative to GAPDH mRNA, and transcript levels standardised to those of quiescent cells in G0 (0 hour). Each time point represents 3 experimental repeats with 3 technical repeats in each, showing mean  $\pm$  S.D.

Western blot analysis revealed that Ciz1 protein accumulated during G1 and increased into S phase. Ciz1 accumulation correlated with cyclin A accumulation and phosphorylation at T293 from 16 hours, suggesting that Ciz1 phosphorylation could potentially promote Ciz1 accumulation. The increase in Ciz1 levels correlated with cyclin A expression and T293 phosphorylation, and its phosphorylation on S331 site resembled cyclin E expression. These findings were consistent with the temporal separation of CDK2 activation by cyclin E and then cyclin A (Coverley et al., 2002). Ciz1 protein expression is temporally regulated in G1 phase and protein accumulation correlates with known G1 – S regulators Cyclin E, Cyclin A, and Dbf4 (lanes 4-6). Cyclin E, Cyclin A, and Dbf4 are transcriptionally regulated by the E2F-Rb pathway. Next the transcript levels for E2F regulated transcripts and Ciz1 were compared (Figure 3.3: B). This RT-qPCR analysis of mRNA levels from G0 to S phase (0-24 hours) revealed that cyclin E1 and E2 transcription peaked up to 15-20 fold, cyclin A2 10-fold, Dbf4 increased 6-fold, and Ciz1 increased 1.3-fold. The relatively small change in Ciz1 transcript levels suggests that post-translational regulation may contribute to Ciz1 accumulation.

#### **3.4. Ciz1 is destabilised by kinase inhibition in asynchronous 3T3 population**

To assess the role of CDK activity for the accumulation of Ciz1 levels in G1 phase, small molecule kinase inhibitors were used. Initially, asynchronous 3T3 cells were treated for 4 hours with CDK4/6i – PD-0332991 (palbociclib), DDKi - PHA-767491, and CDK2i – Roscovitine.

The IC<sub>50</sub> of CDK4/6 inhibitor PD-0332991 is 11 nM for CDK4 and 16 nM for CDK6 in *in vitro* kinase assays (Fry et al., 2004). The IC<sub>50</sub> of DDK inhibitor PHA-767491 is 10

nM for Cdc7 in cell free and on average 3.17  $\mu$ M in 61 cell lines (Montagnoli et al., 2008; Natoni et al., 2011; Sasi et al., 2014). Further, the IC<sub>50</sub> of CDK2 inhibitor – Roscovitine is 0.7  $\mu$ M in cell free assays (Ali et al., 2009). Therefore, the concentrations of kinase inhibitors were selected and tested accordingly, choosing the concentration range providing the effect in molecular level, but leaving the cells phenotypically unchanged and viable.

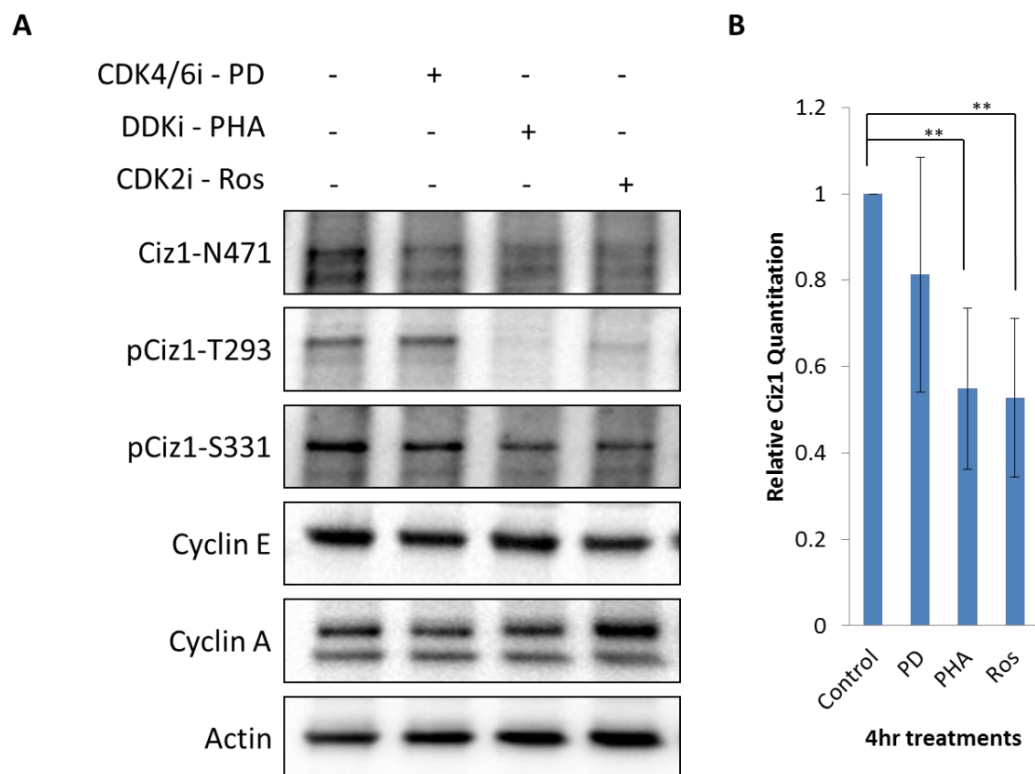


**Figure 3.4. Ciz1 levels are reduced by inhibition of CDK2 (Roscovitine) and DDK (PHA-767491).** **A)** Asynchronous population of 3T3 were treated with kinase inhibitors 10  $\mu$ M CDK4/6i – PD-0332991, 10  $\mu$ M DDKi - PHA-767491, and 30  $\mu$ M CDK2i – Roscovitine for 4 hours. Immunoblots were probed with Ciz1, pCiz1-T293, pCiz1-S331, Cyclin E, Cyclin A, and Actin antibodies. **B)** The quantitation of Ciz1 protein in relation to Actin loads, presented as the mean  $\pm$  S.D. The significant difference between control and treatment was observed after DDKi - PHA-767491 and CDK2i – Roscovitine treatment (one-way ANOVA Tukey’s post-hoc test: PHA-767491  $p < 0.01$ , Roscovitine  $p < 0.01$  (\*\*), where  $n = 4$ ).

Interestingly, PHA-767491, Roscovitine, and Palbociclib reduced Ciz1 levels (PHA-767491  $p < 0.01$ , Roscovitine  $p < 0.01$ , PD-0332991 NS,  $n=4$ ) encouraging the further research into the dependence of Ciz1 accumulation from phosphorylation. Further, the phosphorylation of Ciz1 on CDK2 phosphorylation site T293 site was significantly reduced after DDKi – PHA-767491 and CDK2i – Roscovitine treatments, and marginally reduced on S331 site. This finding was unexpected at first, as PHA-767491 is widely described as DDK inhibitor rather than CDK2 inhibitor. However, there is literature available stating that PHA-767491 has 20-fold lower affinity for CDK2 (IC50 of 200 nM) (Montagnoli et al., 2008), that may be responsible for the effect on Ciz1 stability via inhibition of CDK2. This will be further characterised in Chapter 5.

### **3.5. A model of Ciz1 phosphorylation and accumulation analysis using small molecule kinase inhibitors**

The accumulation of Ciz1 in G1 phase correlates with the expression of cyclin E and A that mediate the rising CDK activity gradient at the G1 – S transition (Figure 3.3) (Lo and Uhlmann, 2011; Pisu et al., 2015). To fully characterise the contribution of specific cyclin - CDK complexes the following experimental strategy was designed (Figure 3.5). In murine 3T3 cells released from quiescence, restriction point occurs between 14-16 hours after release (Figure 3.2) and this time point correlates with the initial accumulation of Ciz1 (Figure 3.3). To assess the role of cyclin D - CDK4/6 activity in promotion of Ciz1 accumulation, cells will be treated with PD-0332991 prior to restriction point. DDK activity (PHA - 767491 and XL - 413) and cyclin E - CDK2 activity (Roscovitine and CVT-313) will be inhibited prior to restriction point. As CDK activity increases post-restriction, DDK and CDK activity will be inhibited from 16 to

20 hours post-release that coincides with the G1/S transition. Analysis of each time point will assess the requirement for CDK or DDK activity during the G1/S transition.

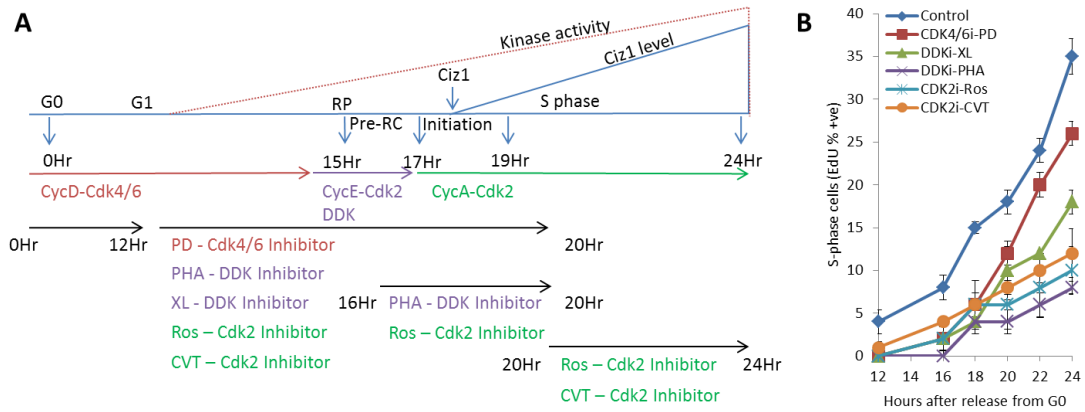


**Figure 3.5. The model of active kinase complexes and Ciz1 accumulation in G1 – S transition and experimental overview. A) Experimental overview.** 3T3 cells were synchronised in G0, released into fresh medium, and treated with 10  $\mu$ M of CDK4/6 inhibitor – PD-0332991, Cdc7-Dbf4 (DDK) inhibitors - 10  $\mu$ M of PHA-767491 and 10  $\mu$ M of XL-413, and CDK2 inhibitors – 30  $\mu$ M of Roscovitine and 10  $\mu$ M of CVT-313 at the time points indicated. **B)** 3T3 cells were treated with kinase inhibitors at 12 hours after G0 release and were 30 min pulse EdU labelled prior every time point indicated. The cells were quantified counting EdU positive calls against DAPI counterstained total nuclei using confocal microscope, each dot presents the mean  $\pm$  S.D., n=6.

In order to understand the effect of kinase inhibitors on cell cycle progression, synchronised 3T3 cells were treated with CDK4/6, DDK, and CDK2 inhibitors at 12 hours after G0 release (Figure 3.5: B). All kinase inhibitors reduced S phase entry, with DDKi – PHA-767491, and CDK2 inhibitors being most efficient. This is consistent with the requirement of rising kinase activity for successful DNA replication (Parker et al., 2017; Takeda and Dutta, 2005; Yeeles et al., 2015).

### **3.6. Phosphorylation of Ciz1 promotes its accumulation in pre-restriction point cells**

The effect of CDK and DDK inhibition on Ciz1 protein levels was determined in pre-restriction point cells. To ensure that selected kinase inhibitors were targeting the proposed kinases, two kinase inhibitors were used for DDK (PHA-767491 and XL-413) and CDK2 (Roscovitine and CVT-313). The XL-413 inhibitor was shown to be more specific for Cdc7 with IC<sub>50</sub> of 3.4 nM *in vitro*, and 2.7 μM for Colo-205 cells (Koltun et al., 2012; Sasi et al., 2014). Similarly, CVT-313 has fewer off target effects than Roscovitine and has an improved IC<sub>50</sub> of 0.5 μM *in vitro*, and for cell application of 6.25 μM (Faber and Chiles, 2007). The distinct CDK2 and DDK inhibitors with different chemical backbones were selected to minimise potential crosstalk with off-target pathways (Maddox, 2016; Sun et al., 2016; Wynn et al., 2011).

Thorough analysis of kinase inhibition at 12-20 hr after G0 release revealed that Ciz1 was reduced by both DDK and both CDK2 inhibitors (PHA-767491 p<0.01, Roscovitine p<0.01, CVT-313 p<0.05), however, the XL-413 did not significantly affect Ciz1 accumulation (Figure 3.6: A and B). Interestingly, CDK4/6 inhibition had no effect and even increased Ciz1 levels in late G1 phase.

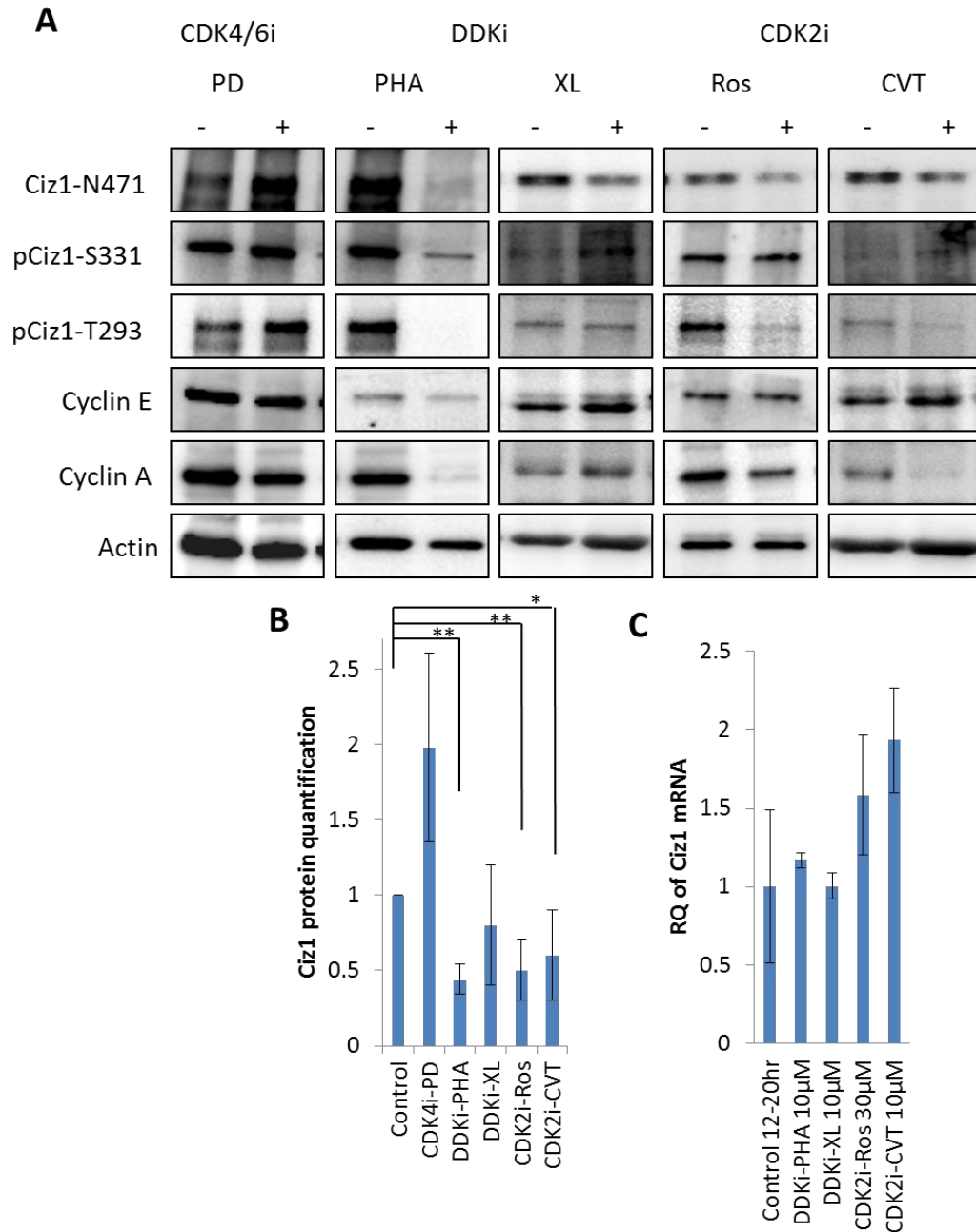


**Figure 3.6. Inhibition of CDK or DDK activity reduces Ciz1 protein levels, but not Ciz1 transcription, in pre-restriction point cells. A)** 3T3 cells were treated with small molecule kinase inhibitors from 12-20 hr after release from G0. Western blot analysis with Ciz1, pCiz1-T293, pCiz1-T293, Cyclin E, Cyclin A, and Actin antibodies. **B)** Quantitation of Ciz1 protein against actin load control, presented as the mean  $\pm$  S.D.,  $p < 0.01$  for PHA-767491 and Roscovitine,  $p < 0.05$  for CVT-313, One Way ANOVA, Post Hoc Tukey, SPSS,  $n = 6$  for PHA-767491 and Roscovitine,  $n = 3$  for PD, XL, and CVT. **C)** Cells were treated with kinase inhibitors 12 - 24 hours. Ciz1 mRNA was quantified using RT-qPCR against GAPDH, and plotted using control as 1,  $n = 3$  (3 technical repeats in each of 3 experimental repeats).

Analysis revealed that PHA-767491 treatment reduced Ciz1 phosphorylation on both CDK2 phosphorylation sites T293 and S331, which contrasted with XL-413 that did not affect Ciz1 phosphorylation and led to a moderate decrease in Ciz1 levels that was not statistically significant (Figure 3.6). These observations support the hypothesis that phosphorylation of Ciz1 at T293 and S331 increases Ciz1 levels. Finally, pre-RP analysis revealed further distinct effects for DDK inhibitors PHA-767491 and XL-413. PHA-767491 was a potent inhibitor of T293 phosphorylation and abolished cyclin A accumulation (Figure 3.6: A, column 2: lanes 3 and 5), whereas XL-413 did not affect either cyclin A levels or Ciz1 phosphorylation. Indeed, PHA-767491 showed differential effects to the DDK inhibitor XL-413, yet produced a similar effect to the CDK2 inhibitors Roscovitine and CVT-313. This is consistent with the published inhibitory effect of PHA-767491 on CDK2 that is 20-fold lower than its IC<sub>50</sub> for Cdc7 (IC<sub>50</sub> of 10 nM for Cdc7, 34 nM for CDK9, and 200 nM for CDK2) (Montagnoli et al., 2008; Montagnoli et al., 2010; Natoni et al., 2011; Natoni et al., 2013; Vanotti et al., 2008).

Finally, the Ciz1 transcript analysis revealed that Ciz1 transcription was not affected by DDK and CDK2 inhibition (Figure 3.6: C). This further suggests that the downregulation of Ciz1 protein levels depends on post-translational Ciz1 regulatory pathways rather than Ciz1 transcription.

### **3.7. CDK2 and DDK inhibition destabilises Ciz1 levels post-restriction point**

Next, the role of CDK and DDK activity in promoting Ciz1 accumulation was assessed in post-restriction point cells. Synchronised 3T3 cells were treated with CDK4/6i – PD-0332991, DDKi – PHA-767491, and CDK2i – Roscovitine 16 – 20 hours after G0

release to assess the role of kinase activity for Ciz1 accumulation in post-RP cells (Figure 3.7).

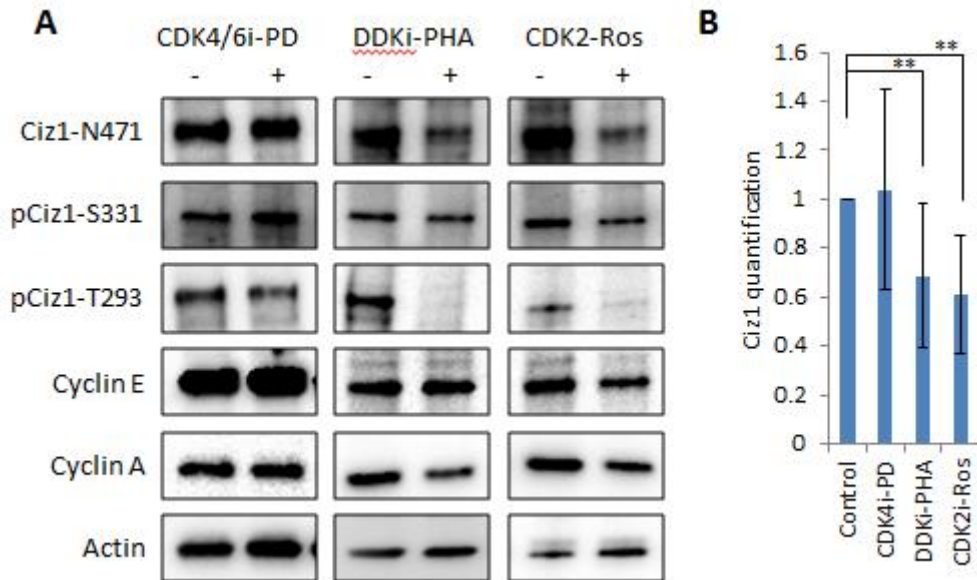


**Figure 3.7. Ciz1 levels are reduced by inhibition of CDK2 or DDK in post-restriction point murine fibroblasts. A)** G0 synchronised cells were treated with small molecule kinase inhibitors 16 – 20 hours after G0 release. WB of protein samples probed with Ciz1, pCiz1-T293, pCiz1-S331, Cyclin E, Cyclin A, and Actin antibodies. **B)** Quantitation of Ciz1 protein level against Actin loading control, presented as the mean ± S.D., significance measured with One-Way ANOVA, Post Hoc, Tukey,  $p < 0.01$  for PHA-767491 and Roscovitine,  $n = 4$ .

Analysis of post-restriction point cells revealed that DDKi - PHA-767491 and CDK2i – Roscovitine efficiently reduced Ciz1 levels ( $p < 0.01$ ,  $n = 4$ ). However, CDK4/6i – PD-0332991 did not affect Ciz1 levels (Figure 3.7), possibly due to the limited CDK4/6 activity in late G1 phase. Both PHA-767491 and Roscovitine inhibitors prevented phosphorylation on T293 site (Figure 3.7: lane 3). In contrast to results shown for pre-restriction point cells, cyclin A levels were less affected after CDK2 or DDK inhibition 16 – 20 hour treatment (Figure 3.7: lane 5). In pre-restriction point cells, this may prevent establishment of the CDK2 positive feedback loop to activate E2F1-3 (Bertoli et al., 2013b). Ciz1 expression is not affected by CDK4/6 kinase inhibition

(Figure 3.6: C), yet PHA-767491 and Roscovitine prevent phosphorylation of Ciz1 at T293 and reduce Ciz1 protein levels (Figure 3.7). This indicates that phosphorylation of Ciz1 may regulate Ciz1 accumulation post-restriction point.

In addition, phosphorylation of Ciz1 at S331 was not affected by CDK2 or DDK inhibition in post-restriction point cells (Figure 3.7), suggesting that S331 was phosphorylated earlier in the cell cycle. S331 phosphorylation might contribute to its accumulation in early G1 phase promoting stabilisation of the protein. Taken together the data suggest that during G1 phase, Ciz1 accumulation is dependent on the activities of DDK and CDK2, as inhibition of CDK or DDK activity reduces Ciz1 levels. This implicates CDK and DDK pathways in the regulation of Ciz1 levels from early and late G1 phase.

### **3.8. Ciz1 is stabilised by phosphorylation after the entry to S phase**

To evaluate whether kinase inhibition reduces Ciz1 levels at the G1/S transition, the late G1/ early S phase time point 20 – 24 hours after G0 release was selected. At this time point 32.6 % of cells are already in S-phase (Figure 3.1). Western blot analysis revealed that inhibition of CDK2 activity using 2 chemical inhibitors reduced Ciz1 levels. This reduction in Ciz1 levels correlates with the significant reduction in Ciz1 phosphorylation at T293 (Figure 3.8). This suggests that CDK mediated phosphorylation of Ciz1 is required to maintain its protein levels in S phase.

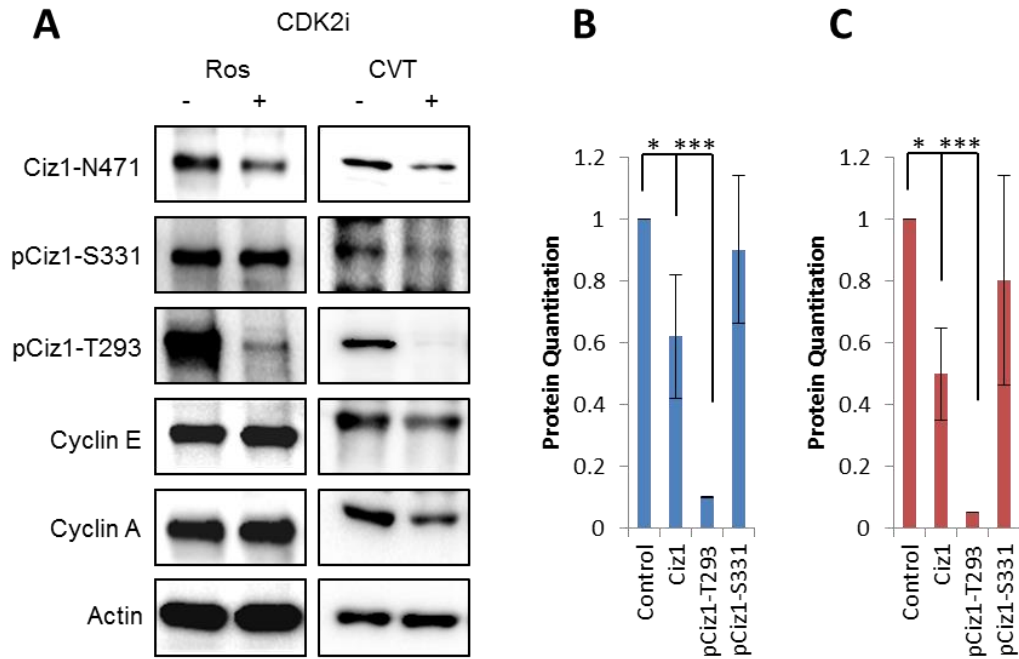


**Figure 3.8. CDK2 phosphorylation stabilises Ciz1 in S phase. A)** Synchronised 3T3 cells were treated with CDK2 inhibitors Roscovitine (Ros) and CVT-313 (CVT) from 20 – 24 hours after G0 release. Western blots were probed with Ciz1, pCiz1-S331, pCiz1-T293, Cyclin E, Cyclin A, and Actin. **B)** Quantitation of Ciz1, pCiz1-S331, pCiz1-T293 level against Actin loading control, for Roscovitine treatment, presented as the mean  $\pm$  S.D., significance measured with One-Way ANOVA, Post Hoc, Tukey,  $p < 0.05$  for Ciz1;  $p < 0.001$  for pCiz1-T293,  $n = 3$ . **C)** as for B, but for CVT-313 treatment.

### 3.9. Genetic depletion of G1 – S regulators reduces S phase entry

The data presented thus far, utilised small molecule inhibitors to evaluate the requirement for CDK and DDK activity in regulation of Ciz1 levels. Due to a high degree of structural similarity in protein kinases, there is invariably cross talk with other kinase families (Breen and Soellner, 2015; Davis et al., 2011; Klaeger et al., 2017; Knight and Shokat, 2005; Wynn et al., 2011; Zhang et al., 2009). To support and complement the small molecule dataset, siRNAs were used to provide an alternative method to reduce specific DDK or cyclin-CDK complexes during cell cycle re-entry from quiescence. Synchronised murine fibroblasts were transfected with siRNAs

against Cdc7-Dbf4, cyclin E1,2 or cyclin A2 and the effect on cell cycle progression and Ciz1 accumulation was determined (Figures 3.9 and 3.10).

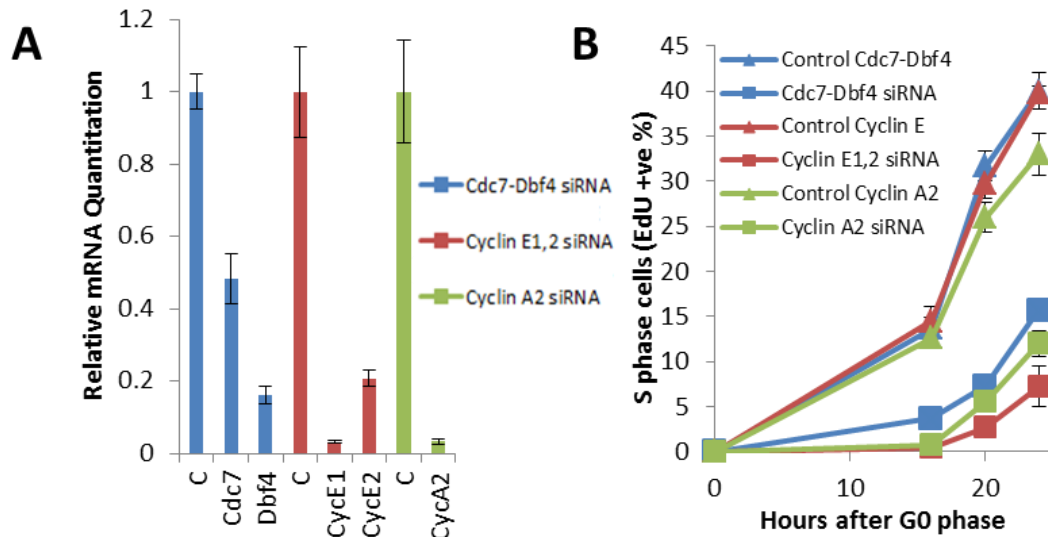


**Figure 3.9. Genetic depletion of G1 – S transition regulators reduce S phase entry.** **A)** G0 synchronised 3T3 cells were transfected with anti- Cdc7-Dbf4, Cyclin E1,E2, and Cyclin A2 siRNAs, harvested 20 hours after release for Cdc7-Dbf4 and cyclin E1,E2, and 24 hours after release for cyclin A2 analysis. mRNA levels were quantified by RT-qPCR relative to GAPDH. One Way ANOVA were performed using Post Hoc analysis using the Tukey method,  $p < 0.001$ ,  $n = 6$  (3 technical repeats in each experimental repeat). **B)** Percentage of S phase (EdU positive) cells were determined at indicated time points for each siRNA and control and show mean  $\pm$  S.D.,  $n = 6$ .

To confirm the efficacy of the depletion, transcript levels were quantified by RT-qPCR relative to GAPDH (Figure 3.9: A). This revealed that Dbf4, Cyclin E1,2, and Cyclin A2 mRNA levels were reduced to less than 20%. Cdc7 transcripts were not reduced as efficiently and required a dual treatment with anti- Cdc7 and Dbf4 siRNA to affect cell cycle progression (Figure 3.9: B). Cell cycle re-entry from G0 was assessed by EdU incorporation and showed that the efficiency of S phase entry was reduced by at least 80% after all depletions (Figure 3.9: B).

### **3.10. Ciz1 is destabilised by G1 – S regulator depletion**

To determine whether Ciz1 protein level was destabilised after genetic depletions of G1 – S regulators, western blot analysis was performed on transfected cells. The investigation revealed that on average Dbf4 protein level was reduced down to 30%, cyclin E was down to 50-60%, with a high variance between experiments and antibodies used. However, the success of cyclin E depletion could be indirectly determined by almost complete ablation of cyclin A expression after cyclin E1, E2 depletion, which is cyclin E – CDK2 dependent. Cyclin A was completely abolished ( $p < 0.01$  for all,  $n=4$ ) (Figure 3.10: A and B).

The Ciz1 levels were reduced in all cases (Figure 3.10: A and C), consistent with small molecule inhibitor studies, which showed that kinase activity was required for Ciz1 accumulation. Interestingly, Cdc7-Dbf4 co-depletion did not affect Ciz1 phosphorylation on T293 or S331 sites (Figure 3.10: A, column 1, lane 1-3), but was still able to destabilise Ciz1 accumulation by 30 %. This may suggest that Ciz1 is phosphorylated on multiple sites by DDK and CDK that collaboratively contribute to its stability and accumulation. Importantly, similar results were achieved using different sequences of siRNA against the same targets (only one is shown on western blot).

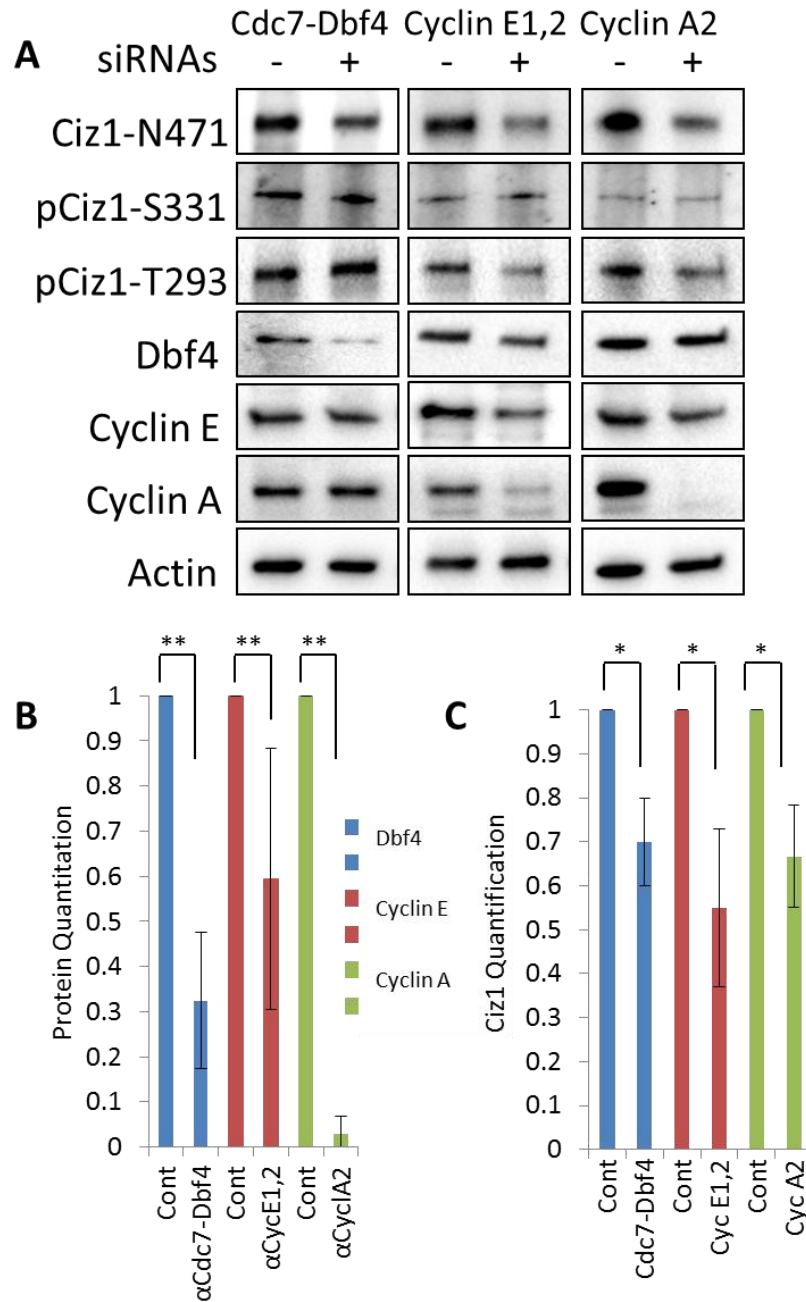


**Figure 3.10. Ciz1 is destabilised by G1 – S regulator depletion. A)** Western blot analysis of control and siRNA depleted samples at 20 hours after Cdc7-Dbf4 and cyclin E1,E2 siRNA transfection, and 24 hours after cyclin A2 siRNA transfection as indicated. **B)** Quantitation of Dbf4 protein after anti-Cdc7-Dbf4 siRNAs co-transfection, Cyclin E protein after anti-Cyclin E1,E2 siRNAs co-transfection, and Cyclin A after anti-Cyclin A2 siRNA transfection. Protein levels shown standardised to actin showing mean  $\pm$  S.D., n=4 (statistical significance analysis performed with One-Way ANOVA, Post Hoc, Tukey,  $p < 0.01$  for all, n=4). **C)** Quantitation of Ciz1 protein levels relative to actin load controls showing mean  $\pm$  S.D.,  $p < 0.05$  for all, n=4.

### 3.11. Ciz1 is regulated by the proteasome in asynchronous and synchronised 3T3 cells

The data presented in this chapter demonstrate that Ciz1 levels are lower in CDK2 or DDK inhibited cells in G1 phase. This effect could be mediated by either reduced cell cycle progression after CDK and DDK inhibition or perhaps through an active process that leads to degradation of Ciz1 levels. To assess the potential role for the proteasome in regulation of Ciz1 levels, cells were treated with a combination of Roscovitine and the proteasome inhibitor MG132 (Figure 3.11).

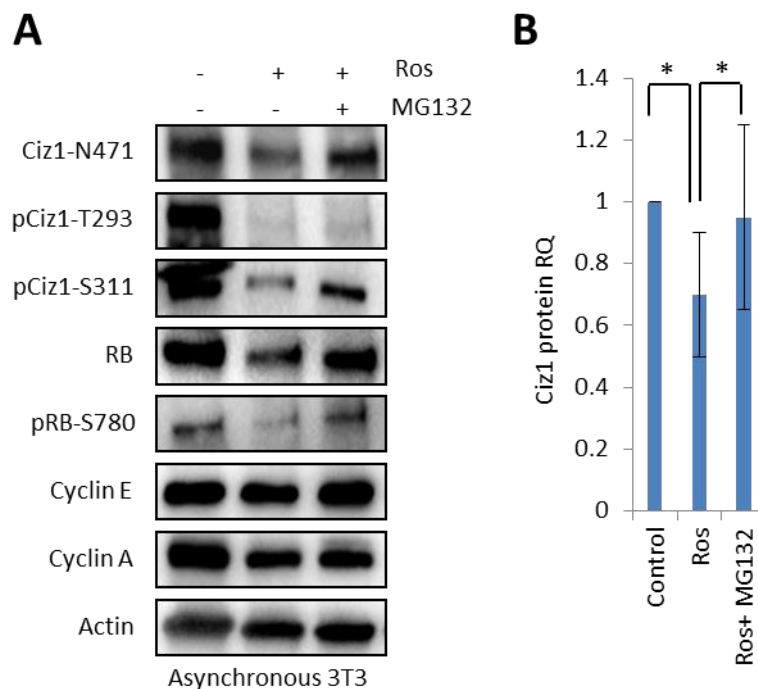


**Figure 3.11. MG132 recovers Ciz1 levels destabilised by kinase inhibitors in asynchronous population. A)** Asynchronous 3T3 were treated with 30  $\mu$ M of Roscovitine and 10  $\mu$ M of MG132 at 70 % confluency for 4 hours. Immunoblot showing Ciz1, pCiz1-T293, pCiz1-S331, RB, pRB-S780, Cyclin E, Cyclin A, and Actin. **B)** Quantitation of Ciz1 protein levels. Protein levels presented standardised to actin showing mean  $\pm$  S.D., where n=3. Statistical significance analysis performed with One-Way ANOVA, Post Hoc, Tukey, p<0.05.

In asynchronous 3T3 cells, Roscovitine efficiently reduced Ciz1 levels (Figure 3.11: A). The levels of pT293 and pS331 were reduced suggesting efficient CDK inhibition. Similarly, the level of Rb phosphorylation (S780) was also reduced. Importantly, the levels of Ciz1 were significantly recovered by addition of MG132, suggesting that the proteasome promotes degradation of Ciz1 after inhibition of CDK activity (Figure 3.11: B).

Following this observation, a more detailed analysis of CDK and DDK inhibition in G1 phase was performed using PHA-767491 and Roscovitine with or without MG132 (Figure 3.12). Using synchronised cells the results revealed more profound destabilisation of Ciz1 after CDK or DDK inhibition. Significantly, the reduction of Ciz1 after kinase inhibition could be efficiently reversed by proteasomal inhibition (Figure 3.12). Consistent with the previous findings in synchronised cells, S331 phosphorylation was not significantly affected by kinase inhibitors (Figure 3.12: A and C, lanes 2), suggesting that this site was phosphorylated earlier in the cell cycle. However, the Ciz1 T293 phosphorylation was efficiently reduced similar to earlier experiments (Figures 3.6 - 8) and was unaffected by proteasomal inhibition. Similarly, cyclin A levels were significantly reduced by PHA-767491 and Roscovitine (Figure 3.12: A and C, lanes 3 and 5), and were only marginally recovered by proteasomal inhibitor.

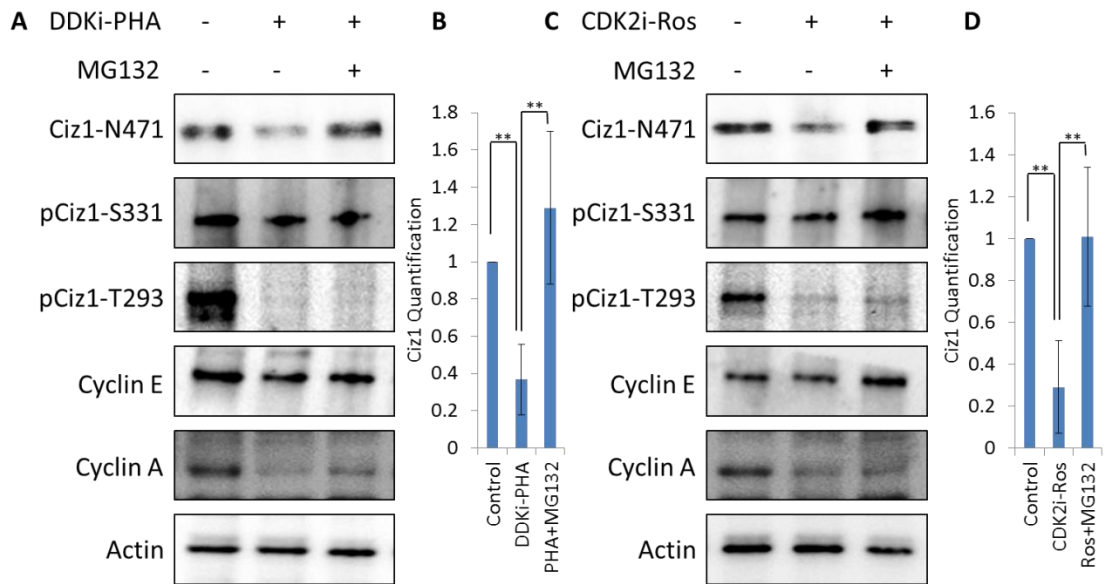


**Figure 3.12. Proteasomal inhibition recovers Ciz1 levels after kinase inhibition.** 3T3 were synchronised and treated 12 – 20 hour after G0 release. **A)** WB of cells treated with PHA-767491 +/- MG132 as indicated. **B)** Quantitation of Ciz1 levels against actin control. Protein levels presented standardised to actin showing mean  $\pm$  S.D., where  $n=4$ . (\*\*) shows  $p<0.01$  for control vs PHA-767491 and PHA vs PHA+MG132, significance was measured by One-Way ANOVA, Post-Hoc, Tukey,  $n=4$ . **C)** as in A except for Roscovitine. **D)** as for B but for Roscovitine,  $n=4$ .

Next, to assess if inhibition of CDK activity promotes proteasomally mediated degradation in late G1 and early S phase, CDK2 inhibitors (Roscovitine and CVT-313) with and without MG132 were added from 20 – 24 hours after G0 release. The results showed that CDK2 inhibition reduced Ciz1 levels (Figure 3.13: A and C). In addition, proteasomal inhibition significantly recovered Ciz1 level ( $p<0.05$ ) that was reduced with CDK2 inhibition (Figure 3.13). This suggests that Ciz1 accumulation is regulated by opposing CDK and ubiquitin ligase activities.

As seen for small molecule inhibition earlier (Figures 3.7 and 3.8), cyclin A level was less affected by CDK2 inhibition after 20 – 24 hour than after 12 -20 hour treatment (Figure 3.13: A and C, lane 5). This may be related to differences in cyclin expression

levels when CDK2 activity is inhibited prior to restriction point bypass and will be discussed further in Chapter 5.

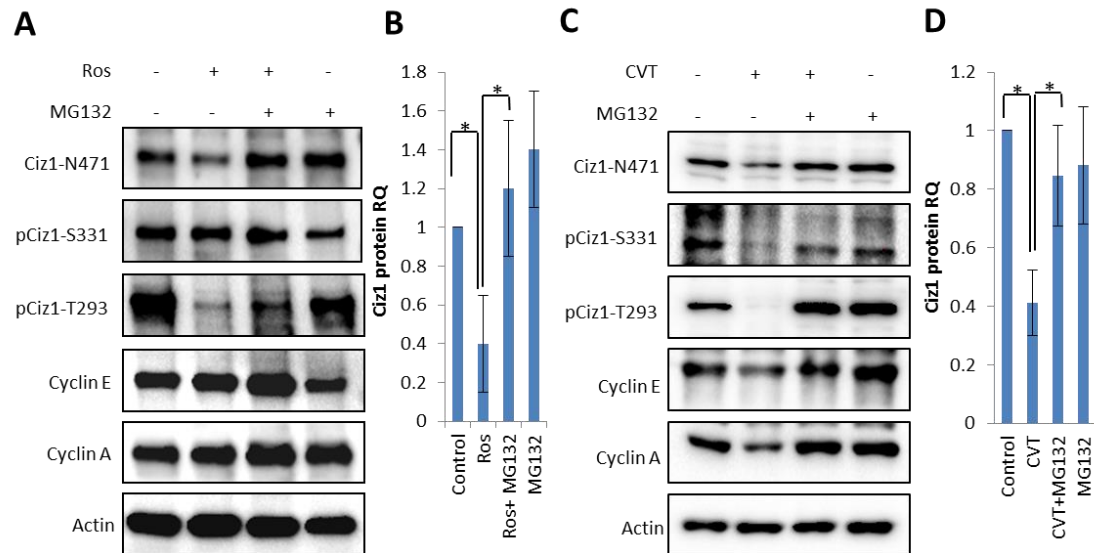


**Figure 3.13. MG132 recovers Ciz1 levels in S phase after reduction by CDK2 inhibitors.** **A)** 3T3 were synchronised and treated 20 – 24 hours after G0 release. WB of cells treated with 30  $\mu$ M of Roscovitine and 10  $\mu$ M of MG132. **B)** Quantitation of Ciz1 protein against actin load control. Protein levels presented standardised to actin and bars show mean  $\pm$  S.D., where n=3. Significance measured by One-Way ANOVA, Post-Hoc, Tukey, (\*) p<0.05 for Control vs Ros and Ros vs Ros+MG132, n=3. **C)** as in A but for 10  $\mu$ M of CVT-313. **D)** as in B but for CVT-313, p<0.05 for Control vs CVT and CVT vs CVT+MG132, n=3.

### 3.12. Proteasomal inhibition recovers Ciz1 levels after genetic cyclin A depletion

To complement and support the data generated using a small molecule inhibition approach, genetic depletion of cyclin A2 was performed using siRNA. To assess whether Ciz1 is degraded by the proteasome after CDK2 inhibition, cyclin A2 was depleted using anti-cyclin A2 siRNA and MG132 was added from 20 hours after release for 4 hours. Western blot analysis revealed that cyclin A expression was completely abolished and transcript levels were reduced by more than 90 %, showing successful depletion (Figure 3.14: A and C).

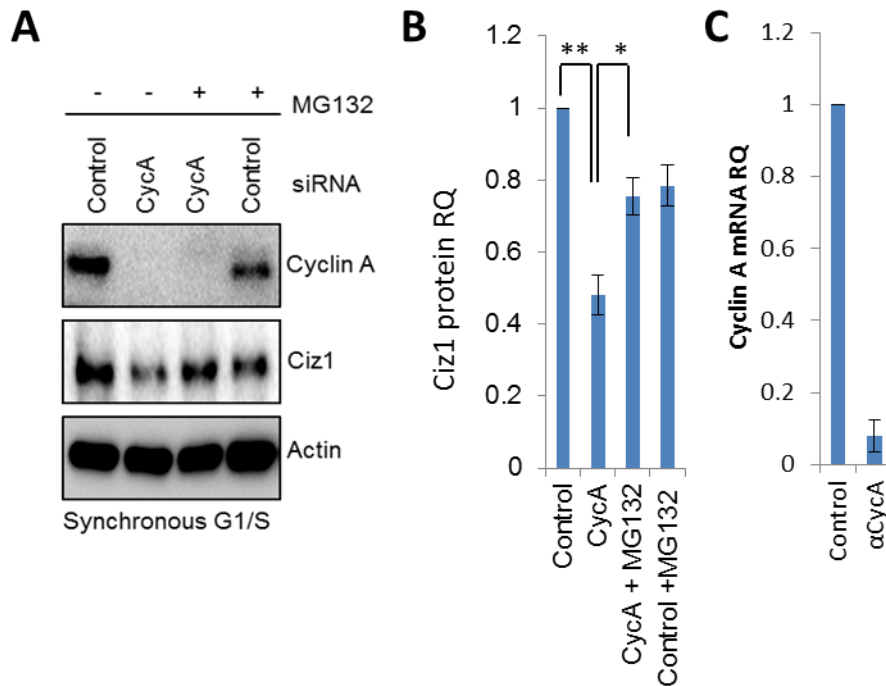


**Figure 3.14. MG132 recovers Ciz1 after genetic cyclin A depletion.** 3T3 cells were synchronised and transfected with anti-cyclin A2 siRNA at the point of release from G0. Cells were treated with 10  $\mu$ M of MG132 20 – 24 hours after release/transfection. **A)** WB of soluble protein 24 hours after transfection, probed with Ciz1 and cyclin A antibodies. **B)** Quantitation of Ciz1 protein levels shown standardised to actin and bars show mean  $\pm$  S.D., where n=3. Significance measured by One-Way ANOVA, Post-Hoc, Tukey, (\*\*)  $p < 0.01$  for Control vs Ros, (\*)  $p < 0.05$  for Ros vs Ros+MG132, n=3. **C)** Cyclin A mRNA levels were quantified control vs anti-cyclin A siRNA treated by RT-qPCR relative to GAPDH. One Way ANOVA was performed using Post Hoc analysis using the Tukey method,  $p < 0.001$ , n=3 (3 technical repeats in each experimental repeat).

In the absence of cyclin A2, Ciz1 protein levels were reduced to 50% of control levels, which was efficiently reversed by addition of MG132 recovering Ciz1 levels to 75-80% of the control levels (Figure 3.14: B). This observation supports the hypothesis that Ciz1 is regulated by opposing kinase and proteasomal activities. The findings are consistent with a model where CDK and DDK kinase activity is required for Ciz1 accumulation, and that inhibition of CDK or DDK kinase activity promotes proteasomally mediated degradation of Ciz1 as protein levels can be maintained by

the inhibition of the proteasome. This suggests that Ciz1 is tightly controlled by opposing kinase and proteasome activities in G1 phase in order to reach sufficient levels for DNA replication initiation in a highly controlled manner.

### 3.13. Ciz1 is ubiquitylated *in vivo*

To directly determine if Ciz1 is poly-ubiquitylated, two complimentary approaches were used. HA-tagged ubiquitin or His-tagged ubiquitin expressing plasmids were transfected into 3T3 cells independently (Figure 3.15). Ubiquitylated proteins were enriched by either immunoprecipitation (HA) or immobilized on Ni-NTA beads (His<sub>6</sub>) and then resolved on SDS-PAGE gel. The western blot analysis revealed the ubiquitylation characteristic smear pattern (Figure 3.15: A) going upwards from the original Ciz1 band at around 110 kDa. This implied that the multiple ubiquitin molecules (8 kDa) were bound onto Ciz1 increasing its molecular weight from 100kDa to >150 kDa, consistent with poly-ubiquitylation (Figure 3.15 A).

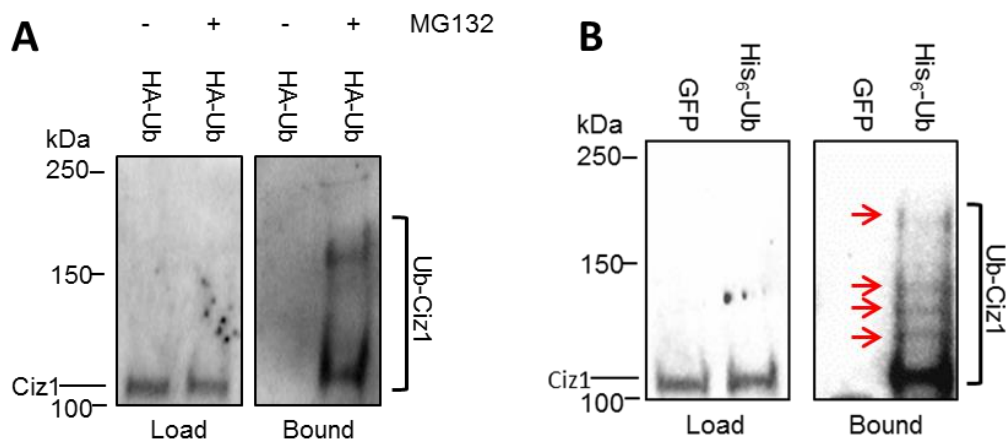


**Figure 3.15. Ciz1 is ubiquitylated *in vivo*.** NIH-3T3 cells were transfected with ubiquitin-hemagglutinin (HA) or ubiquitin-histidines (His<sub>6</sub>) plasmids with or without 10 μM MG132. **A)** Ubiquitylated Ciz1 was anti-HA immunoprecipitated, resolved on 4-15% SDS-PAGE gel and probed with Ciz1 antibody. **B)** Ubiquitylated Ciz1 was immobilised on Ni-NTA resin (IMAC), resolved on 4-15% SDS-PAGE gel and probed with Ciz1 antibody. Red arrows indicate ubiquitylation characteristic bands.

Additionally, the multiple bands from 100 kDa to >150 kDa above Ciz1 protein were observed after Ub-His<sub>6</sub>-Ni-NTA immobilized metal affinity chromatography (IMAC) (Figure 3.15: B). This suggested that Ciz1 was poly-ubiquitylated or poly- mono-ubiquitylated in 3T3 cells, encouraging the further research in Ciz1 ubiquitylation. Notably, the ubiquitylation specific pattern was only observed after MG132 treatment, which allowed its accumulation by inhibition of proteasomally mediated degradation.

### **3.14. Discussion**

Quiescent synchronised embryonic mouse fibroblasts were used to research G1 – S transition in more controlled and interpretable manner. First, the kinetics of cell re-entry from G0 was established using EdU, a thymidine analogue, which enabled visualising actively replicating cells that enter the S phase (Figure 3.1). This technique was used to determine the timing of the restriction point of post-quiescent cells (Moser et al., 2018; Pardee, 1974; Spencer et al., 2013). Actively replicating cells may not encounter G1 restriction point due to residual moderate CDK2 activity and low p21 upon the mitotic exit. However, the post-quiescent cells retain dependency on mitogenic signalling and active G1 restriction point (Figure 3.2), which was used here to temporally organise the G1 – S transition and analysis.

Ciz1 protein acts as a molecular link between origins of replication and CDK2 (Copeland et al., 2010; Copeland et al., 2015; Pauzaite et al., 2017) contributing to the efficiency of DNA replication initiation that occurs in G1 phase (Ainscough et al., 2007; Coverley et al., 2005). Additionally, Ciz1 is phosphorylated by CDK, although only 3 of the sites have been functionally characterised. In murine Ciz1 there are 14

putative CDK sites that may contribute to the regulation of Ciz1 expression and activity.

Here, the expression of Ciz1 was followed from quiescence to early S phase. Ciz1 protein levels and phosphorylation status on 2 sites (T293 and S331) were determined (Figure 3.3). Ciz1 protein accumulation correlated closely with its phosphorylation on T293 and cyclin A expression. The T293 site has been previously validated as a CDK site (Copeland et al., 2015), and results presented here suggest that increasing cyclin A–CDK2 activity promotes T293 phosphorylation at the G1 - S transition (Figure 3.3). Ciz1 protein levels resembled E2F cell cycle regulators: cyclin E1, E2, A2, and Dbf4, accumulation in G1 phase. Ciz1 transcription was compared with E2F regulated Dbf4, cyclin E1, E2, A2 (Harbour and Dean, 2000; Ohtani et al., 1995; Yamada et al., 2002) and was found to be considerably lower than the canonical E2F transcripts despite protein levels mirroring cyclin A expression. The relatively low variation in transcript abundance of Ciz1 suggests that Ciz1 may be regulated post-translationally (Figure 3.3: B).

The potential for CDK mediated phosphorylation to regulate Ciz1 accumulation in late G1 phase was assessed. This approach investigated 3 time points: pre-restriction time point (12 – 20 hours from G0 release), post-restriction point (16 – 20 hours), and late G1 – early S phase time point (20 – 24 hours) (Figures 3.2 and 3.5). The small molecule kinase inhibitor studies (Figures 3.6 - 3.8) suggested that Ciz1 accumulation required the activities of DDK and CDK2 during G1 phase. In addition, CDK2 mediated phosphorylation of T293 site correlated closely with Ciz1 stability and accumulation. The genetic depletion of Dbf4-Cdc7, Cyclin E1, E2, and Cyclin A2 offered similar effect

on Ciz1 accumulation to chemical kinase inhibitors. However, Dbf4-Cdc7 depletion reduced Ciz1 accumulation without affecting T293 phosphorylation (Figure 3.10), suggesting that Ciz1 is phosphorylated by both CDK2 and DDK on various sites that contribute to its stability and accumulation. This is consistent with the collaborative efforts of CDK2 and DDK kinases driving the cell cycle described in the literature (Wan et al., 2008; Yeeles et al., 2015).

Next, the potential role of the UPS mediated degradation in regulation of Ciz1 was assessed. The proteasomal inhibition recovered Ciz1 levels after being destabilised by a lack of phosphorylation (Figures 3.11-3.14). Ciz1 proteasomal down-regulation was confirmed by *in vivo* ubiquitylation, IMAC and IP experiments, which showed that Ciz1 is poly-ubiquitylated in 3T3 cells (Figure 3.15).

The emerging model for Ciz1 accumulation proposes that Ciz1 is stabilised or protected from degradation by rising kinase activities in G1 phase. Furthermore, in the absence of CDK2 or DDK activity Ciz1 is degraded by the UPS to precisely regulate the abundance of Ciz1. This model suggests that an imbalance in either CDK or UPS activity could promote an increase or decrease in Ciz1 levels. For example, overexpression of cyclin E or A leading to hyperactivation of CDK2, or down-regulation of E3 ligases or the entire ubiquitin proteasome system, could lead to the overexpression of Ciz1 that has been linked to a number of major cancers (Den Hollander et al., 2006; Greaves et al., 2012; Higgins et al., 2012; Mitsui et al., 1999; Pauzaite et al., 2017; Yin et al., 2013; Zhou et al., 2018).

Over-expression of Ciz1 is associated with tumour growth in xenograft models (Pauzaite et al., 2017; Wu et al., 2016; Yin et al., 2013; Zhang et al., 2015).

Importantly, in each case reducing Ciz1 levels by genetic depletion has been found to reduce tumour growth. This suggests that Ciz1 is a viable drug target in common tumour types. The analysis presented here suggests that Ciz1 is regulated by opposing CDK and UPS activities, and, significantly, this work has demonstrated that the reduction of Ciz1 can be induced using repurposed small molecule kinase inhibitors. For this approach to be viable, a detailed understanding of the signalling mechanisms that control Ciz1 levels is required. In particular, identification of the E3 ligase(s) would be particularly important as inactivation of the E3 ligase may lead to overexpression of Ciz1 in some tumour types. This mechanism was found in breast cancers where inactivation of PARK2 promotes overexpression of cyclin E that drives proliferation (Gong et al., 2014). The identification of the E3 ligase(s) that regulate Ciz1 will be performed using an *in vitro* ubiquitylation assay (Chapter 7).

In addition, having identified that CDK mediated phosphorylation stabilises Ciz1 in 3T3 cells, the question emerged on which specific phosphorylation sites are responsible for Ciz1 accumulation (Chapter 4). Site directed mutagenesis of CDK phosphorylation sites (S/TP) within Ciz1 may be able to identify which sites regulate Ciz1 accumulation *in vitro*. Using over-expression of exogenous Ciz1 and phosphomimetic aspartate or unphosphorylatable alanine mutants may provide insight into this process. In addition, CRISPR-Cas9 and homology directed repair approaches, in order to replace CDK sites with phosphomimetic aspartate or unphosphorylatable alanine, will be applied. This would allow identification of specific phosphorylation sites that contribute to Ciz1 stability and analysis of its effect on the cell cycle progression.

In addition, the differences between DDK inhibitors PHA-767491 and XL-413 have been observed (Figure 3.6) in context of potential CDK2 targeting by PHA-767491. In particular, PHA-767491 decreases both Ciz1 and cyclin A expression, whereas XL-413 has no significant effect. Differences in PHA-767491 and XL-413 have been noted previously regarding their effects on cancer cell proliferation (Natoni et al., 2011; Rainey et al., 2017; Sasi et al., 2014). Further characterisation of the differential effects of PHA-767491 and XL-413 in relation to cell cycle progression, CDK2 targeting and Ciz1 stability are required (Chapter 5).

Ciz1 has been implied as a driver of development of certain cancer types and the depletion of Ciz1 reduced cancer growth in xenograft models, as well as inhibited cancer cell proliferation and migration (Higgins et al., 2012; Lei et al., 2016; Pauzaite et al., 2017; Wang et al., 2014; Wu et al., 2016; Yin et al., 2013). This suggests that targeting Ciz1 accumulation and stability may be of therapeutic relevance. Therefore, in this work a number of cancer cell lines will be screened for Ciz1 dependency, and treated with already existing CDK and DDK chemical kinase inhibitors. Assuming that some cancer cell lines depend on Ciz1 and have functional UPS, the treatment with small molecule kinase inhibitors would have a dual effect against proliferation. This would make cancer cells more sensitive to the therapies and potentially provide a strategy for patient stratification (Chapter 6).

# **Chapter 4**

## **Evaluation of the role of CDK mediated phosphorylation for Ciz1 stability**

#### 4.1. Introduction

The temporal regulation of the cell cycle is mediated by the activities of cyclin dependent kinases, which impose a rising gradient of activity from G1 phase to mitosis (Coudreuse and Nurse, 2010b; Henderson et al., 2006; Lo and Uhlmann, 2011; Malumbres, 2014; Pauzaite et al., 2017). The importance of protein phosphatases in the temporal control of protein phosphorylation has been demonstrated in yeast, where PP2A-Cdc55 provides temporal separation of serine and threonine phosphorylation status, by showing a preference for threonine (Cundell et al., 2016; Godfrey et al., 2017). Importantly, similar phosphorylation kinetics are seen with Ciz1, where S331 is phosphorylated earlier than T293, which is maximally phosphorylated in S phase (Copeland et al., 2015) (Chapter 3). Ciz1 is first phosphorylated on S331 site correlating closely with cyclin E expression in early G1 phase and then on T293 site that resembles cyclin A accumulation in late G1 – S phase (Figure 3.3: A). The results presented in Chapter 3 suggest that CDK and potentially DDK mediated phosphorylation of Ciz1 has a protective role, preventing UPS mediated degradation of Ciz1 (Figure 3.6 - 8). This protective role is in addition to the regulatory role that controls Ciz1 DNA replication function via CDK mediated phosphorylation on T144, T192, and T293 sites that inhibit DNA replication function of Ciz1 (Copeland et al., 2015). These observations suggest that differential phosphorylation of Ciz1 has a profound effect on its function. The focus of this chapter is to determine whether phosphorylation of Ciz1 increases its stability by specifically reducing UPS mediated degradation *in vitro* and *in vivo*.

Here, the role of CDK mediated phosphorylation of Ciz1 in regulation of its stability will be assessed. To evaluate the role of phosphorylation for the regulation of Ciz1 stability exogenous overexpression of GFP-Ciz1 constructs with phosphomimetic (aspartyl) and non-phosphorylatable (alanine) mutations will be assessed. In addition, CRISPR-Cas9 (clustered regularly interspaced short palindromic repeat–CRISPR-associated system) will be used to introduce site specific phosphomimetic (aspartyl) and non-phosphorylatable (alanine) mutations within the Ciz1 gene.

#### **4.2. CRISPR-Cas9 and homology directed repair (HDR) mediated point mutations in genomic Ciz1 DNA**

In order to pinpoint the function of individual CDK2 phosphorylation sites of endogenous Ciz1 protein, CRISPR-Cas9 was used to introduce double strand breaks; and homology directed repair (HDR), using a synthetic single stranded oligonucleotides (ssODNs), was used to introduce alanine or aspartic acid mutations in T192, T293, and S331 sites (Figure 4.1).

The T192 site was chosen as it possessed multiple DDK and CDK2 phosphorylation sites that could have been targeted with a single ssODN. DDK sites are often located directly adjacent to CDK sites (Wan et al., 2008). There is currently no information regarding the site specificity for the DDK in Ciz1 and preliminary data supports a stabilising role of DDK (Figure 3.6 - 7). To establish whether T192 or adjacent putative CDK/ DDK phosphorylation sites were important regulatory sites, CRISPR-Cas9 was used with ssODN transfection and HDR. In addition, the potential regulatory effect of phosphorylation at position T293 was targeted, as it was shown to be phosphorylated late in G1 phase and it regulates Ciz1 DNA replication activity

(Copeland et al., 2015). Significantly, phosphorylation of T293 correlates with both Ciz1 and cyclin A accumulation (Figure 3.3). In addition, phosphorylation on T293 site was reduced by Roscovitine, CVT-313, and PHA-767491 that results in reduction of Ciz1 consistent with an important role in the stabilisation of Ciz1 (Figures 3.6-7). Finally, S331 site was selected, as it was phosphorylated early in G1 phase potentially leading to Ciz1 accumulation.

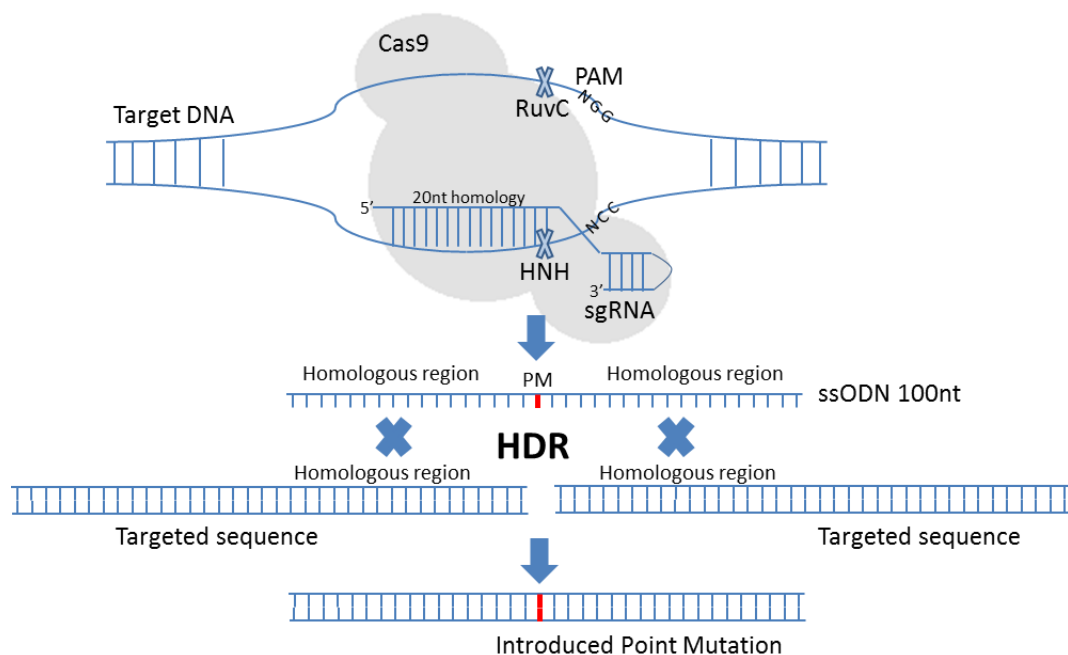


**Figure 4.1. Introduction of the point mutation (PM) by homology directed repair (HDR) pathway.** Single-guide RNA (sgRNA) with introduced 20 nucleotide homology after Protospacer adjacent motif (PAM) sequence guides Cas9 endonuclease to target DNA. HNH and RuvC nuclease domains cut target genomic DNA 3-5 nucleotides after the PAM (NGG) sequence introducing double strand DNA break. Homology directed repair (HDR) mechanism uses 100 nucleotide single-strand ODN sequence with point mutation surrounded by 40-50 nucleotide sequences homologous to genomic DNA for genomic DNA repair.

The Cas9 nuclease of the type II CRISPR-Cas system (Figure 4.2: A) possesses 2 nuclease active domains (Figure 4.1). The HNH nuclease domain cleaves complementary strand and RuvC-like nuclease domain introduces break in non-

complementary strand to guide-RNA around 3-5 nucleotides from PAM sequence (Gasiunas et al., 2012). To introduce point mutations via RNA-guided CRISPR-Cas9 technology, the 20 nucleotide guide sequence complementary to genomic DNA site of interest was incorporated into short guide RNA, which in turn was able to target Cas9 nuclease to PAM sites adjacent to CDK sites in Ciz1 (Figure 4.2). The cells were co-transfected with Cas9 plasmid and single strand ODN sequences (Table 2.5) that include desired point mutations in order to facilitate the introduction of mutations in specific sites by homology directed repair mechanism (HDR) (Figure 4.1).

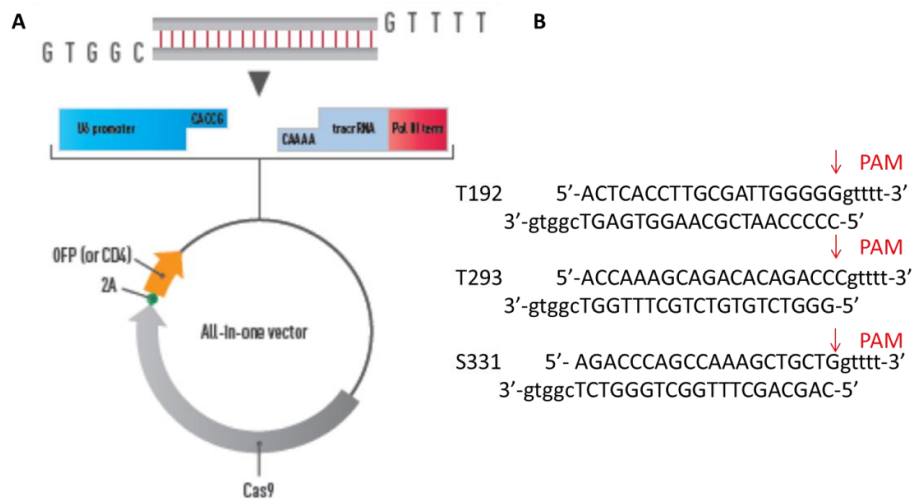


**Figure 4.2. The type II CRISPR-Cas system. A)** The CRISPR-Cas is composed of a complementary CRISPR RNA (crRNA), a trans-activating crRNA (tracrRNA), and the Cas9 endonuclease. **B)** The 20 nucleotide guide sequence, complementary to specific loci in genomic DNA, has a PAM (NGG) sequence, and is ligated in crRNA completing the guide RNA. The three different single-guide RNAs were designed targeting T192, T293 and S331 phosphorylation sites in Ciz1.

#### 4.3. Screening for CDK site specific point mutations in Ciz1 gene

After the double strand DNA breaks were introduced by Cas9 nuclease, the ssODNs, carrying point mutations, were used as templates for HDR knocking-in the mutations in genomic DNA (Prykhodzhiy et al., 2017). Specific ssODNs were generated for each

phosphorylation site, and were carrying alanine (Gcx) or aspartic acid (GAu/c) (where capital letters show introduced point mutations) point mutations surrounded by approximately 40 nucleotide homologous regions for genomic DNA (Figure 2.5). The T192 ODN sequence was 99 nt in length, 5 point mutations were approximately 15-30nt away from cutting site and the homology arms were 30 nt and 50 nt in length. The T293 ODN sequence was 92nt in length, the point mutation was within 10bp from the nuclease cutting point, the homology arms were 48 and 44 nucleotides in length. The S331 ODN sequence was 98nt in length, the point mutation was around 25bp from the nuclease cutting point and the homology arms were 50 and 48 nucleotides in length (Table 2.5). The ssODN sequences were co-transfected into the cells with CRISPR-Cas9 plasmid. The restriction enzymes were selected using NEB cutter V2.0 ([www.neb.com](http://www.neb.com)) in order to determine the locations of cutting sites in the amplified region and specificity for the introduced point mutations (Table 2.6 and Figure 4.3).

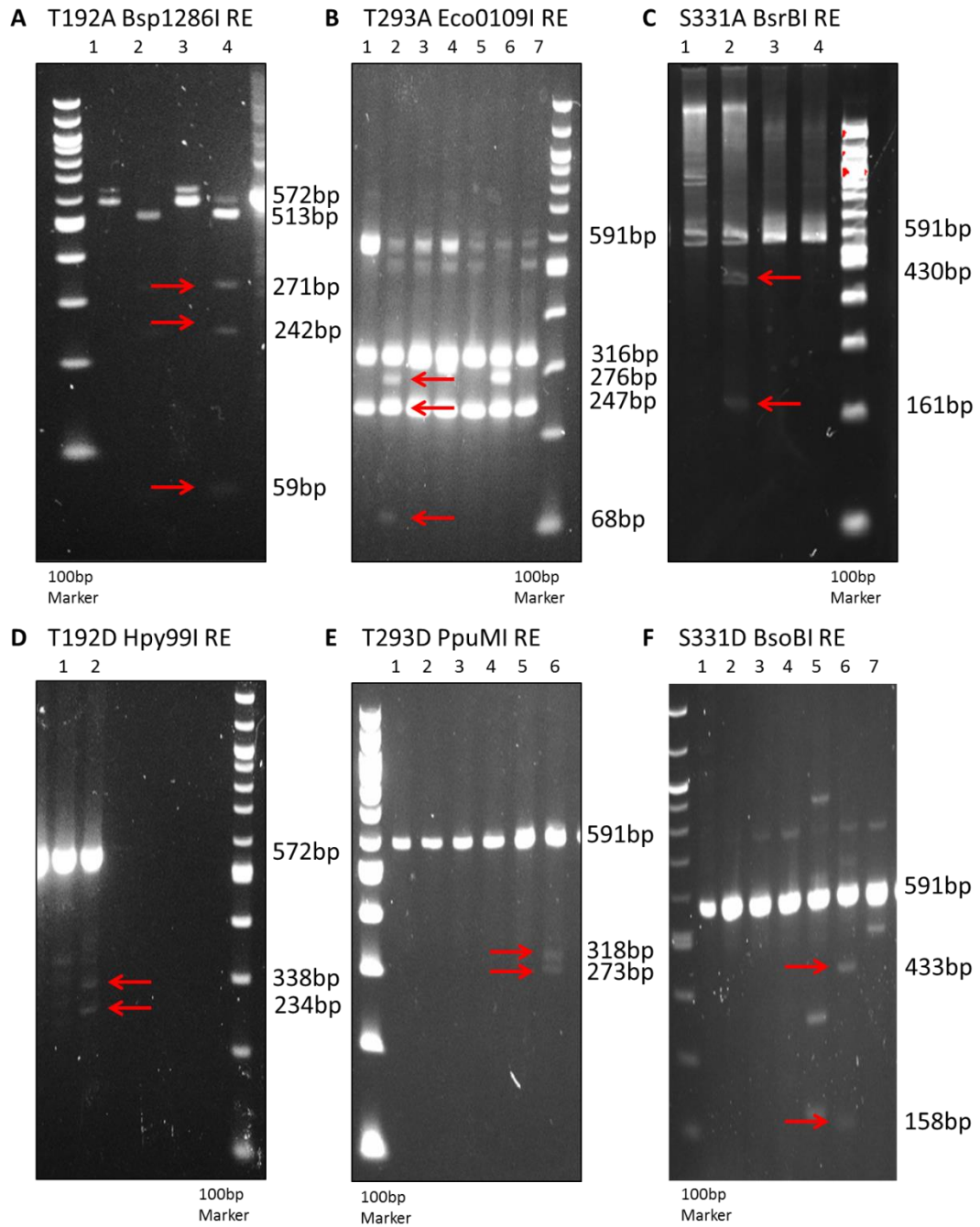


**Figure 4.3. ssODN knock-in screening using point mutation specific restriction enzymes.** DNA was PCR amplified from purified genomic DNA and products screened with point mutation specific restriction enzymes to identify clones with desired mutations **A)** T192A – Bsp1286I lane 4 is partially successful with bands of expected size (red arrows) (Table 2.6). **B)** T293A – Eco0109I. **C)** S331A – BsrBI. **D)** T192D – Hpy99I. **E)** T293D – PpuMI. **F)** S331D – BsoBI.

PCR amplification and restriction enzyme screening allowed identification of clones with the potential point mutations. However, it also revealed that for each clone there was heterogeneity in the population. This suggested that either the restriction digest was incomplete, or that mutations had not been successfully introduced into both copies of the chromosomal DNA. In addition, there could simply be a mixed lineage of cells from wild type and mutant populations from single cell wells through contamination or oversight during the expansion phase from single cells.

Prolonged overnight restriction digestion revealed similar results (data not shown), suggesting that reactions had gone to completion. To ensure that there is not a mixed lineage of cells, cells were diluted to single cells and expanded prior to restriction digest analysis that showed results identical to the original analysis. This left the third option suggesting that the successful point mutation was introduced in only one allele within one cell (Paquet et al., 2016). The haploid mutants were targeted for a second round of CRISPR-Cas9 treatment. In principle, repeating the CRISPR-Cas9 directed cleavage should target the wild type chromosomes specifically as there are mismatches in the guide RNA from incorporation of desired mutations. However, despite selecting a number of clones, screening revealed that they were either identical to previous cells or unhealthy and did not expand well after being subjected to two rounds of transfection, enrichment and CRISPR-Cas9 treatment.

These results are consistent with the low efficiency of homologous recombination in mammalian cells, meaning that acquiring two successful point mutations in single cell is difficult. Finally, the second cutting event by left-over Cas9 may have occurred after the successful point mutation introduction (Hruscha et al., 2013; Kwart et al.,

2017; Prykhozhij et al., 2017). This would lead to introduction of a point mutation via homologous directed repair followed by the second cut repair by non-homologous end joining. This way single allele would contain a point mutation and second non-specific mutation leading to a frame shift and protein truncation. To test that, the amplified DNA fragments were cloned into TOPO10 Blunt cloning vector, and were sequenced using M13 forward and reverse primers (Figure 4.4).

#### **4.4. DNA sequencing of mutated sites after CRISPR-Cas9 and HDR**

The sequencing results from 3 different clones revealed that the point mutations were introduced into at least one of the DNA copies. However, the homology directed repair was not performed with high fidelity (Table 4.1). Many of the sequences had the point mutation introduced together with some nucleotides missing or looped in, producing the frame shift after the PAM – Cas9 cutting site, introducing Ciz1 protein truncations rather than point mutations (Table 4.1 and Figure 4.4). Additionally, it revealed that some cells had the wild type and mutated sequence, which would not allow for further research in Ciz1 protein stability and cellular phenotypes. Finally, in the S331A case, the full homologous recombination and replacement by chromosome 11 had been observed (Table 4.1), which meant that the genome was highly disturbed and unorganised after CRISPR-Cas9 transfection.

**A T192 A: introduced Alanine mutation and frame shift further in the sequence**

```
Query 276 GAACACCCAGAAACAGGCCAGAGGCCCCCTCTTCCACCACCC 316
          |||
Sbjct 623 GAACACCCAGAAACAGGCCAGAACCCCTCTTCCACCACCC 663
```

**B T192 D: TCCACCACCCCAATCGC -> TCCGAC introduced aspartic acid mutation, 12 nucleotides missing, no frame shift**

```
Query 374 AGGAACACCCAGAAACAGGCCAGAACCCCTCTTCC-----GA-CGCAAG 423
          |||
Sbjct 220824 AGGAACACCCAGAAACAGGCCAGAACCCCTCTTCCACCACCCCAATCGCAAG 220883
```

**C T293 A: GGTC -> GGC introducing Alanine + frame shift**

```
Query 310 CTTCTGGTGGCTCAGGCAGCCGATCCGGGG-CTGTGTCTGCTTTGGTGCTGTCA 368
          |||
Sbjct 1142 CTTCTGGTGGCTCAGGCAGCCGATCCGGGGTCTGTGTCTGCTTTGGTGCTGTCA 1083
```

**D T293 D: CGGGGTC -> CGGGTC introducing Aspartic acid + frame shift**

```
Query 312 GGACTTCTGGTGGCTCAGGCAGCCGATCCGGGGG-TCGTGTCTGCTTTGGTGCCGTCA 370
          |||
Sbjct 1142 GGACTTCTGGTGGCTCAGGCAGCCGATCCGGGGTCTGTGTCTGCTTTGGTGCTGTCA 1083
```

**E S331 A: TCT replaced by GCT introducing Alanine mutation, additional 12 nucleotides, but no frame shift**

```
Query 474 TGCCTTTGGCTGGGTCTGAGGCAGGCACAGACACAGACC GCTCCAGAGCACTTGCGG 533
          ||
Sbjct 1190 TG-----CTGAGGCAGGCACAGACACAGACCTCTCCAGAGCACTTAGCG 1237
```

**F S331 D: Aspartic acid mutation and silence proline mutation introduced**

```
Query 495 ACACAGACC GATCCC GAGCACTTGCGCCCCAGCAGGAT 533
          |||
Sbjct 224411 ACACAGACCTCTCCAGAGCACTTAGCGCCCCAGCAGGAT 224449
```

**Figure 4.4. The representative sequences of Ciz1 phospho- sites point mutations.** The point mutations were introduced following CRISPR-Cas9 cut in genomic DNA and ssODN carrying point mutation knock-in via homology directed repair. Introduced mutations in the regions around the PAM site are shown for **A)** T192 Alanine point mutation introduced causing frame shift after PAM. **B)** T192 Aspartic acid mutation introduced. **C)** T293 Alanine introduced with frame shift after PAM. **D)** T293 Aspartic acid introduced with frame shift after PAM. **E)** S331 Alanine introduced. **F)** S331 Aspartic acid point mutation introduced.

ssODN used	Outcome
T192A	1) Frame shift after PAM 2) No change 3) Introduced Alanine mutation + frame shift further in the sequence
T192D	1) No change 2) No change 3) Aspartic acid mutation
T293A	1) CCCC is missing after PAM sequence, replacing Proline with Glutamate + frame shift 2) Alanine mutation introduced + frame shift after PAM 3) Alanine mutation introduced + frame shift after PAM
T293D	1) Aspartic acid mutation introduced + frame shift after PAM 2) Aspartic acid mutation introduced + frame shift after PAM 3) GG missing, Threonine is missing + frame shift after PAM
S331A	1) Introduced Alanine and silent Leucine mutation + 12 nucleotides, but no frame shift 2) No change 3) Recombination with chromosome 11
S331D	1) Frame shift 2) Aspartic acid mutation + frame shift after PAM 3) AGCT looped in creating frame shift, CTC -> CGA mutation causing Leu to Arg mutation, AGA -> CGA mutation causing silent Arg mutation

**Table 4.1. Summary of point mutations introduced by homology directed repair.**

The point mutations were introduced following CRISPR-Cas9 cut in genomic DNA and ssODN carrying point mutation knock-in via homology directed repair. The Ciz1 phosphorylation sites that were replaced by Alanine or Aspartic acid were T192, T293, and S331. The PCR amplified regions spanning the mutation sites were cloned into TOPO10 Blunt cloning vector and transformed into Top10 competent cells. The plasmids were sequenced using M13 forward and reverse primers.

Overall, the homology directed repair introduced significant mutations in the process of knocking-in the ssODN sequence into genomic DNA. In each case, the sequencing results revealed that the desired mutation was not produced. In many cases there were unintended mutations or frame shifts introduced adjacent to PAM sequences that were not repaired using HDR in an orderly manner. Finally, as we were unable to produce the desired mutations, the further investigation of the role of site specific phosphorylation of Ciz1 was not possible.

#### **4.5. Endogenous Ciz1 stability after translational inhibition**

In order to determine if CDK mediated phosphorylation promotes Ciz1 stability, it is necessary to determine its stability in the absence of protein production. Protein synthesis was inhibited by addition of 50 µg/ml of cycloheximide to murine 3T3 cells and Ciz1 levels were monitored every 4 hours after translation inhibition. This revealed that Ciz1 levels were reduced by 60% after 4 hours and by 90% after 8 hours (Figure 4.5 A and B), indicating that Ciz1 was a labile and dynamic protein.

Next, to determine if Roscovitine (CDK2 inhibitor) or PHA-767491 (DDK inhibitor) enhanced the Ciz1 destabilisation, cells were incubated with both cycloheximide and kinase inhibitors. Roscovitine and PHA-767491 addition did not increase degradation of Ciz1 where Ciz1 production had been prevented (Figure 4.5: C, lane 1). Cycloheximide treatment also reduced cyclin A levels (Figure 4.5: C, lane 3), potentially reducing CDK2 activity in the presence of cycloheximide. Indeed, treatment with cycloheximide alone reduces phosphorylation of Ciz1 at T293, a verified CDK site within Ciz1. Significantly, this phosphorylation site correlates with Ciz1 abundance in synchronised 3T3 cells (Figure 3.3).

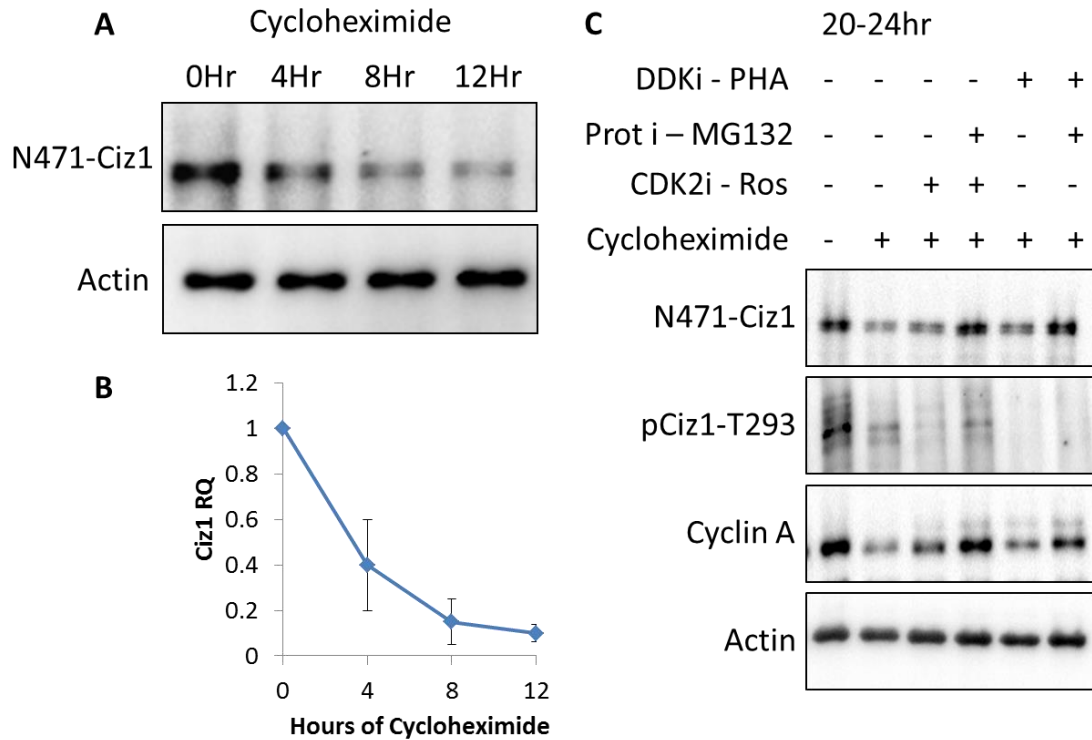


**Figure 4.5. Ciz1 is a labile protein rapidly degraded after translational inhibition. A)** Western blot of asynchronous 3T3 cells that were treated with 50  $\mu\text{g}/\text{ml}$  of translational inhibitor cycloheximide for time points indicated. **B)** Ciz1 protein quantitation against actin loading control, each dot presents the mean  $\pm$  S.D.,  $n=3$ . **C)** WB of synchronised 3T3 were treated with 50  $\mu\text{g}/\text{ml}$  of Cycloheximide, 30  $\mu\text{M}$  of CDK2i - Roscovitine, 10  $\mu\text{M}$  of DDK/CDK2i – PHA-767491, and 10  $\mu\text{M}$  of proteasomal inhibitor MG132 20 – 24 hours after G0 release.

Importantly, inhibition of the proteasome promotes recovery of Ciz1 and cyclin A to similar levels to controls in all contexts. This recovery of Ciz1 and cyclin A by proteasomal inhibition suggests that both proteins are regulated by UPS mediated degradation (Chapter 3).

Overall, this analysis revealed that Ciz1 is labile protein, which could be rapidly degraded after translational inhibition. Inhibition of protein synthesis results in reduced cyclin A levels that correlated with a reduction in CDK mediated phosphorylation of Ciz1 at a potentially key regulatory site T293, leading to a reduction in Ciz1 levels (Figure 4.5: C). However, because of the concomitant cyclin A

and Ciz1 reduction after inhibition of protein synthesis it is difficult to separate the contribution of kinase activity in this context.

#### **4.6. Evaluation of the role of phosphorylation at 4 CDK sites within Ciz1**

To minimise complexity and potential crosstalk between perturbations in CDK activity and Ciz1 levels after inhibition of protein synthesis, the effect of phosphomimetic or non-phosphorylatable mutations within Ciz1 were assessed. Ciz1 has 6 putative phosphorylation sites (T138, T144, T187, T192, T293, and S331), 3 of which have been functionally characterised (T144, T192, and T293) and inhibit Ciz1 DNA replication function when phosphorylated (Copeland et al., 2015). In addition, S331 site, which is phosphorylated early in G1 phase prior to T293 phosphorylation, potentially suggests that it may play a role in Ciz1 stabilisation (Figure 3.3). Whole - plasmid mutagenesis was performed on a GFP – E-Ciz1 construct in order to introduce alanine or aspartic acid mutations in either S331 site or T144, T192, T293, and S331 sites in combination (Appendix 1).

The transfection of Ciz1 has been associated with cell cycle arrest in other studies. To ensure that the expression levels of Ciz1 were low at the point of cycloheximide treatment a time course of expression was performed (Figure 4.6: A). This enables comparison of the expression kinetics of Ciz1 and its mutants post-nucleofection. Transfection using the nucleofection approach (LONZA) promotes expression of exogenous genes more quickly than lipid based approaches. The GFP –Ciz1/ AAAA/ DDDD mutants were expressed in 3T3 as early as 6 – 8 hours after transfection with a comparable intensity (Figure 4.6: A).

Initial experiments 24 hours after transfection showed no discernible differences in Ciz1 stability after protein synthesis has been inhibited (Figure 4.6: B). This was different from endogenous Ciz1 degradation after cycloheximide that was reduced by approximately 80% after 8 hours of translational inhibition (Figure 4.5: A and B). Similarly inhibition of CDK2 activity also revealed no differences in Ciz1 stability with concomitant inhibition of protein synthesis with cycloheximide (Figure 4.5: C, 4.6: C).

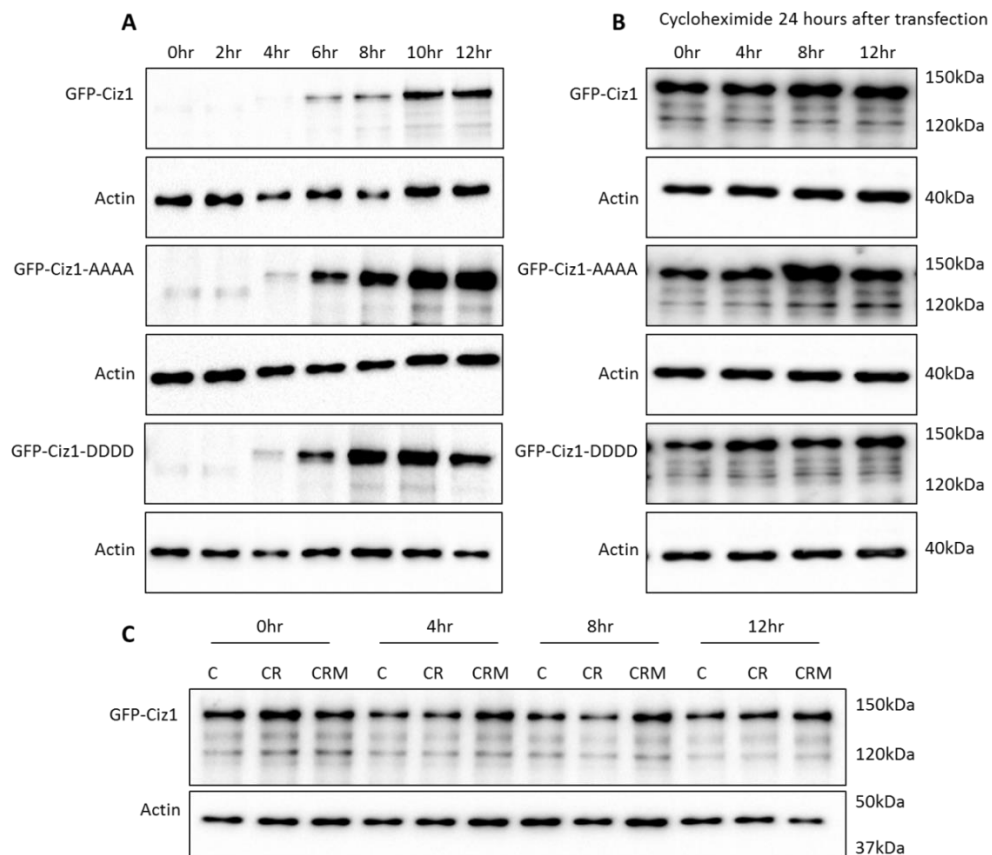


**Figure 4.6. GFP – E-Ciz1/ -AAAA/ -DDDD overexpression profile.** **A)** Asynchronous 3T3 were transfected with GFP-E-Ciz1, GFP-E-Ciz1-AAAA (T144A, T192A, T293A, and S331A), and GFP-E-Ciz1-DDDD (T144D, T192D, T293D, and S331D) plasmids using nucleofector technology. Western blot analysis of cells harvested every 2 hours after transfection, probed with anti-N471 antibody. **B)** Transfected cells were treated with 100 µg/ml of cycloheximide at 24 hours after transfection. Protein levels were determined by western blotting at time points indicated. **C)** GFP-E-Ciz1 transfected cells were treated with 100 µg/ml of cycloheximide (labelled as C), 30 µM of CDK2i Roscovitine (CR), and 10 µM of proteasomal inhibitor MG132 (CRM) 24 hours after transfection for the time intervals indicated. Protein levels were determined by western blotting after 0, 4, 8, and 12 hours of drug treatment.

#### **4.7. Analysis of GFP – E-Ciz1/ S331A/ S331D stability**

To prevent overexpression of Ciz1 from potentially affecting the ability of the UPS to degrade Ciz1, the time point when exogenous protein was readily expressed but had not plateaued was used to prevent saturation of the UPS for degradation of Ciz1. In order to determine whether the early phosphorylation of Ciz1 at S331 site contributes to its stability and accumulation in G1 phase, alanine and aspartic acid mutations were introduced in S331 site of GFP – E-Ciz1. The GFP – E-Ciz1, 8 hours after transfection, was rapidly degraded down to approximately 30% after 6 hours of cycloheximide treatment (Figure 4.7) that was consistent with endogenous Ciz1 degradation (Figure 4.5). These data indicate that high levels of exogenous protein at 24 hour after transfection impaired the efficiency of Ciz1 degradation (Figure 4.6: B). This may be due to cell cycle arrest, inactivated UPS, or GFP-Ciz1 levels being too high to be affected by 100 µg/ml of cycloheximide.

The results revealed that both mutations reduced the rate of Ciz1 degradation. This suggests that mutation of S331 may cause a structural change that affects recognition by the UPS. Additionally, it may propose that S331 site is not responsible for Ciz1 stabilisation and the early phosphorylation might simply mean that S331 site is phosphorylated by the early activated kinases, such as Cyclin E – CDK2.

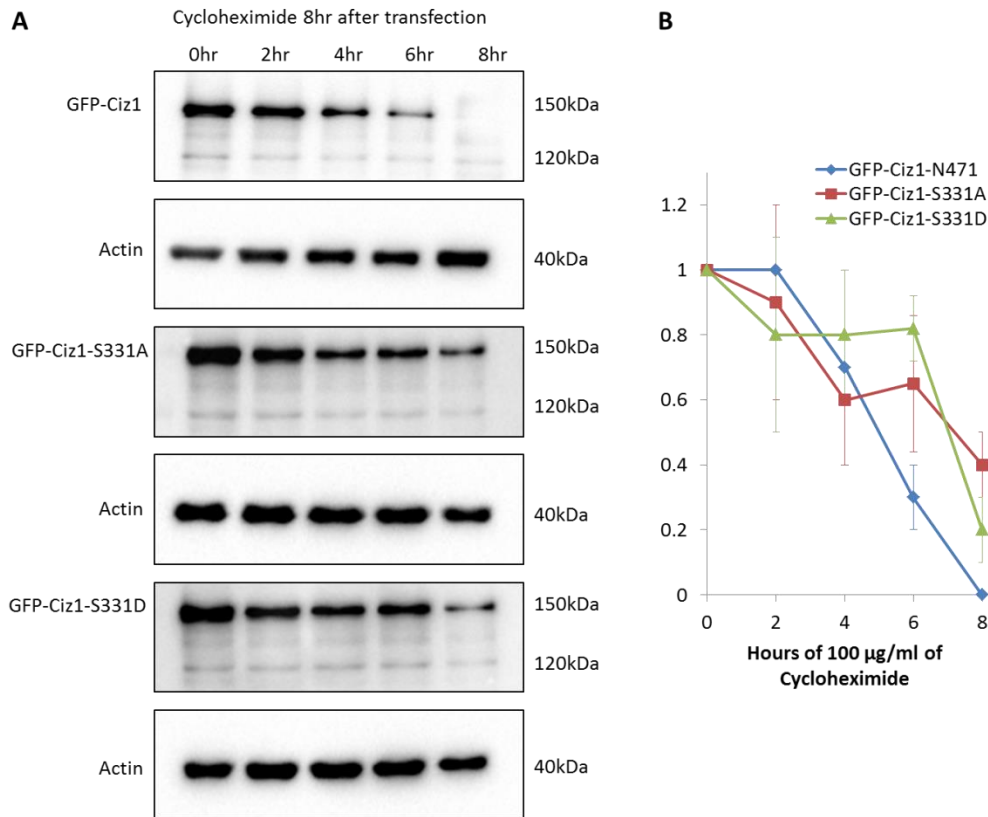


**Figure 4.7. Both GFP-E-Ciz1-S331A and -S331D reduced protein degradation. A)** 3T3 cells were treated with 100 µg/ml of Cycloheximide 8 hours after transfection with GFP – E-Ciz1, -S331A, and -S331D plasmids. Western blot analysis of cells harvested every 2 hours after translational inhibitor treatment 0 – 8 hours. **B)** Protein quantitation against actin loading control, each dot presents the mean ± S.D., n=3.

#### 4.8. Phospho-mutant stability after translational inhibition

Analysis of the S331 site alone did not result in a differential effect for non-phosphorylatable or phosphomimetic mutations. Next, to evaluate all of the key regulatory sites identified within Ciz1, 4 phosphorylation sites were mutated to either alanine or aspartate to determine the relative stability of GFP – E-Ciz1, -AAAA, and -DDDD. Cells were transfected with each construct and cycloheximide was administered 8 hours after transfection when exogenous protein was already expressed and detectable (Figure 4.6: A). The 8 hour time course after translational inhibition revealed that GFP – E-Ciz1 was more readily degraded than GFP – E-Ciz1 –

AAAA or -DDDD mutated protein (Figure 4.8). This suggested that unphosphorylatable (-AAAA) and phospho-mimetic (-DDDD) mutations both stabilised Ciz1. These observations are not entirely consistent with the previous findings; however, it may have exposed an underlying problem with this approach. The extensive mutations may have changed protein conformation or interactions, this way slowing down its degradation. In addition, an alternative possibility is that results could have been confounded by different levels of expression that was not determined in this experimental setting.

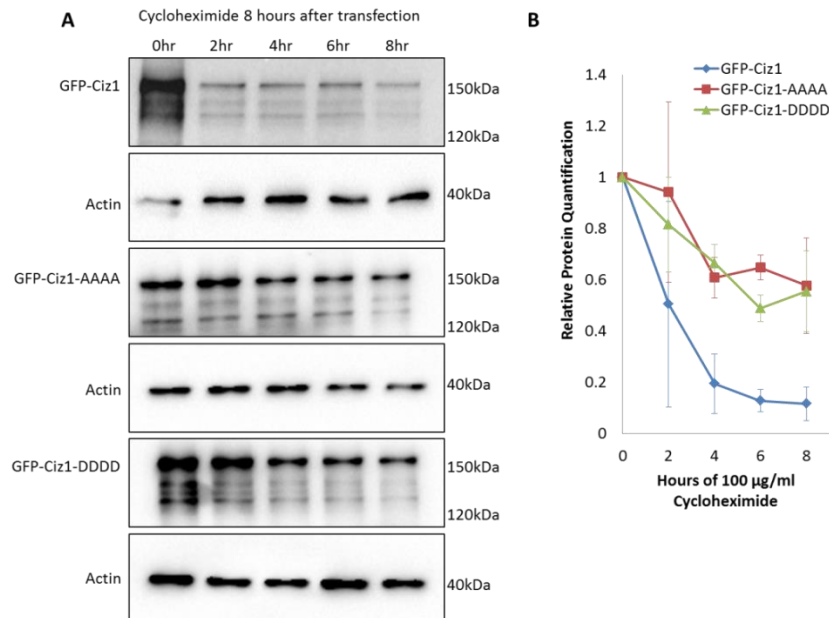


**Figure 4.8. GFP – E-Ciz1 is more prone to degradation than GFP – E-Ciz1 –AAAA or –DDDD.** 3T3 cells were treated with 100 µg/ml of Cycloheximide 8 hours after transfection with GFP – E-Ciz1, -AAAA, and -DDDD plasmids. **A)** Western blot analysis of cells harvested every 2 hours after translational inhibitor treatment 0 – 8 hours. **B)** Quantitation of exogenous GFP - Ciz1/ -AAAA/ -DDDD protein after Cycloheximide treatment against loading control Actin, 0 hour is plotted as relative 1, each dot presents the mean ± S.D., n=3.

Additionally, full length murine Ciz1 has 14 CDK phosphorylation sites (Copeland et al., 2015), and any of them could be responsible for endogenous Ciz1 stabilisation observed from small molecule chemical kinase inhibitor experiments. Therefore,

selecting 4 putative CDK phosphorylation sites may have not included the sites responsible for Ciz1 stability and accumulation that was observed in endogenous experiments (Chapter 3).

#### **4.9. Discussion**

Overall, the site directed mutagenesis (SDM) in exogenous GFP – E-Ciz1 and CRISPR-Cas9 mediated point mutation in genomic Ciz1 DNA did not produce conclusive results. Both of the methods require improvement and development, such as analysing each phosphorylation site individually in case of SDM, and advancing in ssODN introduction and screening methodology in CRISPR-Cas9 technique.

CRISPR-Cas9 technique has been described as a precise genome editing using single stranded template with desired point mutation. However, all clones contained unintended mutations, with either deletion or insertion events present. These events may be caused by re-cutting of the same DNA strand by left-over active Cas9 and repair by non-homologous end joining (NHEJ) (Cong et al., 2013; Inui et al., 2014; Kwart et al., 2017; Mali et al., 2013; Paquet et al., 2016). Therefore, the screening approach was able to identify clones with the desired insertion that was followed by insertion or deletion, thus introducing frameshift in the sequence and truncation in the protein (Figure 4.4 and Table 4.1).

There are methods to avoid re-cutting events including introduction of a Cas9 blocking mutation together with the point mutation of interest (Inui et al., 2014; Paquet et al., 2016). This may prevent the re-repair event of already successfully introduced template sequence. Moreover, the HDR is very rare in mammalian cells; therefore, introducing two successful point mutations in two different alleles in the

single cell is highly unlikely (Paquet et al., 2016). This may be improved by having desired point mutation very close to double strand break introduced by Cas9 (3 – 5 nucleotides after PAM sequence) (Kwart et al., 2017), but this is restricted due to the availability of a suitably positioned PAM sequence. The efficiency of a successful HDR reduces by 50 % when the point mutation is located 10 nucleotides from the cutting site (Kwart et al., 2017; Paquet et al., 2016; Richardson et al., 2016).

CRISPR-Cas9 technology is being developed and strategies for site directed mutagenesis are being evolved, there are a number of ways the knock-in of point mutations in Ciz1 gene could be improved. First, the means of screening could be advanced by adding small tag like HA next to desired point mutation in ssODN, or additional antibiotic resistant cassette could be incorporated in ssODN (Hruscha et al., 2013). This would allow the faster and more efficient screening for positive clones, even though not increasing the recombination efficiency. Further, chemically enhancing HDR by stimulating RS-1 or inhibiting SCR-7 (Song et al., 2016) could be a way of producing more positive clones for screening; however, it would not prevent the errors introduced by HDR or second cutting by Cas9. Additionally, chemical modifications of ssODN, such as phosphorothioate linkages at the ends of ssODNs have been shown to increase HDR efficiency and fidelity (Prykhozhij et al., 2017). Moreover, the asymmetric (36-90nt) anti-sense ssODN was shown to be more readily incorporated in genomic DNA (Richardson et al., 2016).

One of the main reasons why characterising Ciz1 phosphorylation sites individually has proven to be complicated is that the murine Ciz1 possesses 14 putative CDK2 phosphorylation sites and a number of DDK sites as well (Copeland et al., 2015). The

chemical kinase inhibition and genetic depletion of kinase regulators prevented general phosphorylation of Ciz1 on multiple sites. Knowing that kinases collaborate and enhance each other's efficiency (Montagnoli et al., 2006; Pisu et al., 2015; Wan et al., 2008), the extensive lack of phosphorylation may have been the reason of the reduced Ciz1 stability and accumulation, rather than the phosphorylation of one specific site. Additionally, there are 10 sites that have not been evaluated in this work, which may include the regulatory sites that prevent UPS mediated degradation. In addition, there is also a formal possibility that CDK2 and DDK are not directly affecting Ciz1 stability by phosphorylating Ciz1. Phosphorylation of a component of the proposed UPS regulator could regulate its activity or substrate specificity. Further work is required to determine how CDK and the UPS contribute to regulation of Ciz1 stability.

# **Chapter 5**

## **Characterisation of the differential activities of Cdc7-Dbf4 (DDK) inhibitors XL-413 and PHA-767491**

## **5. Characterisation of the differential activities of Cdc7-Dbf4 (DDK) inhibitors XL-413 and PHA-767491**

Since the discovery that the first oncogene was a protein kinase in 1970s, the research on kinase inhibition as a potential therapy has developed significantly (Bhullar et al., 2018; Collett and Erikson, 1978). The use of kinase inhibitors as a therapy was initially criticised due to off-target and toxic effects, acquired drug resistance, and a lack of specificity and selectivity due to the structural conservation of kinases (Davies et al., 2000; Fabbro et al., 2015; Noble et al., 2004). The human kinome consists of approximately 538 kinases and 99 % of kinase inhibitors under investigation today compete for ATP binding site (Breen and Soellner, 2015). This site is highly conserved across 518 human kinases, thus making it challenging to achieve high selectivity and specificity for small molecule inhibitors (Zhang et al., 2009).

However, the discovery of highly selective kinase inhibitors Imatinib and Desatinib for the treatment of BCR-ABL driven acute myeloid leukaemia (AML) and the significant clinical efficacy of this approach has fuelled further interest in small molecule kinase inhibitors (Bhullar et al., 2018; Lombardo et al., 2004; Shah et al., 2004). Currently, there are 37 FDA approved small molecule kinase inhibitors, 31 are used in cancer therapy (Bhullar et al., 2018). Further, more than 150 small molecule kinase inhibitors are in clinical trials and this accounts for 25% of all pharmaceutical research and development performed at present (Bhullar et al., 2018; Klaeger et al., 2017; Knight and Shokat, 2005; Zhang et al., 2009).

The use of small molecule Cdc7 inhibitors has enabled interrogation of the role of DDK in regulation of DNA replication origin activation. In *Xenopus* cell free DNA

replication systems, PHA-767491 blocks helicase activation step, thereby blocking initiation of DNA replication (Poh et al., 2014). PHA-767491 specifically inhibits the initiation phase of DNA replication, but does not inhibit the elongation phase of DNA synthesis (Montagnoli et al., 2008). Both PHA-767491 and XL-413 affect replication fork progression (Rainey et al., 2017; Rodriguez-Acebes et al., 2018), but by differing mechanisms. PHA-767491 inhibits initiation of DNA replication; whereas, XL-413 affects fork progression without affecting initiation of DNA replication (Alver et al., 2017). Importantly, chemical biology approaches using an analogue sensitive Cdc7 mutant (Cdc7as) showed that Cdc7 is an essential gene that is required to phosphorylate the MCM2-7 helicase, and to promote initiation of DNA replication (Rainey et al., 2017). This phenotype was achieved with very high XL-413 concentrations; however, still failed to explain the reduction in replication fork speed seen after the XL-413 challenge.

Consistent with its role in promoting cell cycle progression, Cdc7 is commonly overexpressed in breast, colon, and lung tumours (Bonte et al., 2008; Montagnoli et al., 2008). Therapeutic targeting of Cdc7 may be an approach in cancer therapy, as Cdc7 inhibition selectively kills cancer cells without promoting apoptosis in healthy cells (Montagnoli et al., 2004; Montagnoli et al., 2010). DDK inhibition promotes cell cycle arrest in normal cells and increases apoptosis in cancer cell lines and xenograft models (Jin et al., 2018; Natoni et al., 2011; Natoni et al., 2013). However, there are distinct differences in potency of the DDK inhibitors PHA-767491 and XL-413 in cancer cell lines. XL-413 displays higher affinity for DDK. Atomic structures for PHA-767491 and XL-413 bound to DDK revealed more contacts between XL-413 and DDK providing a molecular basis for its improved potency and selectivity (Hughes et al.,

2012). XL-413 is a potent inhibitor of Colo-205 proliferation *in vitro* and in xenograft models (Koltun et al., 2012), but its activity is limited in other cancer cell lines relative to PHA-767491 (Sasi et al., 2014). Comparison of PHA-767491 and XL-413 in cancer cells lines suggest that differences in potency may be related to bioavailability or specificity (Montagnoli et al., 2008; Natoni et al., 2011; Natoni et al., 2013; Sasi et al., 2014).

The effect of the pyrrolopyridine PHA-767491 on Ciz1 stability was significant and correlated with that of CDK2 inhibitors (Chapter 3). Therefore, the second selective Cdc7 inhibitor (XL-413), which has a different chemical backbone was selected to confirm that the effect was due to DDK inhibition (Koltun et al., 2012). The benzofuropyrimidinone XL-413 shares similar inhibition potency and affinity towards Cdc7 with PHA-767491 (Rainey et al., 2017; Sasi et al., 2014). However, in Ciz1 stability studies, PHA-767491 consistently reduced Ciz1 levels, whereas XL-413 had no significant effect (Chapter 3). In addition, PHA-767491 was more efficient in inhibiting cell cycle than XL-413. PHA-767491 was found to reduce Ciz1 phosphorylation on the CDK specific (S/TPxK/R) threonine 293 (Copeland et al., 2015) and cyclin A levels (Figure 3.6). To further investigate the differences in activity, the effect of PHA-767491 and XL-413 were evaluated in normal 3T3 fibroblasts.

### **5.1. PHA-767491 and XL-413 display different effects on cell cycle progression**

PHA-767491 and XL-413 are Cdc7-Dbf4 (DDK) inhibitors with similar inhibitory constants for DDK *in vitro* (IC<sub>50</sub> 10 nM and 3.4 nM respectively) (Hughes et al., 2012; Koltun et al., 2012; Vanotti et al., 2008), but with distinct effects on DNA replication and cancer cells (Rainey et al., 2017; Sasi et al., 2014). This raised the question

whether PHA-767491 and XL-413 displayed differential activities due to PHA-767491 having additional off target effects. Therefore, thorough analysis of the cell cycle progression after PHA-767491 and XL-413 treatment was performed (Figure 5.1).

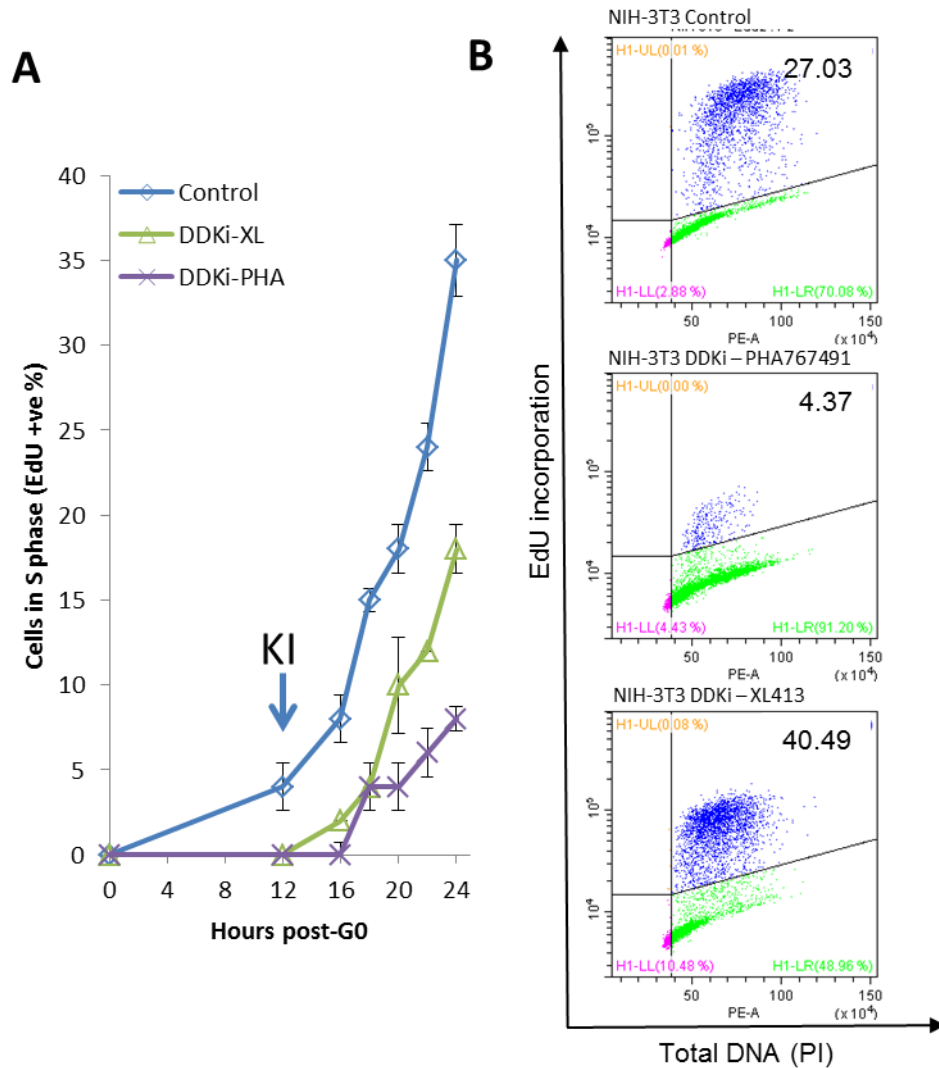


**Figure 5.1. Different effect of PHA-767491 and XL-413 on cell cycle progression. A)** 3T3 cells were synchronised in G0 and treated with 10  $\mu$ M of PHA-767491 (PHA) and 10  $\mu$ M of XL-413 (XL) 12 - 24 hours after release. Cells were pulse labelled with EdU 30 minutes prior each time point indicated. S phase cells were quantified using confocal fluorescence microscopy DAPI stained total nuclei and expressed as percentage. Data show mean  $\pm$  S.D., where n=6. Blue arrow shows the time point (12 hours) of kinase inhibitor (KI) treatment. **B)** Multiparameter flow cytometry dot plot of asynchronous NIH-3T3 were treated with 10  $\mu$ M of PHA-767491 and 10  $\mu$ M of XL-413 for 24 hours, pulse labelled with EdU showing replicating DNA (y axis), fixed and counter-stained with propidium iodide (PI) showing total DNA (x axis). Numbers on the chart show proportion (%) of S phase cells for each condition.

Both kinase inhibitors reduced S phase entry in synchronised 3T3 cells re-entering the cell cycle from quiescence with PHA-767491 reducing S phase cells by 80 % and XL-413 by 50 % (Figure 5.1: A). This observation was verified by addition of both DDK inhibitors to asynchronous NIH-3T3 cells for 24 hours. Cells were pulse labelled with EdU and analysed by flow cytometry (Figure 5.1: B). The analysis showed that PHA-767491 reduced S phase entry by 70-80 % for NIH-3T3. However, XL-413 treatment increased the total amount of cell in S phase by 40 % (Figure 5.1: B, lane 3). This may indicate less efficient progression through S phase leading to an enrichment of cells in S phase and demonstrated that S phase entry is not inhibited by XL-413. Interestingly, flow cytometry after XL-413 treatment revealed reduced EdU - Alexa Fluor 488 fluorescence intensity relative to control cells, consistent with less DNA replication. Other studies, that have investigated the effects of XL-413 on DNA replication fork progression, found that reduced replication rates were compensated by the increased number of origins fired and potentially increased replication fork length (Montagnoli et al., 2008; Rainey et al., 2017). Overall, EdU incorporation analysis revealed the distinct effects for PHA-767491 and XL-413 with respect to the cell cycle progression and the proportion of cells entering the S phase.

## **5.2. PHA-767491 and XL-413 efficiently reduce DDK activity, but only PHA-767491 reduces CDK2 activity**

In order to explore why PHA-767491 was more efficient in inhibiting replication origin firing than XL-413, key DDK mediated phosphorylation events that regulate helicase activation were monitored. The phosphorylation of MCM2 at pS53 is mediated by DDK and is a key regulatory site for the activation of MCM2-7 helicase

activity (Montagnoli et al., 2006). In addition, a second DDK/CDK site, pS40/pS41 (Tsuji et al., 2006), was monitored during the G1 – S transition (Figure 5.2).

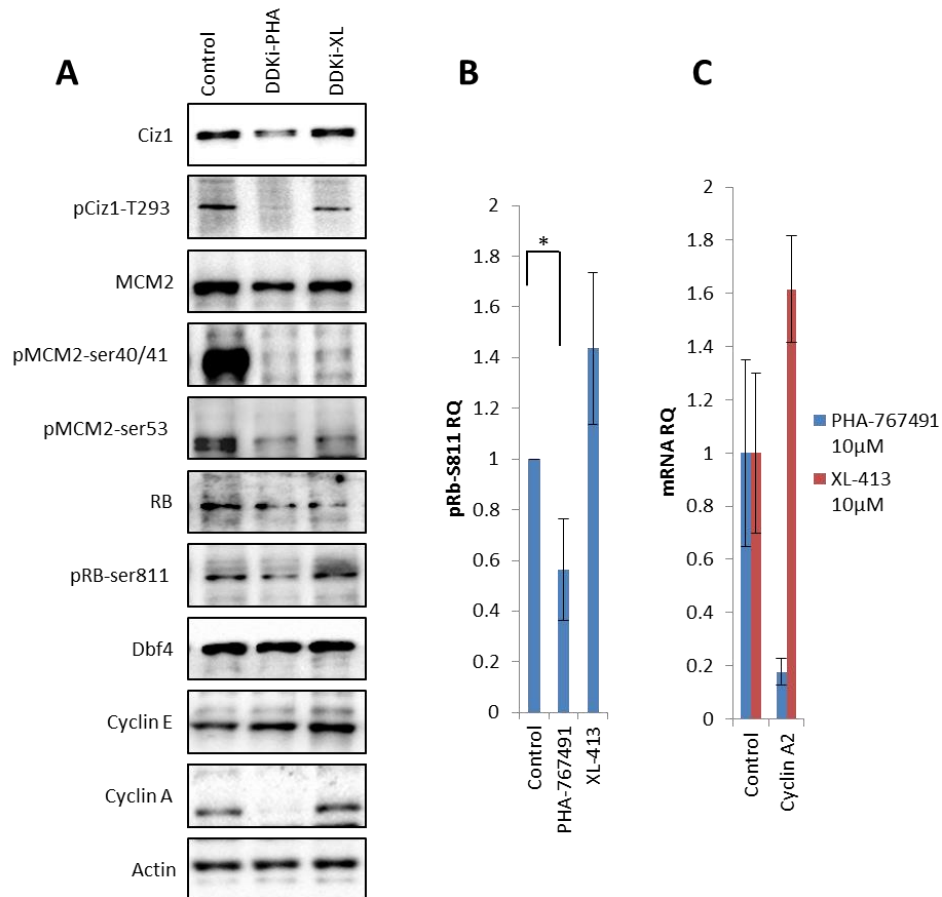


**Figure 5.2. Distinct PHA-767491 and XL-413 activities in Rb phosphorylation. A)** 3T3 cells were synchronised in G0 and treated with 10 µM of PHA-767491 and 10 µM of XL-413 from 12 - 20 hours after release. Western blot probed with Ciz1, p-Ciz1-T293, MCM2, pMCM2-ser40/41, pMCM2-ser53, Rb, pRb-ser811, Dbf4, Cyclin E, Cyclin A, and Actin antibodies. **B)** The quantitation of pRb-ser811 relative to total Rb control. Bar chart presents mean ± S.D., n=3. Significance measured using paired two-tailed Student’s T-test, (\*) p≤0.05. **C)** RT-qPCR analysis of E2F transcript cyclin A2 after 12-20 hour kinase inhibition. Transcript levels are displayed relative to GAPDH, bars present mean ± S.D., n=3 each with 3 technical repeats.

Both inhibitors reduced MCM2 phosphorylation with PHA-767491 being slightly more potent. This suggests that both inhibitors PHA-767491 and XL-413 were effective in inhibiting DDK specific phosphorylation of MCM2 at sites pS40/41 and pS53. Importantly, Ciz1 and cyclin A protein levels were significantly reduced by PHA-

767491 treatment relative to control and XL-413 treated cells. Ciz1 accumulation correlates with cyclin A expression (Figure 3.1) and cyclin A phosphorylation of T293-Ciz1 is closely linked with total Ciz1 levels (Figure 5.2, 5.3, 3.6, and 3.7). The correlation between Ciz1 levels and cyclin A levels may be related to a reduction in cyclin A-CDK2 activity that is required for the accumulation of Ciz1 (Figure 3.3). Cyclin A levels are transcriptionally regulated by Rb-E2F pathway. As CDK mediated phosphorylation of Rb is required for E2F mediated transcription of cyclin A2 (Bertoli et al., 2013b; Mittnacht, 1998), this suggests that PHA-767491 may target CDK2 activity in addition to DDK. Importantly, the data demonstrated a reduction in Rb phosphorylation at CDK site S811 in PHA-767491 treated cells (Figure 5.2: A, B). This is consistent with previously demonstrated PHA-767491 targeting of multiple kinases, such as Cdc7, CDK9, and CDK2 (Montagnoli et al., 2008; Natoni et al., 2011; Natoni et al., 2013; Vanotti et al., 2008). Conversely, XL-413 treatment did not significantly affect Ciz1, cyclin A or Rb phosphorylation (Figure 5.2: lanes 1, 7, and 10). Therefore, XL-413 and PHA-767491 have distinct activities that differentially affect CDK signalling networks by inhibition of Rb phosphorylation at S811. The reduction in cyclin A levels suggests that PHA-767491 may inhibit CDK2 activity thereupon affecting Ciz1 accumulation. This was not observed after XL-413 treatment consistent with a more specific inhibitory activity of XL-413 with fewer off target effects (Koltun et al., 2012).

In order to determine whether PHA-767491 influences cyclin A2 transcription, synchronous 3T3 cells were treated with PHA-767491 and XL-413 12–20 hours after release. This revealed that PHA-767491 reduced cyclin A2 transcription by at least 90% (Figure 5.2: C, blue bars). The combination of a reduction in Rb phosphorylation

and reduced transcription of cyclin A2 suggests that PHA-767491 may be inhibiting CDK2 activity and thereby reduces E2F mediated transcription. This off-target activity of PHA-767491 has been noted previously with an *in vitro* IC50 of 200 nM for CDK2 (Montagnoli et al., 2008).

### **5.3. PHA-767491 is a potent DDK and CDK2 inhibitor**

In order to determine the potency of PHA-767491 in inhibiting CDK2 during G1 phase, DDK inhibitors PHA-767491 and XL-413 were titrated between 1 - 10  $\mu$ M. 10  $\mu$ M of PHA-767491 inhibited phosphorylation at DDK phospho-sites pS40/41 and pS53 of MCM2 as well as on CDK2 phospho-site S811 of Rb (Figure 5.3). However, 1 and 5  $\mu$ M of PHA-767491 did not reduce Rb phosphorylation significantly (Figure 5.3: B). In comparison, XL-413 reduced phosphorylation of pS40/41 and pS53 in MCM2, but did not affect Rb phosphorylation. In addition, PHA-767491 reduced phosphorylation of Ciz1 at the CDK specific site T293 and also reduced total Ciz1 levels at 5 and 10  $\mu$ M. However, Ciz1 levels and phospho-T293 level were not affected by XL-413 treatment (Figure 5.3: A, lanes 1 and 2). Similarly, PHA-767491 significantly reduced levels of cyclin A at concentrations greater than 1  $\mu$ M (Figure 5.3: A, lane 10), which was striking relative to XL-413 that did not affect cyclin A. Additionally, PHA-767491 was more potent (5 – 10  $\mu$ M) in preventing MCM2 phosphorylation on S40/41 site (Figure 5.3: A, lane 4), potentially through dual inhibition of DDK and CDK2 that is required for phosphorylation of S40 and S41 respectively. These data are consistent with the notion that PHA-767491 acts on both DDK and CDK2 kinases, leading to a greater reduction in S40/41 phosphorylation than that exhibited by XL-413 inhibitor. The data here suggest that

PHA-767491 may be a potent DDK and CDK2 inhibitor effective in a low concentration range (1 - 10  $\mu$ M).

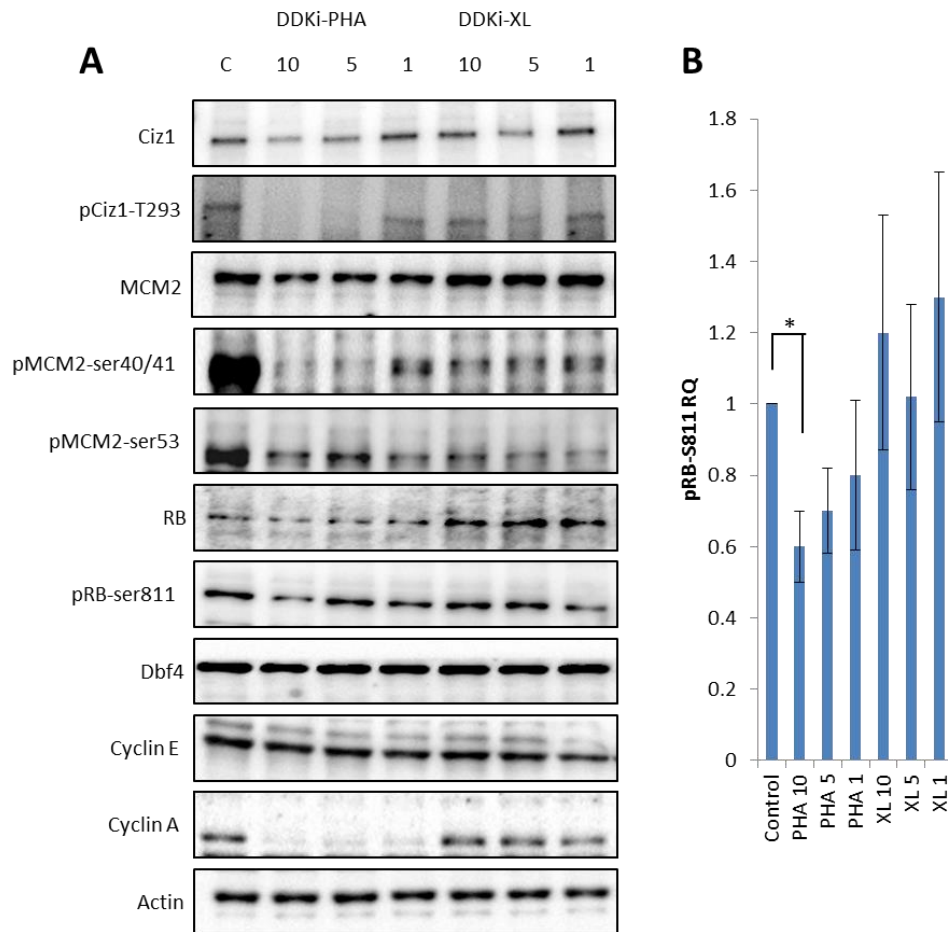


**Figure 5.3. PHA-767491 is a potent DDK and CDK2 inhibitor.** **A)** Synchronised 3T3 were treated 12 – 20 hours after G0 release. WB of cells after 8 hours of 1, 5, and 10  $\mu$ M PHA-767491 and XL-413 treatment, probed with Ciz1, pCiz1-T293, MCM2, pMCM2-ser40/41, pMCM2-ser53, Rb, pRb-ser811, Dbf4, Cyclin E, Cyclin A, and Actin antibodies. **B)** pRB-ser811 protein quantitation relative to total Rb protein control, taking control as relative 1. Bars present mean  $\pm$  S.D., n=3. Significance was measured by paired two-tailed Student’s T-test, (\*)  $p \leq 0.05$  for 10  $\mu$ M PHA-767491 vs. control.

#### 5.4. PHA-767491 displays a similar inhibitory activity to classical CDK2 inhibitors

##### Roscovitine and CVT-313

To determine whether PHA-767491 is inhibiting CDK2 activity and Rb-E2F mediated transcriptional regulation, PHA-767491 and XL-413 were directly compared with

CDK2 inhibitors Roscovitine and CVT-313. CDK2 inhibition has been shown to inhibit Rb phosphorylation, thus reducing E2F mediated transcription of cyclins in G1 phase (Bertoli et al., 2013b; Leone et al., 1999). Using synchronised 3T3 cells that were treated with PHA-767491, XL-413, Roscovitine, and CVT-313 from 12 – 20 hours after release from quiescence, showed that PHA-767491 reduced MCM2 phosphorylation on S40/41 with the same efficiency as Roscovitine and CVT-313 (Figure 5.4).

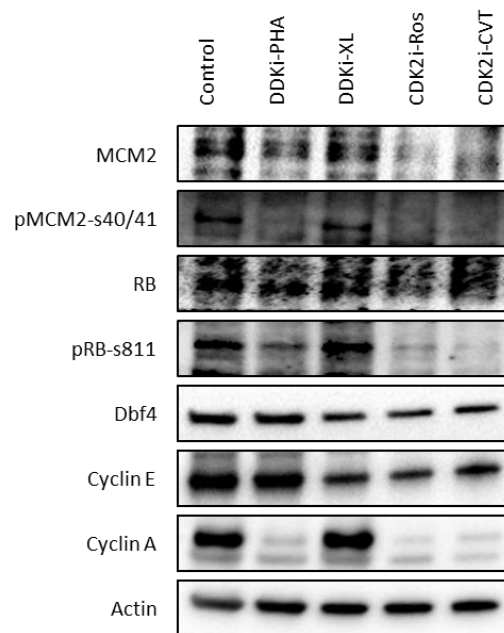


**Figure 5.4. PHA-767491 inhibits Rb phosphorylation and cyclin A expression consistent with inhibition of CDK2.** Western blot analysis of synchronised 3T3 cells treated with 10  $\mu$ M of PHA-767491, 10  $\mu$ M of XL-413, 30  $\mu$ M of Roscovitine, and 10  $\mu$ M of CVT-313 12 – 20 hours after G0 release probed with MCM2, pMCM2-ser40/41, pMCM2-ser53, Rb, pRb-ser811, Dbf4, Cyclin E, Cyclin A, and Actin antibodies.

However, the effect of XL-413 was limited, possibly due to targeting only the S40 site. In addition, MCM2 levels were reduced by PHA-767491, Roscovitine, and CVT-313 as seen elsewhere (Thacker, 2017). The reduction in MCM2 levels may contribute to the reduction in pS40/41 and pS53 observed by western blotting (Figure 5.4). This analysis also revealed that PHA-767491 inhibited Rb phosphorylation on S811 site,

and completely abolished cyclin A expression, consistent with the CDK2 inhibitors Roscovitine and CVT-313 (Figure 5.4). This indicates that PHA-767491 inhibitory activity mirrors those of CDK2 inhibitors. Importantly these effects are not seen after XL-413 treatment highlighting their differential activities.

### **5.5. PHA-767491 inhibits E2F-Rb mediated transcription consistent with off target CDK2 inhibition**

The principle difference in activity between PHA-767491 and XL-413 appears to be related to the regulation of the Rb-E2F pathway (Figure 5.2-5). This activity may be related to the increased potency of PHA-767491 preventing cell cycle progression from G1 to S phase that were not observed with XL-413 (Figure 5.1). To directly determine if PHA-767491 inhibits Rb-E2F transcription, synchronised pre-restriction point 3T3 cells were treated with 1, 5 or 10  $\mu$ M of PHA-767491, XL-413, and compared with CDK2 inhibitors CVT-313 and Roscovitine. The E2F regulated transcripts: cyclin E1, cyclin E2, and cyclin A2, were quantified with specific Taqman probes using RT-qPCR (Figure 5.5).

The results were consistent to the published IC50 values of kinase inhibitors. CVT-313 inhibits CDK2 with IC50 of 500 nM (Brooks et al., 1997), Roscovitine – 650 nM (Lauren, 1997), and PHA-767491 – 200 nM (Hughes et al., 2012; Montagnoli et al., 2008). The analysis revealed that PHA-767491 was as efficient as CDK2 inhibitors in reducing cyclin transcription at high concentrations (10  $\mu$ M) (Figure 5.5: left column), it was comparable with CVT-313 at mid concentrations (5  $\mu$ M) (Figure 5.5: middle column); however, Roscovitine seemed to be less effective at its mid concentration (15  $\mu$ M) to that of PHA-767491 or CVT-313. Only CVT-313 was able to inhibit E2F

transcription at 1  $\mu\text{M}$  concentration (Figure 5.5: right column), possibly due to being highly selective for CDK2, thus even low concentration of CVT-313 was sufficient to inhibit E2F transcription (Brooks et al., 1997). XL-413 did not significantly reduce E2F regulated transcription (Figure 5.5).

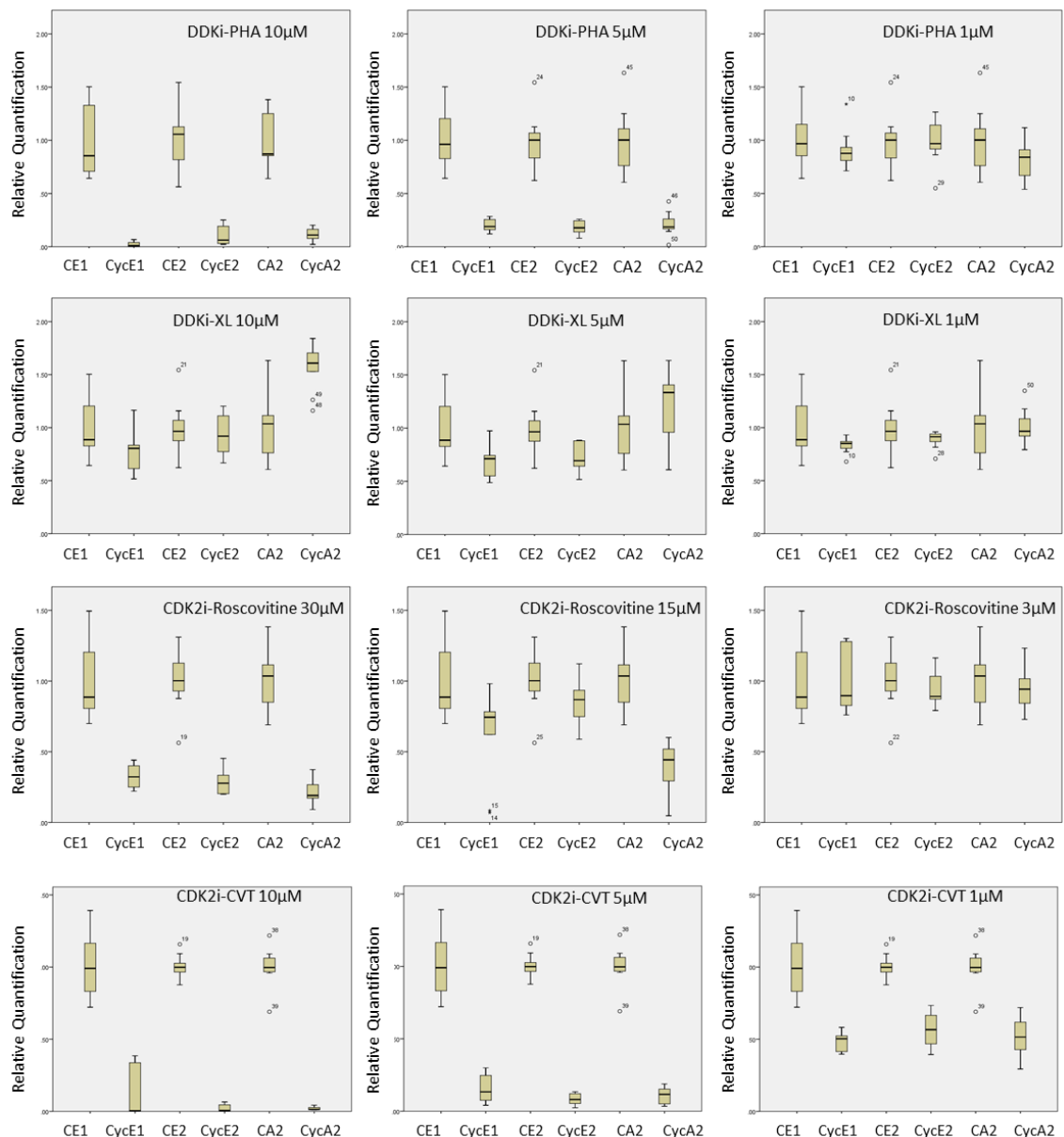


**Figure 5.5. PHA-767491 is a potent E2F-Rb transcriptional pathway inhibitor.** 3T3 cells were synchronised and treated with 1, 5, and 10  $\mu\text{M}$  of PHA-767491, XL-413, CVT-313, and 3, 15, and 30  $\mu\text{M}$  of Roscovitine 12 – 20 hours post – G0. RT-qPCR analysis of cyclin E1, E2, and A2 relative to GAPDH. Box-and-whisker plots showing mean, upper and lower quartiles, whiskers showing maximal and minimal values, and asterisks showing outliers outside the range. Data shown are 3 experimental replicates consisting of 3 technical repeats per experiment.

PHA-767491 inhibited E2F pathway in the concentration range of 5 - 10  $\mu$ M ( $p < 0.001$ ), Roscovitine at 30  $\mu$ M ( $p < 0.001$ ) and cyclin A2 transcription at 15  $\mu$ M ( $p < 0.001$ ), and CVT-313 in a range of 1 – 10  $\mu$ M ( $p < 0.001$ ) (Table 5.1). Overall, the results revealed that PHA-767491 was a potent CDK2 inhibitor that affected Rb-E2F mediated transcription with similar potency to the CDK2 inhibitors Roscovitine and CVT-313. However, XL-413 did not reduce E2F regulated transcription, displaying a different inhibitory activity to PHA-767491.

Inhibitor treatment 12-20hr post G0 release	Transcript Relative Quantification		
	Cyclin E1	Cyclin E2	Cyclin A2
DDKi PHA-767491 10 $\mu$ M	P<0.001 ***	P<0.001 ***	P<0.001 ***
DDKi PHA-767491 5 $\mu$ M	P<0.001 ***	P<0.001 ***	P<0.001 ***
DDKi PHA-767491 1 $\mu$ M	P=0.977	P=1.000	P=0.689
DDKi XL-413 10 $\mu$ M	P=0.344	P=0.988	P<0.001 ***
DDKi XL-413 5 $\mu$ M	P=1.000	P=0.266	P=0.587
DDKi XL-413 1 $\mu$ M	P=0.589	P=0.889	P=1.000
CDK2i Roscovitine 30 $\mu$ M	P<0.001 ***	P<0.001 ***	P<0.001***
CDK2i Roscovitine 15 $\mu$ M	P<0.05 *	P=0.837	P<0.001***
CDK2i Roscovitine 3 $\mu$ M	P=1.000	P=0.991	P=0.982
CDK2i CVT-313 10 $\mu$ M	P<0.001 ***	P<0.001 ***	P<0.001 ***
CDK2i CVT-313 5 $\mu$ M	P<0.001 ***	P<0.001 ***	P<0.001 ***
CDK2i CVT-313 1 $\mu$ M	P<0.001 ***	P<0.001 ***	P<0.001 ***

**Table 5.1. Statistical analysis of PHA-767491, XL-413, Roscovitine, and CVT-313 in reducing E2F regulated transcription.** Post-G0 3T3 were treated with 1, 5, and 10  $\mu$ M of PHA-767491, XL-413, CVT-313, and 3, 15, and 30  $\mu$ M of Roscovitine 12 – 20 hours. The transcription was analysed with RT-qPCR relative to GAPDH. The significance of cyclin E1, E2, and A2 transcription after drug treatment vs. control was measured using SPSS, One-Way ANOVA, Post-Hoc Tukey, analysis, where n=3 experimental replicates, each with 3 technical repeats.

The results shown here demonstrate that XL-413 is a selective DDK inhibitor and does not have off-target effects via inhibition of CDK2 (Figure 5.2 and 5.3) or E2F mediated transcription (Figure 5.5). The analysis also suggests that CVT-313 is more potent CDK2 inhibitor than the earlier generation Roscovitine, consistent with

published IC50 values and selectivity for CDK2 (Brooks et al., 1997; Lauren, 1997). In addition, PHA-767491 is more effective CDK2 inhibitor than Roscovitine, showing an increased potency in inhibition of Rb phosphorylation and E2F mediated transcription of cyclin E1, E2, and A2 (Figure 5.5).

#### **5.6. The effect on E2F-Rb transcription is not due inhibition of CDK9 - RNA Polymerase II transcriptional activity**

PHA-767491 is a dual kinase inhibitor with IC50 of 10 nM for Cdc7 and 34 nM for CDK9 (Montagnoli et al., 2008; Vanotti et al., 2008). PHA-767491 has been shown to inhibit CDK9 in chronic lymphocytic leukaemia (CLL) and multiple myeloma models (Natoni et al., 2011; Natoni et al., 2013). PHA-767491 exhibits cytostatic and apoptotic activities that have been explained by PHA-767491 targeting both Cdc7 and CDK9. CDK9 enhances RNA polymerase II activity at elongation step (Bowman and Kelly, 2014; Hahn, 2004; Kim et al., 2002; Phatnani and Greenleaf, 2006). The CDK9 phosphorylation of RNA polymerase II is conserved in all eukaryotes and is essential for CDK12 activity in higher eukaryotes (Bowman and Kelly, 2014). As PHA-767491 could be affecting E2F1-3 mediated transcription by inhibition of CDK9 and potentially reducing the activity of RNA polymerase II, it was speculated that PHA-767491 may inhibit CDK9 mediated RNA Polymerase II phosphorylation at serine 2, this way inhibiting global transcription (Natoni et al., 2011; Natoni et al., 2013).

To ensure that PHA-767491 effect on E2F transcription was not due to the inhibition of CDK9 mediated phosphorylation of RNA polymerase II, the RT-qPCR analysis was repeated using 18S rRNA as a control instead of GAPDH. The rationale for this experiment was that GAPDH mRNA is transcribed by RNA polymerase II, while 18S

rRNA is produced by RNA polymerase I. Given that PHA-767491 inhibits CDK9 with nanomolar affinity (34 nM) (Montagnoli et al., 2008; Natoni et al., 2011; Natoni et al., 2013), the reduction in E2F1-3 transcripts may be due to a reduction in RNA polymerase II activity globally. To mitigate for the potential confounding effect of PHA-767491 inhibition of RNA polymerase II global transcription, the RNA polymerase I transcript 18S rRNA was used as a standard for comparison of transcript levels. The RT-qPCR analysis using 18S rRNA as a control was performed and the results were compared to the quantitation using GAPDH (Figure 5.6).

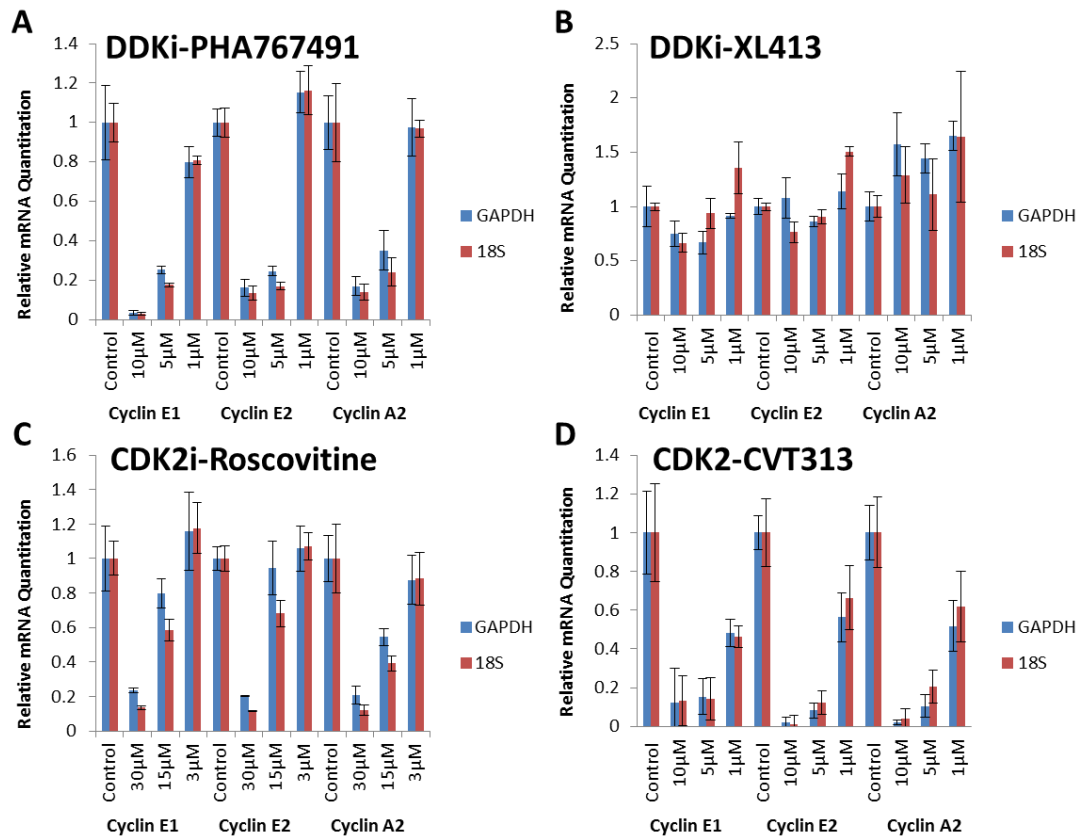


**Figure 5.6. PHA-767491 affected E2F transcription by inhibiting CDK2 rather than CDK9. A, B, C, and D)** 3T3 were synchronised and treated with 1, 5, and 10 μM of PHA-767491, XL-413, CVT-313, and 3, 15, and 30 μM of Roscovitin 12 – 20 hours post – G0 as indicated. RT-qPCR analysis of cyclin E1, E2, and A2 transcription relative to GAPDH (blue) and 18S rRNA (red) controls. Bars present mean ± S.D., 3 experimental repeats each with 3 technical repeats.

This approach showed that there were no significant differences in transcript levels after relative quantitation using either GAPDH mRNA or 18s rRNA. PHA-767491 does not appear to have mediated any effect on transcript levels via inhibition of CDK9 at concentrations less than 10  $\mu$ M. Therefore, the data presented here are consistent with PHA-767491 mediated inhibition of CDK2 that results in suppression of E2F1-3 mediated transcription. This off-target inhibition may contribute to the increased potency of PHA-767491 relative to XL-413 and also potentially explains different effects on G1/S transition (Figure 5.1).

### **5.7. Genetic depletion of Cdc7-Dbf4 does not inhibit E2F transcription**

In order to confirm that PHA-767491 effect on E2F transcription was not due to its inhibition of DDK activity, gene specific siRNAs were used to co-deplete Cdc7-Dbf4 in 3T3 cells (Figure 5.7: A, B: lanes 6 and 7). The genetic depletion of DDK would provide an alternate means of specifically reducing Cdc7-Dbf4 activity, enabling determination of the effect on cell cycle progression and transcription due to DDK inhibition. Cyclin E1, E2, and A2 protein levels and transcription were monitored after depletion of Cdc7 and Dbf4 (Figure 5.7: B and C). RT-qPCR analysis revealed that Cdc7 mRNA level was down to 50% and Dbf4 mRNA was below 20% (Figure 5.7: A); however, depletion of Dbf4 and Cdc7 did not significantly affect cyclin transcription (E1:  $p = 0.759$ , E2:  $p = 0.177$ , A2:  $p = 1.000$ ,  $n=3$ ) (Figure 5.7: B). This was consistent with the western blot analysis of the whole cell extract and detergent resistant chromatin fraction, which showed that cyclin E and cyclin A protein levels remained unchanged (Figure 5.7: C, lanes 8 and 9).

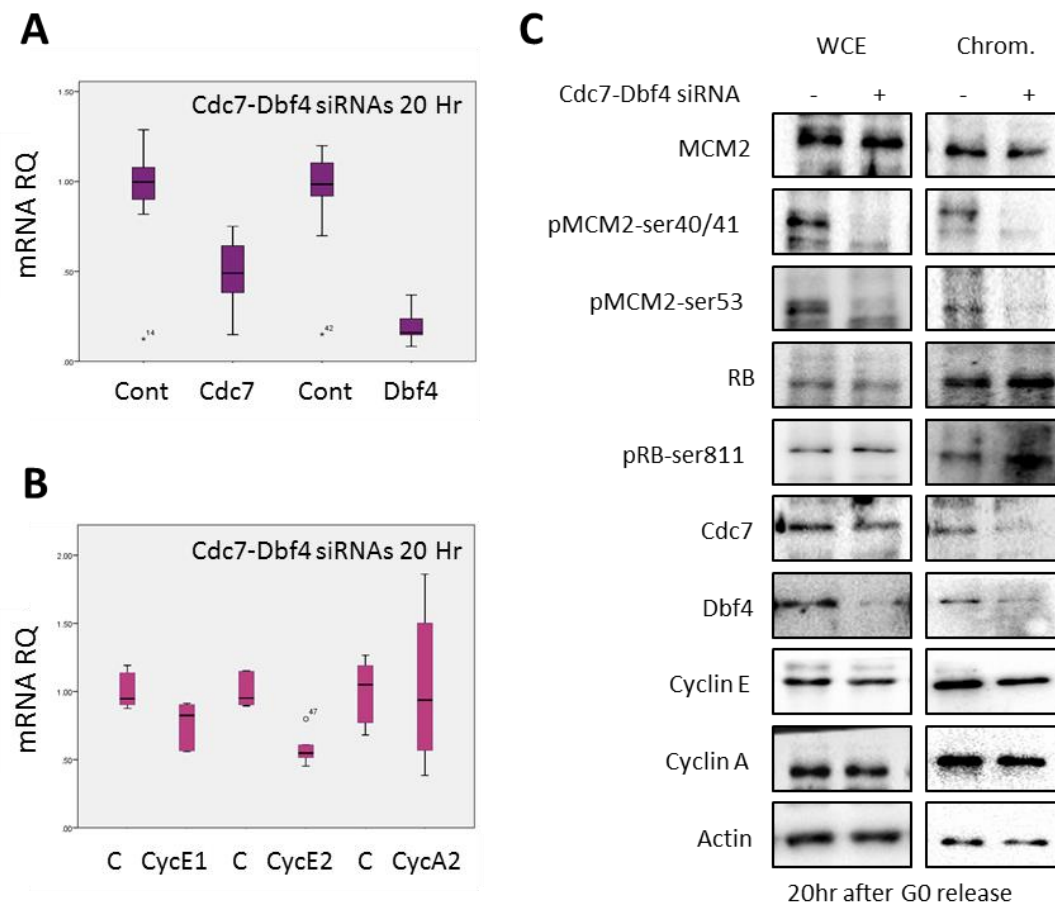


**Figure 5.7. Cdc7-Dbf4 co-depletion does not reduce E2F transcription. A)** 3T3 were synchronised and co-transfected with anti-Cdc7 and anti-Dbf4 siRNAs upon release from G0. RT-qPCR analysis of control siRNA and Cdc7 and Dbf4 siRNA treated cells 20 hours after transfection relative to GAPDH. Box-and-whisker plot shows mean, upper and lower quartiles and whiskers show data range, where n=3 (3 experimental replicates, each with 3 technical replicates). **B)** as for A, except for Cyclin E1, E2, and A2 transcription. **C)** WB of whole cell extracts and chromatin fraction, +/- transfection, probed with MCM2, pMCM2-ser40/41, pMCM2-ser53, Rb, pRb-ser811, Cdc7, Dbf4, Cyclin E, Cyclin A, and Actin antibodies.

In addition, the western blot analysis revealed that Cdc7-Dbf4 co-depletion reduced MCM2 phosphorylation on S40/41 and S53 DDK phosphorylation sites consistent with PHA-767491 and XL-413 results. However, the Rb phosphorylation was not affected on S811 after Cdc7-Dbf4 co-depletion (Figure 5.7: C). This suggests that phosphorylation of Rb at S811 does not require DDK activity and that Rb can be efficiently phosphorylated by CDK2 despite the reduction in DDK activity. These

observations are consistent with the results of XL-413 mediated inhibition of DDK (Figure 5.2 and 5.3). However, genetic depletion of DDK revealed distinct effects from those observed with PHA-767491 (Figure 5.3: lane 5), which reduced Rb-S811 phosphorylation (Figures 5.2 and 5.3). These data suggest that PHA-767491 is a potent DDK and CDK2 inhibitor (Montagnoli et al., 2008) and efficiently inhibits E2F transcription with similar efficacy to Roscovitine and CVT-313 (Figure 5.5).

## **5.8. Discussion**

The characterisation of small molecule kinase inhibitors is crucial in order to progress the research into clinical studies. The comprehensive and thorough analysis of the small molecule inhibitor molecular targets and phenotypic effects is key in reducing the amount of drugs that fail pre-clinical studies. In addition, identifying the off-target effect can reduce undesired toxicities, side-effects, and rejection in clinical trials (Dambach et al., 2016; Hoelder et al., 2012; Schenone et al., 2013). Further, identifying additional targets and effects of small molecule inhibitors may be useful in generating novel therapies.

Due to the distinct activities on the cell cycle progression and Ciz1 stability (Chapter 3), this chapter focused on the comparison between two potent DDK inhibitors, PHA-767491 and XL-413. Here it has been shown that PHA-767491 is more efficient in inhibiting G1 - S transition than XL-413 (Figure 5.1). However, XL-413 reduces EdU fluorescence and prolonged treatment of 24 hours promotes accumulation of cells in S phase. These observations are similar to others that have demonstrated that XL-413 reduces origin firing due to inhibition of MCM2 phosphorylation on serine 53 and serine 40 (Montagnoli et al., 2008), and reduces rate of S phase progression

(Conti et al., 2007; Rainey et al., 2017). Indeed, the speed of replication forks has been shown to increase in order to compensate for the reduction in origin firing after PHA-767491 and XL-413 challenge; however, high concentration of DDK inhibitors still reduce S phase progression (Montagnoli et al., 2008; Rainey et al., 2017).

Both PHA-767491 and XL-413 significantly reduce MCM2 phosphorylation on serine 53 and serine 40/41 sites (Figure 5.2) and this inhibition is concentration dependent (Figure 5.3). In addition, PHA-767491 also inhibits CDK2 mediated phosphorylation of MCM2 serine 41, resulting in a more potent reduction in phosphorylation at this site. Similarly, PHA-767491 inhibits Rb-S811 phosphorylation and reduces cyclin A protein levels (Figure 5.2, 5.3, and 5.4). Analysis of the E2F regulated transcripts revealed that PHA-767491 inhibited transcription of cyclin E1, E2 and A2 genes at micromolar concentrations. Importantly, it was shown that PHA-767491 prevents efficient Rb phosphorylation consistent with RT-qPCR results and with a reduction in E2F mediated transcription.

Rb-E2F pathway regulated transcripts: cyclins E1, E2 and A2, have been quantified and analysed after the increasing concentration of PHA-767491 and XL-413 (Figure 5.5). PHA-767491 alone inhibits E2F transcription with the similar micromolar efficiency as CDK2 inhibitors, Roscovitine and CVT-313. The transcript analysis has been confirmed using RNA polymerase II transcript GAPDH mRNA and RNA polymerase I transcript 18S rRNA to relatively quantify E2F transcripts abundance (Figure 5.6). This reduces the confounding effect of the reduced global RNA polymerase II transcription due to inhibition of CDK9 by PHA-767491 (Natoni et al., 2011; Natoni et al., 2013). These results clearly demonstrate that PHA-767491

reduces E2F regulated transcripts and cyclin A protein levels with the same potency as CDK2 inhibitors (Figure 5.4).

The genetic co-depletion of Cdc7 – Dbf4 has no significant effect on E2F transcription, Rb phosphorylation on CDK2 site, or cyclin A protein accumulation (Figure 5.7). This is consistent with DDK function in MCM2 phosphorylation to initiate DNA replication, but not Rb-E2F pathway (Chuang et al., 2009; Francis et al., 2009; Montagnoli et al., 2006; Montagnoli et al., 2010; Sasi et al., 2014; Tsuji et al., 2006). Taken together the results suggest that PHA-767491 has significant off target effects via CDK2 inhibition. These effects may contribute to the increased efficacy in reducing cancer cell proliferation (Giacinti and Giordano, 2006; Harbour and Dean, 2000; Zhu and Mao, 2015).

Overall, the reduction of DNA replication initiation has been observed with PHA-767491 and less with XL-413 (Figure 5.1). This is consistent with their role in phosphorylating MCM2 (Tsuji et al., 2006). However, the degree of restriction in G1 phase after PHA-767491 can only be explained by additional inhibition of CDK2 mediating its effect at both the transcriptional levels via the Rb-E2F pathway and the inhibition of helicase activation (Montagnoli et al., 2008; Rainey et al., 2017). The additional inhibition of CDK2 could explain the distinct effects of PHA-767491 and XL-413 observed in Ciz1 stability and accumulation experiments (Chapter 3), where PHA-767491 reduced Ciz1 levels with the same efficiency to CDK2 inhibitors and XL-413 had a limited success.

The data presented here offers a potential mechanism to explain the enhanced cytotoxic effect of PHA-767491 relative to XL-413 in cancer cell lines (Sasi et al.,

2014). PHA-767491 inhibits both DDK and CDK2 kinase activities in micromolar concentrations. Thus, PHA-767491 potentially affects cell cycle progression via a dual inhibition of DDK and CDK2 networks that regulate restriction point bypass, helicase activation and initiation of DNA replication. This also explains why PHA-767491 prevents initiation of DNA replication, whereas XL-413 does not. The initiation phase of DNA replication requires both DDK and CDK2 activities, and the requirement for DDK mediated activation of helicase activation occurs earlier (Deegan and Diffley, 2016; Diffley, 2004; Siddiqui et al., 2013; Yeeles et al., 2015; Yeeles et al., 2017). These observations suggest that PHA-767491 has potentially significant anti-proliferative effects and provides a basis for the reinterpretation of results generated using this inhibitor. Finally, a critical analysis of the effect of PHA-767491 in cancer cell lines with respect to the potential inhibition of the Rb-E2F axis is required. This may provide a more detailed understanding of differences in XL-413 and PHA-767491 cytotoxic effects in cancer cells.

# **Chapter 6**

## **Enhancing UPS mediated degradation of Ciz1 with small molecule DDK and CDK2 inhibitors**

## 6.1. Introduction

Conventional anti-cancer chemotherapeutic drugs target cell proliferation, DNA replication and mitotic microtubule assembly (Jackson et al., 2007; Ke and Shen, 2017). Despite being the first line therapy, chemotherapeutic agents target dividing cells and this non-selective approach is associated with severe side effects and reduced quality of life. Therefore, there is a need to improve the efficacy of conventional drugs and reduce side effects to improve patient tolerance to treatments. This may be achieved by the rational targeting of angiogenesis, signalling cascades, splice variants or gene fusions, inhibitors of apoptosis, and promotion of differentiation pathways (Blattman and Greenberg, 2004; Herr and Brummer, 2015). A number of molecularly targeted anticancer therapies have been approved, including the blockade of receptor tyrosine kinases (RTK) using antibodies or small molecules that inhibit RTK activity. These include targeted strategies against human epidermal growth factor receptor 2 (HER2) in breast cancer and epidermal growth factor receptor (EGFR) in non-small cell lung cancer (Eliyatkin et al., 2016; Hirsch et al., 2016; Perez et al., 2017). However, targeted therapies come at higher cost and are often associated with cancer cells developing resistance mechanisms (Pantziarka et al., 2014; Shakhnovich, 2018).

Current research focuses on potential ways to make cancer therapies more successful and cost efficient. Strategies to reduce costs include data sharing, patient stratification, early diagnosis and re-purposing of existing drugs (Edginton and Models, 2018; Ledford, 2008; Shakhnovich, 2018). The main benefits of drug repurposing are knowledge on drug pharmacokinetics, bioavailability, toxicities, and

dosing that reduces the length of clinical trials. It is imperative to understand the molecular mechanisms that underpin tumorigenesis in order to develop rationally designed small molecules for the treatment of cancers. However, this approach has a long lead-time to clinical use of the compound, typically of the order of 15 to 20 years. This process can be reduced to 3-12 years and reduce costs by greater than 50% when existing drugs are repurposed to target novel molecular pathways for cancer therapy (Hernandez et al., 2017; Ke and Shen, 2017; Klaeger et al., 2017; Liu et al., 2018; Pantziarka et al., 2014; Yoo et al., 2017).

A number of cancers have been shown to depend on Ciz1 for proliferation, migration, aggressiveness, and high Ciz1 levels are associated with poor patient outcomes (Den Hollander and Kumar, 2006; Higgins et al., 2012; Nishibe et al., 2013; Pauzaite et al., 2017; Yin et al., 2013; Zhang et al., 2015; Zhou et al., 2018). Ciz1 overexpressing cancers belong to the most prevalent cancer types including colorectal, gallbladder, prostate, breast, liver, and lung cancers. Significantly, the depletion of Ciz1 has been shown to inhibit tumour growth in xenograft models and cancer cell proliferation and migration *in vitro* (Higgins et al., 2012; Lei et al., 2016; Wu et al., 2016; Zhang et al., 2015). Therefore, representative cancer cell lines were selected to test for Ciz1 dependency for proliferation and viability. The aim was to identify Ciz1 dependent cancer cell lines and to determine whether Ciz1 levels could be decreased by CDK and DDK inhibitors in human cancer cell lines. The cancer cell lines screened for Ciz1 dependency were androgen independent prostate adenocarcinoma PC3 (Tai et al., 2011), primary colon cancer cell line SW480, and the metastatic SW620 from the same patient (Maamer-Azzabi et al., 2013). Additionally, the oestrogen (ER), progesterone (PR) and other hormone receptor positive, Rb

positive, and HER2 negative breast cancer cell lines MCF7 and T47D were analysed (Aka and Lin, 2012; Azizi et al., 2010; Bosco et al., 2007; Radde et al., 2015).

In murine fibroblasts, disruption of CDK2/DDK activity and expression promotes UPS mediated degradation of Ciz1 (Chapter 3). This observation suggests that CDK or DDK inhibitors may be repurposed to reduce Ciz1 levels through shifting the equilibrium of opposing CDK and UPS networks that regulate Ciz1 abundance (Figure 6.1).

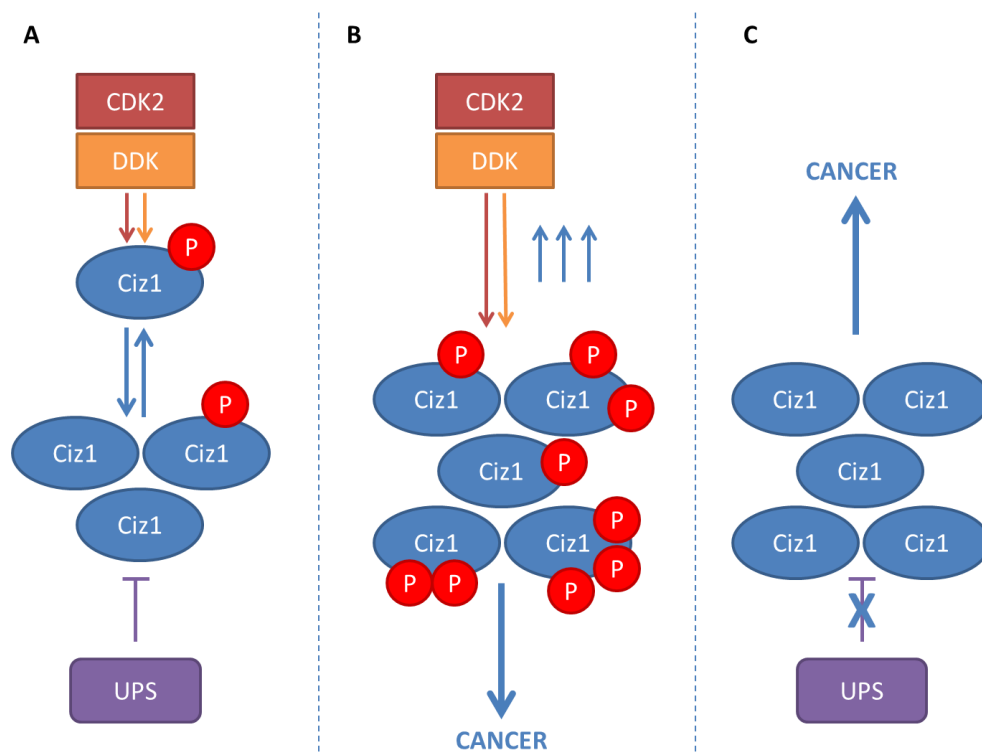


**Figure 6.1. Model of opposing regulation of Ciz1 protein levels by CDK and DDK kinase activity and UPS mediated degradation. A)** Normal Ciz1 levels are regulated by CDK and DDK phosphorylation stabilising Ciz1 and protecting it from degradation, thus positively contributing to Ciz1 accumulation in G1 phase. Ciz1 level is down-regulated by UPS mediated degradation, providing tight regulation of Ciz1 abundance in the cell cycle. **B)** Increased CDK activity may lead to Ciz1 hyper-phosphorylation, which in turn leads to Ciz1 over-accumulation facilitating increased rate of Ciz1 dependent cancer proliferation. **C)** Mutations and loss-of-function in UPS responsible for normal Ciz1 degradation leads to over-accumulation of Ciz1 contributing to tumourigenesis.

In this model, the targeting of CDK/DDK activity may increase the rate of UPS mediated degradation of Ciz1. Here the feasibility of utilising small molecule CDK or DDK inhibitors to reduce Ciz1 levels is assessed. In addition, the effect of CDK and DDK inhibition in suppression of the Rb-E2F pathway will be determined. The molecular characterisation of this effect of CDK2 and DDK inhibition may be the first step towards the preclinical investigations for the rational targeting of Ciz1 levels.

## **6.2. Kinase inhibition reduced Ciz1 levels in cancer cell lines**

The clinical use of CDK4/6 inhibitors has demonstrated the efficacy of kinase inhibition for treatment of oestrogen receptor (ER<sup>+</sup>) positive and human epidermal growth factor receptor 2 (HER2<sup>-</sup>) negative breast cancer (Asghar et al., 2017; Lynce et al., 2018; Pernas et al., 2018; VanArsdale et al., 2015). The observation that Ciz1 is regulated by opposing CDK activity and UPS mediated degradation suggests that CDK2 inhibition may shift this equilibrium promoting UPS mediated degradation of Ciz1 (Chapter 3, Figure 6.1). Ciz1 has both tumour suppressor activities in normal levels and facilitates the growth of tumours when over-expressed (Higgins et al., 2012; Nishibe et al., 2013; Ridings-Figueroa et al., 2017; Sunwoo et al., 2017; Wu et al., 2016; Yin et al., 2013). This suggests that the reduction of Ciz1 levels in cancers may reduce proliferation. To determine whether CDK2i and DDKi can be used to reduce Ciz1 levels in cancer cell lines, PC3 and SW480 cell lines were used. Preliminary data in asynchronous colorectal (SW480, SW620, and Caco-2), prostate (PC3), cervical (HeLa), and breast carcinoma (MCF7, T47D, and BT549) cell lines, that were treated with PHA-767491, Roscovitine, and CVT-313 for 24 hours, revealed some reduction in Ciz1 levels (data not shown). To assess whether there are cell cycle

specific effects of CDK/DDK inhibitors, early G1 phase synchronised cells were produced. Cells were synchronised at the metaphase checkpoint and treated for 8 hours from 4 – 12 hours after M phase release. These conditions are analogous to the data shown for G1 phase progression in murine fibroblasts (Chapter 3). PC3 and SW480 cells were treated with DDK inhibitors (PHA-767491 and XL-413) and CDK2 inhibitors (Roscovitine and CVT-313) between 4 – 12 hours after the release from the nocodazole block. The results revealed that all inhibitors, except XL-413, significantly reduced Ciz1 levels in cancer cells (Figure 6.2).

The DDK specific phospho-S53 in MCM2 was reduced after both DDK inhibitors PHA-767491 and XL-413 (Figure 6.2: A and B, lane 4). Additionally, CDK2 specific phosphorylation of Ciz1 (pT293-Ciz1) and Rb (pS811-Rb) was reduced after PHA-767491, Roscovitine, and CVT-313 treatments (Figure 6.2: A and B, lanes 2 and 6). This suggests that PHA-767491 inhibits both DDK and CDK2 activity in cancer cell lines consistent with the observed effect in murine 3T3 fibroblasts (Chapters 3 and 5). Further, cyclin A levels were reduced after PHA-767491, Roscovitine, and CVT-313 inhibition (Figure 6.2: A and B: lane 9). This suggests that, similarly to normal fibroblasts, CDK2 inhibitors and PHA-767491 affect regulation of Rb-E2F pathway that is required for efficient G1 phase progression. However, XL-413 efficiently reduces MCM2 S53 phosphorylation but does not affect cyclin A expression.

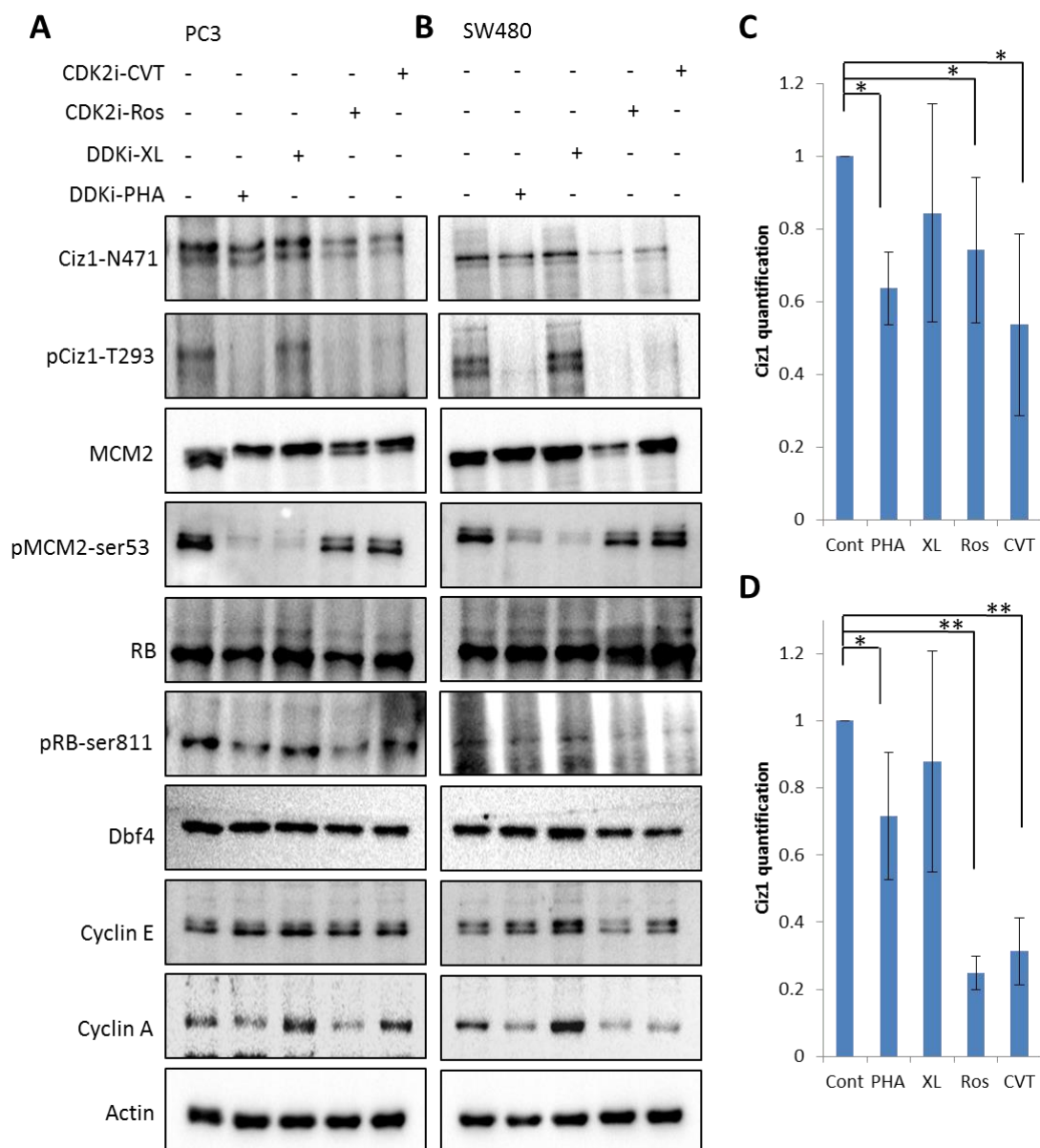


**Figure 6.2. Kinase inhibition reduces Ciz1 levels in PC3 and SW480 cancer cells. A)** Cell cycle synchronised PC3 cells were treated with 10  $\mu$ M of PHA-767491, 10  $\mu$ M of XL-413, 30  $\mu$ M of Roscovitine, and 10  $\mu$ M of CVT-313 4 – 12 hours after release from M phase. Western blot of PC3 cells harvested after 8 hours of kinase inhibition probed with Ciz1, pCiz1-T293, MCM2, pMCM2-ser53, Rb, pRb-ser811, Dbf4, Cyclin E, Cyclin A, and Actin antibodies. **B)** as for A but for SW480 cells. **C)** Quantitation of Ciz1 levels in PC3 cells relative to actin loading control, control plotted as relative 1. Bars present mean  $\pm$  S.D., n=3. Significance measured with One-Way ANOVA, Post Hoc, Tukey, (\*) p<0.05 for PHA, Ros, and CVT. **D)** as for C except for SW480, (\*) p<0.05 for PHA, (\*\*) p<0.01 for Ros and CVT.

### **6.3. Ciz1 is degraded by the UPS after CDK2 or DDK inhibition in PC3 and SW480 cancer cell lines**

The model presented here suggests that Ciz1 is regulated by opposing activities of CDK/ DDK and UPS mediated degradation (Figure 6.1). This model suggests that inhibition of kinase activity may reduce Ciz1 protein levels. Therefore, targeting CDK2 activity to reduce Ciz1 levels may provide with the novel therapeutic means to target Ciz1 dependent cancers. For kinase inhibitor therapy to be successful in Ciz1 dependent cancers, the UPS mediated Ciz1 degradation mechanism should be functional. Only cells possessing functional UPS could degrade Ciz1 effectively after kinase inhibition treatment. Consequently, it is important to determine whether cancer cell lines retain functional UPS and are able to recover Ciz1 levels (Figure 6.3).

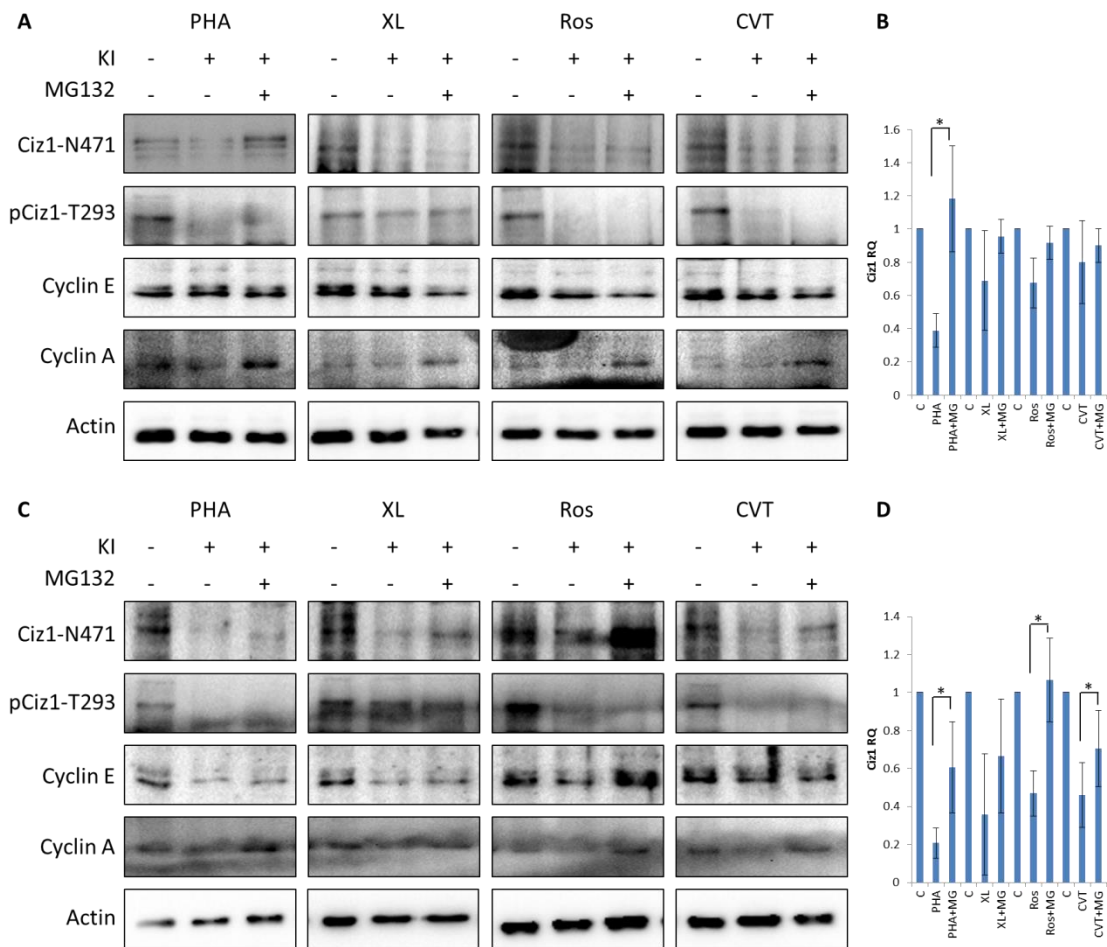


**Figure 6.3. Ciz1 recovery with MG132 in PC3 and SW480 cancer cell lines. A)** WB of PC3 cells that were synchronised in M phase and treated with 10  $\mu$ M of PHA-767491, 10  $\mu$ M of XL-413, 30  $\mu$ M of Roscovitine, and 10  $\mu$ M of CVT-313 with or without 10  $\mu$ M of MG132 4 – 12 hours after release. **B)** Quantitation of Ciz1 levels for PC3 cells relative to actin load control. Bars present mean  $\pm$  S.D., n=3. Significance measured by One-Way ANOVA, Post Hoc, Tukey, (\*) p<0.05 for PHA. **C and D)** as for A except for SW480, (\*) p<0.05 for PHA, Ros, and CVT.

To determine whether kinase inhibition increases the rate of proteasomal mediated degradation of Ciz1, the prostate cancer cell line PC3, and the colorectal cancer cell line SW480 were treated with kinase inhibitors with or without MG132 (Figure 6.3). In PC3 cells, proteasomal inhibition promoted recovery of Ciz1 in PHA-767491 treated cells, but did not in XL-413, Roscovitine or CVT-313 treated cells. The statistically significant recovery of Ciz1 after PHA-767491 suggests that the proteasome is functional in PC3 cells. This may reflect differences in the activity of

each inhibitor used and the complexity of molecular pathways exploited by different cancer cell lines. In all cases where Ciz1 levels are affected, there was a reduction in phosphorylation of CDK2 site T293-Ciz1 (Figure 6.3). The T293 phosphorylation correlated closely with Ciz1 levels, consistent with the earlier observations in murine fibroblasts (Chapter 3). CDK2 and DDK inhibition in the colorectal cell line SW480 were consistent with results obtained in normal fibroblasts (Figure 6.3: C, D; Chapter 3). In SW480 cells, Ciz1 levels were reduced after all drug treatments, and significantly recovered with proteasomal inhibition in PHA-767491, Roscovitine, and CVT-313 treated cells (Figure 6.3). In addition, in SW480 cells, PHA-767491, Roscovitine, and CVT-313 treatment resulted in reduced cyclin A levels and reduced phosphorylation of T293 within Ciz1.

The data presented so far demonstrate a strong correlation between Ciz1 phosphorylation at T293 and Ciz1 stability. In addition, the reduction in cyclin A levels suggests that kinase inhibition potentially affects the Rb-E2F pathway that requires further investigation. Here, the reduction of cyclin A after kinase inhibition correlated with the loss of T293 phosphorylation that was not recovered by proteasomal inhibition. Further, Ciz1 recovery with proteasomal inhibitor varied greatly between cell lines, potentially indicating the heterogeneity of molecular pathways cancer cells utilise in order to proliferate. However, each cell line tested here demonstrated a reduction of Ciz1 levels after CDK2 or DDK inhibition that was recovered by proteasomal inhibition with one or more of inhibitors tested. These results suggest that the E3 pathway that regulates Ciz1 is intact in the cell lines tested as the Ciz1 levels were recovered to some extent after being downregulated by kinase inhibition.

#### 6.4. CDK2 inhibitors reduced E2F transcription in cancer cell lines

As CDK2 and DDK inhibition reduced cyclin A levels (Figure 6.3), this suggests that kinase inhibition may be affecting the transcription of E2F regulated genes. Importantly, cell lines used for this analysis (PC3, SW480, and SW620) are Rb positive cancer cell lines. In murine fibroblasts, PHA-767491, Roscovitine, and CVT-313 efficiently reduced E2F transcripts (Figures 5.5 and 5.6). Therefore, E2F regulated transcripts cyclin E1, cyclin E2, and cyclin A2 mRNA were quantified by RT-qPCR after CDK2 and DDK inhibition in cancer cell context (Figure 6.4, Table 6.1).

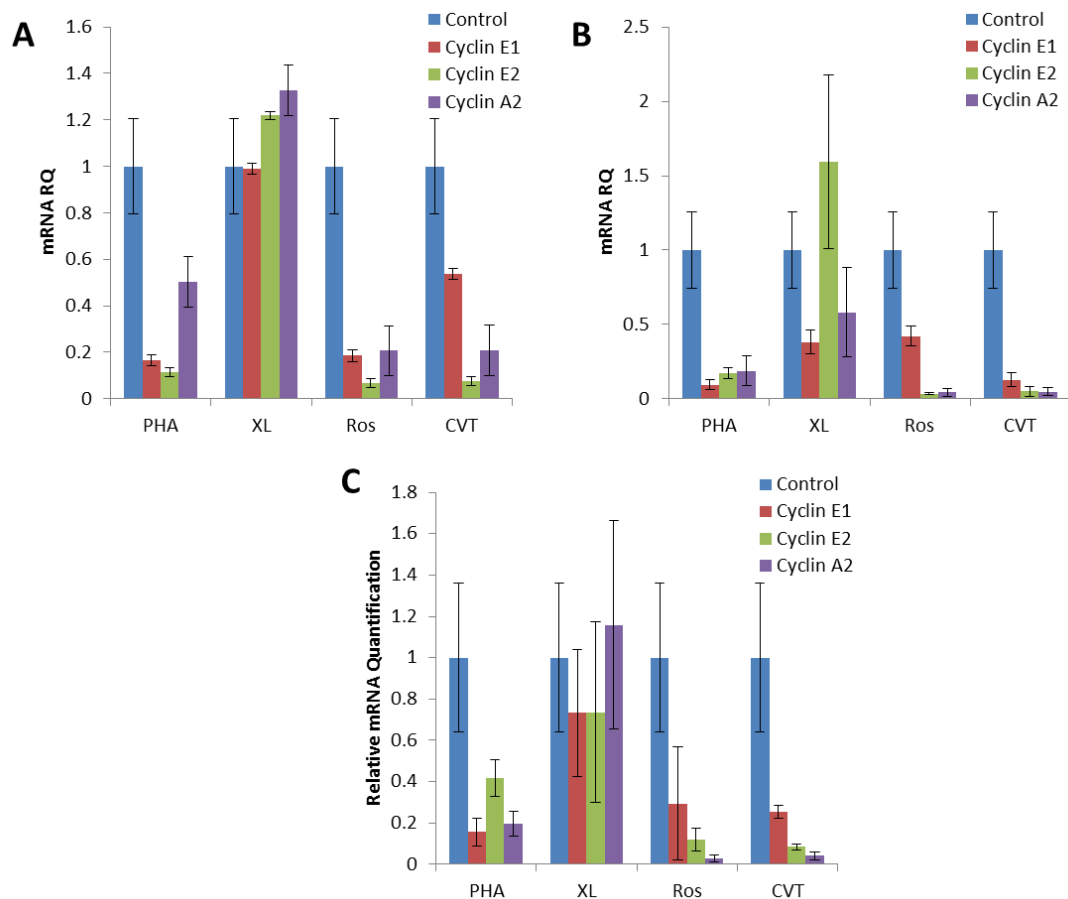


**Figure 6.4. Roscovitine, CVT-313 and PHA-767491 inhibit E2F transcription in cancer cells.** **A)** Synchronised PC3 cells were treated with 10  $\mu$ M of PHA-767491, 10  $\mu$ M of XL-413, 30  $\mu$ M of Roscovitine, and 10  $\mu$ M of CVT-313 4 – 12 hours after release. RT-qPCR of cyclin E1, E2, and A2 relative to GAPDH, control is plotted as 1, bars show mean  $\pm$  S.D., 3 experimental with 3 technical repeats in each. **B)** as for A but for SW480. **C)** as for A but for SW620.

p values		PHA-767491	XL-413	Roscovitine	CVT-313
PC3	Cyclin E1	0.0021 **	0.9413	0.0025 *	0.0183 *
	Cyclin E2	0.0003 ***	0.0623	0.0002 ***	0.0002 ***
	Cyclin A2	0.0475 *	0.6899	0.0422 *	0.0428 *
SW480	Cyclin E1	0.0461 *	0.1345	0.0432 *	0.0413 *
	Cyclin E2	0.0053 **	0.3268	0.0029 **	0.0032 **
	Cyclin A2	0.0032 **	0.1140	0.0011 **	0.0012 **
SW620	Cyclin E1	0.0442 *	0.1556	0.0389 *	0.0491 *
	Cyclin E2	0.0220 *	0.2489	0.0512	0.0232 *
	Cyclin A2	0.0140 *	0.8321	0.0233 *	0.0179 *

**Table 6.1. Quantitation of RT-qPCR analysis of cyclin E1, E2, A2 after kinase inhibitors.** The quantitation of mRNA transcription from Figure 6.4. The statistical analysis was performed with student paired t-test, 3 experimental repeats with 3 technical repeats in each. Significance (\*)  $p < 0.05$ , (\*\*)  $p < 0.01$ , (\*\*\*)  $p < 0.001$ .

Similar to results seen in 3T3 cells (Chapter 3 and Figures 5.5 and 5.6), E2F mediated cyclin E1, E2, and A2 transcription was reduced with Roscovitine and CVT-313 (Figure 6.4 and Table 6.1). In addition, the DDK inhibitor PHA-767491 reduced E2F mediated transcription of cyclin E1, E2 and A2 consistent with its off-target CDK2 inhibitory activity (Montagnoli et al., 2008; Montagnoli et al., 2010) (Chapter 5). The results for XL-413 showed that although the cyclin E1, E2 and A2 transcript levels were reduced in SW480, the reduction was not statistically significant ( $p > 0.1$  in all cases, Table 6.1). In addition, XL-413 did not affect cyclin E1, E2 or A2 expression in PC3 or SW620 cells. These results are consistent with the earlier data showing that XL-413 does not affect E2F regulated transcription (Chapter 5).

To ensure that PHA-767491 acts via CDK2 inhibition and not via CDK9 inhibition, qRT-PCR was performed using 2 housekeeping genes: RNA polymerase II regulated GAPDH and 18S rRNA that is produced by RNA polymerase I (Bowman and Kelly, 2014; Goodfellow and Zomerdijk, 2012; Hahn, 2004; Kim et al., 2002; Natoni et al.,

2011; Natoni et al., 2013; Phatnani and Greenleaf, 2006). The relative quantitation values generated using either GAPDH mRNA or 18S rRNA were not significantly different (Table 6.2) consistent with the hypothesis that PHA-767491 does not affect global transcription (Chapter 5).

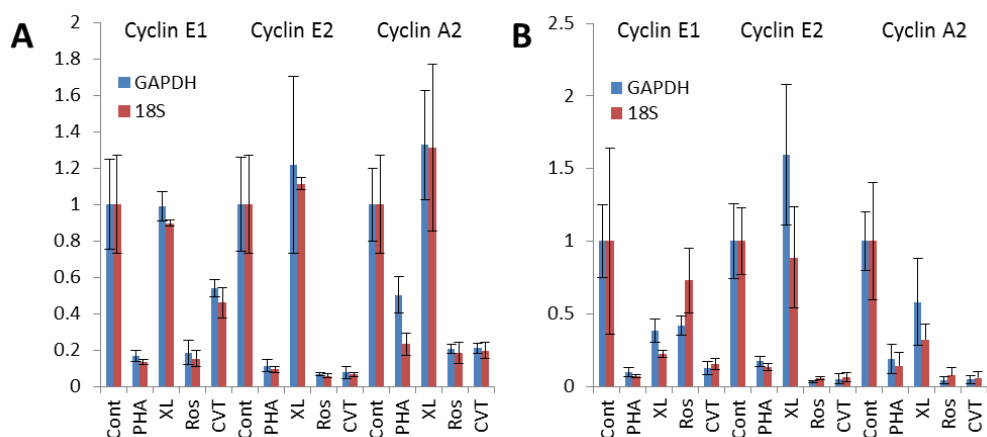


**Figure 6.5. PHA-767491, Roscovitine, and CVT-313 inhibit E2F - Rb axis transcription in cancer cell lines. A)** Synchronised PC3 cells were treated with 10  $\mu$ M of PHA-767491, 10  $\mu$ M of XL-413, 30  $\mu$ M of Roscovitine, and 10  $\mu$ M of CVT-313 4 – 12 hours after release. RT-qPCR of cyclin E1, E2, and A2 relative to GAPDH (blue) and 18S (red). Control is plotted as relative 1, bars present mean  $\pm$  S.D., 3 experimental with 3 technical repeats in each. **B)** as for A but for SW480.

	GAPDH vs 18S in PC3			GAPDH vs 18S in SW480		
	Cyclin E1	Cyclin E2	Cyclin A2	Cyclin E1	Cyclin E2	Cyclin A2
<b>Control</b>	p = 1.0	p = 1.0	p = 1.0	p = 1.0	p = 1.0	p = 1.0
<b>PHA-767491</b>	p = 1.0	p = 1.0	p = 1.0	p = 1.0	p = 1.0	p = 1.0
<b>Control</b>	p = 1.0	p = 1.0	p = 1.0	p = 1.0	p = 1.0	p = 1.0
<b>XL-413</b>	p = 1.0	p = 1.0	p = 1.0	p = 1.0	p = 0.3	p = 1.0
<b>Control</b>	p = 1.0	p = 1.0	p = 1.0	p = 1.0	p = 1.0	p = 1.0
<b>Roscovitine</b>	p = 1.0	p = 1.0	p = 1.0	p = 1.0	p = 1.0	p = 1.0
<b>Control</b>	p = 1.0	p = 1.0	p = 1.0	p = 1.0	p = 1.0	p = 1.0
<b>CVT-313</b>	p = 1.0	p = 1.0	p = 1.0	p = 1.0	p = 1.0	p = 1.0

**Table 6.2. The statistical analysis of the difference between GAPDH mRNA and 18S rRNA.** Synchronised PC3 and SW480 cells were treated with 10  $\mu$ M of PHA-767491, 10  $\mu$ M of XL-413, 30  $\mu$ M of Roscovitine, and 10  $\mu$ M of CVT-313 4 – 12 hours after release. The significance of the difference of quantitation values (Figure 6.5) of RT-qPCR of cyclin E1, E2, and A2 relative to GAPDH and 18S was analysed using One-Way ANOVA Post-Hoc Tukey, SPSS, n=3.

Taken together (Figures 6.4 and 6.5), the data demonstrate that in Rb positive cancer cell lines CDK2 inhibitors Roscovitine and CVT-313, and DDK/CDK2 inhibitor PHA-767491 reduced Rb-E2F regulated transcription, resulting in reduced cyclin expression. This effect may potentially reduce Ciz1 accumulation by reducing CDK2 activity, predisposing Ciz1 for UPS mediated destruction in normal and cancer cell lines.

### 6.5. CDK or DDK inhibition does not affect Ciz1 transcription in PC3 and SW480 cancer cell lines

In order to investigate whether CDK2 or DDK inhibitors reduce Ciz1 transcription, RT-qPCR was performed. This revealed that Ciz1 transcript levels were not significantly affected by CDK2 or DDK inhibitors in PC3 and SW480 cell lines (Figure 6.6). This is consistent with Ciz1 transcriptional analysis after small molecule kinase inhibitors in murine fibroblasts (Figure 3.6: C) and is consistent with the hypothesis that Ciz1 is post-translationally regulated by the UPS.

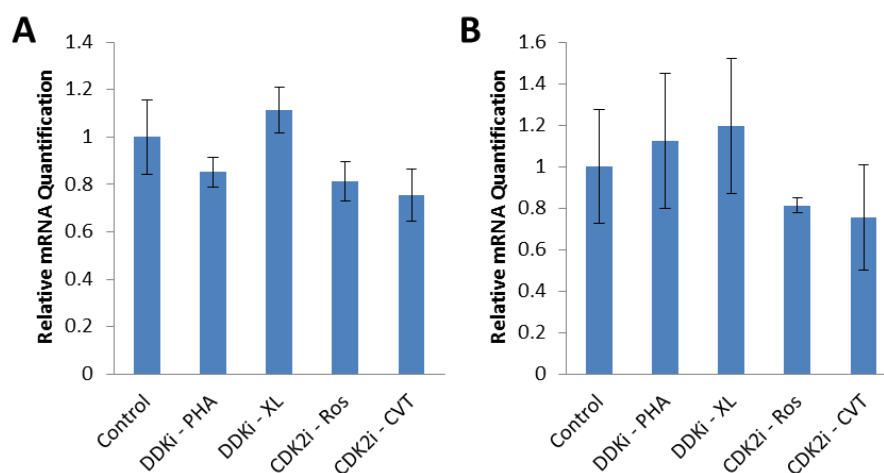


**Figure 6.6. Ciz1 transcription is unaffected by CDK2 or DDK inhibition.** A) Synchronised PC3 cells were treated 4 – 12 hours after release from M phase. RT-qPCR of Ciz1 relative to GAPDH. Control is plotted as a relative 1, bars show mean  $\pm$  S.D., 3 experimental with 3 technical repeats in each. B) as for A but for SW480.

## **6.6. CDK2 or DDK inhibition reduces cellular proliferation and S phase entry in Rb positive cancer cells**

Next, to determine the effect of CDK2 or DDK inhibition on cellular proliferation, M phase synchronised cancer cell lines were treated with CDK2 or DDK inhibitors between 4 – 12 hours after release. To determine the percentage of the population in S-phase, cells were pulse EdU labelled for 1 hour and harvested at 12 hours after release from mitotic block. The results revealed that all kinase inhibitors reduced S phase entry and that XL-413 was the least potent inhibitor (Figure 6.7: A). PHA-767491 reduced S phase entry by 80 – 85% between three cell lines, Roscovitine by 90 – 95%, and CVT-313 by 75 – 80%. In all cases, PHA-767491, Roscovitine, and CVT-313 showed statistically significant reduction in S-phase cells (PHA-767491 and CVT-313  $p < 0.01$ , Roscovitine  $p < 0.05$ ). XL-413 treatment was more effective in reducing S phase entry in PC3 cells than in SW480 and SW620 (Figure 6.7: A), although this reduction was not significant (Figure 6.7: B). This is consistent to previous research stating that XL-413 has a limited and cell type specific activity. This difference has been attributed to limited XL-413 bioavailability (Sasi et al., 2014), but the data presented here suggest that this effect may be related to the differences in target specificity, as XL-413 does not affect E2F mediated transcription (Figures 6.4 and 6.5; Table 6.1). Overall, these data suggest that CDK2 kinase inhibitors are able to reduce S phase entry in Rb positive cancer cell lines (Figure 6.7), decrease E2F transcription (Figure 6.5), and reduce Ciz1 levels (Figure 6.2, 6.3).

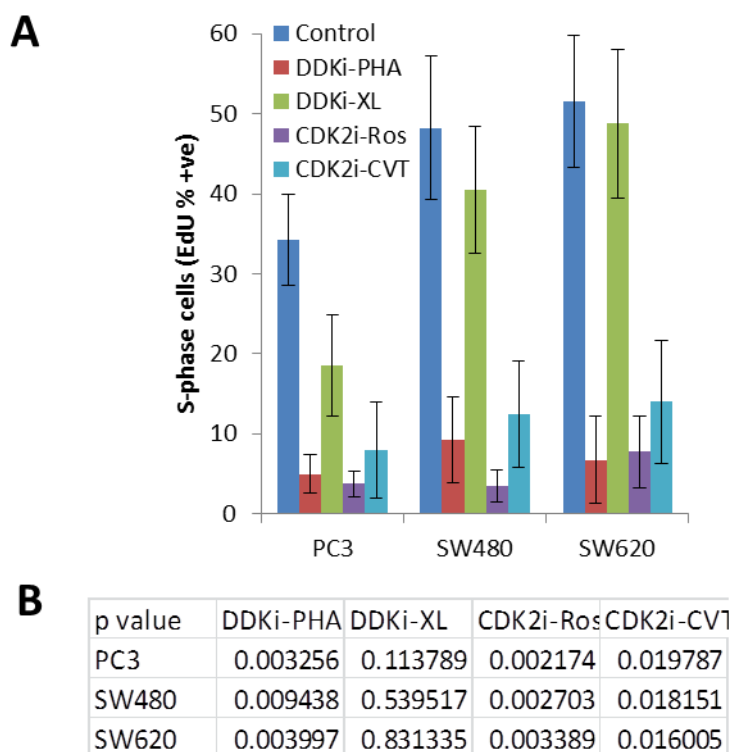


**Figure 6.7. CDK2 kinase inhibition prevents S phase entry of Rb positive cancers. A)** Cancer cell lines were treated with 10  $\mu$ M of PHA-767491, 10  $\mu$ M of XL-413, 30  $\mu$ M of Roscovitine, and 10  $\mu$ M of CVT-313 4 – 12 hours after release. Bars show the mean percentage of EdU positive nuclei  $\pm$  S.D., where n=4. **B)** The significance (p value) was measured using One-Way ANOVA, using Tukey Post-Hoc analysis for each treatment against control, where n=4.

### 6.7. PHA-767491, Roscovitine and CVT-313 reduce proliferation in PC3, SW480 and SW620 cancer cell lines

To further assess the effect of CDK2 and DDK inhibition on the cell cycle progression, flow cytometry analysis of asynchronous PC3, SW480 and SW620 cancer cell lines was performed after 24 hours of kinase inhibitor treatment. Cells were pulse labelled with EdU for 1 hour prior to harvesting and fluorescently labelled using CLICK-IT chemistry. This enabled both nascent and total DNA levels to be detected by flow cytometry (Figure 6.8).

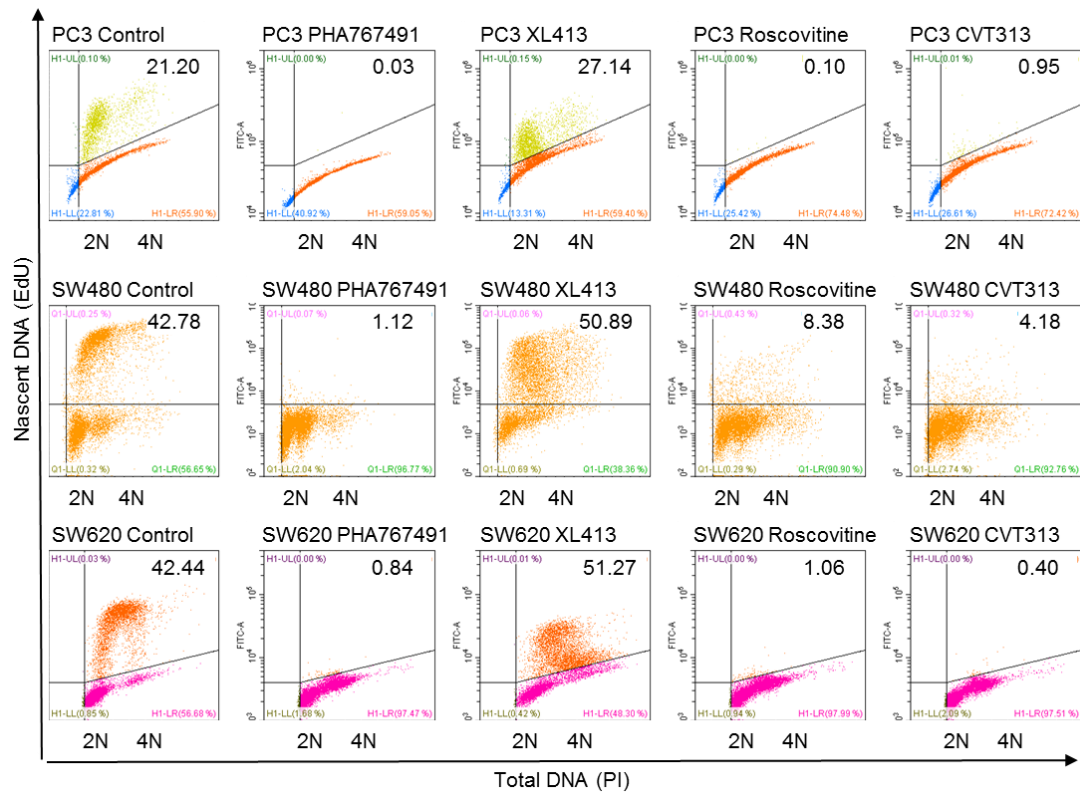


**Figure 6.8. PHA-767491 resembles CDK2 inhibitors in cancer cell lines.** Flow cytometry of asynchronous PC3, SW480, and SW620 cells after treatment with 10  $\mu$ M of PHA-767491, 10  $\mu$ M of XL-413, 30  $\mu$ M of Roscovitine, or 10  $\mu$ M of CVT-313 for 24 hours. The cells were labelled with propidium iodide (x axis) for total DNA and EdU alexafluor 488 (y axis) for nascent DNA synthesis. The percentage of cells in S phase is shown in the top right corner. 2N presents cell population in G1 phase, 4N shows S and G2 phase cells.

The results showed that PHA-767491, Roscovitine, and CVT-313 inhibited S phase entry in PC3, SW480, and SW620 cancer cell lines (Figure 6.8). In contrast, XL-413 did not inhibit G1 – S transition, and led to an increase in the number of S phase cells (Figure 6.8, third column). This may indicate a prolonged S phase, rather than a cell cycle checkpoint activation preventing S phase entry. In addition, the reduction in fluorescence intensity on FITC (EdU 488 nm) axis after XL-413 treatment suggests that there was a reduction in DNA synthesis, consistent with the DNA replication stress (Bertoli et al., 2016; Herlihy and De Bruin, 2017; Yeeles et al., 2017; Zeman and Cimprich, 2014). This response was noted previously as XL-413 increased replication

origin firing from cryptic origins to offset the reduction in DNA replication initiation (Alver et al., 2017; Rainey et al., 2017). Overall, the data show that PHA-767491, Roscovitine, and CVT-313 efficiently reduce proliferation and S phase entry in Rb positive cancer cell lines.

### **6.8. Identification of Ciz1 dependent cancer cell lines**

The results presented in this chapter have identified that CDK2 and DDK inhibition can reduce Ciz1 levels, most likely via UPS mediated degradation. In addition, CDK2 inhibitors and PHA-767491 reduce cyclin E1, E2 and A2 expression and proliferation. These results suggest that CDK2 and/or DDK inhibition has multifaceted activities that prevent proliferation, which may include reduction of Ciz1 levels. To determine the effect of reducing Ciz1 levels in cancer cell lines, specific siRNA was used to deplete Ciz1 in several cancer cell lines. Each cell line was synchronised in S phase with two thymidine blocks prior to transfection with anti-Ciz1 siRNA. Post-transfection, cells were released back into the cell cycle and cellular proliferation, Ciz1 levels, apoptosis and necrosis were monitored. This showed that Ciz1 was efficiently depleted at both the protein and mRNA level in cell lines PC3, SW480, MCF7, and T47D (Figure 6.9).

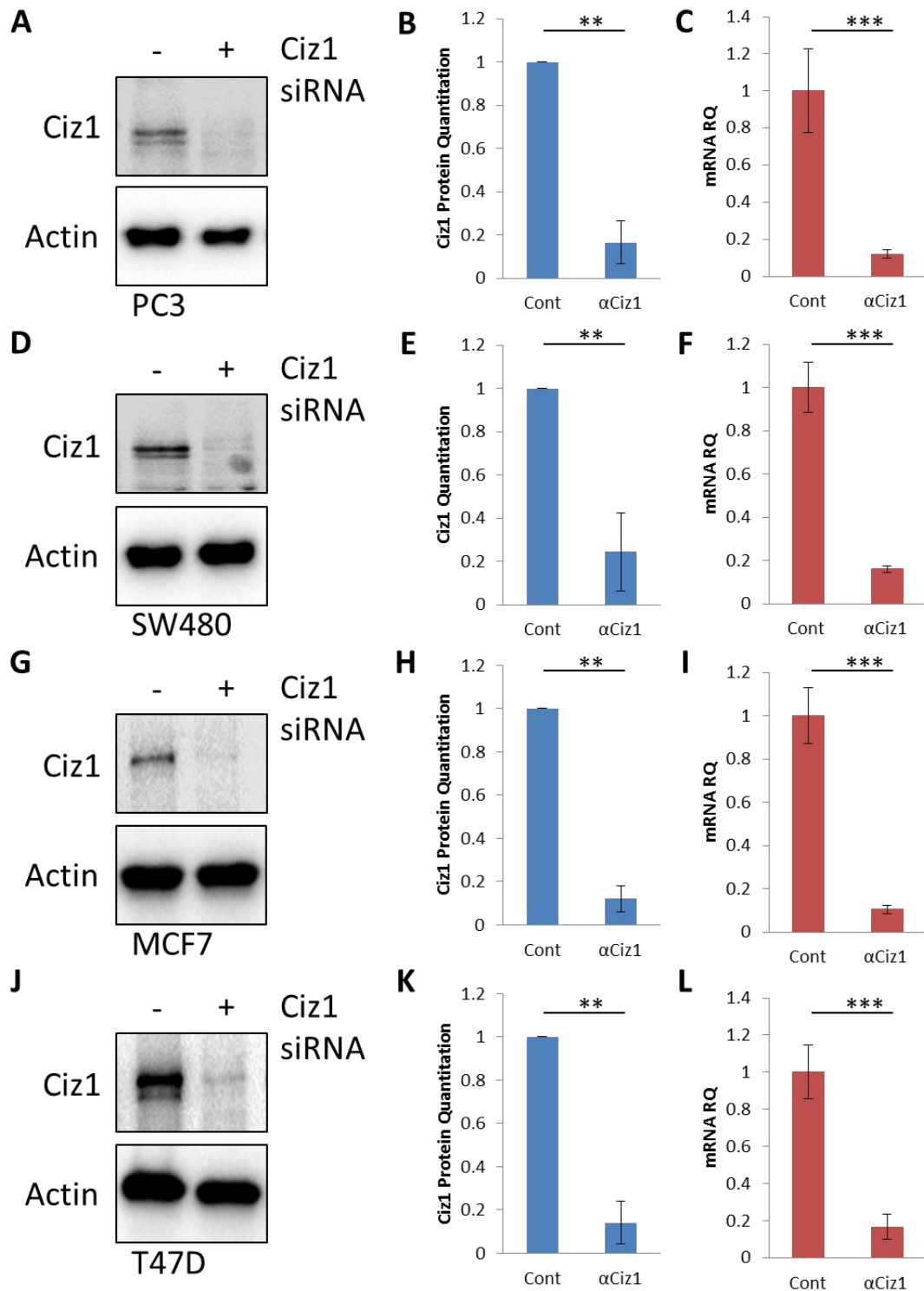


**Figure 6.9. Ciz1 depletion in cancer cell lines. A, D, G, and J)** WB of cells harvested 24 hours after release and transfection, probed with Ciz1 antibody for indicated cell lines. **B, E, H, and K)** Ciz1 protein quantitation relative to actin loading control, control is plotted as relative 1, bars present mean  $\pm$  S.D.,  $n=3$ , significance measured by paired two-tailed t-test, (\*\*\*)  $p \leq 0.005$ . **C, F, I, and L)** RT-qPCR of Ciz1 transcription relative to GAPDH, control is plotted as a relative 1, bars present mean  $\pm$  S.D., 3 experimental repeats with 3 technical repeats in each. Significance measured by one-way ANOVA post-hoc Tukey, (\*\*\*)  $p \leq 0.005$ .

In order to determine whether cancer cells were dependent on Ciz1 for proliferation and viability, EdU incorporation and Ki-67 transcript levels were used as proliferation markers. In addition, mitochondrial activity using MTT assay was monitored in PC3 and SW480 cell lines (Figure 6.10). EdU incorporation was monitored from 12 – 24 hours after siRNA depletion and showed that S phase entry was reduced by 65% at 24 hour time point in Ciz1 depleted PC3 cells relative to control cells (Figure 6.10: A). These data suggest that the androgen independent prostate adenocarcinoma PC3 cell line requires Ciz1 expression to efficiently enter the S phase, consistent with its role in regulation of DNA replication initiation (Coverley et al., 2005).

In Ciz1 depleted PC3 cells, transcription of the KI-67 gene was reduced by 40% (Figure 6.10: C). The Ki-67 is a marker of proliferation that is transcribed in all cell cycle phases except quiescence and peaks prior to mitosis (Sun and Kaufman, 2018). In addition, there was also a reduction in metabolic activity post-depletion of Ciz1 in PC3 cells, with approximately 30% reduction relative to control cells (Figure 6.10: E). Using three independent approaches, depletion of Ciz1 reduces the number of cells in S phase (Figure 6.10: A), reduces KI-67 expression ( $p < 0.05$ ,  $n = 3$ ) (Figure 6.10: C), and decreases metabolic activity (Figure 6.10: E) consistent with a decline in cellular proliferation.

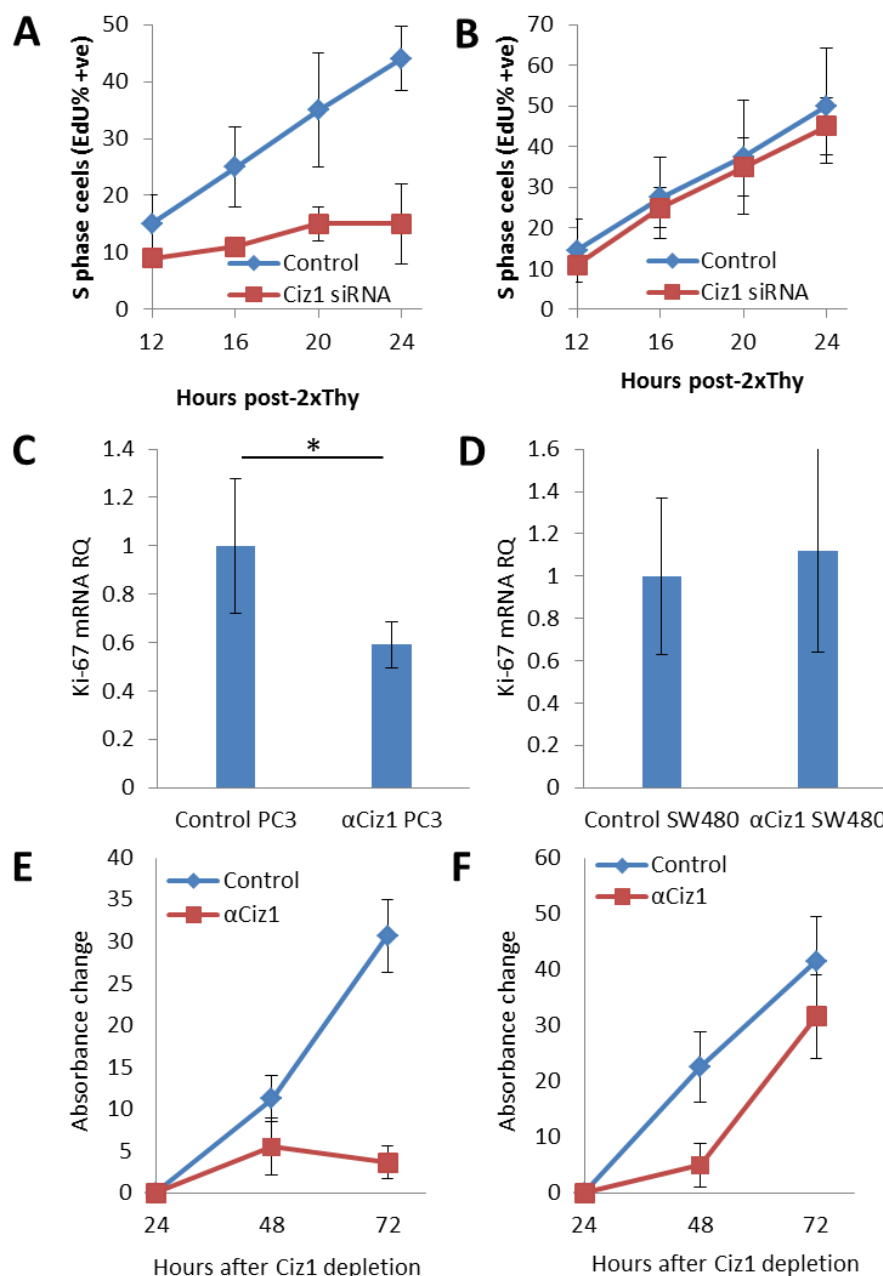


**Figure 6.10. Ciz1 requirement for PC3 and SW480 proliferation.** **A)** PC3 cells were synchronised by 2 x Thymidine block and transfected with anti-Ciz1-siRNA upon release. Cells were 1 hour pulse labelled with EdU prior time points indicated. Plot of percentage of EdU positive cells relative to DAPI counterstained total cells. Each dot shows mean  $\pm$  S.D.,  $n=3$ . **B)** same as A, but for SW480. **C)** PC3 cell line RT-qPCR of Ki-67 relative to GAPDH, control plotted as a relative 1, bars show mean  $\pm$  S.D., 3 experimental repeats with 3 technical repeats in each. Significance measured by one-way ANOVA post-hoc Tukey, (\*)  $p \leq 0.05$ . **D)** same as C, but for SW480. **E)** PC3 cells MTT cell viability assay, 24, 48, and 72 hour after transfection. 24 hour time point is plotted as relative 0, and the time points 48 and 72 hour were plotted as an absorbance change after 24 hours (%),  $n=3$  (in triplicate). **F)** same as E, but for SW480.

In contrast, SW480 grade II colorectal cancer cell line was not affected. Ciz1 depletion did not reduce the proportion of cells in S-phase, KI-67 expression or cellular metabolism measured by the MTT assay (Figure 6.10: B, D, and F).

Overall, these data show clear differences in PC3 and SW480 cells. The aggressive androgen independent PC3 cells required Ciz1 for efficient cell proliferation rate, cellular metabolism, and cell viability. In contrast the Grade II colorectal carcinoma cell line SW480 is Ciz1 independent for growth and proliferation. These observations suggest that PC3 cells are an attractive model to evaluate small molecule inhibitors that reduce Ciz1 levels, with the potential exploitation in more complex models and clinical settings.

#### **6.9. Ciz1 depletion shows differential effects in Luminal A cancer cell lines T47D and MCF7**

Next, to further expand this analysis, the luminal A (ER<sup>+</sup>/ PR<sup>+</sup>/ HER<sup>-</sup>) breast cancer cell lines T47D and MCF7 (Holliday and Speirs, 2011; Radde et al., 2015) were used to determine the requirement for Ciz1 for cell proliferation. Both T47D and MCF7 cell lines retain functional oestrogen receptor (ER), which was previously shown to collaborate with Ciz1 in ER driven tumourigenesis (Den Hollander and Kumar, 2006; Den Hollander et al., 2006). MCF7 and T47D cells were transfected with anti-Ciz1 siRNA and pulse labelled with EdU at 24, 48, and 72 hours. The cell cycle distribution was analysed by multiparameter flow cytometry staining for total DNA and EdU labelling. This approach revealed that Ciz1 depletion did not affect T47D proliferation. Cell cycle progression and the percentage of cells in S phase were indistinguishable between control and Ciz1 depleted cells (Figure 6.11: C and D).

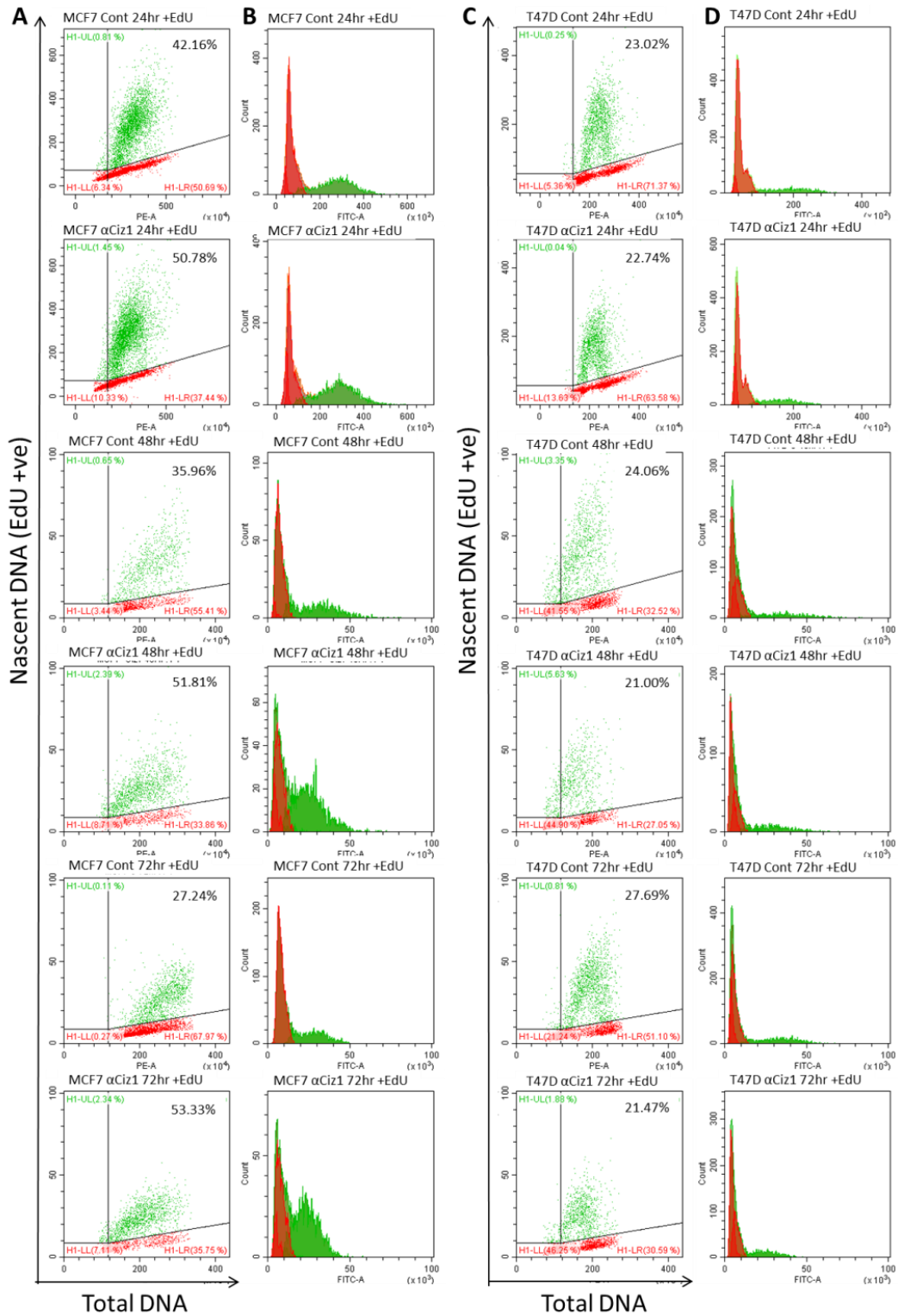


**Figure 6.11. Flow cytometry analysis of MCF7 and T47D showing cell cycle progression after Ciz1 depletion. A)** The asynchronous population of MCF7 were transfected with anti-Ciz1 siRNA, 1 hour pulse labelled prior each 24, 48, and 72 hour time point. Flow cytometry multiparameter dot blot, EdU replicating cells (FITC – 488 nm - y axis) vs. PI total DNA (PE-A - 620 nm - x axis). Number in the top right corner shows the proportion of cells in S phase. **B)** Histogram of the cell count (y axis) vs. EdU positive (x axis). **C)** as for A but for T47D. **D)** as for B except for T47D.

However, Ciz1 depletion in MCF7 cell line increased the proportion of cells in S phase (24 hours after the depletion: 42.16% control vs 50.78% Ciz1 depletion, 48 hours: 35.96% vs 51.81%, 72 hours: 27.24% vs 53.33%) (Figure 6.11: A). After plotting of the cell count against EdU intensity, a clear accumulation of the cells in S phase was detected (Figure 6.11: B). The data show an increase in S phase cells after Ciz1 depletion that may suggest increased proliferation. An alternative hypothesis to explain the increased number of cells in S phase could be via slowed replication or DNA replication stress phenotype, which can prolong S phase (Herlihy and De Bruin, 2017; Toledo et al., 2017).

#### **6.10. Ciz1 depletion reduced proliferation in MCF7 breast cancer cell line**

The cell cycle profiling of MCF7 and T47D revealed differential effects. T47D cells do not alter their cell cycle profile after Ciz1 depletion (Figure 6.11: C and D), whereas the MCF7 cell line showed an enrichment of cells within S phase (Figure 6.11: A and B). This could reflect an increased rate of proliferation or potentially a delay in S phase progression due to a DNA replication stress like phenotype (Bertoli et al., 2016; Herlihy and De Bruin, 2017; Toledo et al., 2017). To further evaluate the proliferation rate of MCF7 and T47D cells, KI-67 levels, a cell proliferation marker, were determined by qRT-PCR. The KI-67 transcription was significantly reduced in MCF7 cell lines after Ciz1 depletion relative to controls ( $p < 0.05$ ,  $n=3$ ) (Figure 6.12: A) and slightly reduced in T47D cells, although this was not statistically significant (NS,  $n=3$ ) (Figure 6.12: B). Further, cell viability measured by MTT assay showed a marginal reduction in MCF7 cells ( $p=0.095$ ,  $n=3$ ), but not in T47D (Figure 6.12: C and D). However, the reduction of mitochondrial activity was not statistically significant

in both cases. The enrichment in S phase cells, reduced KI-67 levels and reduced cellular proliferation suggest that MCF7 cells may undergo DNA replication stress after Ciz1 depletion.

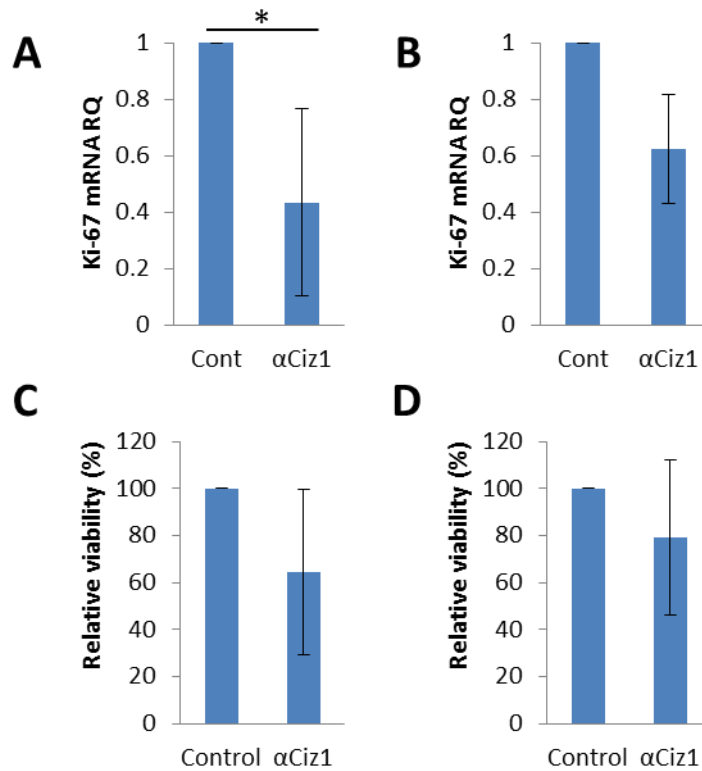


**Figure 6.12. Ciz1 depletion reduces proliferation in MCF7.** **A)** MCF7 24 hours after transfection with anti-Ciz1 siRNA, RT-qPCR of KI-67 relative to GAPDH, control expressed as relative 1, bars show mean  $\pm$  S.D., significance measured using One-Way ANOVA, Post-Hoc, Tukey, (\*)  $p < 0.05$ , 3 experimental with 3 technical repeats in each. **B)** as for A but for T47D, non-significant,  $n=3$ . **C)** MTT assay of MCF7 48 hours after transfection, control is plotted as 100%, non-significant, bars show mean  $\pm$  S.D.,  $n=3$ . **D)** as for C but for T47D.

### 6.11. Ciz1 depletion reduces proliferation without inducing cell death

To determine if Ciz1 depletion increased cell death, cells were labelled with Annexin V - alexafluor 488 and analysed by flow cytometry (Figure 6.13). Annexin V (FITC 525/40 nm) specifically binds to phosphatidylserine externalised on the outer surface

of the plasma membrane during apoptosis (Monceau et al., 2004). In addition, propidium iodide (PE-A 585/42 nm), a membrane impermeant dye was used to label necrotic cells that are characterised by the loss of membrane integrity (Zhang et al., 2018).

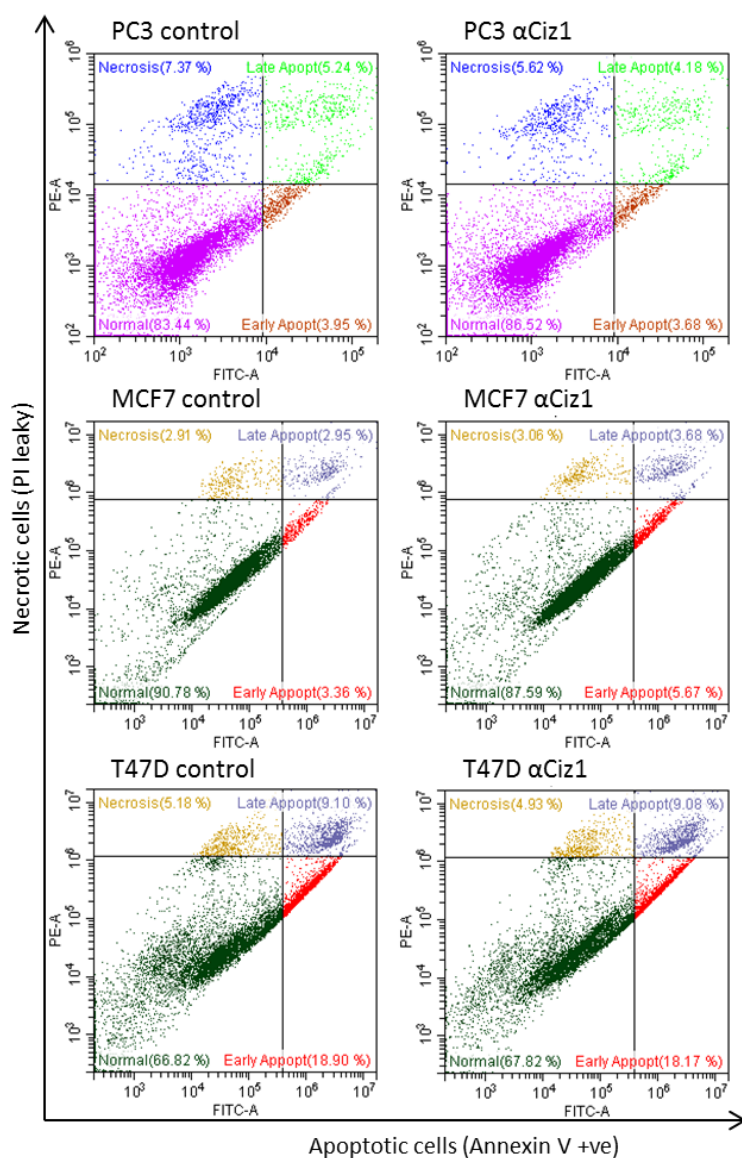


**Figure 6.13. Quantitation of apoptotic and necrotic cells after Ciz1 depletion in PC3, MCF7, and T47D cell lines.** The cells were transfected with anti-Ciz1 siRNA, harvested at 48 hours after depletion and labelled with Annexin V and propidium iodide (PI). Multiparameter dot plot using flow cytometry shows Annexin V labelled apoptotic cells (x axis) and PI leaky necrotic cells (y axis). Cells scoring high on FITC axis, but low on PE axis were classified as the early apoptotic cells, high in both – late apoptosis, high in PE – necrosis, low in PE – normal cells.

%	PC3 Control	PC3 $\alpha$ Ciz1	MCF7 Control	MCF7 $\alpha$ Ciz1	T47D Control	T47D $\alpha$ Ciz1
Normal	83.44	86.52	90.78	87.69	66.82	67.82
Early Apoptosis	3.95	3.68	3.36	5.67	18.9	18.17
Late Apoptosis	5.24	4.18	2.95	3.68	9.10	8.08
Necrosis	7.37	5.62	2.91	3.06	5.18	4.93

**Table 6.3. The quantitation of cell fate after Ciz1 depletion in PC3, MCF7, and T47D.** The quantitation of flow cytometry analysis in Figure 6.13. The cells were analysed using flow cytometry channels FITC 525/40 nm for Annexin V, and PE-A 585/42 nm for PI.

Flow cytometry analysis of PC3, MCF7, and T47D showed that Ciz1 depletion did not increase apoptosis or necrosis at 24, 48, or 72 hours after the transfection (Figure 6.13 and Table 6.3 only presents 48 hour time point). Taken together, the data suggest that Ciz1 has a cytostatic effect in PC3 and MCF7 that reduces proliferation and cellular metabolism without increasing cellular death.

## 6.12. Discussion

The aim of this chapter was to evaluate whether the hypothesis that Ciz1 is regulated by opposing CDK2 and UPS activities could be used to promote degradation of Ciz1 by CDK2 inhibition. The data presented here suggest that Ciz1 levels can be efficiently reduced by CDK2 inhibitors Roscovitine and CVT-313, and by CDK2/DDK inhibitor PHA-767491 in PC3 and SW480 cancer cell lines (Figure 6.2), which is consistent with normal mice fibroblasts (Chapters 3 and 5). The reduction in Ciz1 levels correlates closely to cyclin A levels and the phosphorylation at T293 site within Ciz1, consistent with a potential stabilising role of phosphorylation at T293 site (Chapter 3). In addition, PHA-767491, Roscovitine, and CVT-313 inhibitors reduce Rb-

E2F transcription in Rb positive cancer cell lines that is responsible for cyclin expression (Figure 6.4 and Chapter 5). Importantly, reduced E2F transcription does not affect Ciz1 transcription in cancer cell lines (Figure 6.6) suggesting that Ciz1 downregulation is post-translationally regulated. The degradation of Ciz1 after CDK2 inhibition or PHA-767491 treatment in PC3 and SW480 cell lines is likely UPS mediated, as MG132, a proteasomal inhibitor, efficiently recovered Ciz1 levels in some cases (Figure 6.3). This suggests that PC3 and SW480 cells have a functional UPS that could potentially be exploited in Ciz1 reducing kinase inhibition therapies. However, in PC3 cells, the Ciz1 levels were recovered only after PHA-767491 treatment, possibly indicating different drug efficacies or the complexity of molecular pathways utilised by various cancer cell lines. This further emphasises the importance of identification of the exact molecular pathway regulating Ciz1 abundance in normal and cancer cell lines; and molecular screening of cancer cell lines in order to design successful therapies and predict treatment outcomes.

Further analysis of kinase inhibition in cancer cell lines revealed that CDK2 inhibitors Roscovitine and CVT-313 efficiently inhibit Rb-E2F transcription (Figure 6.4) in Rb positive cancer cell lines. The reduced E2F transcription seen in PHA-767491 cells required further evaluation to ensure that results were not confounded by inhibition of global transcription via CDK9 – RNA polymerase II axis (Figure 6.5). Comparison of the relative quantitation (RQ) values for GAPDH and 18s rRNA revealed no significant differences (Table 6.2), consistent with the notion that the reduction in Rb-E2F regulated transcription was due to a reduction in CDK2 activity. The inhibition of E2F transcription in Rb positive cancer cell lines may be a reason for successful inhibition

of S phase entry and the reduction in cancer cell proliferation rate observed after PHA-767491, Roscovitine, and CVT-313 challenge (Figures 6.7 and 6.8).

Normal fibroblasts and cancer cell analysis revealed that PHA-767491 is a potent Cdc7 and CDK2 inhibitor (Figures 6.2, 6.4, and 6.5; Chapter 5) explaining the superior efficiency of PHA-767491 over XL-413 in cell cycle inhibition and cancer cell killing (Montagnoli et al., 2008; Rainey et al., 2017; Sasi et al., 2014). This additional feature of PHA-767491 inhibitor could be useful in targeting various cancers relying on different molecular pathways for proliferation. However, the research and data interpretation of PHA-767491 should be performed with care, being aware of PHA-767491 targeting the CDK2-Rb-E2F pathway.

Given that PHA-767491, Roscovitine, and CVT-313 inhibitors efficiently reduce Rb positive cancer proliferation and Ciz1 levels, cancer cells were screened for Ciz1 dependency for proliferation. This approach may help identifying cancer cell lines that would have increased sensitivity to kinase inhibitor therapies, affecting kinase activity dependent proliferation as well as Ciz1 dependent proliferation. Genetic depletion of Ciz1 via siRNA transfection in PC3, SW480, MCF7, and T47D cancer cell lines reduced Ciz1 mRNA and protein levels (Figure 6.9). The androgen receptor (AR) negative human prostate cancer cell line (PC3) is dependent on Ciz1 for S phase entry, proliferation rate and viability (Figure 6.10) that is consistent with normal fibroblasts and previously described prostate cancer (Liu et al., 2015; Liu et al., 2016).

Interestingly, Ciz1 depleted ER and Rb positive breast cancer cell line MCF7 exhibited different phenotype, accumulating cells in S phase (Figure 6.11). Together with the reduced proliferation rate (Figure 6.12), it potentially suggests the replication stress

like phenotype in MCF7 after Ciz1 depletion (Herlihy and De Bruin, 2017; Toledo et al., 2017). However, there were no observed changes in S phase progression for T47D cells (Figure 6.11: C and D), no significant changes in KI-67 expression (Figure 6.12: B) or cellular metabolism (Figure 6.12: D). Both MCF7 and T47D are Luminal A breast cancer cell lines; however, proteomic analyses have identified differential expression of crucial proteins for cell proliferation and survival. For instance, T47D expresses higher levels of cell growth, anti-apoptotic and tumourigenic genes, as well as carries mutated P53 (Aka and Lin, 2012; Lim et al., 2009). Contrary, the MCF7 expresses higher amount of transcriptional repression and apoptotic genes than T47D, and retains wild type P53 (Aka and Lin, 2012; Lim et al., 2009; Radde et al., 2015). These might be underlying reasons between the different response of MCF7 and T47D to Ciz1 depletion.

Finally, Ciz1 depletion appears to execute cytostatic effect on cancer cell lines rather than cause apoptosis (Figure 6.13) that has been shown previously in other cancer types (Lei et al., 2016; Liu et al., 2016; Wang et al., 2014; Wu et al., 2016; Yin et al., 2013). This work shows that CDK2/DDK inhibitors PHA-767491, Roscovitine and CVT-313 can efficiently reduce Ciz1 level in cancer cell lines that is UPS dependent. Additionally, kinase inhibitors successfully reduce Rb positive cancer cell proliferation. This may provide basis for further exploration of Ciz1 dependent Rb positive cancer targeting with repurposed kinase inhibitors. This approach would provide multifaceted targeting of cancer cell line proliferation, inhibiting kinase activity dependent cell cycle progression, and Ciz1 dependent proliferation. These data emphasise the importance of molecular cancer cell screening in order to design effective personalised treatment and predict potential therapy outcomes.

# **Chapter 7**

## **Identification of putative Ciz1 regulators by cellular fractionation and mass spectrometry**

## **7. Ciz1 is regulated by ubiquitin proteasome system (UPS) and kinase/phosphatase activities**

The principle aim of this work is to better understand the regulatory mechanisms that contribute to the accumulation of Ciz1 protein. Identification of the signalling networks that regulate Ciz1 levels could possibly facilitate the molecular targeting of Ciz1 by repurposing small molecule inhibitors. Ciz1 accumulates in G1 phase, mirroring the rising CDK activity at the G1/S transition and small molecule kinase inhibitors can successfully reduce Ciz1 levels in normal murine fibroblasts (Chapter 3) and cancer cell lines (Chapter 6). Ciz1 is poly-ubiquitylated *in vivo* (Figure 3.15) and proteasomal degradation is enhanced by CDK2 inhibition (Figure 3.12 – 3.14). Having identified that Ciz1 is regulated by opposing CDK2/DDK and UPS activities, this raises the potential to target Ciz1 through the repurposing of CDK2 inhibitors to increase UPS mediated degradation of Ciz1. Importantly, for CDK inhibition strategies to reduce Ciz1 levels, a fully functional UPS system is prerequisite for efficacy.

The indirect targeting of Ciz1 levels through CDK2 inhibition requires a detailed understanding of the UPS system. In fact this approach requires cancer cells to possess functional ubiquitin proteasome system for efficient Ciz1 degradation. Consequently, there is a need to identify and characterise the E3 ligase(s) that target Ciz1 to facilitate identification of cancers that may be resistant to this strategy. This could provide insight and identify cancer types that may be responsive to this approach and potentially aid in patient stratification for selection of effective therapies.

In addition, as CDK2 mediated phosphorylation promotes accumulation of Ciz1 through prevention of UPS mediated degradation; this suggests that the signalling networks could be influenced by phosphatase activities as well. CDK2 mediated phosphorylation of Ciz1 at position T293 mirrors the increase in Ciz1 levels (Figures 3.3, 3.4, 3.6-8, and 3.10). Therefore, phosphatase enzymes that dephosphorylate Ciz1 at this site may contribute to the regulation of Ciz1 activity.

Serine/threonine (S/T) phosphatases directly oppose S/T kinases during the cell cycle progression. Interestingly, more than 400 kinases are expressed in human genome, and they are counter-regulated by approximately 100 S/T phosphatases (Wlodarchak and Xing, 2016). This is achieved by the formation of highly heterogeneous complexes, such as PP1 class of phosphatases form approximately 400 heterodimeric holoenzymes, and PP2A form around 100 heterotrimeric holoenzymes (Wlodarchak and Xing, 2016). This variability is the reason that phosphatases are involved in every phase of the cell cycle, the deregulation of any element of the holoenzymes may lead to cancer, and the therapeutic targeting is in its infancy due to functional redundancy of the specific subunits (Boutros et al., 2007; Rudolph et al., 2004; Ruvolo, 2016; Winkler et al., 2015; Wlodarchak and Xing, 2016).

To illustrate the multitude of functions performed by S/T phosphatases, the PP1 phosphatase is most active in mitotic phase (Winkler et al., 2015). However, it has been shown to regulate phosphorylation state of Rb in G1 phase. In addition, PP1 control timely MCM4 phosphorylation by opposing Cdc7-Dbf4 activity in S phase, PP1 dephosphorylates Cdc25 and thereby stimulates CDK1 dephosphorylation and drives G2 to M transition. In mitosis PP1 regulates Aurora A and B kinase activities (Bollen

et al., 2009; Hiraga et al., 2014; Ludlow et al., 1993; Margolis et al., 2006; Winkler et al., 2015). The inhibition of PP1 has been shown to cause mitotic catastrophe and apoptosis of cancer cells, suggesting the selective targeting of PP1 as a potential cancer therapeutic (Winkler et al., 2015). Additionally, PP2A possesses more than 300 substrates in eukaryotes, thus it regulates all major signalling pathways and cell cycle checkpoints, including G1 to S transition, DNA synthesis, and mitotic initiation (Grallert et al., 2015; Jiang, 2006; Kim et al., 2007; Kolupaeva and Janssens, 2013; Mochida et al., 2009; Ruvolo, 2016; Weber et al., 2015; Wlodarchak and Xing, 2016). PP2A displays a preference for phospho-threonine over phospho-serine, which is consistent with Ciz1 phosphorylation profile (Chapter 3) (Cundell et al., 2016; Godfrey et al., 2017).

The mutations and suppression in PP2A have been implicated in a number of solid tumours and leukaemias. Therefore, PP2A is a tumour suppressor, which opposes overexpressed kinase activities that have been linked with a multitude of cancers (Bhullar et al., 2018; Klaeger et al., 2017; Perrotti and Neviani, 2013; Ruvolo, 2016; Zhang et al., 2009). Therefore, the pharmacological activation and restoration of normal PP2A function is one of the promising avenues in cancer research (Perrotti and Neviani, 2013; Ruvolo, 2016).

This chapter has two aims. First, using an established biochemical fractionation approach to identify ubiquitin ligase(s) activity that poly-ubiquitylates Ciz1 (Section 7.1). Next, this approach was adapted to monitor phosphatase activity of Ciz1 at a specific site using phospho-specific antibodies against pT293 in Ciz1 (Section 7.2).

These approaches aim to identify potential regulatory enzymes that contribute to deregulation of Ciz1 levels in cancer cells.

### **7.1. Identification of putative E3 ligases that regulate Ciz1 accumulation**

In order to identify ubiquitin E3 ligases that regulate Ciz1 levels an *in vitro* ubiquitylation assay was utilised (Parsons et al., 2008; Parsons et al., 2009; Parsons et al., 2011). This approach uses an ubiquitin activating enzyme (E1), 9 ubiquitin conjugating enzymes (E2) and ubiquitin ligase activity (E3) from HeLa lysates to ubiquitylate the target protein (Parsons et al., 2008; Parsons et al., 2009; Parsons et al., 2011). Using recombinant Ciz1 and HeLa whole cell extract the aim here was to identify potential E3 ligases that may regulate Ciz1 using sequential chromatography steps to enrich for E3 proteins for identification by mass spectrometry analysis.

*In vitro* ubiquitylation assays utilise recombinant proteins, therefore Ciz1 protein was expressed in *E. coli* and purified using Immobilized Metal Affinity Chromatography (IMAC) and anion exchange chromatography. First, the ECiz1 was PCR amplified to introduce NcoI and Sall restriction sites and to add 6xHis tag onto C-terminal of ECiz1 (Figure 7.1: A and C). The 6xHis tag was added to the C-terminus, as in previous attempts to purify Ciz1 using an N-terminal GST tag produced a truncated Ciz1 fragment, potentially due to proteolysis of the natively disordered N-terminal region of Ciz1. Utilising a C-terminal may improve yields of Ciz1 after purification. The C-terminus is predicted to have a defined secondary structure and has domains that have been structurally determined, including zinc finger protein and matrix domains (Ainscough et al., 2007).

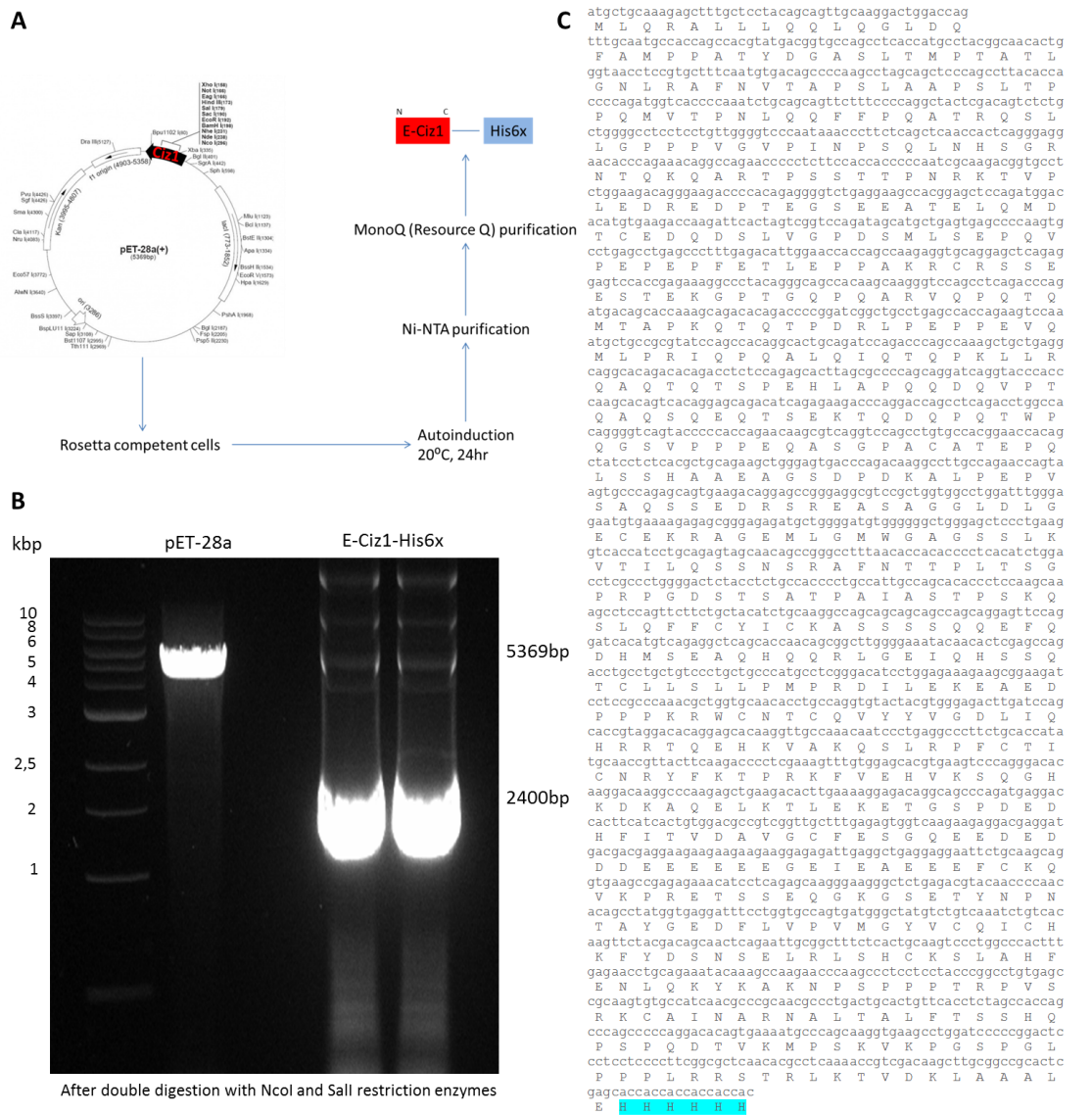


**Figure 7.1. Recombinant ECiz1-His6x cloning.** **A)** The diagram of ECiz1 cloning, expression and purification. **B)** Amplified and linearised pET-28a vector (5364 bp) and ECiz1 (2400 bp) after double digestion with restriction enzymes NcoI and SalI. **C)** The sequence of ECiz1 cloned in pET-28a obtained using T7 forward and reverse primers. The nucleotide sequence was translated into amino acid sequence using ExpASY translate ([www.expasy.ch](http://www.expasy.ch)). The 6xHis tag is highlighted in light blue.

The 708 amino acid ECiz1 was cloned from mouse embryo derived cDNA (Coverley et al., 2005) that partially lacks 2, 6, and 8 exon (Ainscough et al., 2007). The ECiz1 isoform is more efficiently expressed than the full length Ciz1 protein, which contains poly-glutamine motifs that may cause aggregation of proteins. Consequently, ECiz1 was used to aid purification, by increasing Ciz1 solubility and stability (Ainscough et

al., 2007; Copeland et al., 2010; Coverley et al., 2005). ECiz1 was cloned into pET-28a vector that included a C-terminal His tag (Figure 7.1: A and B). The plasmid was sequenced to confirm the construct and the presence of 6xHis tag (Figure 7.1: C). Finally, pET-28a-ECiz1-His6x was transformed into *E. coli* Rosetta (DE3) competent cells (Figure 7.1: B). The Rosetta supplied the system with tRNAs for translation of rare codons to aid expression.

### **7.1.1. Overexpression and purification of ECiz1-His<sub>6</sub>**

In order to determine the best strategy of ECiz1 expression, a number of conditions were tested. IPTG was used at different temperatures and concentrations to optimise expression. In addition, the autoinduction approach was utilised that used catabolite repression and lactose to promote expression of target proteins in mid log growth.

The expression of Ciz1 by IPTG induction at 37 °C for 3 hours or at 37 °C then reducing temperature to 20 °C was poor (Figure 7.2). In contrast, using autoinduction at 20 °C for 24 hours produced a protein that was identified using coomassie staining (Figure 7.2, right lane). The IPTG induction and higher temperatures appeared to be too fast inducing insoluble inclusion body formation sequestering Ciz1.

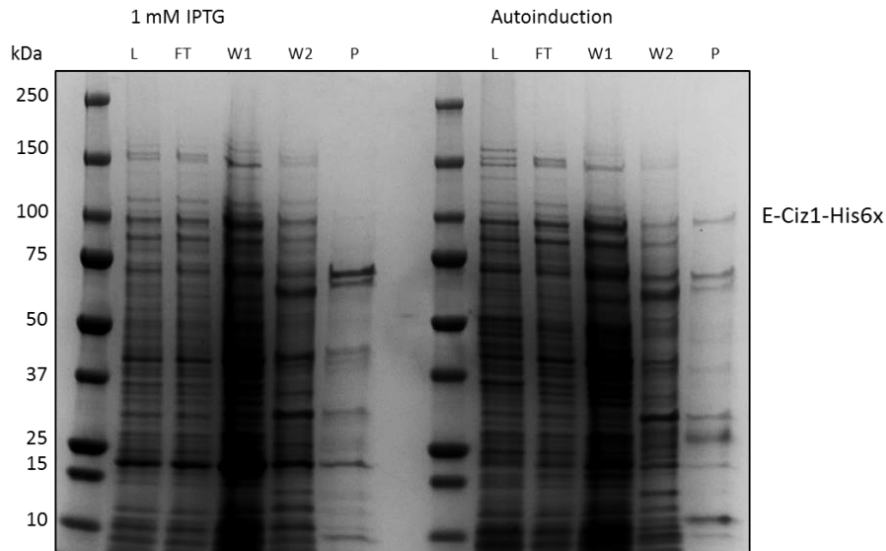


**Figure 7.2. ECiz1-His<sub>6</sub> purification with Ni-NTA resin. LEFT)** The induction of Ciz1 expression with 1 mM IPTG for 3 at 37°C, and incubation of 21 hours at 20°C. **RIGHT)** The gradual autoinduction in rich ZY medium for 24 hours at 20°C. L - lysate of cells after sonication, FT – flow through after the bead binding, W1 – wash 1 with 10 mM of Imidazole, W2 – wash 2 with 25 mM of Imidazole, P – Protein that was eluted with 250 mM of Imidazole. The gel was stained with instant blue.

Immobilized metal affinity chromatography was used to purify ECiz1-His<sub>6</sub> (Figure 7.2). ECiz1 was immobilised on Ni-NTA beads and eluted using stepped imidazole washes (Figure 7.2). However, due to the presence of impurities the sample was diluted with no salt buffer, and a second purification step was performed using anion exchange using a 1 ml Resource Q column (Figure 7.3: A). The western blotting of fractions C1-4 revealed that the protein was pure enough for *in vitro* ubiquitylation assays (Figure 7.3: B and C). The probing with His-tag antibody revealed that the sample was still contaminated with predicted *Escherichia coli* Sly-D protein (Figure 7.3: C) that interacted with nickel ions (Martino et al., 2009) and was negative in charge: pI of 4.23 vs Ciz1 pI 4.8, therefore was co-purified with ECiz1 using Resource Q column. The identity of impurity was not confirmed and Sly-D was only a predicted protein that often contaminates recombinant proteins expressed in *E. coli* (Mokhonov et al.,

2018). However, the size of two proteins was significantly different to prevent the interference in *in vitro* ubiquitylation assays, thus allowing us to use it without any additional purification steps.

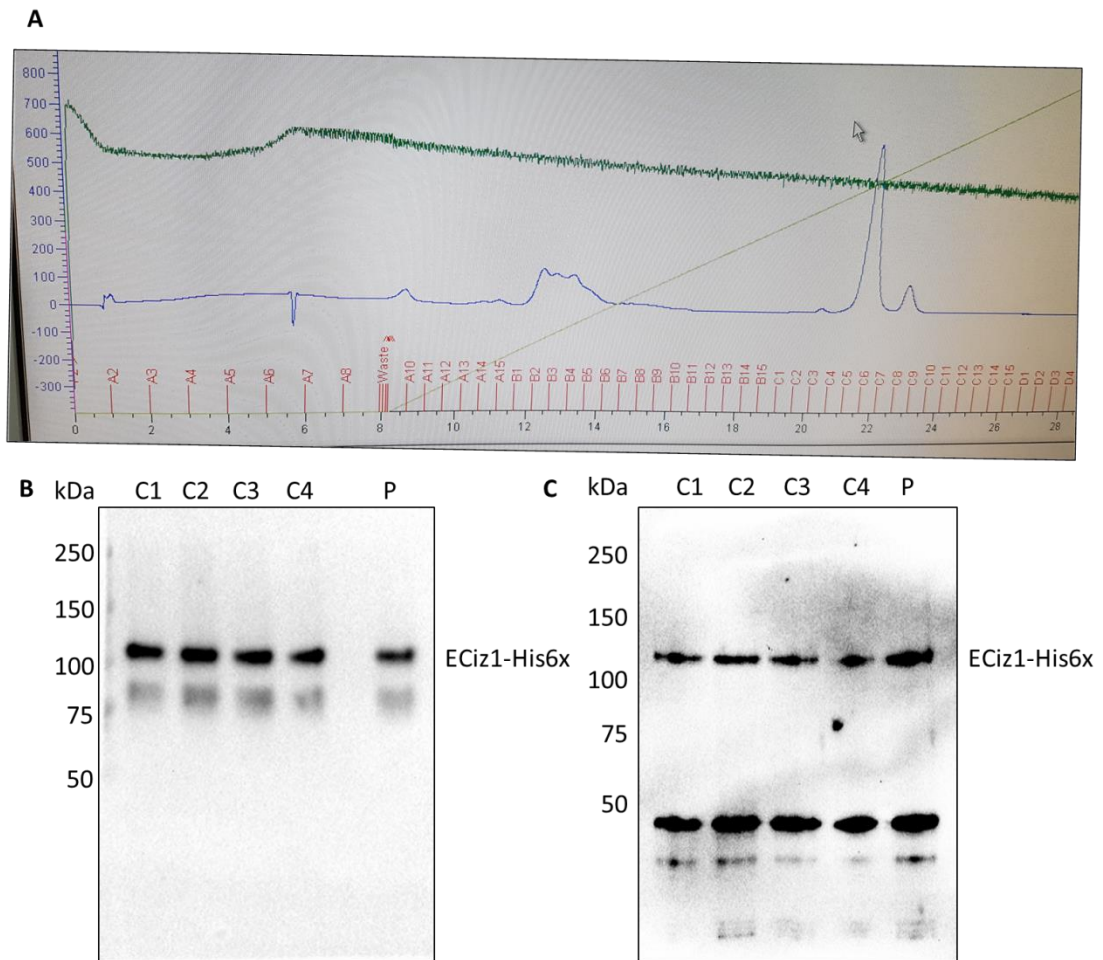


**Figure 7.3. Ciz1 purification with Resource Q 1 ml column. A)** Picture showing the chromatogram of ECiz1-His6x purification. Ni-NTA purified protein was subjected to Resource Q 1 ml column, and eluted using KCl 50 – 1000 mM gradient, 0.5 ml / fraction for 20 ml gradient, gradient starts at fraction A8. Fractions and volume on x axis, absorbance (mAU at UV 280 nm) on y axis. Absorbance in blue line, salt concentration in green. The ECiz1-His6x eluted at fractions C1-4 (620 – 691.25 mM of KCl gradient). **B)** WB of C1-4 fractions probed with Ciz1 antibody, indicating ECiz1-His6x at 120 kDa. **C)** WB of C1-4 fractions probed with His tag antibody, indicating ECiz1-His6x at 120 kDa.

### 7.1.2. *In vitro* ubiquitylation assay of Ciz1

To determine whether recombinant ECiz1 protein was ubiquitylated *in vitro* and to narrow down the list of E3 ligases specifying Ciz1 for degradation, HeLa whole cell extract (WCE) was used as a source of E3 ligases. The WCE was subjected to a series of chromatography steps (Figure 7.4: A) where the ligase activity was determined in *in vitro* ubiquitylation reactions for alternate fractions. Active fractions underwent sequential purification steps, to further enrich for E3 ligase activity. This approach (Figure 7.4) enabled identification of putative E3 ligases by MS.

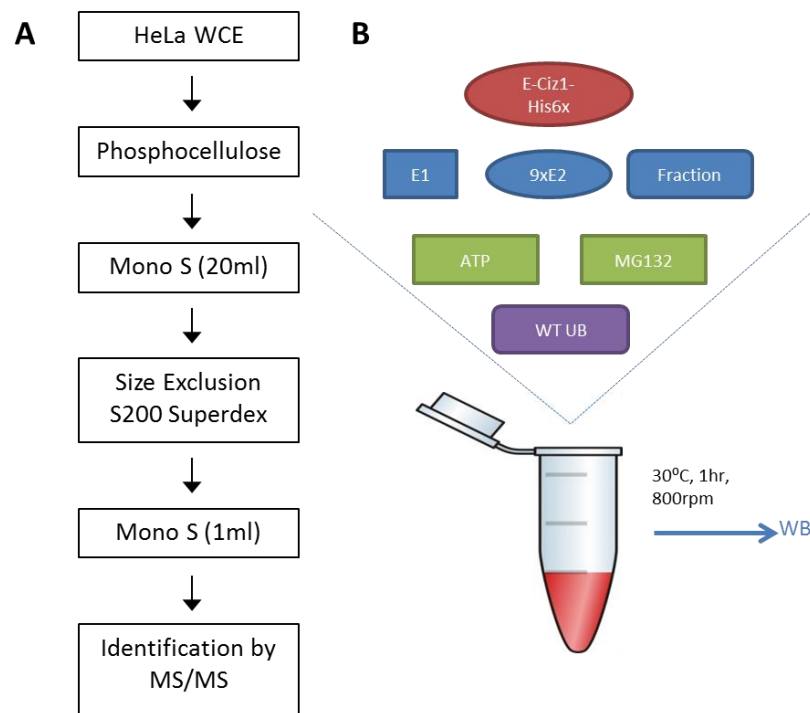


**Figure 7.4.** The diagram of chromatography steps and *in vitro* ubiquitylation reaction involved in identification of E3 ligase. **A)** HeLa WCE was subjected to Phosphocellulose column, phosphocellulose binding fraction (P1000) was put through 20 ml MonoS column, then active fractions were subjected to size exclusion column, then to analytical 1 ml MonoS column, and active fractions were sent for liquid chromatography–mass spectrometry (LC-MS/MS) analysis. **B)** The reaction combines 200 ng of recombinant ECiz1-His6x, recombinant E1, 9 x E2 (Ubch2, His-Ubch3, Ubch5a, Ubch5b, Ubch5c, His-Ubch6, Ubch7, Ubch8, His-Ubch10) and a fraction from chromatography steps as a source of E3s.

### **7.1.3. Phosphocellulose fractionation of HeLa extracts identified that Ciz1 is poly-ubiquitylated *in vitro***

In order to determine the charge of the fraction ubiquitylating Ciz1, the HeLa WCE was subjected to 100 ml phosphocellulose ion exchange column. Two crude fractions were identified, namely phosphocellulose flow through fraction (P150) that had a negative charge and did not bind phosphocellulose column, and the positive fraction (P1000) that bound the column.

To determine the E3 ligase activity present in each fraction, *in vitro* ubiquitylation assays were performed on a 2 step purification using phosphocellulose column producing a low salt eluate (P150) and high salt eluate (P1000). The ubiquitin ligase activity was determined in *in vitro* ubiquitylation assays. This revealed a laddering of bands in HeLa whole cell extract and the high salt eluate that was detected using both anti-Ciz1 and anti-His<sub>6</sub> antibodies independently, consistent with poly-ubiquitylation of Ciz1 (Figure 7.5). Importantly, the ubiquitin ligase activity was contained within the high salt fraction (P1000) with little activity in the low salt fraction (P150). Therefore the P1000 fraction was used for further fractionation using a 20 ml cation exchange sulphopropyl (SP) resin for fractionating of positively charged proteins.

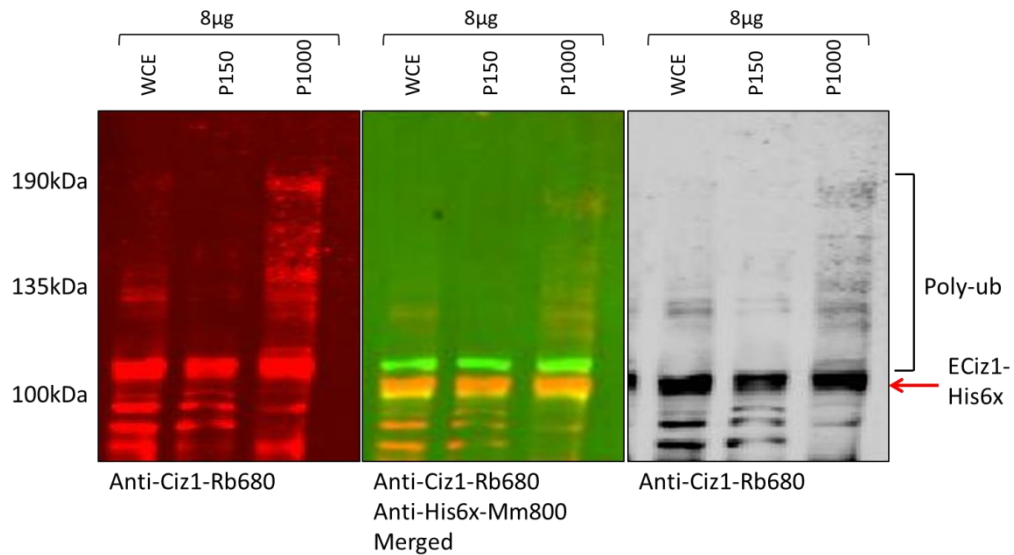


**Figure 7.5. Ciz1 ubiquitylation by phosphocellulose column fractions.** Western blot of *in vitro* Ciz1 ubiquitylation reactions using 8  $\mu$ g of HeLa WCE, P150 phosphocellulose unbinding fraction, and P1000 phosphocellulose binding fraction. The blots were probed with Ciz1 and His tag antibodies, and fluorescent anti-Rabbit-680nm and anti-Mouse-800nm secondary antibodies. The blots were developed with Odyssey Imaging System. Red arrow indicated ECiz1-His6x recombinant protein band. His tag antibody also probes recombinant E1-His6x running slightly higher than ECiz1-His6x. Brackets show the range of poly-ubiquitylation (poly-ub) of Ciz1.

#### 7.1.4. Fractionation of high salt extracts using cation exchange chromatography

The P1000 fraction was dialysed and loaded onto the 20 ml HiLoad MonoS Sepharose-SP column. The flow through was discarded and eluted proteins collected. Even numbered fractions were assayed for ubiquitin ligase activity *in vitro* for fractions 4-60. Fractions were collected, concentrated, protein levels quantified and 8  $\mu$ g of protein was loaded in each ubiquitylation assay. Western blot analysis of *in vitro* ubiquitylation assays revealed that fractions 24-26 had the highest ubiquitylation activity that was most visible using anti-His tag antibody (Figure 7.6: B, bottom blot). Notably, the recombinant E1 was purified with his tag as well, and E1-His<sub>6</sub> run slightly higher than ECiz1-His<sub>6</sub>. Nevertheless, the laddering pattern can still be observed in fractions 24-26 (Figure 7.6: B). Several lanes had single bands that

could represent ubiquitylation. Only fractions that contained poly-ubiquitylation in both anti-Ciz1 and anti-His antibody western blots were chosen for further analysis (Figure 7.6: B). Therefore, fractions 24-26 were pooled concentrated and further purified.

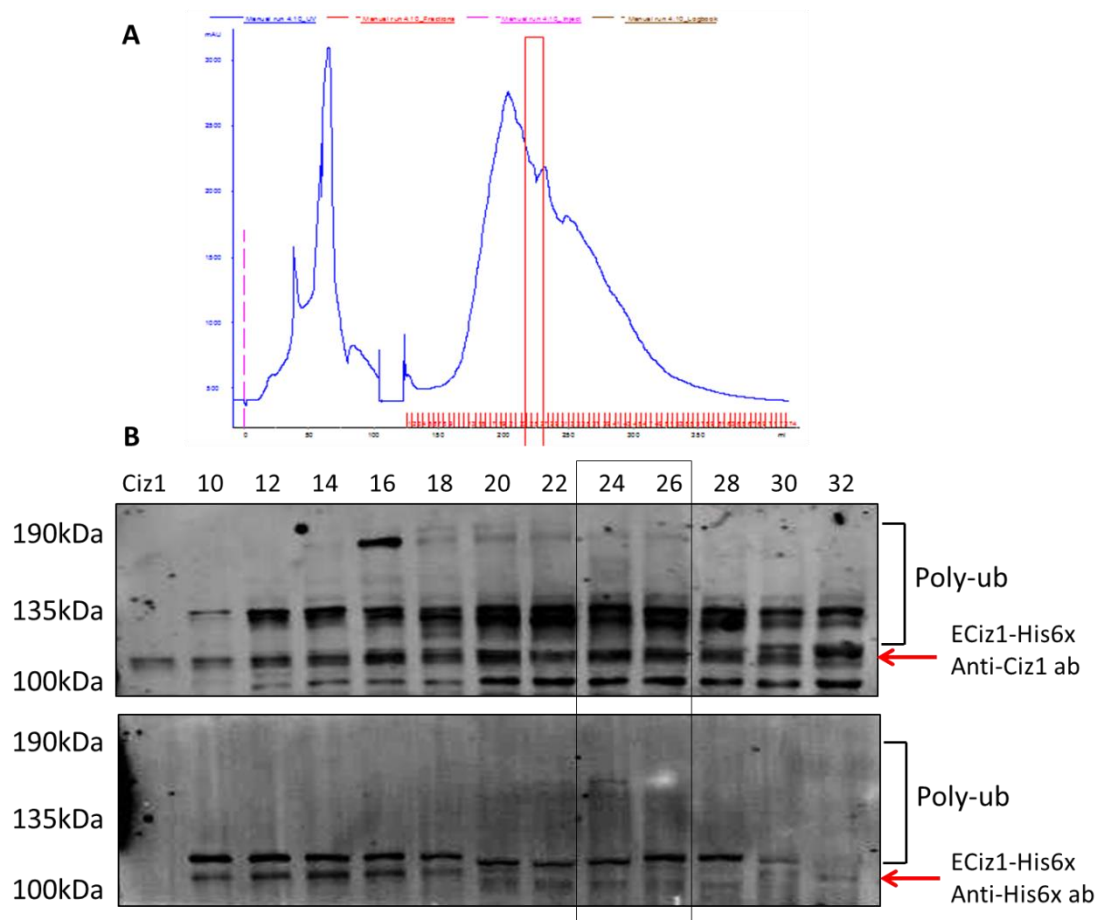


**Figure 7.6. Ciz1 ubiquitylation by fractions after Mono S cation exchange chromatography column. A)** Chromatogram of MonoS fractionation, fraction number on x axis, UV absorbance at 280 nm (mAU) on y axis. Selected fractions indicated in red. **B)** WB after *in vitro* ubiquitylation assay, probed for Ciz1 (upper panel) and His tag (bottom) antibodies. The highest ubiquitylation intensity observed in 24 – 26 fractions that eluted with 335 – 358.75 mM of KCl concentration. Red arrow indicates ECiz1-His6x recombinant protein band. Brackets show the range of poly-ubiquitylation (poly-ub) of Ciz1.

After dialysis and concentration, pooled fractions were loaded onto an analytical S200 size exclusion column (Figure 7.7).

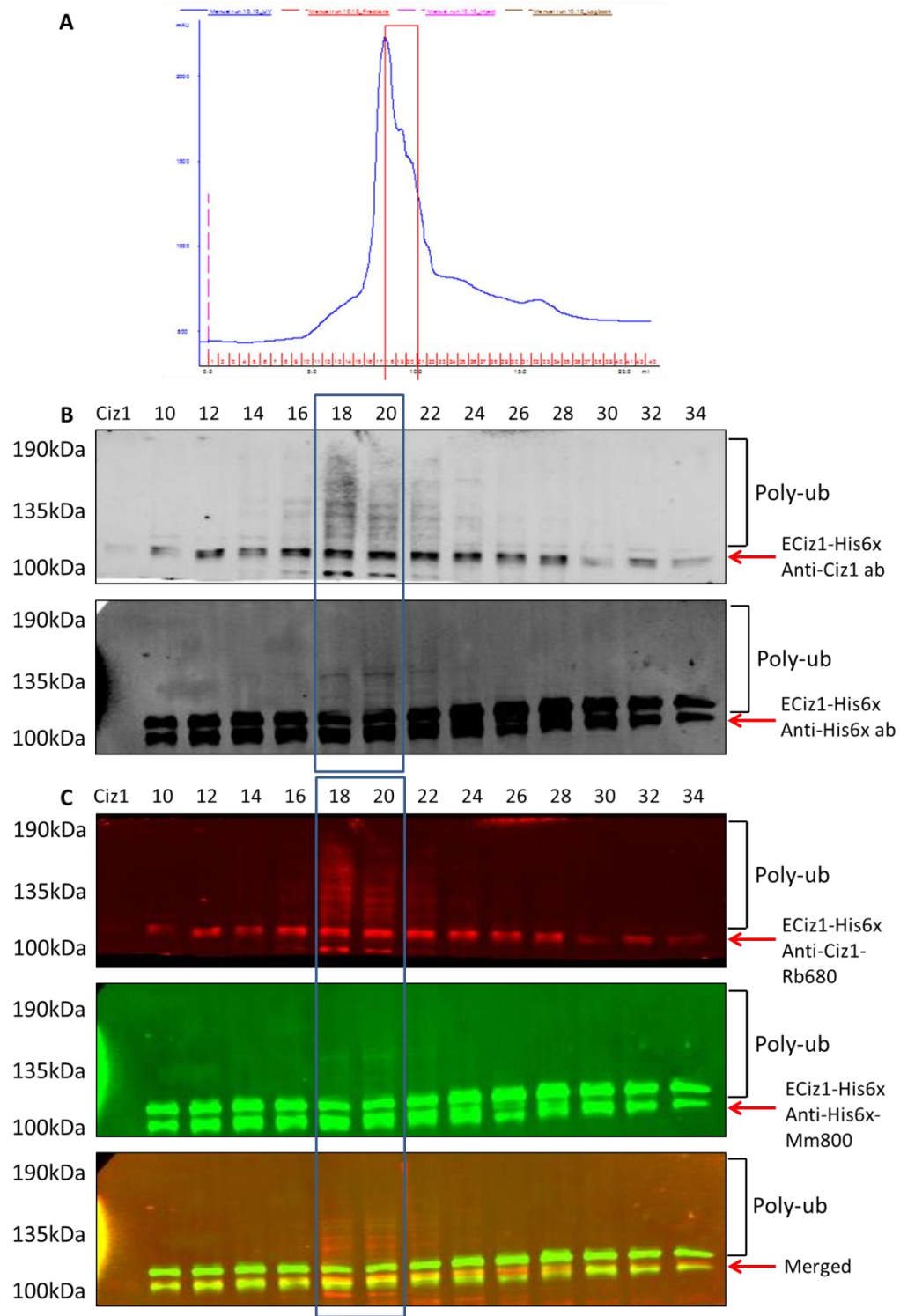


**Figure 7.7. Ciz1 ubiquitylation with fractions after SEC. A)** The chromatogram of SEC fractionation, fraction and volume on x axis, UV absorbance at 280 (mAU) on y axis. Red – selected fractions. **B)** The WB grey field of fractions used in Ciz1 ubiquitylation assays. **C)** The fluorescent field of *in vitro* ubiquitylation assays. WB was probed with Ciz1 and His tag antibody, and fluorescent secondary antibodies: Rabbit 680 nm (red), Mouse 800 nm (green), the blots were developed with Odyssey Imaging System. Red arrow indicates ECiz1-His6x recombinant protein band. Brackets show the range of poly-ubiquitylation (poly-ub) of Ciz1.

The chromatogram revealed the rapid peaking of A280 starting at column void volume of around 8 ml (Figure 7.7: A). To identify fractions containing E3 ligase activity, even fractions between 8 – 40 were assayed in *in vitro* ubiquitylation assays. Fractions 18 – 20 contained the highest ubiquitylation activity, producing ubiquitylation characteristic multiple bands above Ciz1 with both anti-Ciz1 and anti-His antibodies by Western blot (Figure 7.7: B and C). The Superdex200 calibration performed in University of Liverpool indicated that the size of the protein that eluted between 9 - 10 ml would be approximately 400 - 700 kDa in size, suggesting that the potential E3 ligase may be a large protein or working in a multimeric complex. Fractions 18-20 were pooled and loaded onto an analytical MonoS column for a final polishing step (Figure 7.8).

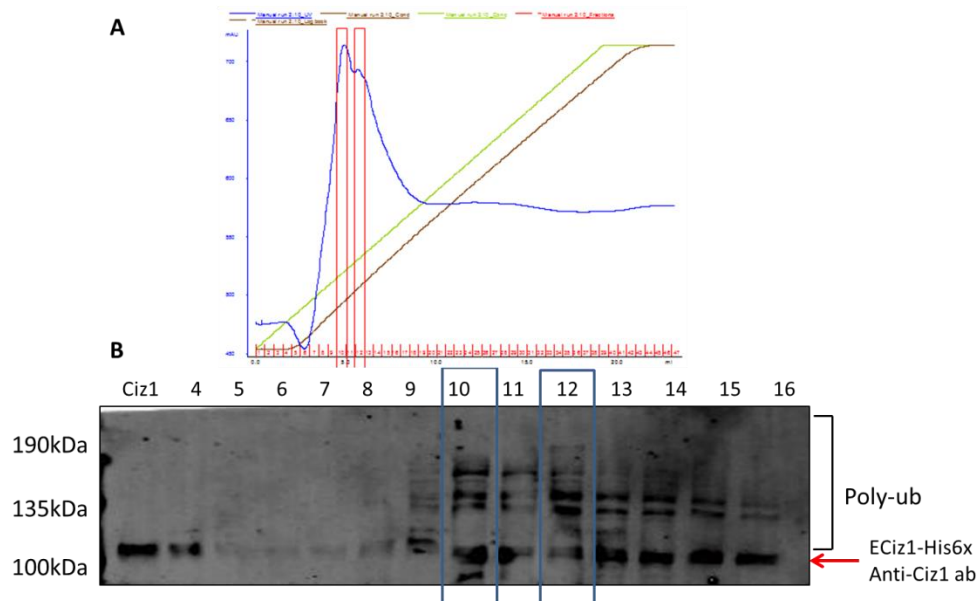


**Figure 7.8. Ciz1 ubiquitylation by MonoS 1ml fractions. A)** The chromatogram of MonoS fractions, fractions and volume on x axis, UV absorbance at 280nm (mAU) on y axis. Green line shows KCl concentration gradient, brown line – conductivity, blue line – absorbance, and red – the fractions selected for LC-MS analysis. **B)** WB of *in vitro* Ciz1 ubiquitylation fractions probed with Ciz1 antibody. Red arrow indicates ECiz1-His6x recombinant protein band. Brackets show the range of poly-ubiquitylation (poly-ub) of Ciz1.

*In vitro* ubiquitylation assays revealed the two main peaks at fractions 10-11 and 12-13 (Figure 7.8: A). After *in vitro* ubiquitylation analysis of even fractions from 2 – 40, fractions 10 and 12 were selected giving the highest intensity of ubiquitylation characteristic banding (Figure 7.8: B). These fractions exhibited slightly different ubiquitylation pattern as well, potentially indicating that there is more than one E3 ligase present, making them a good target for liquid chromatography–mass spectrometry analysis (LC-MS/MS).

### 7.1.5. Potential E3 ligase identification via LC-MS/MS analysis

The results of LS-MS/MS revealed 362 proteins in fraction 10 and 488 proteins in fraction 12 (Figure 7.9). Further analysis identified one potential E3 ligase in fraction 10: F-box only protein 38. Two potential E3 ligase candidates were identified in fraction 12; namely, (E3-independent) E2 ubiquitin-conjugating enzyme, and E3 ubiquitin-protein ligase UBR5 (Table 7.1).

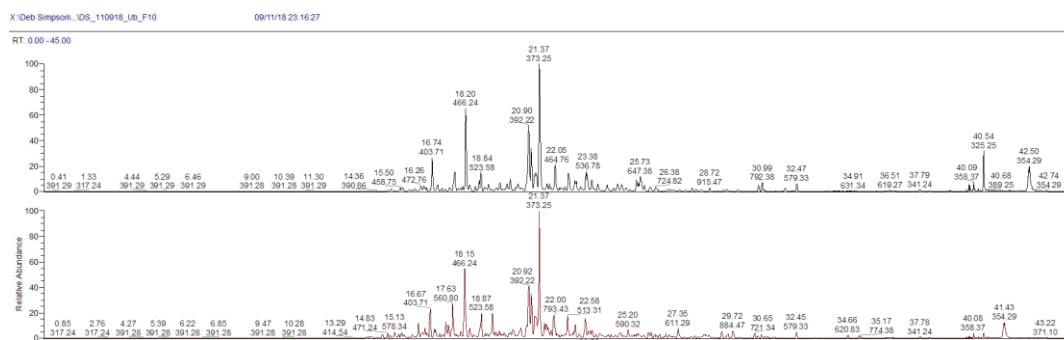


**Figure 7.9. The chromatogram of LC-MS/MS analysis.** The fraction 10 (top) and 12 (bottom) were analysed identifying 362 proteins in F10 and 488 in F12. The chromatogram presents relative abundance against time.

Title	Score	Coverage	MW (kDa)	Calc. pI
(E3-independent) E2 ubiquitin-conjugating enzyme OS=Homo sapiens GN=UBE2O PE=1 SV=3 - [UBE2O_HUMAN]	63.27	2.86%	141	5.1
E3 ubiquitin-protein ligase UBR5 OS=Homo sapiens GN=UBR5 PE=1 SV=2 - [UBR5_HUMAN]	29.26	0.54%	309	5.8
F-box only protein 38 OS=Homo sapiens GN=FBXO38 PE=1 SV=3 - [FBX38_HUMAN]	75.36	2.10%	133.9	6.33

**Table 7.1. The potential E3 ligases revealed after LC-MS/MS analysis.** Table shows individual protein score - sum of all peptides above the threshold; coverage – number of amino acids in found peptide divided by total number of amino acids in the protein; MW – molecular weight of the protein; Calc. pI – calculated isoelectronic point of the protein.

F-box only protein 38 is not extensively studied. Fbxo38 is 135 kDa in size and is predicted to target phosphorylated proteins for degradation, which is characteristic to the F-box E3 ligases. The hybrid E2/E3 enzyme UBE2O was shown to be ubiquitously expressed in various tissues preferably in central nervous system (CNS) and testis (Berleth and Pickart, 1996; Hormaechea-agulla et al., 2018; Klemperer et al., 1989), and could ubiquitylate multiple protein with consensus sequence K/R and VLI patches: [KR][KR][KR]-X(1,3)-[VLI]-X-[VLI]-X-X-[VLI] (Mashtalir et al., 2014). However, it was usually found in cytoplasm, and had a limited amount of information on cell cycle expression and control. Additionally, UBR5 E3 ligase was shown to regulate many proteins responsible for cell cycle progression, CDK9 – RNA Pol II mediated transcription, and DNA damage responses (Shearer et al., 2015). The UBR5 ubiquitin ligase is proposed to have tumour suppressor activity, and was correlated with multiple cancers including colorectal and prostate adenocarcinomas (Kim et al., 2010; Shearer et al., 2015).

Overall, this approach has identified three potential E3 ligases targeting Ciz1 for degradation. Further analysis of these ligases is required in order to confirm which E3 ligase is responsible for Ciz1 degradation.

## **7.2. Identification of phosphatases opposing Ciz1 regulating CDK2 activity**

### **7.2.1. Overexpression and purification of GST-Ciz1-N471**

In order for Ciz1 to be phosphorylated and stabilised by rising kinase activity in G1 phase, the hypo-phosphorylated state of Ciz1 has to be re-set in the end of cell cycle. If Ciz1 is left in hyper-phosphorylated state, the binding to cyclin A and DNA proliferative activity would be inhibited (Copeland et al., 2015).

Ciz1 has been shown to be phosphorylated by multiple kinases contributing to its accumulation, stability, and possibly protection from ubiquitylation and degradation. In the cell, CDK and opposing phosphatase activity precisely regulate the phosphorylation status of target proteins during the G1 – S transition. This serves to ensure precise temporal regulation of events and ensure that sufficient CDK activity is present to drive the cell cycle (Lo and Uhlmann, 2011).

The phosphorylation of Ciz1 appears to be dynamic and increases through the G1 – S transition (Figure 3.3). Additionally, if phosphorylation stabilises Ciz1 and protects it from degradation, then phosphatases may oppose this effect down-regulating Ciz1. A range of cancers has been linked with mutated/deleted phosphatases leading to a rise in kinase activity and cellular proliferation (Bhullar et al., 2018; Khanna et al., 2013; Wlodarchak and Xing, 2016). This could be of relevance when considering Ciz1 overexpressing cancers. Given that Ciz1 phosphorylation contributes to its stability

and protects it from degradation (Chapter 3), targeting kinase opposing phosphatases may be a novel therapeutic avenue in Ciz1 overexpressing cancers. Activation and functional restoration of phosphatases is a newly emerging field in cancer therapies (Mastellos et al., 2013).

To identify protein phosphatases that reverse CDK2 mediated phosphorylation of Ciz1 at pT293, a biochemical approach was used. This approach used the same sequential chromatography of the HeLa cellular extracts coupled to a novel *in vitro* phosphatase assay. In this experiment, a N-terminal Ciz1 construct that retains full DNA replication activity was used (Ciz1-N471) (Copeland et al., 2010; Copeland et al., 2015). This Ciz1 construct is efficiently phosphorylated using recombinant cyclin A-CDK2 (Copeland et al., 2015). The construct of p-GEX-6P-3-GST-Ciz1-N471 was acquired from Justin Ainscough's lab and DNA sequenced to ensure the correct construct (Figure 7.10: A).

GST-N471 was expressed in BL-21 *E. coli* cells via autoinduction in rich ZY medium for 24 hours at 20 °C. The protein was purified using glutathione sepharose 4B resin and the GST tag removed by 3C PreScission Protease (Figure 7.10: B). The results revealed that N471 was co-purified with *E. Coli* HSP-70 (70 kDa) (Figure 7.10: C). The identity of the impurity was not experimentally confirmed; however, HSP-70 was the most likely candidate in *E. coli* expression system. HSP-70 was previously detected as a co-purifying contaminant in other studies (Copeland et al., 2015). However, this impurity did not affect the *in vitro* phosphorylation or de-phosphorylation assays as it is not visible on western blots. Nevertheless, a refolding step (5 mM ATP) was



antibody was already determined using T293A mutations and *in vitro* kinase assays (Copeland et al., 2015). As a first step to validation of this approach, the reversibility of phosphorylation at T293 was demonstrated using recombinant cyclin A – CDK2 and Lambda protein phosphatase (Figure 7.11).

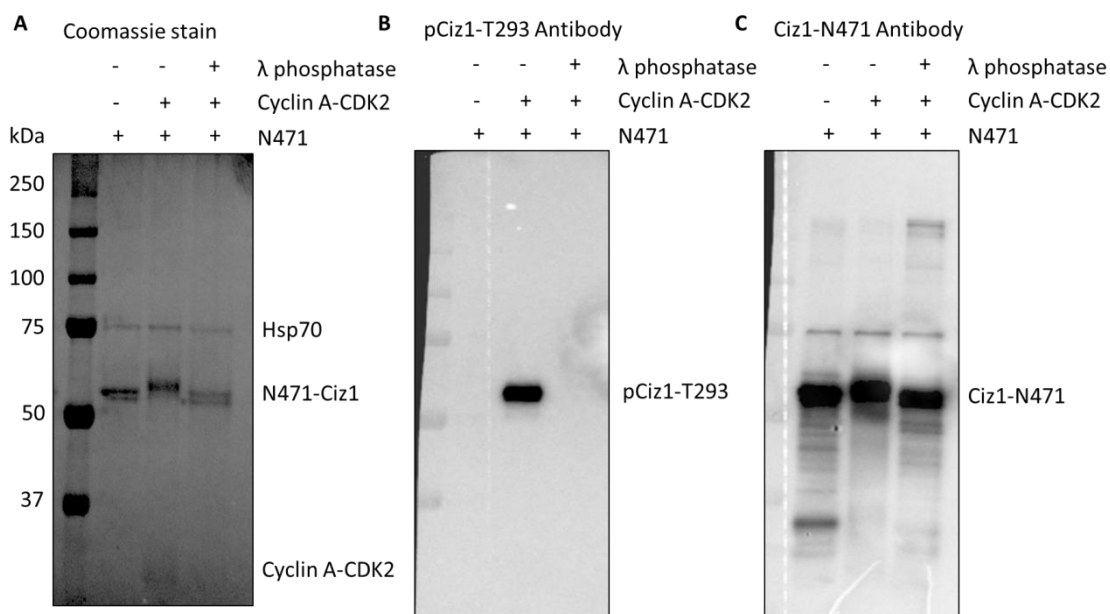


**Figure 7.11. The T293 antibody is specific for pCiz1.** *In vitro* phosphorylation was performed using recombinant Ciz1-N471, Cyclin A – CDK2, and lambda phosphatase as a negative control. **A)** Coomassie stained 10% SDS-PAGE gel showing Hsp70 at 75 kDa, Ciz1-N471 at 60 kDa, Cyclin A (50 kDa) – CDK2 (25 kDa). Phosphorylation of Ciz1 caused an anomalous upwards shift of pCiz1-N471. **B)** WB probed with T293 antibody was specific for phosphorylated Ciz1. **C)** WB re-probed with Ciz1 antibody for total protein as a loading control.

The coomassie staining revealed that pCiz1-N471 migrates anomalously when phosphorylated by cyclin A – CDK2 (Figure 7.11: A). Western blotting revealed that phospho-T293 antibody was highly specific for cyclin A-CDK2 phosphorylated Ciz1-N471 (Figure 7.11: B), and did not cross-react with total Ciz1 or when lambda phosphatase was introduced into the reaction preventing phosphorylation. Finally, the re-probing of the same blot with Ciz1 antibody indicated that each lane had similar protein loads (Figure 7.11: C). These data confirmed the specificity of

phospho-T293 antibody for phosphorylated Ciz1, demonstrating its suitability to monitor dephosphorylation of Ciz1.

### **7.2.3. Developing a strategy to identify phosphatase activity by classical biochemistry approaches**

Identification of putative regulatory phosphatases was performed using a similar approach to that used for identification of the regulatory E3 ligases. All chromatography steps were identical and the loss of phosphorylation from T293 was monitored by western blotting. To produce phosphorylated Ciz1 as the substrate for *in vitro* phosphatase assays, Ciz1 was phosphorylated using 200 ng of pCiz1-N471 and 20 ng of recombinant cyclin A-CDK2. All assays have a positive control pT293-Ciz1 and a reduction in phosphorylation at this site is used to determine fractions containing phosphatase activity. The *in vitro* phosphatase assays have an excess of Roscovitine to inhibit recombinant and endogenous CDK activity that may have masked phosphatase activity (Figure 7.12: B). HeLa whole cell extract was used to provide a source of phosphatase activity that would be sequentially purified by classical biochemical fractionation and phosphatases identified by LC-MS/MS.

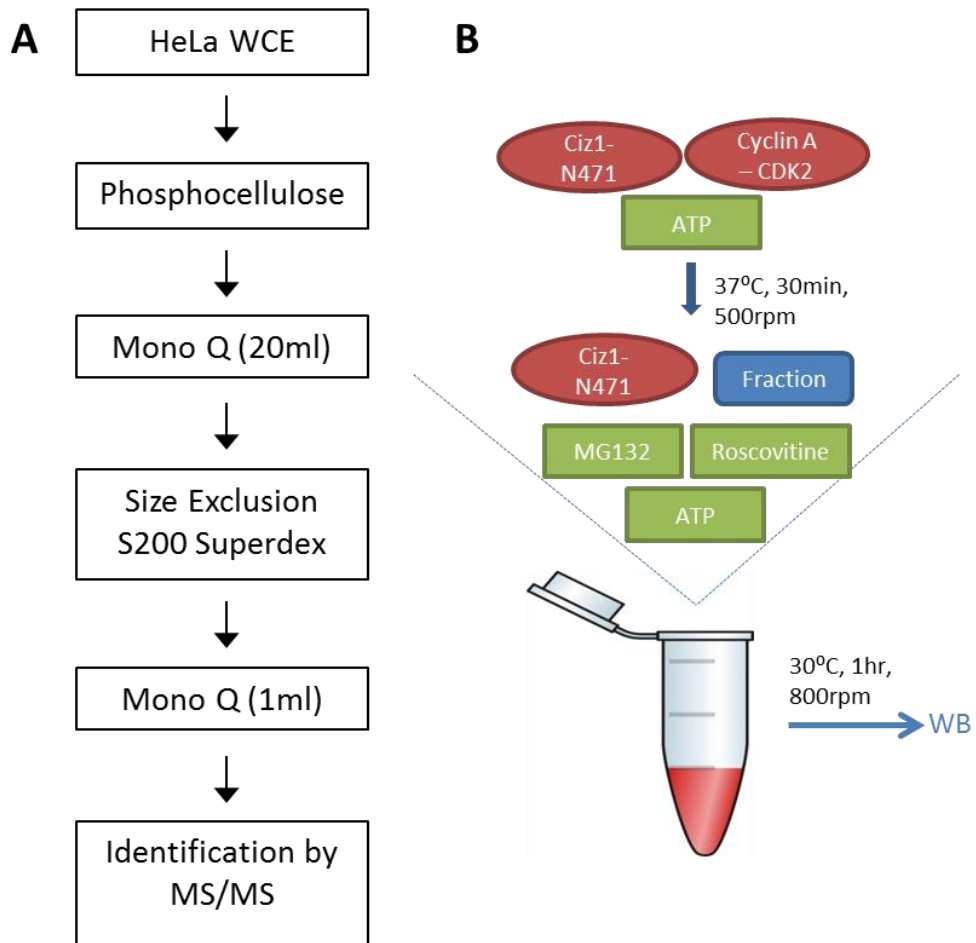


**Figure 7.12. Strategic overview for the identification of phosphatase activity.** **A)** A chain of chromatography steps used in phosphatase identification, 100 ml phosphocellulose, 20 ml MonoQ, 24 ml SEC, 1 ml MonoQ, LC-MS/MS. **B)** The diagram of *in vitro* phosphorylation assay and de-phosphorylation assay using chromatography fractions as a source of potential phosphatases.

#### 7.2.4. Fractionation of low salt extracts exhibiting phosphatase activity using anion exchange chromatography

Initially, HeLa whole cell extract was fractionated into 2 fractions: a low salt (P150) and high salt (P1000) fraction using a phosphocellulose column (Figure 7.5 and 7.13). Protein concentration was determined for each fraction and 0, 4 and 8  $\mu\text{g}$  of protein were used to identify phosphatase activity *in vitro* (Figure 7.13).

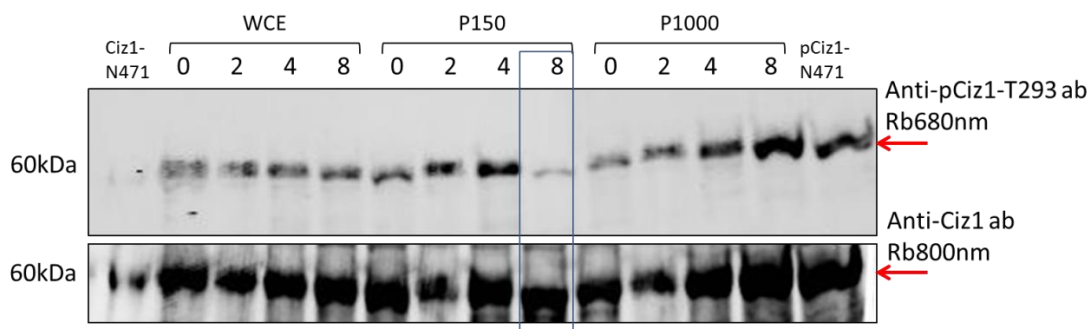


**Figure 7.13. p-Ciz1-N471 is de-phosphorylated by phosphocellulose P150 fraction.** The 0 – 8  $\mu$ g of HeLa WCE, P150 and P1000 fractions were tested. The Ciz1-N471 was used as a negative control and pCiz1-N471 as a positive control. The blots were probed with Ciz1-pT293 antibody specific for phosphorylated Ciz1, and re-probed with Ciz1 antibody specific for total Ciz1 protein. The fluorescent secondary antibodies Rabbit 680 nm and Mouse 800 nm were used as indicated and developed using Odyssey Imaging System. Red arrow indicates Ciz1-N471 recombinant protein band.

Phosphatase activity was detected in the P150 fraction eluted from the phosphocellulose column (Figure 7.13). To ensure that the reduction in signal was due to dephosphorylation of T293 and not degradation of Ciz1, total Ciz1 levels were determined (Figure 7.13: bottom panel). This showed that the activity was likely to be mediated by phosphatase activity and not due to proteolytic digestion of Ciz1.

Subsequently, the P150 fraction was loaded onto a 20 ml MonoQ column. The eluted proteins were fractionated over 80 fractions and the phosphatase activity was determined for all even numbered fractions. This revealed a reduction of pT293 Ciz1 signal in several fractions (Figure 7.14). The fractions 22, 28 – 30, and 40 – 42 showed an apparent reduction in phosphorylation (Figure 7.14: A, C, and D, upper blot). However, only fractions 28 – 30 showed a reduction in pT293 signal with no change in total Ciz1 levels. For fractions 22 and 40-42 there was a reduction in both pT293-Ciz1 and total Ciz1 signals, suggesting that the reduction in signal may be due

to proteolysis of Ciz1 (Figure 7.14: A and B, lower blot, indicated in blue outline).

Therefore, the fractions 28 – 30 were selected for further analysis.

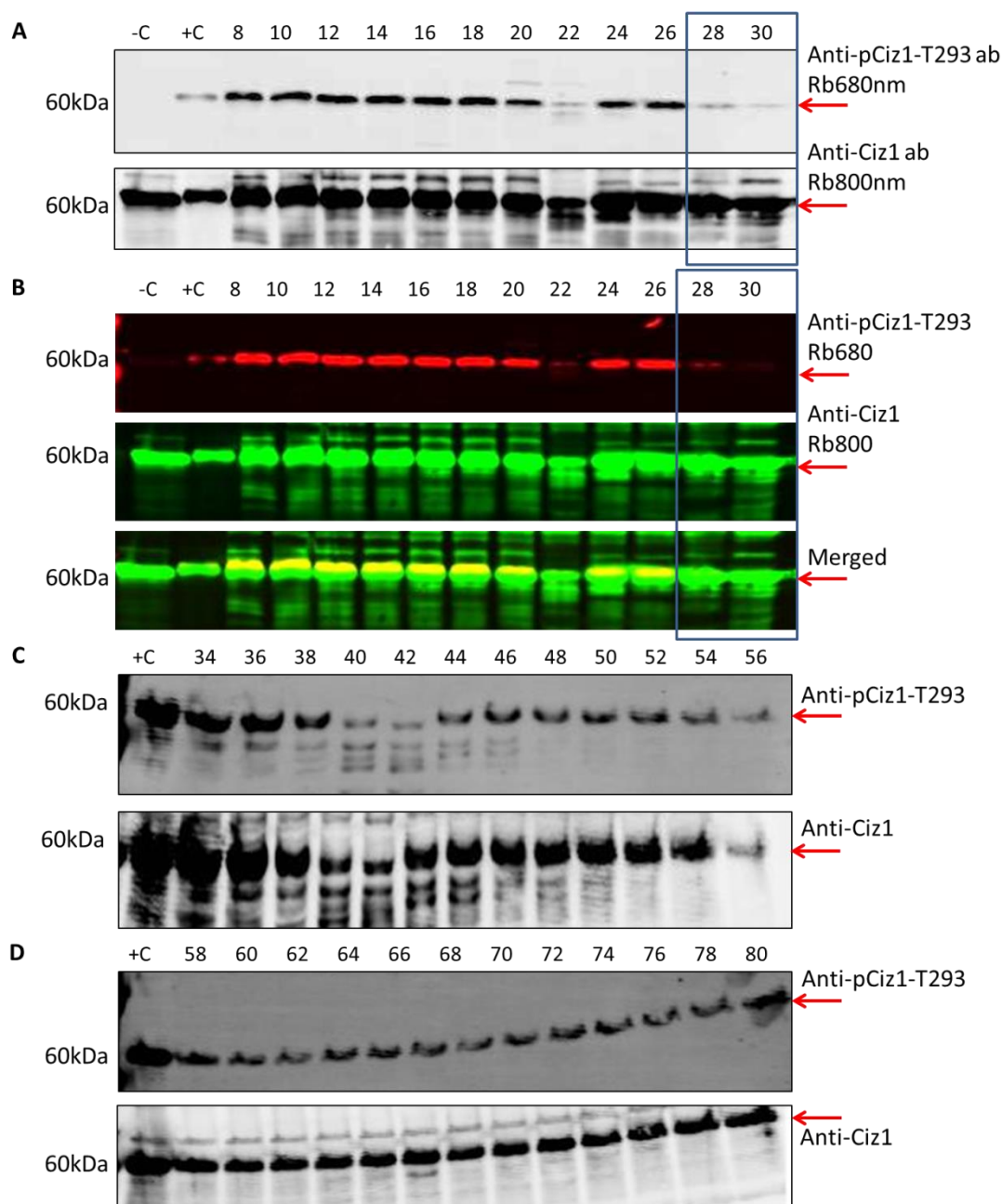


**Figure 7.14. Phosphatase activity assays of anion exchange fractions. A)** WB of fractions 8 – 30 probed with pCiz1-T293 and re-probed with Ciz1-N471 antibodies. **B)** Fluorescent field of 8 – 30 fractions developed using Odyssey Imaging System, red for pCiz1-T293-Rb680nm, green for Ciz1-N471-Rb800nm antibodies, and merged fields of both. **C)** WB of fractions 34 – 56 probed for phospho-T293 and total Ciz1. **D)** WB of fractions 58 – 80. Recombinant Ciz1-N471 was used as a negative control (C-), pCiz1-N471 as a positive control (C+). Red arrow indicates Ciz1-N471 recombinant protein band.

Subsequently, Fractions 28-30 were pooled and concentrated down to 500  $\mu$ l for further purification by size exclusion chromatography (SEC) (Figure 7.12: A). All even fractions were assayed for phosphatase activity, which revealed that phosphatase activity was present in fractions 24 – 26 (Figure 7.15: B). The fractions eluted at 11.5 – 13 ml of Superdex200 10/300 (24 ml) SEC (Figure 7.15: A, indicated in red), and predicted to be 125-250 kDa according to the Superdex200 calibration (Section 7.1.4). Importantly, dephosphorylation of phospho-T293 did not reduce the total Ciz1 levels (Figure 7.15). Fractions 24-26 were pooled, concentrated and loaded onto the final column, an analytical 1ml MonoQ anion exchange column.

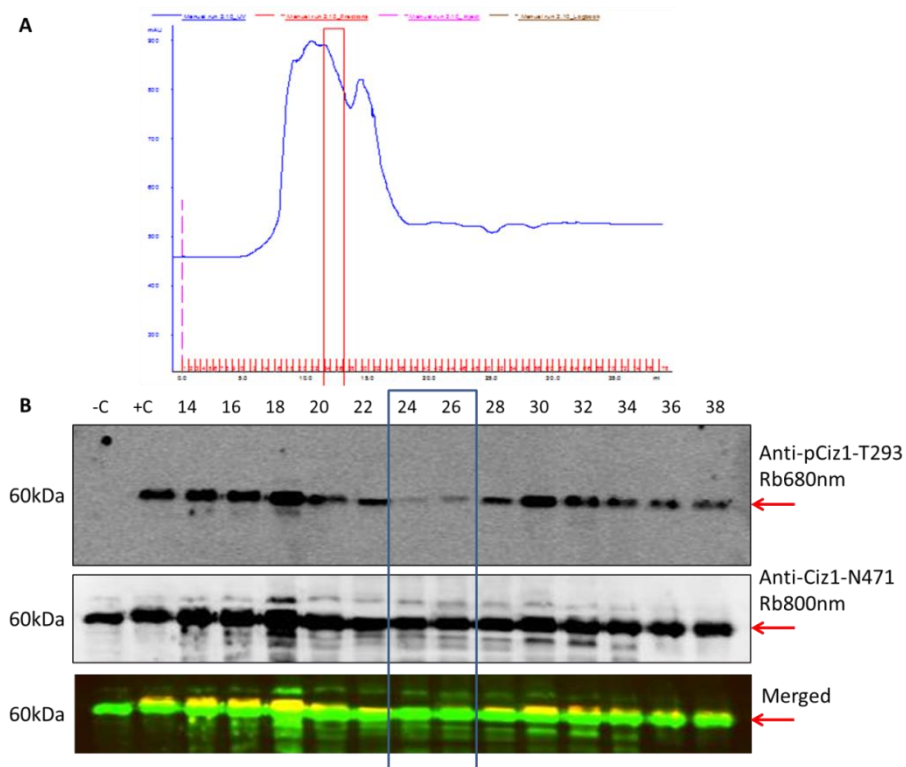


**Figure 7.15. Phosphatase assays of SEC fractions showing phosphatase active fractions. A)** Chromatogram of SEC, fraction number and volume on x axis, UV 280 nm absorbance (mAU) on y axis. Selected fractions indicated in red. **B)** WB of fractions 14 – 38 probed with Ciz1-N471 pT293-Rb680nm and Ciz1-Rb800nm antibodies, Ciz1-N471 (C-), Ciz1-N471 pT293 (C+). Red arrow indicates Ciz1-N471 recombinant protein band.

Phosphatase assays of fractions from the MonoQ column revealed that fractions 13-16 contained the highest phosphatase activity (Figure 7.16: B). Fractions 13 and 14 were selected for LC-MS/MS analysis, as they presented the highest absorbance and good resolution.

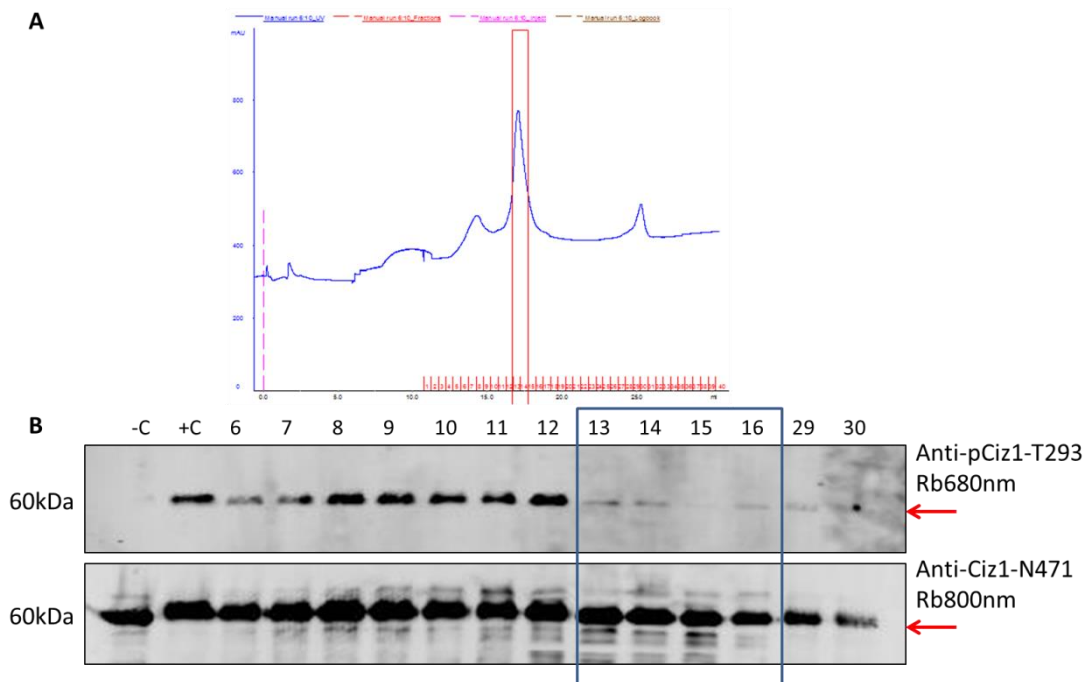


**Figure 7.16. Phosphatase assays of MonoQ fractions. A)** A chromatogram of MonoQ column fractions, 1 - 40 fractions on x axis, Absorbance at UV 280 nm (mAU) on y axis, selected fractions indicated in red. **B)** WB of *in vitro* assays probed with pCiz1-T293 and Ciz1 antibodies, Ciz1-N471 (-C), Ciz1-N471 pT293 (+C). Red arrow indicates Ciz1-N471 recombinant protein band.

### 7.2.5. Identification of putative regulatory phosphatases by LC-MS/MS

The LC-MS/MS analysis was performed as a service by the Centre for Proteome research Liverpool in collaboration with Professor Rob Beynon. Analysis of fractions 13 and 14 identified 467 proteins and 536 respectively (Figures 7.17 and 7.18). After filtering the results for serine/threonine phosphatases, this identified regulatory and catalytic subunits for both PP2A and PP1 phosphatases in each fraction (Table 7.2

and Table 7.3). This suggests that both PP1 and PP2A may have de-phosphorylated Ciz1. This activity is consistent with PP1 and PP2A reversing CDK mediated phosphorylation and aiding regulation of the cell cycle (Jiang, 2006; Kolupaeva and Janssens, 2013; Mochida et al., 2009; Ruvolo, 2016; Weber et al., 2015; Wlodarchak and Xing, 2016).

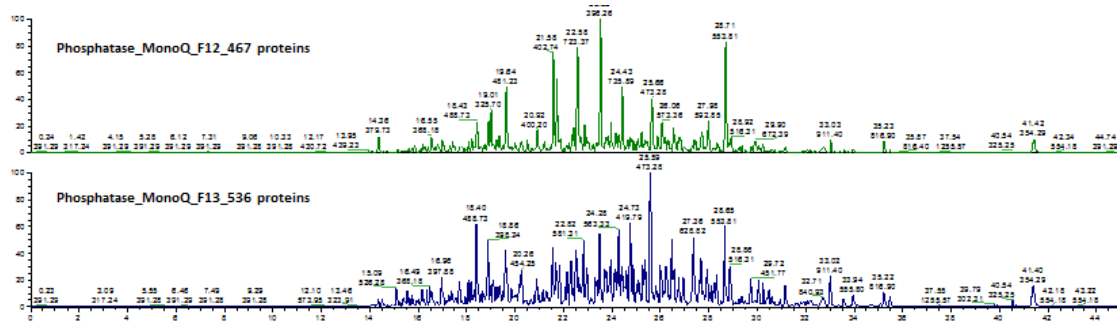


**Figure 7.17. The chromatogram of LC-MS/MS analysis.** The fractions 13 and 14 were analysed by LC-MS/MS. The 467 protein in F13 and 536 – F14 were identified.

PP2A is active in G1 – S transition, and both PP2A and PP1 are responsible for mitotic exit (Grallert et al., 2015; Jiang, 2006; Johnson and Latimer, 2005; Wlodarchak and Xing, 2016). Both phosphatases have been described in various pathologies including cancer (Jiang, 2006; Kim et al., 2007; Kolupaeva and Janssens, 2013; Mochida et al., 2009; Ruvolo, 2016; Wlodarchak and Xing, 2016). However, due to a high variability of the structural, regulatory, and catalytic subunits comprising the holoenzymes of phosphatases, it is not possible to identify the specific complexes due to this complexity (Figure 7.18).

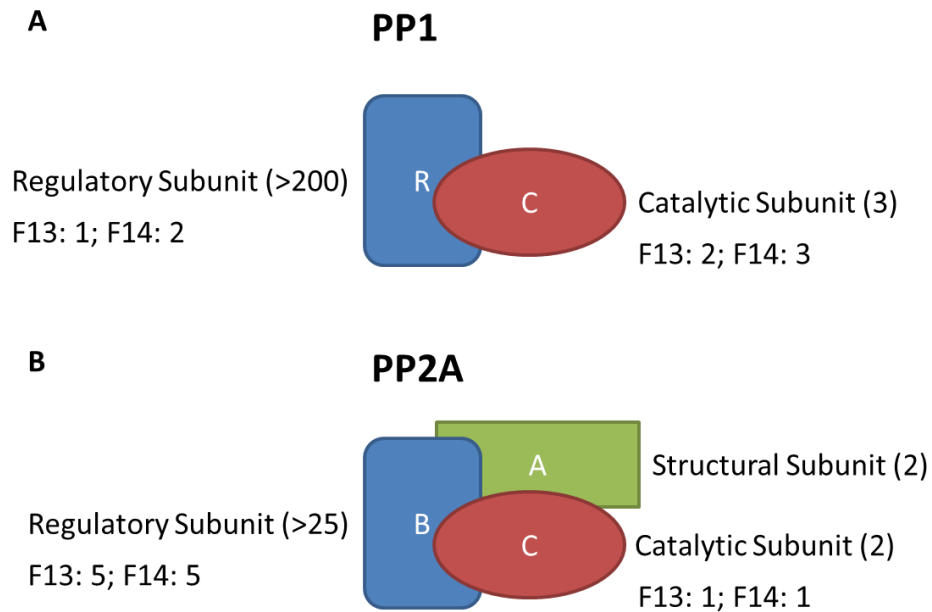


**Figure 7.18. The diagram of structures of serine/threonine protein phosphatases PP1 and PP2A. A)** Protein phosphatase 1 (PP1) is composed of highly variable regulatory subunit (R) with more than 200 different subunits identified, and catalytic subunit (C) with 3 possible variations. 1 regulatory subunit was identified in fraction 13 and 2 different regulatory subunits were identified in fraction 14; 2 catalytic subunits in fraction 13 and 3 in fraction 14. **B)** Protein phosphatase 2A (PP2A) has structural scaffold subunit (A) with two possible subunits identified, highly variable regulatory subunit (B) with more than 25 variations, and 2 different catalytic subunits (C). 5 regulatory subunits were identified in fraction 13 and 5 in fraction 14; 1 catalytic subunit in fraction 13 and 1 in fraction 14 (Weber et al., 2015).

Description	Score	Coverage	MW (kDa)	Calc pl
Serine/threonine-protein phosphatase 2A 55 kDa regulatory subunit B alpha isoform OS=Homo sapiens GN=PPP2R2A PE=1 SV=1 - [2ABA_HUMAN]	461.51	49.66 %	51.7	6.2
Serine/threonine-protein phosphatase PP1-alpha catalytic subunit OS=Homo sapiens GN=PPP1CA PE=1 SV=1 - [PP1A_HUMAN]	408.38	32.73 %	37.5	6.33
Serine/threonine-protein phosphatase PP1-gamma catalytic subunit OS=Homo sapiens GN=PPP1CC PE=1 SV=1 - [PP1G_HUMAN]	362.09	28.74 %	37	6.54
Serine/threonine-protein phosphatase 2A catalytic subunit alpha isoform OS=Homo sapiens GN=PPP2CA PE=1 SV=1 - [PP2AA_HUMAN]	267.11	32.04 %	35.6	5.54
Serine/threonine-protein phosphatase 2A 65 kDa regulatory subunit A alpha isoform OS=Homo sapiens GN=PPP2R1A PE=1 SV=4 - [2AAA_HUMAN]	251.41	16.81 %	65.3	5.11
Serine/threonine-protein phosphatase 2A 65 kDa regulatory subunit A alpha isoform OS=Homo sapiens GN=PPP2R1A PE=1 SV=4 - [2AAA_HUMAN]	215.45	23.06 %	41.5	4.91
Serine/threonine-protein phosphatase 2A 55 kDa regulatory subunit B delta isoform OS=Homo sapiens GN=PPP2R2D PE=2 SV=1 - [2ABD_HUMAN]	208.69	19.21 %	52	6.39
Serine/threonine-protein phosphatase 2A 56 kDa regulatory subunit gamma isoform OS=Homo sapiens GN=PPP2R5C PE=1 SV=3 - [2A5G_HUMAN]	172.46	11.07 %	61	6.87
Protein phosphatase 1 regulatory subunit 11 OS=Homo sapiens GN=PPP1R11 PE=1 SV=1 - [PP1RB_HUMAN]	159.7	19.05 %	13.9	7.01

**Table 7.2. The serine/threonine protein phosphatases identified by LC-MS/MS.** The catalytic and regulatory subunits of PP2A and PP1 phosphatases were identified in fraction 13.

Description	Score	Coverage	MW (kDa)	Calc pl
Serine/threonine-protein phosphatase 2A 55 kDa regulatory subunit B alpha isoform OS=Homo sapiens GN=PPP2R2A PE=1 SV=1 - [2ABA_HUMAN]	591.88	51.01 %	51.7	6.2
Serine/threonine-protein phosphatase 2A catalytic subunit alpha isoform OS=Homo sapiens GN=PPP2CA PE=1 SV=1 - [PP2AA_HUMAN]	490.46	44.34 %	35.6	5.54
Serine/threonine-protein phosphatase 2A 65 kDa regulatory subunit A alpha isoform OS=Homo sapiens GN=PPP2R1A PE=1 SV=4 - [2AAA_HUMAN]	411.42	22.24 %	65.3	5.11
Serine/threonine-protein phosphatase 2A 56 kDa regulatory subunit gamma isoform OS=Homo sapiens GN=PPP2R5C PE=1 SV=3 - [2A5G_HUMAN]	383.77	25.00 %	61	6.87
Serine/threonine-protein phosphatase PP1-alpha catalytic subunit OS=Homo sapiens GN=PPP1CA PE=1 SV=1 - [PP1A_HUMAN]	379.68	26.97 %	37.5	6.33
Serine/threonine-protein phosphatase PP1-beta catalytic subunit OS=Homo sapiens GN=PPP1CB PE=1 SV=3 - [PP1B_HUMAN]	345.21	22.63 %	37.2	6.19
Serine/threonine-protein phosphatase PP1-gamma catalytic subunit OS=Homo sapiens GN=PPP1CC PE=1 SV=1 - [PP1G_HUMAN]	333.8	22.91 %	37	6.54
Serine/threonine-protein phosphatase 2A 55 kDa regulatory subunit B delta isoform OS=Homo sapiens GN=PPP2R2D PE=2 SV=1 - [2ABD_HUMAN]	333.67	25.17 %	52	6.39
Serine/threonine-protein phosphatase 2A 56 kDa regulatory subunit epsilon isoform OS=Homo sapiens GN=PPP2R5E PE=1 SV=1 - [2A5E_HUMAN]	333.34	15.20 %	54.7	6.95
Protein phosphatase 1 regulatory subunit 7 OS=Homo sapiens GN=PPP1R7 PE=1 SV=1 - [PP1R7_HUMAN]	300.27	25.83 %	41.5	4.91
Protein phosphatase 1 regulatory subunit 11 OS=Homo sapiens GN=PPP1R11 PE=1 SV=1 - [PP1RB_HUMAN]	143.94	19.05 %	13.9	7.01
Protein phosphatase 1A OS=Homo sapiens GN=PPM1A PE=1 SV=1 - [PPM1A_HUMAN]	131.58	15.97 %	42.4	5.36

**Table 7.3. The serine/threonine protein phosphatases identified by LC-MS/MS.** The catalytic and regulatory subunits of PP2A and PP1 were identified in fraction 14.

### 7.3. Discussion

Overall, this work has identified that Ciz1 is regulated by opposing kinase and ubiquitin mediated degradation. Ciz1 protein levels are tightly controlled by rising CDK2/DDK kinase activities in G1 phase (Chapters 3 and 5), and is down-regulated by UPS (Chapter 3, 6, and 7). Ciz1 phosphorylation stabilises Ciz1, protects Ciz1 from degradation, or inactivates one of the components of UPS targeting Ciz1 for degradation (Figure 7.19: A). In order to identify the regulatory E3 ligase(s) that target Ciz1 cellular fractionation and LC-MS/MS was used, which identified three possible E3 ligases that target Ciz1, namely FBXO38, UBE2O, and UBR5.

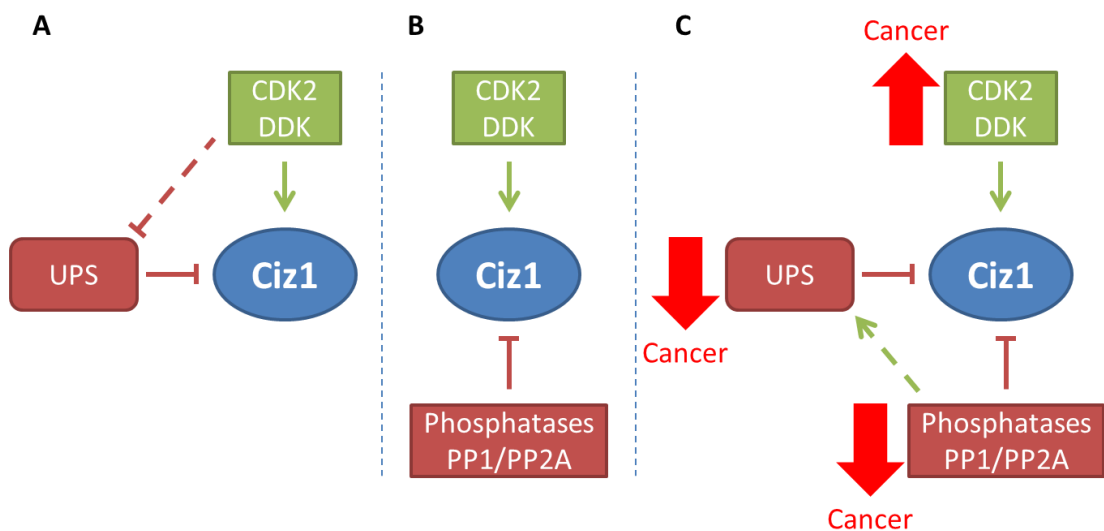


**Figure 7.19. Model of Ciz1 protein level regulation by opposing activities of kinases vs UPS and kinases vs phosphatases. A)** Ciz1 level is upregulated by rising CDK2 and DDK kinase activities in G1 phase (green arrow) (Chapters 3 and 5), and is downregulated by ubiquitin proteasome system mediated degradation (red line with the endpoint) (Chapters 3 and 7). The phosphorylation either protects Ciz1 from UPS, or inactivates UPS (red dashed line). **B)** Ciz1 level is upregulated by CDK2/DDK that is opposed by PP1 and PP2A phosphatases (red line with endpoint) (Chapter 7). **C)** Ciz1 is upregulated by CDK2/DDK, and down-regulated by both UPS and phosphatases. Phosphatases may dephosphorylate Ciz1 for effective UPS degradation, or dephosphorylate and re-activate UPS (green dashed arrow) for Ciz1 degradation. Upregulation in kinase activity or down-regulation in UPS and phosphatase activities may lead to Ciz1 overexpression driving Ciz1 dependent tumourigenesis (Chapter 6).

In this context, the opposing kinase and phosphatase activities that modulate phospho-T293 levels could play an important regulatory role in Ciz1 accumulation (Figure 7.19: B). Using a similar biochemical approach two putative phosphatase regulators of Ciz1 were identified. Multiple catalytic and regulatory subunits of PP1 and PP2A phosphatases were identified after extensive purification and enrichment of phosphatase activity from HeLa cells. The PP1 and PP2A phosphatases efficiently remove CDK2 mediated phosphorylation of Ciz1 at T293 (pT293). This is consistent with the requirement of Ciz1 dephosphorylation in order to re-set its cyclin A binding and Ciz1 DNA replicative function (Copeland et al., 2015). Also, the temporal separation of serine and threonine phosphorylation of Ciz1 in G1 phase (Figure 3.3) is consistent with PP2A's catalytic preference for phospho-threonine over phosphoserine (Cundell et al., 2016; Godfrey et al., 2017). Given that Ciz1 phosphorylation aids its accumulation in G1 phase (Chapters 3 and 5), the de-phosphorylation of Ciz1 may increase its poly-ubiquitylation and thereby reduce Ciz1 protein levels (Figure 7.19: B).

The proposed model aims to integrate the potential for UPS, CDK and phosphatase activity regulating Ciz1 accumulation. Deregulation of CDK activity is associated with tumorigenesis (Barnum and O'Connell, 2014; Canavese et al., 2012; Deshpande et al., 2005; Pauzaite et al., 2017; Vijayaraghavan et al., 2018). In a deregulated CDK context, we propose that high CDK activity may inactivate the E2/ E3 ligase responsible for Ciz1 degradation and in this way increases Ciz1 levels (Figure 7.19: A). The model proposed here suggests that Ciz1 is regulated by opposing kinase and UPS/phosphatase activities. The precise molecular mechanism is yet to be elucidated; however, this work led to a number of new questions that will be

addressed in the near future. First aim will be to determine the identity of E3 ligase targeting Ciz1 for degradation. Next, the interplay between UPS and CDK activity will require further investigation. Finally, further analysis of Ciz1 dephosphorylation is going to be performed.

The regulatory molecular pathways that control Ciz1 activity are interlinked. In the context of Ciz1 overexpression, hyper-activation of CDK2 activity or down-regulation in UPS/phosphatase activities may promote Ciz1 over-expression and potentially drive Ciz1 dependent cancer proliferation (Chapter 6) (Figure 7.19: C). Increased CDK activity is a common event in cancer, which contributes to increased cancer cell proliferation, evasion of cell cycle checkpoints, DNA replication stress and DNA damage (Bhullar et al., 2018; Caetano et al., 2014; Canavese et al., 2012; Heldt et al., 2018a; Malumbres, 2014; Pauzaite et al., 2017; Zhang et al., 2009). In contrast, downregulation and loss-of-function mutations in UPS have been linked to tumorigenesis, cancer aggressiveness, and poor patient outcomes. There are increasing interest in development of UPS components as therapeutic targets and biomarkers for cancer detection and prognosis (Kitagawa et al., 2009; Pal et al., 2014; Rizzardi and Cook, 2012; Shearer et al., 2015; Sun, 2006; Zheng et al., 2016).

This suggests potential research avenues in targeting Ciz1 overexpressing/dependent cancers. This work has already explored small molecule CDK2/DDK kinase inhibitors in Ciz1 dependent prostate adenocarcinoma (PC3) cell line (Chapter 6). Targeting CDK2/DDK activity may provide two-pronged attack reducing both CDK activity and Ciz1 levels. The kinase inhibition therapy targeting Ciz1 levels would only be successful if cells possess intact UPS. This demonstrates the importance of

identification of E3 ligases targeting Ciz1 for degradation as well as other components in the future (Chapter 7). Indeed, the research in pharmaceutical targeting of UPS is still in its infancy, with only handful of drugs approved, such as Thalidomide targeting Cereblon E3 ligase in multiple myeloma and mantle cell lymphoma (Galdeano, 2017; Morrow and Lin, 2015; Pal et al., 2014; Weathington and Mallampalli, 2014). Additionally, many cancers have mutated and down-regulated UPS leading to oncogene accumulation; therefore, contrary to kinase inhibition therapies, successful intervention should aim to restore UPS function rather than inhibit it. This may be achieved by allosteric regulation; however, currently only computational predictive models of UPS activation have been proposed (Galdeano, 2017).

Further, the observation that Ciz1 may be dephosphorylated by PP1 and PP2A that reverse CDK2 mediated phosphorylation of Ciz1 suggests that inactivation of PP1 or PP2A would lead to Ciz1 overexpression (Figure 7.19: C). PP1 and PP2A regulate cell cycle progression, DNA replication and damage responses. Both phosphatases are deregulated in cancer (Section 7) and have been proposed as potential therapeutic targets (Alver et al., 2017; Grallert et al., 2015; Hiraga et al., 2014; Kim et al., 2007; Kolupaeva and Janssens, 2013; Margolis et al., 2006; Mochida et al., 2009; Perrotti and Neviani, 2013; Ruvolo, 2016; Wlodarchak and Xing, 2016). Strategies to reduce Ciz1 levels would aim to stimulate PP1 and PP2A activity to increase the rate of Ciz1 dephosphorylation. PP1 phosphatases are heterodimers composed of a catalytic and regulatory subunit. PP2A heterotrimer consists of scaffold and catalytic subunits that bind highly variable regulatory subunit, which dictates timing of enzyme activation and its localisation (Figure 7.18) (O'Connor et al., 2018). The therapeutic targeting of

phosphatases is complicated due to the plethora of subunits that can make up the holoenzyme and potential for functional redundancy of isoforms (Wlodarchak and Xing, 2016). However, there are two potential mechanisms to increase phosphatase activity. First, reducing or inactivating endogenous phosphatase inhibitors would lead to the activation of target phosphatase. Second, modulation of regulatory post-translational modifications in phosphatases activating the desired phosphatase (Ahola et al., 2007; Boutros et al., 2007; Janghorban et al., 2019; Khanna et al., 2013; Lazo et al., 2017; Mazhar et al., 2019; McConnell and Wadzinski, 2009; O'Connor et al., 2018; Perrotti and Neviani, 2013; Rudolph et al., 2004; Ruvolo, 2016; Winkler et al., 2015).

Several approaches that activate protein phosphatase PP2A are currently in various stages of research or clinical trials. For instance, Phenothiazine and SMAP bind to the scaffold subunit and promote conformational changes that activate PP2A. This approach has been shown to promote PP2A dependent apoptosis in leukaemias and inhibit KRAS dependent tumour growth (Gutierrez et al., 2014; Sangodkar et al., 2017).

This overview of pharmaceutical targeting of kinases, phosphatases and UPS activities, demonstrates the importance of molecular screening of cancer patients to identify the underlying mutations driving cancer progression and potential therapeutic targets. In Ciz1 dependent cancers, Ciz1 overexpression may be the result of upregulated kinase activity or due to loss-of-function mutations in UPS and phosphatases. The effective targeting of Ciz1 for UPS mediated degradation via inhibition of CDK2 activity would require a functional UPS system. Both deregulations

of the UPS and/or phosphatase activities could potentially affect the efficacy of this approach. Identification of tumours that have functional UPS and phosphatase activities would be important clinical biomarkers that would aid in patient stratification.

In addition, the increase in Ciz1 level that is present and necessary for tumour proliferation to arise, may be a consequence of inactivation of the regulatory E3 ligase. In this context CDK2 inhibition would not be suitable as the effect on Ciz1 levels would be minimal. Further work is required to fully understand the interplay between the regulatory signalling networks that modulate Ciz1 levels and establish whether these networks can be targeted to reduce Ciz1 levels in a clinical setting.

# **Chapter 8**

## **General discussion**

### **8.1. Ciz1 level is upregulated by kinase phosphorylation in G1 phase**

The deregulation of Ciz1 levels has been linked with the defects in DNA replication, DNA repair, and cell cycle progression (Ainscough et al., 2007; Copeland et al., 2010; Copeland et al., 2015; Coverley et al., 2005; Greaves et al., 2012; Liu et al., 2016; Łukasik et al., 2008; Pauzaite et al., 2017). Abnormal Ciz1 levels have been identified in various pathologies. The overexpression of Ciz1 has been reported as a facilitator of tumorigenesis, cancer cell migration, tumour vascularisation, and aggressiveness (Den Hollander et al., 2006; Den Hollander et al., 2006; Lei et al., 2016; Wang et al., 2014; Wu et al., 2016; Yin et al., 2013; Zhang et al., 2015). Additionally, the overexpression of Ciz1 and its variants have also been identified as potential biomarkers in cancer diagnosis (Coverley et al., 2017; Higgins et al., 2012; Wang et al., 2014; Zhou et al., 2018). Nonetheless, Ciz1 ablation in murine models showed that loss of Ciz1 increases cell sensitivity to irradiation, predisposes cells to viral oncogenic transformation, and increase incidence of lymphoid tumours in female lineages due to affecting X chromosome silencing and epigenetics (Nishibe et al., 2013; Ridings-Figueroa et al., 2017; Stewart et al., 2019; Sunwoo et al., 2017). Therefore, Ciz1 may serve as a tumour suppressor at unperturbed levels, but overexpression of Ciz1 may have oncogenic properties. To further emphasise the importance of maintenance of the correct levels of Ciz1 expression, low Ciz1 expression promotes neurodegeneration and other brain defects (Khan et al., 2018; Xiao et al., 2016; Xiao et al., 2018). These data suggest that Ciz1 homeostasis is crucial to maintain normal cell cycle progression, regulation of DNA replication, and tissue function. However, the molecular mechanisms that control Ciz1 levels have not been determined.

Ciz1 phosphorylation has been implied as a regulator of Ciz1 DNA replicatory activity (Copeland et al., 2010; Copeland et al., 2015; Pauzaite et al., 2017). The phosphorylation of 3 CDK regulatory sites (T144, T192, T293) has collaborative inhibitory effect over Ciz1 and cyclin A binding, thus over its DNA replication initiation activity. Ciz1 may play a role in prevention of DNA re-replication. This work provided basis for further research on the importance of Ciz1 phosphorylation. Further, previous research has shown that newly synthesised and localised Ciz1 is required for successful DNA replication initiation (Ainscough et al., 2007; Copeland et al., 2010; Copeland et al., 2015; Coverley et al., 2005). Therefore, this work focused on the importance of Ciz1 phosphorylation on Ciz1 accumulation and stability. Understanding the molecular mechanisms that regulate Ciz1 levels may allow its targeting in cancer. Therefore, this research focused on determining the molecular mechanism that regulates Ciz1 abundance in normal mice fibroblasts and human cancer cell lines.

First, Ciz1 accumulation was determined in post-quiescent embryonic mice fibroblasts (3T3) (Figure 3.3). Ciz1 was found to accumulate through G1 phase in order to reach sufficient levels for initiation of DNA replication (Copeland et al., 2010; Copeland et al., 2015; Coverley et al., 2005). The accumulation of Ciz1 mirrors its phosphorylation on two CDK phosphorylation sites, threonine 293 (T293) and serine 331 (S331). There is a strict temporal separation of phosphorylation of S331 in early G1, and phosphorylation of T293 in late G1 – S phase that correlates with Ciz1 accumulation. The phosphorylation of Ciz1 at T293 inhibits Ciz1 DNA replicative function in order to prevent DNA re-replication (Copeland et al., 2015). The phosphorylation of Ciz1 at S331 correlates with Dbf4 and cyclin E, and T293

phosphorylation correlates with cyclin A expression (Figure 3.3). The increase in Ciz1 protein levels appears to be driven by post-translational modification with both CDK mediated phosphorylation and UPS mediated degradation contributing to the regulation of Ciz1 levels with little change at the transcript levels (Figure 3.3). The accumulation of Ciz1 correlates with E2F regulated transcripts, Dbf4, cyclin E, and cyclin A (Giacinti and Giordano, 2006; Harbour and Dean, 2000; Ohtani et al., 1995). Therefore, the relationship between increasing kinase activity and Ciz1 accumulation has been assessed.

According to cyclin expression and kinase activation profiles (Figures 1.1 and 1.2) (Hochegger et al., 2008), post-quiescent cells have been treated with specific small molecule kinase inhibitors to target the relevant cyclin-CDK and DDK complexes throughout G1 phase (Figure 3.5). Ciz1 accumulation is affected by two DDK inhibitors PHA-767491 and XL-413 (Koltun et al., 2012; Vanotti et al., 2008), and two CDK2 inhibitors Roscovitine and CVT-313 (Faber and Chiles, 2007; Lauren, 1997). However, PHA-767491 reduces cell cycle progression more potently than XL-413. In addition, PHA-767491 decreases Ciz1 phosphorylation on T293 site that is more similar to the effect of CDK2 inhibitors Roscovitine and CVT-313 (Figure 3.6 and 3.7). This is consistent with the off target CDK2 activity of PHA-767491 with an IC50 of 200 nM (Hughes et al., 2012; Montagnoli et al., 2008; Rainey et al., 2017). In murine cells, PHA-767491 abolishes cyclin A protein levels at 1 micromolar concentration and significantly reduces E2F mediated transcription of cyclin E1, E2, and A2 with a similar potency to CDK2 inhibitors Roscovitine and CVT-313 (Figure 3.6, 5.4, and 5.5). Consistent with CDK2 inhibition, PHA-767491 inhibits retinoblastoma protein (Rb) phosphorylation on CDK phosphorylation site serine 811 (Figures 5.2-4) (Rubin,

2013). These data are consistent with PHA-767491 targeting both G1 – S kinases, DDK and CDK2, in micromolar concentrations (Rainey et al., 2017).

In order to characterise the activity of PHA-767491 with respect to inhibition of the Rb – E2F transcription axis, the E2F regulated transcripts have been analysed after PHA-767491 treatment. The analysis has been performed using GAPDH mRNA and 18S rRNA housekeeping genes. Use of both the RNA polymerase I and RNA polymerase II transcripts as housekeeping genes reduces the possibility that quantitative PCR would be affected by off-target CDK9 activity of PHA-767491 (Natoni et al., 2011; Natoni et al., 2013). The effect of PHA-767491 on E2F transcription is independent from CDK9 – RNA polymerase II axis in 1 - 10  $\mu$ M range in normal mouse fibroblasts and human cancer cell lines (Figure 5.6 and 6.11). These data suggest that PHA-767491 influences both DDK and CDK activities and reduces E2F mediated transcription that is required for cell cycle progression from G1 to S phase. This dual activity against both DDK and CDK2 at 1 micromolar concentrations may explain the superior efficacy of PHA-767491 over XL-413 in multiple cancer cell lines (Sasi et al., 2014).

## **8.2. Genetic depletion of cyclins and DDK suggests that kinase activity is required for Ciz1 accumulation**

The genetic co-depletion of Cdc7–Dbf4, cyclin E1, 2, and depletion of cyclin A2 reduces cell cycle progression through G1 - S due to limiting kinase activity and not activating pre-replication complex (Coudreuse and Nurse, 2010a; Hochegger et al., 2008; Lim and Kaldis, 2013; Malumbres, 2014) (Figure 3.9). Additionally, the depletion of G1 – S regulators reduces Ciz1 protein accumulation (Figure 3.10). CDK2

inhibition prevents T293 phosphorylation that closely correlates with Ciz1 accumulation. However, DDK inhibition does not affect either T293 or S331 phosphorylation, but moderately reduces Ciz1 levels, suggesting that Ciz1 accumulation may require multiple phosphorylation events by various kinases in G1 phase. These observations are consistent with the quantitative theory that states that increasing CDK activity is sufficient to coordinate all of the phases of the cell cycle (Figure 1.2) (Coudreuse and Nurse, 2010a; Hochegger et al., 2008). Additionally, many cellular processes depend on the collaborative kinase activity including helicase activation. Here DDK and CDK phosphorylate MCM2 at serine 40/41. Cyclin E – CDK2 phosphorylates serine 41 priming MCM2 for second phosphorylation on serine 40 by DDK (Montagnoli et al., 2006). The accumulation of Ciz1 requires continuous kinase activity and phosphorylation on multiple sites throughout G1 phase that is achieved by the collaboration of multiple kinases.

### **8.3. Ciz1 de-phosphorylation by phosphatases**

This work shows that Ciz1 phosphorylation leads to Ciz1 accumulation in G1 phase (Chapter 3). These data add to published work on phosphorylation importance for Ciz1 DNA replication activity (Copeland et al., 2015) and are consistent with a model that kinase activity plays key role in Ciz1 abundance. Ciz1 phosphorylation by CDK and DDK and its dephosphorylation by PP1 and PP2A suggest that there is a complex network of regulators that regulate Ciz1 accumulation and potentially activity. Various subunits of PP1 and PP2A phosphatases have been identified by purification of fractions that maintain phosphatase activity and mass spectrometry (Figures 7.12-17, Table 7.2 and 7.3). Both PP1 and PP2A phosphatases are implicated in cell cycle

regulation, with PP1 being most active in mitosis where it contributes to the complete dephosphorylation of the retinoblastoma protein (Kolupaeva and Janssens, 2013). PP2A is active throughout the entire cell cycle and responds to various stimuli (Grallert et al., 2015; Kolupaeva and Janssens, 2013; Weber et al., 2015). Therefore, both phosphatases could target CDK2 phosphorylation site threonine 293 of Ciz1 that has been tested.

Multiple catalytic, regulatory and scaffold subunits were identified with mass spectrometry for both PP1 and PP2A (Figure 7.17, Tables 7.2 and 7.3) that will be characterised in the future. A number of PP2A phosphatases have been shown to oppose CDK phosphorylation throughout the entire cell cycle, and display a preference for phospho-threonine over phospho-serine enforcing a temporal order to phosphorylation (Cundell et al., 2016; Godfrey et al., 2017; Hein et al., 2017). The identification of PP1 and PP2A phosphatases is consistent with their roles in opposing CDK mediated phosphorylation and the temporal order of Ciz1 phosphorylation, starting with S331 in early G1 phase and threonine phosphorylation later in G1 (Figures 3.3 and 8.1).

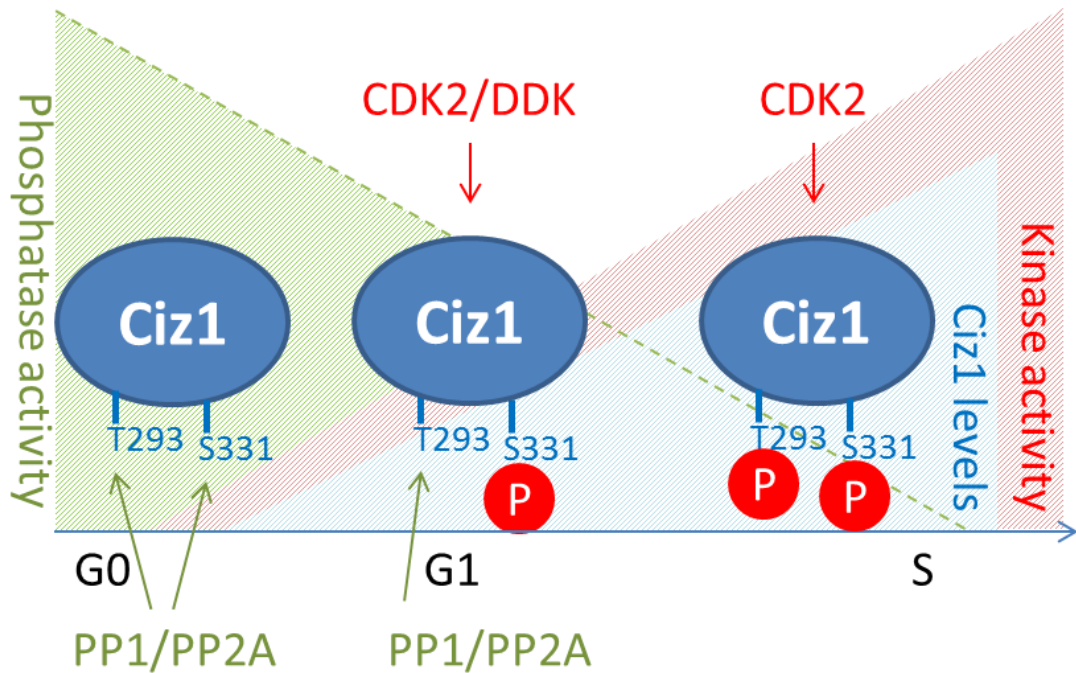


**Figure 8.1. Model of Ciz1 phosphorylation/dephosphorylation in G1 – S transition.** Ciz1 is phosphorylated on multiple sites (representative S331 and T293) by multiple kinases (CDK2 and DDK) in G1 phase leading to its accumulation (light blue shading). Ciz1 accumulation mirrors rising kinase activity (light red shading) in G1 phase (Chapter 3) (Bertoli et al., 2013b; Coudreuse and Nurse, 2010a; Hochegger et al., 2007). Ciz1 phosphorylation on different sites is temporally separated, S331 is phosphorylated prior T293, that is potentially regulated by phosphatase PP1/PP2A (light green) (Cundell et al., 2016; Godfrey et al., 2017) (Chapter 7).

Overall, these data suggest that Ciz1 phosphorylation and accumulation is tightly controlled by opposing activities of kinase phosphorylation and phosphatase dephosphorylation. Upregulated kinase activities and downregulated phosphatase may lead to over-accumulation of Ciz1 that contributes to Ciz1 dependent cancer proliferation (Figure 7.19). Small molecule kinase inhibition is a fast growing field in cancer research (Jorda et al., 2018; Klaeger et al., 2017; Knight and Shokat, 2005; Noble et al., 2004; Wynn et al., 2011; Zhang et al., 2009). However, the stimulation and recovery of downregulated phosphatase activity is a new emerging avenue in cancer research with a number of drugs in pre-clinical research (Boutros et al., 2007;

Khanna et al., 2013; Lazo et al., 2017; Mazhar et al., 2019; McConnell and Wadzinski, 2009; Perrotti and Neviani, 2013). This suggests that Ciz1 overexpressing cancers may be targetable by combination of therapies. However, the exact composition of the phosphatase holoenzymes should be identified. Additionally, full length murine Ciz1 has 14 CDK phosphorylation sites that may contribute to Ciz1 stability. Therefore, the specific function of each phospho- site and their specific phosphatases should be determined in order to use them as therapeutic targets.

#### **8.4. Ciz1 is downregulated by ubiquitin proteasome system in G1 phase**

The ubiquitin proteasome system is a primary protein degradation mechanism in mammalian cells (Melvin et al., 2013). The UPS is essential in oscillation of protein levels during cell cycle progression. For instance, APC/C-CDH1 is responsible for targeting mitotic cyclins for degradation in order to maintain low kinase activity in G1 phase (Huang et al., 2001; Nakayama and Nakayama, 2006; Vodermaier, 2004). In early G1 phase, APC/C-CDH1 targets SCF-SKP2 for degradation maintaining low kinase activity. However, during G1 – S transition, APC/C-CDH1 is phosphorylated by G1 phase cyclin-CDK complexes, the SCF-SKP2 is activated targeting CDK inhibitors for degradation, which leads to the increase in kinase activity driving the cell cycle (Benanti, 2012; Frescas and Pagano, 2008; Nakayama and Nakayama, 2006; Skaar and Pagano, 2009; Vodermaier, 2004). These data suggest that the cell cycle progression is tightly regulated by interlinked kinase and UPS pathways, which is consistent with Ciz1 regulation by opposing kinase and UPS activities observed here (Chapter 3).

Ciz1 accumulates in G1 phase and this increase mirrors the rising CDK activity as the cell cycle progresses towards S phase (Figure 3.3). The data presented here has demonstrated that Ciz1 levels can be reduced via CDK2 inhibition using small molecule inhibitors (Figures 3.6-8) and through siRNA mediated depletion of cyclin E and cyclin A2 (Figure 3.10). The reduction of Ciz1 is due to UPS mediated degradation of Ciz1 that is enhanced after CDK2 inhibition (Figures 3.8, 3.11-14). This process is reversible by proteasomal inhibition, demonstrating that Ciz1 levels are regulated by CDK2 mediated phosphorylation and UPS mediated degradation (Figure 3.11-14). The UPS regulates Ciz1 levels from pre-restriction point (Figure 3.12) and post-restriction point (Figure 3.13) in G1 phase. Perturbation of CDK2 activity in this window promotes Ciz1 degradation consistent with a model where Ciz1 abundance is regulated by opposing kinase phosphorylation and proteasome mediated degradation (Figure 6.1). This is consistent with global control of G1 – S progression by rising kinase activity and reduction of APC/C activity (Figures 1.2 and 1.5) (Frescas and Pagano, 2008; Hochegger et al., 2008; Nakayama and Nakayama, 2006; Rizzardi and Cook, 2012).

Ciz1 has been poly-ubiquitylated in *in vivo* experiments (Figure 3.15), suggesting that the UPS was responsible for Ciz1 degradation. Using an *in vitro* ubiquitylation system and biochemical fractionation of HeLa cell lysates have revealed three putative regulators of Ciz1: F-box only protein 38 [FBX38\_HUMAN], (E3-independent) E2 ubiquitin-conjugating enzyme [UBE2O\_HUMAN], and E3 ubiquitin-protein ligase UBR5 [UBR5\_HUMAN] (Table 7.1). There is limited amount of published literature available on FBX38, only that it is 134 kDa in size, aid phosphorylated protein ubiquitylation and degradation, and is positively linked with neuronal projection

development. F box proteins typically recruit phosphorylated substrates to SCF ubiquitin ligase complex (Skaar and Pagano, 2009; Skaar et al., 2013; Skowyra et al., 1997). However, further work is required to determine whether the phosphorylation of Ciz1 may protect Ciz1 from degradation or phosphorylation of E3 ligase may inactivate E3 ligase/ any UPS component, thus diminishing Ciz1 ubiquitylation efficiency.

UBE2O is a hybrid E2/E3 ligase that displays both ubiquitin conjugating and ligation functions (Ullah et al., 2018; Yokota et al., 2001). The UBE2O is a predominantly cytoplasmic 141 kDa protein, that contains a nuclear localisation sequence (NLS) for nuclear transport, and could therefore potentially target Ciz1 in the nucleus (Mashtalir et al., 2014). The UBE2O possesses multiple phosphorylation sites that are suggested to regulate its function (Liang et al., 2017) that would fit with observation that cyclin A – CDK2 phosphorylation reduced efficiency of Ciz1 ubiquitylation. UBE2O targets many proteins including AMPK $\alpha$ 2 (Vila et al., 2017), BMAL1 (Chen et al., 2018), c-Maf (Ullah et al., 2018), and MLL (Liang et al., 2017). UBE2O can catalyse mono-ubiquitylation, poly mono-ubiquitylation, and poly-ubiquitylation of proteins regulating the targeted protein. The mono-ubiquitylation has been implied in protein signalling, trafficking, and complex formation (Sadowski et al., 2012), and poly-ubiquitylation mainly leads to proteasomal degradation consistent with Ciz1 poly-ubiquitylation and degradation (Ullah et al., 2018). Both inactivating mutations and amplification of UBE2O have been linked with cancer (Chen et al., 2018; Hormaechea-agulla et al., 2018; Liang et al., 2017; Mashtalir et al., 2014; Ullah et al., 2018; Vila et al., 2017; Yanagitani et al., 2017). Interestingly, UBE2O is overexpressed in PC3 prostate cancer cell line (Ullah et al., 2018), which is a cell line that is

dependent on Ciz1 for efficient proliferation (Figure 6.2 and 6.3). It has been shown that ablation of UBE2O delays prostate and breast tumorigenesis and cancer aggressiveness (Hormaechea-agulla et al., 2018; Vila et al., 2017). Therefore, further analysis is required in order to confirm whether UBE2O can regulate Ciz1 levels *in vitro* and *in vivo*.

Third E3 ligase identified by mass spectrometry was UBR5 (Ubiquitin protein ligase E3 component n – recognin 5), which is also known as EDD (E3 identified by Differential Display) (Shearer et al., 2015). The UBR5 is well characterised E3 ligase belonging to HECT group and recognise n – degron sequences (mainly Glycine destabilising residue in N – terminal) via its 70 amino acids UBR box (Tasaki et al., 2009). UBR5 is 310 kDa, contains an NLS and is localised primarily to the nucleus. UBR5 has multiple phosphorylation sites that are targeted by ATM, CHK, and ERK kinases in order to modulate its localisation and function (Eblen et al., 2003; Henderson et al., 2006; Kim et al., 2007; Munoz et al., 2007; Zhang et al., 2014). UBR5 is conserved in metazoan lineage and is essential for mammalian development (Saunders et al., 2004; Shearer et al., 2015).

Either amplification and overexpression, or point and frame shift mutations in UBR5 gene have been linked with cancer (Kim et al., 2010; Shearer et al., 2015). The E3 ligase has multiple partners and targets that regulate cell cycle progression, DNA damage checkpoint response, transcription, and apoptosis (Cojocaru et al., 2011; Muñoz-Escobar et al., 2015; Munoz et al., 2007; Zhang et al., 2014). Therefore, it is challenging to clearly state whether UBR5 is a tumour suppressor or an oncogene. These opposing phenotypes are mediated by depletion and overexpression of UBR5

that can lead to pathologies and tumourigenesis. UBR5 gene amplification has been linked with breast and ovarian cancers, and renders the latter to cisplatin resistance (Liao et al., 2017; Wang et al., 2007). The UBR5 gene is stimulated by progesterone receptor (PR) and in turn UBR5 upregulates PR activity (Rojas-Rivera and Hetz, 2015). Similarly Ciz1 promotes oestrogen sensitisation through interactions with estrogen receptor (ER) in breast cancer (Den Hollander and Kumar, 2006; Den Hollander et al., 2006). However, the UBR5 has been shown to negatively regulate ER levels and activity in MCF7 cancer cell line (Shearer et al., 2015). In addition, the overexpression of UBR5 has been shown to ubiquitylate and stabilise  $\beta$ -catenin - TCF transcription in colorectal cancer (Hay-Koren et al., 2011). These data demonstrate that UBR5 is involved in regulation of signalling pathways and cell cycle control, and has either tumour suppressor or oncogene functions depending on its expression level.

More extensive research is required to confirm which E3 ligase targets Ciz1. This would require E3 ligase overexpression and genetic depletion monitoring how it affects Ciz1 levels in normal and cancer cell lines. Additionally, protein – protein binding experiments would be beneficial in order to confirm functional interaction between Ciz1 and E3. Various cancer therapies targeting E3 ligases are currently being developed (Sun, 2006). Therefore, identification of E3 ligase targeting Ciz1 may provide new avenues in Ciz1 dependent cancer therapy, or the mean of patient stratification according to how well would they respond to small molecule kinase inhibitor therapies.

### **8.5. Ciz1 expression and regulation in cancers**

Normal Ciz1 levels have been shown to temporally and spatially control DNA replication initiation and prevent DNA re-replication (Copeland et al., 2010; Copeland et al., 2015; Coverley et al., 2005). The overexpression of Ciz1 has been linked to major cancers, such as prostate, breast, lung, colon, and liver cancers (Den Hollander and Kumar, 2006; Den Hollander et al., 2006; Lei et al., 2016; Liu et al., 2015; Wang et al., 2014; Wu et al., 2016; Yin et al., 2013; Zhou et al., 2018). In addition, deletion of Ciz1 reveals that Ciz1 is a potential tumour suppressor gene as Ciz1 knockout mice are predisposed to lymphoproliferative disorders (Ridings-Figueroa et al., 2017; Sunwoo et al., 2017), DNA sensitivity to irradiation and oncogenic transformation (Nishibe et al., 2013), and various motor-neuron disorders in mice (Khan et al., 2018; Xiao et al., 2016; Xiao et al., 2018). These data suggest that Ciz1 may be a tumour suppressor in normal levels and an oncogene when overexpressed, and that Ciz1 is key in normal cell cycle progression and tissue development.

This research has determined that aggressive prostate carcinoma, PC3 cell line, and oestrogen and progesterone receptor positive breast cancer, MCF7 cell line, are dependent on Ciz1 for cell cycle progression (Figure 6.2-5). However, the cell replication profiles after Ciz1 depletion differ between two cell lines. The genetic depletion of Ciz1 in PC3 cells inhibited initiation of DNA replication, thus entry to S phase (Figure 6.3). This is consistent with normal murine fibroblasts (Coverley et al., 2005) and the plethora of data on Ciz1 depletion in cancers, including prostate cancer (Liu et al., 2015). However, Ciz1 depletion in PC3 cell line as well as in MCF7, T47D, and SW480, did not cause apoptotic cell death that has been reported in many

cancer cases (Lei et al., 2016; Liu et al., 2015; Wu et al., 2016; Yin et al., 2013) (Figure 6.6). Interestingly, Ciz1 depletion prolonged S phase in MCF7 cell line, but did not inhibit G1 – S transition (Figure 6.4). This is consistent with Ciz1 depletion data in breast cancer cell lines (Den Hollander and Kumar, 2006; Den Hollander et al., 2006). In addition, Ciz1 depletion promoted accumulation of cells in S phase, but reduced global proliferation in MCF7 cells (Figure 6.4 and 6.5), suggesting that Ciz1 depletion causes DNA replication stress-like state (Bertoli et al., 2016; Herlihy and De Bruin, 2017; Toledo et al., 2017; Zeman and Cimprich, 2014). However, the T47D cell line was not significantly affected by Ciz1 depletion (Figures 6.4 and 6.5). This may be explained by the differential protein expression between two breast cancer cell lines, T47D expressing anti-apoptotic and cell proliferation genes more than MCF7 (Aka and Lin, 2012; Radde et al., 2015).

Treatment of cancer cell lines with small molecule kinase inhibitors successfully reduced Ciz1 levels (Figure 6.7) and similar effects were observed in normal mice fibroblasts (Chapters 3 and 5). Importantly, small molecule CDK2 and DDK inhibitors reduced G1 – S transition in retinoblastoma positive tumours (Maamer-Azzabi et al., 2013; Martino-Echarri et al., 2014; Tai et al., 2011) (Figure 6.8 and 6.9). Further analysis revealed that CDK2 inhibitors and PHA-767491 downregulated the Rb – E2F axis consistent with observations in normal murine fibroblasts (Figures 3.5, 5.2, and 5.5). These data suggest the potential efficacy of small molecule kinase inhibition therapies that could inhibit cell cycle by reducing CDK2 activity and E2F mediated transcription, and reduce Ciz1 levels that are required for proliferation. This may increase cancer cell sensitivity to kinase inhibition therapy and allow stratification of patients.

However, for CDK2 inhibitors to be effective, the UPS must be functional. The recovery of Ciz1 levels after proteasomal inhibition was successful only after some kinase inhibitor treatments and varied between different cancer cell lines (Figure 6.13). This may indicate that functional UPS is present in these cells, but are affected by more complex pathways than in normal fibroblast, where significant Ciz1 rescue was observed after majority of the kinase inhibition treatments (Figures 3.11-14). Additionally, these data may suggest that some cancer cell lines would be more responsive to certain kinase inhibitor therapies, and emphasise the importance in molecular screening of cancer cells in order to determine best possible treatment and intervention.

The data presented here suggest the following model to describe the molecular mechanisms that regulate Ciz1 protein levels (Figure 6.1). The increase in kinase activity during G1 phase is mediated by CDK2 and DDK (Figures 1.1, 1.2, 6.1, 8.1) (Gerard and Goldbeter, 2009; Hochegger et al., 2008) and their activity is proposed to promote accumulation of Ciz1. This rising kinase activity overwhelms phosphatase activity (PP1 and PP2A) and facilitates phosphorylation of Ciz1 or components of the UPS that regulates Ciz1 poly-ubiquitylation (Jiang, 2006; Lo and Uhlmann, 2011; Nakayama and Nakayama, 2006; Rizzardi and Cook, 2012; Wlodarchak and Xing, 2016). This positively regulates Ciz1 accumulation in G1 phase by conferring stability or protecting it from UPS mediated degradation (Figure 3.3). Ciz1 overexpressing tumours may have underlying overexpression of kinases or down-regulation of UPS and phosphatases. This may lead to increased Ciz1 phosphorylation, over-stabilisation and over-protection of Ciz1, and reduced protein clearing. Consequently, increased Ciz1 accumulation may facilitate Ciz1 dependent tumour

proliferation further. The main emphasis of potentially successful Ciz1 dependent cancer therapies could be shifting the equilibrium of kinase activity to enable dephosphorylation of Ciz1 or any component of UPS in order to promote Ciz1 degradation. This work shows that repurposed CDK2 and DDK small molecule kinase inhibitors may be a potential therapy for Rb positive and Ciz1 dependent cancers, reducing cancer cell proliferation by decreasing kinase activity and by down-regulating Ciz1 levels.

#### **8.6. Future perspectives/ Future work**

Tight control of kinase, phosphatase and UPS activities is crucial in the cell cycle progression and for the precise regulation of DNA replication. Any disturbances in these mechanisms may lead to deregulation in Ciz1 levels and activity that potentially contributes to the dysregulation of the cell cycle that is an early event in tumourigenesis. The next step is to characterise the E3 ligases that may regulate Ciz1 function. Understanding these events in molecular detail will facilitate further studies that will fully characterise the potential of CDK2 and DDK inhibition for the regulation of Ciz1 dependent tumours. This will enable molecular screening of cancer cells in order to identify whether there are functional UPS systems that can be manipulated to reduce Ciz1 levels and potentially reduce proliferation of cancer cells.

A full understanding of the interplay between complex networks of regulators would facilitate a rational approach to the manipulation of Ciz1 levels. For example, there are potentially three key regulators that contribute to Ciz1 accumulation that includes cyclin dependent kinases, serine/threonine phosphatase (potentially PP1 and PP2A), and ubiquitin mediated degradation (UPS). Each regulator is a potential

therapeutic target for Ciz1 dependent tumours (Lazo et al., 2017; McConnell and Wadzinski, 2009; Ndubaku and Tsui, 2015; Sun, 2003; Vijayaraghavan et al., 2018). In addition, there is potential for the identification of deubiquitinating enzymes (DUB) that may also contribute to the regulation of Ciz1. This complex network of interlinked pathways contributes to Ciz1 homeostasis and a precise understanding of these networks is required to target Ciz1 for degradation. This further reinforces the importance of research on molecular mechanism of Ciz1 level regulation.

# **Chapter 9**

# **References**

- Ahola, R., Arnold, H., Junttila, M. R., Puustinen, P., Niemela, M., Lin, S., Chan, E. K. L., Wang, X. and Gre, R.** (2007). CIP2A Inhibits PP2A in Human Malignancies. *Cell* **130**, 51–62.
- Ainscough, J. F.-X., Rahman, F. A., Sercombe, H., Sedo, A., Gerlach, B. and Coverley, D.** (2007). C-terminal domains deliver the DNA replication factor Ciz1 to the nuclear matrix. *J. Cell Sci.* **120**, 115–124.
- Aka, J. A. and Lin, S. X.** (2012). Comparison of functional proteomic analyses of human breast cancer cell lines T47D and MCF7. *PLoS One* **7**, 1–9.
- Akutsu, M., Dikic, I. and Bremm, A.** (2016). Ubiquitin chain diversity at a glance. *J. Cell Sci.* **129**, 875–880.
- Aleem, E., Berthet, C. and Kaldis, P.** (2004). Cdk2 as a Master of S phase Entry. *Cell Cycle* **3**, 35–37.
- Ali, S., Heathcote, D. A., Kroll, S. H. B., Jogalekar, A. S., Scheiper, B., Patel, H., Brackow, J., Siwicka, A., Fuchter, M. J., Periyasamy, M., et al.** (2009). The Development of a Selective Cyclin-Dependent Kinase Inhibitor That Shows Antitumor Activity. *Cancer Res.* **69**, 6208–6216.
- Alver, R. C., Chadha, G. S., Gillespie, P. J. and Blow, J. J.** (2017). Reversal of DDK-Mediated MCM Phosphorylation by Rif1-PP1 Regulates Replication Initiation and Replisome Stability Independently of ATR / Chk1. *Cell Rep.* **18**, 2508–2520.
- Arnold, L., Hockner, S. and Seufert, W.** (2015). Insights into the cellular mechanism of the yeast ubiquitin ligase APC/C-Cdh1 from the analysis of in vivo degrons. *Mol. Biol. Cell* **26**, 843–858.

- Asghar, U. S., Barr, A. R., Cutts, R., Beaney, M., Babina, I., Sampath, D., Giltane, J., Lacap, J. A., Crocker, L., Young, A., et al.** (2017). Single-Cell Dynamics Determines Response to CDK4 / 6 Inhibition in Triple-Negative Breast Cancer. *Clin. Cancer Res.* **23**, 5561–5573.
- Azizi, E., Namazi, A., Kaabinejadian, S., Sh, F., Rezaei, P. and Ramezani, M.** (2010). Molecular analysis of MEN1 expression in MCF 7, T47D and MDA-MB 468 breast cancer cell lines treated with adriamycin using RT-PCR and immunocytochemistry. *DARU* **18**, 17–22.
- Bageghni, S. A., Frentzou, G. A., Drinkhill, M. J., Mansfield, W., Coverley, D. and Ainscough, J. F. X.** (2017). Cardiomyocyte--specific expression of the nuclear matrix protein, CIZ1, stimulates production of mono-nucleated cells with an extended window of proliferation in the postnatal mouse heart. *Biol. Open* **6**, 92–99.
- Bajar, B. T., Lam, A. J., Badiie, R. K., Oh, Y. H., Chu, J., Zhou, X. X., Kim, N., Kim, B. B., Chung, M., Yablonovitch, A. L., et al.** (2016). Fluorescent indicators for simultaneous reporting of all four cell cycle phases. *Nat. Methods* **13**, 993–996.
- Barboro, P., Repaci, E., Arrigo, C. D. and Balbi, C.** (2012). The Role of Nuclear Matrix Proteins Binding to Matrix Attachment Regions ( MARs ) in Prostate Cancer Cell Differentiation. *PLoS One* **7**, 1–12.
- Bard, J. A. M., Goodall, E. A., Greene, E. R., Jonsson, E., Dong, K. C. and Martin, A.** (2018). Structure and Function of the 26S Proteasome. *Annu. Rev. Biochem.* **87**, 697–724.

- Barnum, K. and O'Connell, M.** (2014). Cell Cycle Regulation by Checkpoints. *Methods Mol. Biol.* **1170**, 29–40.
- Barr, A. R., Heldt, F. S., Zhang, T., Bakal, C. and Novak, B.** (2016). Article Transition A Dynamical Framework for the All-or-None G1 / S Transition. *Cell Syst.* **2**, 27–37.
- Barr, A. R., Cooper, S., Heldt, F. S., Butera, F. and Stoy, H.** (2017). DNA damage during S-phase mediates the proliferation-quiescence decision in the subsequent G1 via p21 expression. *Nat. Commun.* **8**, 1–17.
- Bassermann, F., Eichner, R. and Pagano, M.** (2014). Biochimica et Biophysica Acta The ubiquitin proteasome system — Implications for cell cycle control and the targeted treatment of cancer. *BBA - Mol. Cell Res.* **1843**, 150–162.
- Bedford, L., Paine, S., Sheppard, P. W., Mayer, R. J. and Roelofs, J.** (2010). Assembly , structure , and function of the 26S proteasome. *Trends Cell Biol.* **20**, 391–401.
- Benanti, J. A.** (2012). Coordination of cell growth and division by the ubiquitin-proteasome system. *Semin. Cell Dev. Biol.* **23**, 492–498.
- Berleth, E. S. and Pickart, C. M.** (1996). Mechanism of ubiquitin conjugating enzyme E2-230K: Catalysis involving a thiol relay? *Biochemistry* **35**, 1664–1671.
- Berthet, C., Aleem, E., Coppola, V., Tessarollo, L. and Kaldis, P.** (2003). Cdk2 Knockout Mice Are Viable. *Curr. Biol.* **13**, 1775–1785.
- Berti, M. and Vindigni, A.** (2016). Replication stress : getting back on track. *Nat. Struct. Mol. Biol.* **23**, 103–109.
- Bertoli, C., Skotheim, J. M., Bruin, R. A. M. De, Street, G. and de Bruin, R. A. M.**

- (2013a). Control of cell cycle transcription during G1 and S phases. *Nat. Rev. Mol. Cell Biol.* **14**, 518–528.
- Bertoli, C., Skotheim, J. M. and De Bruin, R. A. M.** (2013b). Control of cell cycle transcription during G1 and S phases. *Nat. Rev. Mol. Cell Biol.* **14**, 518–528.
- Bertoli, C., Herlihy, A. E., Pennycook, B. R., Kriston-Vizi, J. and De Bruin, R. A. M.** (2016). Sustained E2F-Dependent Transcription Is a Key Mechanism to Prevent Replication-Stress-Induced DNA Damage. *Cell Rep.* **15**, 1412–1422.
- Bhullar, K. S., Lagarón, N. O., McGowan, E. M., Parmar, I., Jha, A., Hubbard, B. P. and Rupasinghe, H. P. V.** (2018). Kinase-targeted cancer therapies : progress, challenges and future directions. *Mol. Cancer* **17**, 1–20.
- Blagosklonny, M. V. and Pardee, A. B.** (2002). The restriction point of the cell cycle. *Cell cycle* **1**, 102–109.
- Blattman, J. N. and Greenberg, P. D.** (2004). Cancer Immunotherapy: A Treatment for the Mass. *Science (80-. )*. **305**, 200–206.
- Blow, J. J. and Hodgson, B.** (2002). Replication licensing - Defining the proliferative state? *Trends Cell Biol.* **12**, 72–78.
- Bollen, M., Gerlich, D. W. and Lesage, B.** (2009). Mitotic phosphatases : from entry guards to exit guides. *Trends Cell Biol.* **19**, 531–541.
- Bonte, D., Lindvall, C., Liu, H., Dykema, K., Furge, K. and Weinreich, M.** (2008). Cdc7-Dbf4 Kinase Overexpression in Multiple Cancers and Tumor Cell Lines Is Correlated with p53 Inactivation. *Neoplasia* **10**, 920–931.

- Boos, D., Yekezare, M. and Diffley, J. F. X.** (2013). Identification of a Heteromeric Complex That Promotes DNA Replication Origin Firing in Human Cells. *Science (80-. )*. **340**, 981–984.
- Bornstein, G., Bloom, J., Sitry-Shevah, D., Nakayama, K., Pagano, M. and Hershko, A.** (2003). Role of the SCFSkp2ubiquitin ligase in the degradation of p21Cip1in S phase. *J. Biol. Chem.* **278**, 25752–25757.
- Bosco, E. E., Wang, Y., Xu, H., Zilfou, J. T., Knudsen, K. E., Aronow, B. J., Lowe, S. W. and Knudsen, E. S.** (2007). The retinoblastoma tumor suppressor modifies the therapeutic response of breast cancer. *J. Clin. Invest.* **117**, 218–228.
- Boutros, R., Lobjois, V. and Ducommun, B.** (2007). CDC25 phosphatases in cancer cells: Key players? Good targets? *Nat. Rev. Cancer* **7**, 495–507.
- Bowman, E. A. and Kelly, W. G.** (2014). RNA Polymerase II transcription elongation and Pol II CTD Ser2 phosphorylation A tail of two kinases. *Nucleus* **5**, 224–236.
- Brandeis, M., Rosewell, I., Carrington, M., Crompton, T., Jacobs, M. A., Kirk, J., Gannon, J. and Hunt, T.** (1998). Cyclin B2-null mice develop normally and are fertile whereas cyclin B1-null mice die in utero. *Proc. Natl. Acad. Sci.* **95**, 4344–4349.
- Breen, M. E. and Soellner, M. B.** (2015). Small molecule substrate phosphorylation site inhibitors of protein kinases: Approaches and challenges. *ACS Chem. Biol.* **10**, 175–189.
- Brooks, E. E., Gray, N. S., Joly, A., Kerwar, S. S., Lum, R., Mackman, R. L., Norman, T. C., Rosete, J., Rowe, M., Schow, S. R., et al.** (1997). CVT-313, a specific and

potent inhibitor of CDK2 that prevents neointimal proliferation. *J. Biol. Chem.* **272**, 29207–29211.

**Burke, J. R., Deshong, A. J., Pelton, J. G. and Rubin, S. M.** (2010). Phosphorylation-induced conformational changes in the retinoblastoma protein inhibit E2F transactivation domain binding. *J. Biol. Chem.* **285**, 16286–16293.

**Burroughs, A. M., Jaffee, M., Iyer, L. M. and Aravind, L.** (2008). Anatomy of the E2 ligase fold: Implications for enzymology and evolution of ubiquitin/Ub-like protein conjugation. *J. Struct. Biol.* **162**, 205–218.

**Caetano, C., Limbo, O., Farmer, S., Klier, S., Dovey, C., Russell, P. and deBruin, R. A. M.** (2014). Tolerance of Deregulated G1/S Transcription Depends on Critical G1/S Regulon Genes to Prevent Catastrophic Genome Instability. *Cell Rep.* **9**, 2279–2289.

**Canavese, M., Santo, L. and Raje, N.** (2012). Cyclin dependent kinases in cancer: Potential for therapeutic intervention. *Cancer Biol. Ther.* **13**, 451–457.

**Cappell, S. D., Mark, K. G., Garbett, D., Pack, L. R., Rape, M. and Meyer, T.** (2018). Emi1 switches from being a substrate to an inhibitor of APC/ CCdh1 to start the cell cycle. *Nature* **558**, 313–317.

**Chau, V., Tobias, J. W., Bachmair, A., Marriott, D., David, J., Gonda, D. K., Varshavsky, A., Chau, V., Tobias, J. W., Bachmair, A., et al.** (1989). A Multiubiquitin Chain Is Confined to Specific Lysine in a Targeted Short-Lived Protein. *Science (80-. )*. **243**, 1576–1583.

**Chen, G. and Deng, X.** (2018). Cell Synchronization by Double Thymidine Block. *Bio*

*Protoc.* **8**, 1–6.

**Chen, S., Yang, J., Zhang, Y., Duan, C., Liu, Q., Huang, Z., Xu, Y., Zhou, L. and Xu, G.**

(2018). Ubiquitin-conjugating enzyme UBE2O regulates cellular clock function by promoting the degradation of the transcription factor BMAL1. *J. Biol. Chem.* **293**, 11296–11309.

**Cheng, T.** (2000). Hematopoietic Stem Cell Quiescence Maintained by p21cip1/waf1.

*Science (80-. ).* **287**, 1804–1808.

**Cheung, T. H. and Rando, T. A.** (2013). Molecular regulation of stem cell quiescence.

*Nat. Rev. Mol. Cell Biol.* **14**, 1–26.

**Chowdhury, A., Liu, G., Kemp, M., Chen, X., Katrangi, N., Myers, S., Ghosh, M., Yao,**

**J., Gao, Y., Bubulya, P., et al.** (2010). The DNA Unwinding Element Binding Protein DUE-B Interacts with Cdc45 in Preinitiation Complex Formation. *Mol. Cell. Biol.* **30**, 1495–1507.

**Chuang, L. C., Teixeira, L. K., Wohlschlegel, J. A., Henze, M., Yates, J. R., Méndez, J.**

**and Reed, S. I.** (2009). Phosphorylation of Mcm2 by Cdc7 Promotes Pre-replication Complex Assembly during Cell-Cycle Re-entry. *Mol. Cell* **35**, 206–216.

**Clare, D. K. and Saibil, H. R.** (2013). ATP-driven molecular chaperone machines.

*Biopolymers* **99**, 846–859.

**Cojocar, M., Bouchard, A., Cloutier, P., Cooper, J. J., Varzavand, K., Price, D. H. and**

**Coulombe, B.** (2011). Transcription factor IIS cooperates with the E3 ligase UBR5 to ubiquitinate the CDK9 subunit of the positive transcription elongation factor B. *J. Biol. Chem.* **286**, 5012–5022.

- Coller, H. A.** (2007). From Quiescence Versus Proliferation. *Mol. cell Biol.* **8**, 667–670.
- Collett, M. S. and Erikson, R. L.** (1978). Protein kinase activity associated with the avian sarcoma virus src gene product. *Proc Natl Acad Sci U S A* **75**, 2021–2024.
- Cong, L., Ran, F. A., Cox, D., Lin, S., Barretto, R., Hsu, P. D., Wu, X., Jiang, W. and Marraffini, L. A.** (2013). Multiplex Genome Engineering Using CRISPR/Cas Systems. *Science (80-. )*. **339**, 819–823.
- Conti, C., Sacca, B., Herrick, J., Lalou, C., Pommier, Y. and Bensimon, A.** (2007). Replication Fork Velocities at Adjacent Replication Origins Are Coordinately Modified during DNA Replication in Human Cells. *Mol. Biol. Cell* **18**, 3059–3067.
- Copeland, N. A., Sercombe, H. E., Ainscough, J. F. X. and Coverley, D.** (2010). Ciz1 cooperates with cyclin-A-CDK2 to activate mammalian DNA replication in vitro. *J. Cell Sci.* **123**, 1108–1115.
- Copeland, N. A., Sercombe, H. E., Wilson, R. H. C. and Coverley, D.** (2015). Cyclin-A-CDK2-mediated phosphorylation of CIZ1 blocks replisome formation and initiation of mammalian DNA replication. *J. Cell Sci.* **128**, 1518–1527.
- Coudreuse, D. and Nurse, P.** (2010a). Driving the cell cycle with a minimal CDK control network. *Nature* **468**, 1074–1080.
- Coudreuse, D. and Nurse, P.** (2010b). Driving the cell cycle with a minimal CDK control network. *Nature* **468**, 1074–1080.
- Coverley, D., Laman, H. and Laskey, R. A.** (2002). Distinct roles for cyclins E and A during DNA replication complex assembly and activation. *Nat. Cell Biol.* **4**, 523–

528.

**Coverley, D., Marr, J. and Ainscough, J.** (2005). Ciz1 promotes mammalian DNA replication. *J. Cell Sci.* **118**, 101–112.

**Coverley, D., Higgins, G., West, D., Jackson, O. T., Dowle, A., Haslam, A., Ainscough, E., Chalkley, R. and White, J.** (2017). A quantitative immunoassay for lung cancer biomarker CIZ1b in patient plasma. *Clin. Biochem.* **50**, 336–343.

**Cundell, M. J., Hutter, L. H., Bastos, R. N., Poser, E., Holder, J., Mohammed, S., Novak, B. and Barr, F. A.** (2016). A PP2A-B55 recognition signal controls substrate dephosphorylation kinetics during mitotic exit. *J. Cell Biol.* **214**, 539–554.

**Da Fonseca, P. C. A., Kong, E. H., Zhang, Z., Schreiber, A., Williams, M. A., Morris, E. P. and Barford, D.** (2011). Structures of APC/CCdh1 with substrates identify Cdh1 and Apc10 as the D-box co-receptor. *Nature* **470**, 274–280.

**Dahmcke, C. M., Büchmann-Møller, S., Jensen, N. A. and Mitchelmore, C.** (2008). Altered splicing in exon 8 of the DNA replication factor CIZ1 affects subnuclear distribution and is associated with Alzheimer's disease. *Mol. Cell. Neurosci.* **38**, 589–594.

**Dambach, D. M., Simpson, N. E., Jones, T. W., Brennan, R. J., Pazdur, R. and Palmby, T. R.** (2016). CCR FOCUS Nonclinical Evaluations of Small-Molecule Oncology Drugs : Integration into Clinical Dose Optimization and Toxicity Management. *Clin. Cancer Res.* **22**, 2618–2623.

**Davies, S. P., Reddy, H., Caivano, M. and Cohen, P.** (2000). Specificity and

mechanism of action of some commonly used protein kinase inhibitors.

*Biochem. J.* **351**, 95–105.

**Davis, M. I., Hunt, J. P., Herrgard, S., Ciceri, P., Wodicka, L. M., Pallares, G., Hocker, M., Treiber, D. K. and Zarrinkar, P. P.** (2011). Comprehensive analysis of kinase inhibitor selectivity. *Nat. Biotechnol.* **29**, 1046–1051.

**Davis, R. J., Welcker, M. and Clurman, B. E.** (2014). Tumor suppression by the Fbw7 Ubiquitin ligase: Mechanisms and opportunities. *Cancer Cell* **26**, 455–464.

**Deegan, T. D. and Diffley, J. F. X.** (2016). MCM: One ring to rule them all. *Curr. Opin. Struct. Biol.* **37**, 145–151.

**Deegan, T. D., Yeeles, J. T. and Diffley, J. F.** (2016). Phosphopeptide binding by Sld3 links Dbf4-dependent kinase to MCM replicative helicase activation. *EMBO J.* **35**, 961–973.

**Den Hollander, P. and Kumar, R.** (2006). Dynein light chain 1 contributes to cell cycle progression by increasing cyclin-dependent kinase 2 activity in estrogen-stimulated cells. *Cancer Res.* **66**, 5941–5949.

**Den Hollander, P., Rayala, S. K., Coverley, D. and Kumar, R.** (2006). Ciz1, a novel DNA-binding coactivator of the estrogen receptor  $\alpha$ , confers hypersensitivity to estrogen action. *Cancer Res.* **66**, 11021–11029.

**Deshpande, A., Sicinski, P. and Hinds, P. W.** (2005). Cyclins and cdks in development and cancer: A perspective. *Oncogene* **24**, 2909–2915.

**Diffley, J. F. X.** (2004). Regulation of early events in chromosome replication. *Curr.*

*Biol.* **14**, 778–786.

**Donovan, S., Harwood, J., Drury, L. S. and Diffley, J. F.** (1997). Cdc6p-dependent loading of Mcm proteins onto pre-replicative chromatin in budding yeast. *Pnas* **94**, 5611–6.

**Donzelli, M. and Draetta, G. F.** (2003). Regulating mammalian checkpoints through Cdc25 inactivation. *EMBO Rep.* **4**, 671–677.

**Duzdevich, D., Warner, M. D., Ticau, S., Ivica, N. A., Bell, S. P. and Greene, E. C.** (2015). The dynamics of eukaryotic replication initiation: Origin specificity, licensing, and firing at the single-molecule level. *Mol. Cell* **58**, 483–494.

**Eblen, S. T., Kumar, N. V., Shah, K., Henderson, M. J., Watts, C. K. W., Shokat, K. M. and Weber, M. J.** (2003). Identification of novel ERK2 substrates through use of an engineered kinase and ATP analogs. *J. Biol. Chem.* **278**, 14926–14935.

**Edginton, A. N. and Models, P.** (2018). Using Physiologically Based Pharmacokinetic Modeling for Mechanistic Insight : Cases of Reverse Translation. *Clin. Transl. Sci.* **11**, 109–111.

**Eliyatkin, N. O., Aktas, S., Ozgur, H., Ercetin, P. and Kupelioglu, A.** (2016). The role of p95HER2 in trastuzumab resistance in breast cancer. *J. B.U.ON.* **21**, 382–389.

**Fabbro, D., Cowan-Jacob, W. S. and Moebitz, H.** (2015). Ten things you should know about protein kinases : IUPHAR Review 14. *Br. J. Pharmacol.* **172**, 2675–2700.

**Faber, A. C. and Chiles, T. C.** (2007). Inhibition of cyclin-dependent kinase-2 induces apoptosis in human diffuse large b-cell lymphomas. *Cell Cycle* **6**, 2983–2989.

**Francis, L. I., Randell, J. C. W., Takara, T. J., Uchima, L. and Bell, S. P. (2009).**

Incorporation into the prereplicative complex activates the Mcm2-7 helicase for Cdc7-Dbf4 phosphorylation. *Genes Dev.* **23**, 643–654.

**Frescas, D. and Pagano, M. (2008).** Deregulated proteolysis by the F-box proteins

SKP2 and  $\beta$ -TrCP: Tipping the scales of cancer. *Nat. Rev. Cancer* **8**, 438–449.

**Fry, D. W., Harvey, P. J., Keller, P. R., Elliott, W. L., Meade, M., Trachet, E.,**

**Albassam, M., Zheng, X., Leopold, W. R., Pryer, N. K., et al. (2004).** Specific inhibition of cyclin-dependent kinase 4 / 6 by PD 0332991 and associated antitumor activity in human tumor xenografts. **3**, 1427–1438.

**Galdeano, C. (2017).** Drugging the undruggable: targeting challenging E3 ligases for personalized medicine. *Future Med. Chem.* **9**, 347–350.

**Gasiunas, G., Barrangou, R., Horvath, P. and Siksnys, V. (2012).** Cas9-crRNA

ribonucleoprotein complex mediates specific DNA cleavage for adaptive immunity in bacteria. *Proc. Natl. Acad. Sci.* **109**, E2579–E2586.

**Gavet, O. and Pines, J. (2010).** Activation of cyclin B1–Cdk1 synchronizes events in

the nucleus and the cytoplasm at mitosis. *J. Cell Biol.* **189**, 247–259.

**Geng, Y., Yu, Q., Sicinska, E., Das, M., Schneider, J. E., Bhattacharya, S., Rideout, W.**

**M., Bronson, R. T., Gardner, H. and Sicinski, P. (2003).** Cyclin E ablation in the mouse. *Cell* **114**, 431–443.

**Geng, Y., Lee, Y. M., Welcker, M., Swanger, J., Zagozdzon, A., Winer, J. D., Roberts,**

**J. M., Kaldis, P., Clurman, B. E. and Sicinski, P. (2007).** Kinase-Independent Function of Cyclin E. *Mol. Cell* **25**, 127–139.

**Gerard, C. and Goldbeter, A.** (2009). Temporal self-organization of the cyclin/Cdk network driving the mammalian cell cycle. *Proc. Natl. Acad. Sci.* **106**, 21643–21648.

**Gérard, C. and Goldbeter, A.** (2012). From quiescence to proliferation : Cdk oscillations drive the mammalian cell cycle. *Front. Physiol.* **3**, 1–18.

**Giacinti, C. and Giordano, A.** (2006). RB and cell cycle progression. *Oncogene* **25**, 5220–5227.

**Godfrey, M., Touati, S. A., Kataria, M., Jones, A., Snijders, A. P., Uhlmann, F.,**

**Godfrey, M., Touati, S. A., Kataria, M., Jones, A., et al.** (2017). Phosphorylation by Opposing Threonine Article PP2A Cdc55 Phosphatase Imposes Ordered Cell-Cycle Phosphorylation by Opposing Threonine Phosphorylation. *Mol. Cell* **65**, 393–402.e3.

**Gong, Y., Zack, T. I., Morris, L. G. T., Lin, K., Hukkelhoven, E., Raheja, R., Tan, I.,**

**Turcan, S., Veeriah, S., Meng, S., et al.** (2014). Pan-cancer genetic analysis identifies PARK2 as a master regulator of G1 / S cyclins. *Nat. Commun.* **46**, 588–596.

**Goodfellow, S. J. and Zomerdijk, J. C. B. M.** (2012). Basic Mechanisms in RNA

Polymerase I Transcription of the Ribosomal RNA Genes. *Subcell. Biochem.* **61**, 1–26.

**Grallert, A., Boke, E., Hagting, A., Hodgson, B. and Connolly, Y.** (2015). A PP1 / PP2A phosphatase relay controls mitotic progression. *Nature* **517**, 94–98.

**Greaves, E. A., Copeland, N. A., Coverley, D. and Ainscough, J. F. X.** (2012). Cancer-

associated variant expression and interaction of CIZ1 with cyclin A1 in differentiating male germ cells. *J. Cell Sci.* **125**, 2466–2477.

**Grice, G. L., Lobb, I. T., Weekes, M. P., Gygi, S. P., Antrobus, R. and Nathan, J. A.**

(2015). The proteasome distinguishes between heterotypic and homotypic lysine-11-Linked polyubiquitin chains. *Cell Rep.* **12**, 545–553.

**Gutierrez, A., Look, A. T., Aster, J. C., Gutierrez, A., Pan, L., Groen, R. W. J.,**

**Baleyrier, F., Kentsis, A., Poglio, S., Uzan, B., et al.** (2014). Phenothiazines induce PP2A-mediated apoptosis in T cell acute lymphoblastic leukemia. *J. Clin. Invest.* **124**, 644–655.

**Hahn, S.** (2004). Structure and mechanism of the RNA Polymerase II transcription machinery. *Nat. Struct. Mol. Biol.* **11**, 394–403.

**Hanahan, D. and Weinberg, R. A.** (2011). Review Hallmarks of Cancer : The Next Generation. *Cell* **144**, 646–674.

**Hanahan, D., Weinberg, R. A. and Francisco, S.** (2000). The Hallmarks of Cancer Review University of California at San Francisco. *Cell* **100**, 57–70.

**Harbour, J. W. and Dean, D. C.** (2000). The Rb/E2F pathway: Expanding roles and emerging paradigms. *Genes Dev.* **14**, 2393–2409.

**Hay-Koren, A., Caspi, M., Zilberberg, A. and Rosin-Arbesfeld, R.** (2011). The EDD E3 ubiquitin ligase ubiquitinates and up-regulates  $\beta$ -catenin. *Mol. Biol. Cell* **22**, 399–411.

**He, J., Chao, W. C. H., Zhang, Z., Yang, J., Cronin, N. and Barford, D.** (2013). Insights

into degron recognition by APC/C coactivators from the structure of an Acm1-Cdh1 complex. *Mol. Cell* **50**, 649–660.

**Hein, J. B. and Nilsson, J.** (2016). Interphase APC/C-Cdc20 inhibition by cyclin A2-Cdk2 ensures efficient mitotic entry. *Nat. Commun.* **7**, 1–10.

**Hein, J. B., Hertz, E. P. T., Garvanska, D. H., Kruse, T. and Nilsson, J.** (2017). Distinct kinetics of serine and threonine dephosphorylation are essential for mitosis. *Nat. Cell Biol.* **19**, 1–15.

**Heldt, F. S., Barr, A. R., Cooper, S., Bakal, C. and Novák, B.** (2018a). A comprehensive model for the proliferation–quiescence decision in response to endogenous DNA damage in human cells. *Proc. Natl. Acad. Sci.* 1–6.

**Heldt, F. S., Barr, A. R., Cooper, S., Bakal, C. and Novák, B.** (2018b). A comprehensive model for the proliferation – quiescence decision in response to endogenous DNA damage in human cells.

**Henderson, M. J., Munoz, M. A., Saunders, D. N., Clancy, J. L., Russell, A. J., Williams, B., Pappin, D., Kum, K. K., Jackson, S. P., Sutherland, R. L., et al.** (2006). EDD mediates DNA damage-induced activation of CHK2. *J. Biol. Chem.* **281**, 39990–40000.

**Herlihy, A. E. and De Bruin, R. A. M.** (2017). The Role of the Transcriptional Response to DNA Replication Stress. *Genes (Basel)*. **8**, 1–15.

**Hernandez, A. J., Prysizlak, M., L., S., Yanchus, C., Kurji, N., Shahani, V. M. and Molinski, S. V.** (2017). Giving Drugs a Second Chance: Overcoming Regulatory and Financial Hurdles in Repurposing Approved Drugs As Cancer Therapeutics.

*Front. Oncol.* **7**, 1–8.

**Herr, R. and Brummer, T.** (2015). BRAF inhibitors in colorectal cancer : Toward a differentiation therapy ? BRAF inhibitors in colorectal cancer : Toward a differentiation therapy ? *Mol. Cell. Oncol.* **2**, e1002709.

**Higgins, G., Roper, K. M., Watson, I. J., Blackhall, F. H., Rom, W. N., Pass, H. I., Ainscough, J. F. X. and Coverley, D.** (2012). Variant Ciz1 is a circulating biomarker for early-stage lung cancer. *Proc. Natl. Acad. Sci.* **109**, E3128–E3135.

**Hiraga, S., Alvino, G. M., Chang, F., Lian, H., Sridhar, A., Kubota, T., Brewer, B. J., Weinreich, M., Raghuraman, M. K. and Donaldson, A. D.** (2014). Rif1 controls DNA replication by directing Protein Phosphatase 1 to reverse Cdc7- mediated phosphorylation of the MCM complex. *Genes Dev.* **28**, 372–383.

**Hirsch, F. R., Suda, K., Wiens, J. and Jr, P. A. B.** (2016). Lung cancer 3 New and emerging targeted treatments in advanced non-small-cell lung cancer. *Lancet* **388**, 1012–1024.

**Hochegger, H., Dejsuphong, D., Sonoda, E., Saberi, A., Rajendra, E., Kirk, J., Hunt, T. and Takeda, S.** (2007). An essential role for Cdk1 in S phase control is revealed via chemical genetics in vertebrate cells. *J. Cell Biol.* **178**, 257–268.

**Hochegger, H., Takeda, S. and Hunt, T.** (2008). Cyclin-dependent kinases and cell-cycle transitions: Does one fit all? *Nat. Rev. Mol. Cell Biol.* **9**, 910–916.

**Hoelder, S., Clarke, P. A. and Workman, P.** (2012). Discovery of small molecule cancer drugs : Successes , challenges and opportunities. *Mol. Oncol.* **6**, 155–176.

- Hoggard, T., Shor, E., Müller, C. A., Nieduszynski, C. A. and Fox, C. A.** (2013). A Link between ORC-Origin Binding Mechanisms and Origin Activation Time Revealed in Budding Yeast. *PLoS Genet.* **9**, 1–23.
- Hole, W.** (2006). *Cell Culture Protocols, HeLa and CHO cells.*
- Holley, R. W. and Kiernan, J. A.** (1968). CONTACT INHIBITION OF CELL DIVISION IN 3T3 CELLS. *Biochemistry* **60**, 300–304.
- Holliday, D. L. and Speirs, V.** (2011). Choosing correct breast cancer cell line. *Breast Cancer Res.* **13**, 1–7.
- Hormaechea-agulla, D., Kim, Y., Song, M. S. and Song, S. J.** (2018). New Insights into the Role of E2s in the Pathogenesis of Diseases : Lessons Learned from. *Mol. Cells* **41**, 168–178.
- Hruscha, A., Krawitz, P., Rechenberg, A., Heinrich, V., Hecht, J., Haass, C. and Schmid, B.** (2013). Efficient CRISPR/Cas9 genome editing with low off-target effects in zebrafish. *Development* **140**, 4982–4987.
- Huang, J. N., Park, I., Ellingson, E., Littlepage, L. E. and Pellman, D.** (2001). Activity of the APCCdh1 form of the anaphase-promoting complex persists until S phase and prevents the premature expression of Cdc20p. *J. Cell Biol.* **154**, 85–94.
- Hughes, S., Elustondo, F., Di Fonzo, A., Leroux, F. G., Wong, A. C., Snijders, A. P., Matthews, S. J. and Cherepanov, P.** (2012). Crystal structure of human CDC7 kinase in complex with its activator DBF4. *Nat. Struct. Mol. Biol.* **19**, 1101–1107.
- Hwang, H. C. and Clurman, B. E.** (2005). Cyclin E in normal and neoplastic cell cycles.

*Oncogene* **24**, 2776–2786.

**Hwang, I. S., Woo, S. U., Park, J. W., Lee, S. K. and Yim, H.** (2014). Two nuclear export signals of Cdc6 are differentially associated with CDK-mediated phosphorylation residues for cytoplasmic translocation. *Biochim. Biophys. Acta - Mol. Cell Res.* **1843**, 223–233.

**Inui, M., Miyado, M., Igarashi, M., Tamano, M., Kubo, A., Yamashita, S., Asahara, H., Fukami, M. and Takada, S.** (2014). Rapid generation of mouse models with defined point mutations by the CRISPR/Cas9 system. *Sci. Rep.* **4**, 1–8.

**Jackson, J. R., Patrick, D. R., Dar, M. M. and Huang, P. S.** (2007). Targeted anti-mitotic therapies : can we improve on tubulin agents ? *Nat. Rev. Cancer* **7**, 107–117.

**Janghorban, M., Farrell, A. S., Allen-petersen, B. L., Pelz, C., Daniel, J., Oddo, J., Langer, E. M., Christensen, D. J., Sears, R. C., Janghorban, M., et al.** (2019). Linked references are available on JSTOR for this article : Targeting c-MYC by antagonizing PP2A inhibitors in breast cancer. *Proc. Natl. Acad. Sci.* **111**, 9157–9162.

**Jiang, Y.** (2006). Regulation of the Cell Cycle by Protein Phosphatase 2A in *Saccharomyces cerevisiae*. *Microbiol. Mol. Biol. Rev.* **70**, 440–449.

**Jin, L., Williamson, A., Banerjee, S., Philipp, I. and Rape, M.** (2008). Mechanism of Ubiquitin-Chain Formation by the Human Anaphase-Promoting Complex. *Cell* **133**, 653–665.

**Jin, S., Ma, H., Yang, W., Ju, H., Wang, L. and Zhang, Z.** (2018). Cell division cycle 7 is

a potential therapeutic target in oral squamous cell carcinoma and is regulated by E2F1. *J. Mol. Med.* **96**, 513–525.

**Johnson, J. M. and Latimer, J. J.** (2005). Analysis of DNA repair using transfection-based host cell reactivation. *Methods Mol. Biol.* **291**, 321–35.

**Jorda, R., Hendrychová, D., Voller, J., Řezníčková, E., Gucký, T. and Kryštof, V.** (2018). How Selective Are Pharmacological Inhibitors of Cell-Cycle-Regulating Cyclin-Dependent Kinases? *J. Med. Chem.* **61**, 9105–9120.

**Kalaszczynska, I., Geng, Y., Iino, T., Mizuno, S. Ichi, Choi, Y., Kondratiuk, I., Silver, D. P., Wolgemuth, D. J., Akashi, K. and Sicinski, P.** (2009). Cyclin A Is Redundant in Fibroblasts but Essential in Hematopoietic and Embryonic Stem Cells. *Cell* **138**, 352–365.

**Kato, J., Matsushime, H., Hiebert, S. W., Ewen, M. E. and Sherr, C. J.** (1993). Direct binding of cyclin D to the retinoblastoma gene product (pRb) and pRb phosphorylation by the cyclin D-dependent kinase CDK4. *Genes Dev.* **7**, 331–342.

**Ke, X. and Shen, L.** (2017). Frontiers in Laboratory Medicine Molecular targeted therapy of cancer : The progress and future prospect. *Front. Lab. Med.* **1**, 69–75.

**Kelly, B. L., Wolfe, K. G. and Roberts, J. M.** (1998). Identification of a substrate-targeting domain in cyclin E necessary for phosphorylation of the retinoblastoma protein. *Proc. Natl. Acad. Sci. U. S. A.* **95**, 2535–40.

**Khan, M. M., Xiao, J., Patel, D. and LeDoux, M. S.** (2018). DNA damage and neurodegenerative phenotypes in aged Ciz1 null mice. *Neurobiol. Aging* **62**,

180–190.

**Khanna, A., Pimanda, J. E. and Westermarck, J.** (2013). Cancerous Inhibitor of Protein Phosphatase 2A , an Emerging Human Oncoprotein and a Potential Cancer Therapy Target. *Cancer Res* **73**, 1–7.

**Kim, Y. and Kipreos, E. T.** (2007). The Caenorhabditis elegans Replication Licensing Factor CDT-1 Is Targeted for Degradation by the CUL-4/DDB-1 Complex. *Mol. Cell. Biol.* **27**, 1394–1406.

**Kim, Y. K., Bourgeois, C. F., Isel, C., Churcher, M. J. and Karn, J.** (2002). Phosphorylation of the RNA Polymerase II Carboxyl-Terminal Domain by CDK9 Is Directly Responsible for Human Immunodeficiency Virus Type 1 Tat-Activated Transcriptional Elongation. *Mol. Cell. Biol.* **22**, 4622–4637.

**Kim, M. A., Kim, H. J., Brown, A. L., Lee, M. Y., Bae, Y. S., Park, J. I., Kwak, J. Y., Chung, J. H. and Yun, J.** (2007). Identification of novel substrates for human checkpoint kinase Chk1 and Chk2 through genome-wide screening using a consensus Chk phosphorylation motif. *Exp. Mol. Med.* **39**, 205–212.

**Kim, Y., Starostina, N. G. and Kipreos, E. T.** (2008). The CRL4Cdt2 ubiquitin ligase targets the degradation of p21Cip1 to control replication licensing. *Genes Dev.* **22**, 2507–2519.

**Kim, M. S., Oh, J. E., Eom, H. S., Yoo, N. J. and Lee, S. H.** (2010). Mutational analysis of UBR5 gene encoding an E3 ubiquitin ligase in common human cancers. *Pathology* **42**, 93–94.

**Kitagawa, K., Kotake, Y. and Kitagawa, M.** (2009). Ubiquitin-mediated control of

oncogene and tumor suppressor gene products. *Cancer Sci.* **100**, 1374–1381.

**Klaeger, S., Heinzlmeir, S., Wilhelm, M., Polzer, H., Vick, B., Koenig, P. and**

**Reinecke, M.** (2017). The target landscape of clinical kinase drugs. *Science* (80-  
). **358**, 1–17.

**Klein, E. A. and Assoian, R. K.** (2008). Transcriptional regulation of the cyclin D1 gene  
at a glance. *J. Cell Sci.* **121**, 3853–3857.

**Klemperer, N. S., Berleth, E. S. and Pickart, C. M.** (1989). A Novel, Arsenite-Sensitive  
E2 of the Ubiquitin Pathway: Purification and Properties. *Biochemistry* **28**, 6035–  
6041.

**Knehr, M., Popper, M., Enulescu, M., Stoehr, M., Schroeter, D. and Paweletz, N.**

(1995). A Critical Appraisal of Synchronization Methods Applied to Achieve  
Maximal Enrichment of HeLa Cells in Specific Cell Cycle Phases. *Exp. Cell Res.*  
**217**, 546–553.

**Knight, Z. and Shokat, K.** (2005). Features of Selective Kinase Inhibitors. *Chem. Biol.*  
**12**, 621–637.

**Koltun, E. S., Tshako, A. L., Brown, D. S., Aay, N., Arcalas, A., Chan, V., Du, H.,**

**Engst, S., Ferguson, K., Franzini, M., et al.** (2012). Discovery of XL413, a potent  
and selective CDC7 inhibitor. *Bioorganic Med. Chem. Lett.* **22**, 3727–3731.

**Kolupaeva, V. and Janssens, V.** (2013). PP1 and PP2A phosphatases – cooperating  
partners in modulating retinoblastoma protein activation. *FEBS J.* **280**, 627–643.

**Kossatz, U., Dietrich, N., Zender, L., Buer, J., Manns, M. P. and Malek, N. P.** (2004).

Skp2-dependent degradation of p27kip1 is essential for cell cycle progression. *Genes Dev.* **18**, 2602–2607.

**Kozar, K., Ciemerych, M. A., Rebel, V. I., Shigematsu, H., Zagodzon, A., Sicinska, E., Geng, Y., Yu, Q., Bhattacharya, S., Bronson, R. T., et al.** (2004). Mouse development and cell proliferation in the absence of D-cyclins. *Cell* **118**, 477–491.

**Kumagai, A., Shevchenko, A., Shevchenko, A. and Dunphy, W. G.** (2011). Direct regulation of Treslin by cyclin-dependent kinase is essential for the onset of DNA replication. *J. Cell Biol.* **193**, 995–1007.

**Kwart, D., Paquet, D., Teo, S. and Tessier-Lavigne, M.** (2017). Precise and efficient scarless genome editing in stem cells using CORRECT. *Nat. Protoc.* **12**, 329–334.

**Ladha, M. H., Lee, K. Y., Upton, T. M., Reed, M. F. and Ewen, M. E.** (1998). Regulation of exit from quiescence by p27 and cyclin D1-CDK4. *Mol. Cell. Biol.* **18**, 6605–15.

**Lauren** (1997). Biochemical and cellular effects of roscovitine, a potent and selective inhibitor of the cyclin-dependent kinases cdc2, cdk2 and cdk5. *EJB* **243**, 527–536.

**Lazo, J. S., McQueeney, K. E. and Sharlow, E. R.** (2017). New Approaches to Difficult Drug Targets: The Phosphatase Story. *SLAS Discov.* **22**, 1071–1083.

**Ledford, H.** (2008). The full cycle. *Nature* **453**, 843–845.

**Lee, K. Y., Bang, S. W., Yoon, S. W., Lee, S. H., Yoon, J. B. and Hwang, D. S.** (2012).

Phosphorylation of ORC2 protein dissociates origin recognition complex from chromatin and replication origins. *J. Biol. Chem.* **287**, 11891–11898.

**Lee, S. B., Kim, J. J., Nam, H. J., Gao, B., Yin, P., Qin, B., Yi, S. Y., Ham, H., Evans, D., Kim, S. H., et al.** (2015). Parkin Regulates Mitosis and Genomic Stability through Cdc20/Cdh1. *Mol. Cell* **60**, 21–34.

**Lei, L., Wu, J., Gu, D., Liu, H. and Wang, S.** (2016). CIZ1 interacts with YAP and activates its transcriptional activity in hepatocellular carcinoma cells. *Tumor Biol.* **37**, 11073–11079.

**Leman, A. R. and Noguchi, E.** (2013). The replication fork: Understanding the eukaryotic replication machinery and the challenges to genome duplication. *Genes (Basel)*. **4**, 1–32.

**Leonard, A. C. and Me, M.** (2013). DNA Replication Origins. *Cold Spring Harb Perspect Biol* **5**, 1–17.

**Leone, G., DeGregori, J., Jakoi, L., Cook, J. G. and Nevins, J. R.** (1999). Collaborative role of E2F transcriptional activity and G1 cyclindependent kinase activity in the induction of S phase. *Proc Natl Acad Sci U S A* **96**, 6626–6631.

**Liang, K., Volk, A. G., Haug, J. S., Marshall, S. A., Woodfin, A. R., Bartom, E. T., Gilmore, J. M., Florens, L., Washburn, M. P., Sullivan, K. D., et al.** (2017). Therapeutic Targeting of MLL Degradation Pathways in MLL-Rearranged Leukemia. *Cell* **168**, 59–72.e13.

**Liao, L., Song, M., Li, X., Tang, L., Zhang, T., Zhang, L., Pan, Y., Chouchane, L. and Ma, X.** (2017). E3 ubiquitin ligase UBR5 drives the growth and metastasis of

- triple-negative breast cancer. *Cancer Res.* **77**, 2090–2101.
- Lim, S. and Kaldis, P.** (2013). Cdks, cyclins and CKIs: roles beyond cell cycle regulation. *Development* **140**, 3079–3093.
- Lim, L. Y., Vidnovic, N., Ellisen, L. W. and Leong, C. O.** (2009). Mutant p53 mediates survival of breast cancer cells. *Br. J. Cancer* **101**, 1606–1612.
- Liu, E., Li, X., Yan, F., Zhao, Q. and Wu, X.** (2004). Cyclin-dependent Kinases Phosphorylate Human Cdt1 and Induce Its Degradation. *J. Biol. Chem.* **279**, 17283–17288.
- Liu, T., Ren, X., Li, L., Yin, L., Liang, K., Yu, H., Ren, H., Zhou, W., Jing, H., Kong, C., et al.** (2015). Ciz 1 promotes tumorigenicity of prostate carcinoma cell. *Front. Biosci.* **20**, 705–715.
- Liu, Q., Niu, N., Wada, Y. and Liu, J.** (2016). The role of Cdkn1A-interacting zinc finger protein 1 (CIZ1) in DNA replication and pathophysiology. *Int. J. Mol. Sci.* **17**, 1–12.
- Liu, H. Y., Tuckett, A. Z., Fennell, M., Garippa, R. and Zakrzewski, J. L.** (2018). Repurposing of the CDK inhibitor PHA-767491 as a NRF2 inhibitor drug candidate for cancer therapy via redox modulation. *Invest. New Drugs* **36**, 590–600.
- Lo, S. and Uhlmann, F.** (2011). A quantitative model for cyclin-dependent kinase control of the cell cycle : revisited. *Philos. Trans. R. Soc.* **366**, 3572–3583.
- Lolli, G. and Johnson, L.** (2005). CAK-Cyclin-dependent activating kinase. *Cell Cycle* **4**,

572–577.

**Lombardo, L. J., Lee, F. Y., Chen, P., Norris, D., Barrish, J. C., Behnia, K., Castaneda, S., Cornelius, L. A. M., Das, J., Doweyko, A. M., et al.** (2004). Discovery of N - ( 2-Chloro-6-methyl- phenyl ) -2- ( 6- ( 4- ( 2-hydroxyethyl ) - ( BMS-354825 ), a Dual Src / Abl Kinase Inhibitor with Potent Antitumor Activity in Preclinical Assays. *J. Med. Chem.* **47**, 6658–6661.

**Lu, Z. and Hunter, T.** (2010). Ubiquitylation and proteasomal degradation of the p21Cip1, p27Kip1 and p57Kip2 CDK inhibitors. *Cell Cycle* **9**, 2342–2352.

**Ludlow, J. W., Glendening, C. L., Livingston, D. M. and Decaprio, J. A.** (1993). Specific Enzymatic Dephosphorylation of the Retinoblastoma Protein. *Mol. Cell. Biol.* **13**, 367–372.

**Łukasik, A., Uniewicz, K. A., Kulis, M. and Kozłowski, P.** (2008). Ciz1, a p21Cip1/Waf1-interacting zinc finger protein and DNA replication factor, is a novel molecular partner for human enhancer of rudimentary homolog. *FEBS J.* **275**, 332–340.

**Lynce, F., Shajahan-haq, A. N. and Swain, S. M.** (2018). Pharmacology & Therapeutics CDK4 / 6 inhibitors in breast cancer therapy : Current practice and future opportunities. *Pharmacol. Ther.* **191**, 65–73.

**Ma, Y.-S., Yang, I.-P., Tsai, H.-L., Huang, C.-W., Juo, S.-H. H. and Wang, J.-Y.** (2014). High Glucose Modulates Antiproliferative Effect and Cytotoxicity of 5-Fluorouracil in Human Colon Cancer Cells. *DNA Cell Biol.* **33**, 64–72.

**Maamer-Azzabi, A., Ndozangue-Touriguine, O. and Bréard, J.** (2013). Metastatic

SW620 colon cancer cells are primed for death when detached and can be sensitized to anoikis by the BH3-mimetic ABT-737. *Cell Death Dis.* **4**, 1–9.

**MacNeill, S. A.** (2010). Structure and function of the GINS complex, a key component of the eukaryotic replisome. *Biochem. J.* **425**, 489–500.

**Maddox, S.** (2016). Enhancing the selectivity of kinase inhibitors in oncology: a chemical biology perspective. *Future Med. Chem.* **8**, 241–244.

**Mali, P., Yang, L., Esvelt, K., Aach, J., Guell, M., DiCario, J., Norville, J. and Church, G.** (2013). RNA-Guided Human Genome Engineering via Cas9. *Science (80-. ).* **339**, 823–826.

**Malumbres, M.** (2014). Cyclin-dependent kinases. *Genome Biol.* **15**, 1–10.

**Margolis, S. S., Perry, J. A., Weitzel, D. H., Freel, C. D., Yoshida, M., Haystead, T. A. and Kornbluth, S.** (2006). A Role for PP1 in the Cdc2 / Cyclin B – mediated Positive Feedback Activation of Cdc25. *Mol. Biol. Cell* **17**, 1779–1789.

**Martino-Echarri, E., Henderson, B. R. and Brocardo, M. G.** (2014). Targeting the DNA replication checkpoint by pharmacologic inhibition of Chk1 kinase: a strategy to sensitize APC mutant colon cancer cells to 5-fluorouracil chemotherapy. *Oncotarget* **5**, 9889–900.

**Martino, L., He, Y., Hands-Taylor, K. L. D., Valentine, E. R., Kelly, G., Giancola, C. and Conte, M. R.** (2009). The interaction of the Escherichia coli protein SlyD with nickel ions illuminates the mechanism of regulation of its peptidyl-prolyl isomerase activity. *FEBS J.* **276**, 4529–4544.

**Mashtalir, N., Daou, S., Barbour, H., Sen, N. N., Gagnon, J., Hammond-Martel, I., Dar, H. H., Therrien, M. and Affar, E. B.** (2014). Autodeubiquitination protects the tumor suppressor BAP1 from cytoplasmic sequestration mediated by the atypical ubiquitin ligase UBE2O. *Mol. Cell* **54**, 392–406.

**Mastellos, D. C., Deangelis, R. A. and Lambris, J. D.** (2013). Inducing and characterizing liver regeneration in mice: Reliable models, essential &quot;readouts&quot; and critical perspectives. *Curr. Protoc. Mouse Biol.* **3**, 141–170.

**Mazhar, S., Taylor, S. E., Sangodkar, J. and Narla, G.** (2019). Targeting PP2A in cancer : Combination therapies. *BBA - Mol. Cell Res.* **1866**, 51–63.

**McConnell, J. L. and Wadzinski, B. E.** (2009). Targeting Protein Serine/Threonine Phosphatases for Drug Development. *Mol. Pharmacol.* **75**, 1249–1261.

**Melvin, A. T., Woss, G. S., Park, J. H., Waters, M. L. and Allbritton, N. L.** (2013). Measuring Activity in the Ubiquitin-Proteasome System: From Large Scale Discoveries to Single Cells Analysis. *Cell Biochem. Biophys.* **67**, 75–89.

**Mendez, J., Zou-Yang, X. H., Kim, S.-Y., Hidaka, M., Tansey, W. P. and Stillman, B.** (2002). Human Origin Recognition Complex Large Subunit Is Degraded by Ubiquitin-Mediated Proteolysis after Initiation of DNA Replication. *Mol. Cell* **9**, 481–491.

**Merrick, K. A., Larochelle, S., Zhang, C., Allen, J. J., Shokat, K. M. and Fisher, R. P.** (2008). Distinct Activation Pathways Confer Cyclin-Binding Specificity on Cdk1 and Cdk2 in Human Cells. *Mol. Cell* **32**, 662–672.

- Meyer, H. J. and Rape, M.** (2014). Enhanced protein degradation by branched ubiquitin chains. *Cell* **157**, 910–921.
- Mitsui, K., Matsumoto, A., Ohtsuka, S., Ohtsubo, M. and Yoshimura, A.** (1999). Cloning and characterization of a novel p21(Cip1/Waf1)-interacting zinc finger protein, Ciz1. *Biochem. Biophys. Res. Commun.* **264**, 457–464.
- Mittnacht, S.** (1998). Control of pRB phosphorylation. *Curr. Opin. Genet. Dev.* **8**, 21–27.
- Mochida, S., Ikeo, S., Gannon, J. and Hunt, T.** (2009). Regulated activity of PP2A-B55 is crucial for controlling entry into and exit from mitosis in *Xenopus* egg extracts. *EMBO J.* **28**, 2777–2785.
- Mokhonov, V. V., Vasilenko, E. A., Gorshkova, E. N., Astrakhantseva, I. V., Novikov, D. V. and Novikov, V. V.** (2018). SlyD-deficient *Escherichia coli* strains: A highway to contaminant-free protein extraction. *Biochem. Biophys. Res. Commun.* **499**, 967–972.
- Monceau, V., Belikova, Y., Kratassiouk, G., Charue, D., Camors, E., Communal, C., Trouvé, P., Russo-Marie, F. and Charlemagne, D.** (2004). Externalization of endogenous annexin A5 participates in apoptosis of rat cardiomyocytes. *Cardiovasc. Res.* **64**, 496–506.
- Montagnoli, A., Tenca, P., Sola, F., Carpani, D., Brotherton, D. and Albanese, C.** (2004). Cdc7 Inhibition Reveals a p53-Dependent Replication Checkpoint That Is Defective in Cancer Cells. *Cancer Res.* **64**, 7110–7116.
- Montagnoli, A., Valsasina, B., Brotherton, D., Troiani, S., Rainoldi, S., Tenca, P.,**

- Molinari, A. and Santocanale, C.** (2006). Identification of Mcm2 phosphorylation sites by S-phase-regulating kinases. *J. Biol. Chem.* **281**, 10281–10290.
- Montagnoli, A., Valsasina, B., Croci, V., Menichincheri, M., Rainoldi, S., Marchesi, V., Tibolla, M., Tenca, P., Brotherton, D., Albanese, C., et al.** (2008). A Cdc7 kinase inhibitor restricts initiation of DNA replication and has antitumor activity. *Nat. Chem. Biol.* **4**, 357–366.
- Montagnoli, A., Moll, J. and Colotta, F.** (2010). Targeting cell division cycle 7 kinase: A new approach for cancer therapy. *Clin. Cancer Res.* **16**, 4503–4508.
- Moore, J. D., Kirk, J. A. and Hunt, T.** (2003). Unmasking the S-phase-promoting potential of cyclin B1. *Science (80- )*. **300**, 987–990.
- Morgan, D. O.** (1995). Principles of CDK regulation. *Nature* **374**, 131–134.
- Morreale, F. E. and Walden, H.** (2016). Types of Ubiquitin Ligases. *Cell* **165**, 248–248.e1.
- Morrow, J. K. and Lin, H.** (2015). Targeting ubiquitination for cancer therapies. *Future Med. Chem.* **7**, 2333–2350.
- Moser, J., Miller, I., Carter, D. and Spencer, S. L.** (2018). Control of the Restriction Point by Rb and p21. *Pnas* **115**, E8219–E8227.
- Muñoz-Escobar, J., Matta-Camacho, E., Kozlov, G. and Gehring, K.** (2015). The MLLE domain of the ubiquitin ligase UBR5 binds to its catalytic domain to regulate substrate binding. *J. Biol. Chem.* **290**, 22841–22850.

- Munoz, M. A., Saunders, D. N., Henderson, M. J., Clancy, J. L., Russell, A. J., Lehrbach, G., Musgrove, E. A., Watts, C. K. W. and Sutherland, R. L.** (2007). The E3 ubiquitin ligase EDD regulates S-phase and G2/M DNA damage checkpoints. *Cell Cycle* **6**, 3070–3077.
- Myung, J., Kim, K. B. and Crews, C. M.** (2001). The ubiquitin-proteasome pathway and proteasome inhibitors. *Med. Res. Rev.* **21**, 245–73.
- Nakayama, K. I. and Nakayama, K.** (2006). Ubiquitin ligases: Cell-cycle control and cancer. *Nat. Rev. Cancer* **6**, 369–381.
- Nathan, J. A., Tae Kim, H., Ting, L., Gygi, S. P. and Goldberg, A. L.** (2013). Why do cellular proteins linked to K63-polyubiquitin chains not associate with proteasomes? *EMBO J.* **32**, 552–565.
- Natoni, A., Murillo, L. S., Kliszczak, A. E., Catherwood, M. A., Montagnoli, A., Samali, A., O'Dwyer, M. and Santocanale, C.** (2011). Mechanisms of Action of a Dual Cdc7/Cdk9 Kinase Inhibitor against Quiescent and Proliferating CLL Cells. *Mol. Cancer Ther.* **10**, 1624–1634.
- Natoni, A., Coyne, M. R. E., Jacobsen, A., Rainey, M. D., O'Brien, G., Healy, S., Montagnoli, A., Moll, J., O'Dwyer, M. and Santocanale, C.** (2013). Characterization of a dual CDC7/CDK9 inhibitor in multiple myeloma cellular models. *Cancers (Basel)*. **5**, 901–918.
- Ndubaku, C. and Tsui, V.** (2015). Inhibiting the deubiquitinating enzymes (DUBs). *J. Med. Chem.* **58**, 1581–1595.
- Nishibe, R., Watanabe, W., Ueda, T., Yamasaki, N., Koller, R., Wolff, L., Honda, Z. I.,**

- Ohtsubo, M. and Honda, H.** (2013). CIZ1, a p21Cip1/Waf1-interacting protein, functions as a tumor suppressor in vivo. *FEBS Lett.* **587**, 1529–1535.
- Noble, M. E. M., Endicott, J. A. and I, L. N. J.** (2004). Protein Kinase Inhibitors : Insights into Drug Design from Structure. *Science (80-. ).* **303**, 1800–1806.
- Nurse, P.** (1997). Checkpoint pathways come of age. *Cell* **91**, 865–867.
- O'Connor, C. M., Perl, A., Leonard, D., Sangodkar, J. and Narla, G.** (2018). Therapeutic Targeting of PP2A Caitlin. *Int J Biochem Cell Biol* **96**, 182–193.
- Ohtani, K., DeGregori, J. and Nevins, J. R.** (1995). Regulation of the cyclin E gene by transcription factor E2F1. *Proc. Natl. Acad. Sci.* **92**, 12146–12150.
- Ortiz, A. B., Garcia, D., Vicente, Y., Palka, M., Bellas, C. and Martin, P.** (2017). Prognostic significance of cyclin D1 protein expression and gene amplification in invasive breast carcinoma. *PLoS One* **12**, 1–14.
- Pal, A., Young, M. A. and Donato, N. J.** (2014). Emerging potential of therapeutic targeting of ubiquitin-specific proteases in the treatment of cancer. *Cancer Res.* **74**, 4955–4966.
- Pantziarka, P., Bouche, G., Meheus, L., Sukhatme, V. and Sukhatme, V. P.** (2014). The Repurposing Drugs in Oncology ( ReDO ) Project. *ecancer* **8**, 1–13.
- Paquet, D., Kwart, D., Chen, A., Sproul, A., Jacob, S., Teo, S., Olsen, K. M., Gregg, A., Noggle, S. and Tessier-Lavigne, M.** (2016). Efficient introduction of specific homozygous and heterozygous mutations using CRISPR/Cas9. *Nature* **533**, 125–129.

- Pardee, A. B.** (1974). A Restriction Point for Control of Normal Animal Cell Proliferation. *Proc. Natl. Acad. Sci.* **71**, 1286–1290.
- Parker, M. W., Botchan, M. R. and Berger, J. M.** (2017). Mechanisms and regulation of DNA replication initiation in eukaryotes. *Crit. Rev. Biochem. Mol. Biol.* **52**, 107–144.
- Parsons, J. L., Tait, P. S., Finch, D., Dianova, I. I., Allinson, S. L. and Dianov, G. L.** (2008). CHIP-Mediated Degradation and DNA Damage-Dependent Stabilization Regulate Base Excision Repair Proteins. *Mol. Cell* **29**, 477–487.
- Parsons, J. L., Tait, P. S., Finch, D., Dianova, I. I., Edelmann, M. J., Khoronenkova, S. V., Kessler, B. M., Sharma, R. A., McKenna, W. G. and Dianov, G. L.** (2009). Ubiquitin ligase ARF-BP1/Mule modulates base excision repair. *EMBO J.* **28**, 3207–3215.
- Parsons, J. L., Dianova, I. I., Khoronenkova, S. V., Edelmann, M. J., Kessler, B. M. and Dianov, G. L.** (2011). USP47 Is a Deubiquitylating Enzyme that Regulates Base Excision Repair by Controlling Steady-State Levels of DNA Polymerase  $\beta$ . *Mol. Cell* **41**, 609–615.
- Pauzaite, T., Thacker, U., Tollitt, J. and Copeland, N. A.** (2017). Emerging roles for ciz1 in cell cycle regulation and as a driver of tumorigenesis. *Biomolecules* **7**, 1–15.
- Perez, E. A., Barrios, C., Eiermann, W., Toi, M., Im, Y., Conte, P., Martin, M., Pienkowski, T., Pivot, X., Iii, H. B., et al.** (2017). Trastuzumab Emtansine With or Without Pertuzumab Versus Trastuzumab Plus Taxane for Human Epidermal

- Growth Factor Receptor 2 – Positive , Advanced Breast Cancer : Primary Results From the Phase III MARIANNE Study. *J. Clin. Oncol.* **35**, 141–158.
- Pernas, S., Tolaney, S. M., Winer, E. P. and Goel, S.** (2018). CDK4 / 6 inhibition in breast cancer : current practice and future directions. *Ther. Adv. Med. Oncol.* **10**, 1–15.
- Perrotti, D. and Neviani, P.** (2013). Protein phosphatase 2A : a target for anticancer therapy. *Lancet Oncol.* **14**, e229–e238.
- Phatnani, H. P. and Greenleaf, A. L.** (2006). Phosphorylation and functions of the RNA polymerase II CTD. *Genes Dev.* **20**, 2922–2936.
- Pickart, C. M.** (2001). MECHANISMS UNDERLYING UBIQUITINATION. *Annu. Rev. Biochem.* **70**, 503–533.
- Pines, J.** (1999). Four-dimensional control of the cell cycle. *Nat. Cell Biol.* **1**, 73–79.
- Pisu, M., Concas, A. and Cao, G.** (2015). A novel quantitative model of cell cycle progression based on cyclin-dependent kinases activity and population balances. *Comput. Biol. Chem.* **55**, 1–13.
- Poh, W. T., Chadha, G. S., Gillespie, P. J., Kaldis, P., Blow, J. J. and Blow, J. J.** (2014). Xenopus Cdc7 executes its essential function early in S phase and is counteracted by checkpoint-regulated protein phosphatase 1. *Open Biol.* **4**, 1–16.
- Prioleau, M. N. and MacAlpine, D. M.** (2016). DNA replication origins—Where do we begin? *Genes Dev.* **30**, 1683–1697.

- Prykhozhij, S. V., Fuller, C., Steele, S. L., Veinotte, C. J., Razaghi, B., McMaster, C., Shlien, A., Malkin, D. and Berman, J. N.** (2017). Successful optimization of CRISPR/Cas9-mediated defined point mutation knock-in using allele-specific PCR assays in zebrafish. *bioRxiv* 1–33.
- Qiao, R., Weissmann, F., Yamaguchi, M., Brown, N. G., VanderLinden, R., Imre, R., Jarvis, M. A., Brunner, M. R., Davidson, I. F., Litos, G., et al.** (2016). Mechanism of APC/C<sup>CDC20</sup> activation by mitotic phosphorylation. *Proc. Natl. Acad. Sci.* **113**, E2570–E2578.
- Radde, B. N., Ivanova, M. M., Mai, H. X., Salabei, J. K., Hill, B. G. and Klinge, C. M.** (2015). Bioenergetic differences between MCF-7 and T47D breast cancer cells and their regulation by oestradiol and tamoxifen. *Biochem. J.* **465**, 49–61.
- Rahman, F. A., Ainscough, J. F. X., Copeland, N. and Coverley, D.** (2007). Cancer-Associated Missplicing of Exon 4 Influences the Subnuclear Distribution of the DNA Replication Factor CIZ1. *Hum. Mutat.* **28**, 993–1004.
- Rahman, F. A., Aziz, N. and Coverley, D.** (2010). Differential detection of alternatively spliced variants of Ciz1 in normal and cancer cells using a custom exon-junction microarray. *BMC Cancer* **10**, 1–12.
- Rainey, M. D., Quachthithu, H., Gaboriau, D. and Santocanale, C.** (2017). DNA Replication Dynamics and Cellular Responses to ATP Competitive CDC7 Kinase Inhibitors. *ACS Chem. Biol.* **12**, 1893–1902.
- Richardson, C. D., Ray, G. J., DeWitt, M. A., Curie, G. L. and Corn, J. E.** (2016). Enhancing homology-directed genome editing by catalytically active and

inactive CRISPR-Cas9 using asymmetric donor DNA. *Nat. Biotechnol.* **34**, 339–344.

**Ridings-Figueroa, R., Stewart, E., Nesterova, T., Coker, H., Pintacuda, G., Godwin, J., Wilson, R., Haslam, A., Lilley, F., Ruigrok, R., et al.** (2017). The nuclear matrix protein CIZ1 facilitates localization of Xist RNA to the inactive X-chromosome territory. *Genes Dev.* **31**, 876–888.

**Riera, A., Barbon, M., Noguchi, Y., Reuter, L. M., Schneider, S. and Speck, C.** (2017). From structure to mechanism— understanding initiation of DNA replication. *Genes Dev.* **31**, 1073–1088.

**Rizzardi, L. F. and Cook, J. G.** (2012). Flipping the Switch from G1 to S Phase with E3 Ubiquitin Ligases. *Genes Cancer* **3**, 634–648.

**Robbins, J. A. and Cross, F. R.** (2010). Regulated degradation of the APC coactivator Cdc20. *Cell Div.* **5**, 1–10.

**Rodriguez-Acebes, S., Mourón, S. and Méndez, X. J.** (2018). Uncoupling fork speed and origin activity to identify the primary cause of replicative stress phenotypes. *J. Biol. Chem.* **293**, 12855–12861.

**Rojas-Rivera, D. and Hetz, C.** (2015). TMBIM protein family: Ancestral regulators of cell death. *Oncogene* **34**, 269–280.

**Rubin, S. M.** (2013). Deciphering the retinoblastoma protein phosphorylation code. *Trends Biochem. Sci.* **38**, 12–19.

**Rudolph, J., Kristja, K. and Carolina, N.** (2004). Cdc25 Phosphatases and Cancer.

*Chem. Biol.* **11**, 1043–1051.

**Ruvolo, P. P.** (2016). The broken “ Off ” switch in cancer signaling : PP2A as a regulator of tumorigenesis , drug resistance , and immune surveillance. *BBACL* **6**, 87–99.

**Sadowski, M., Suryadinata, R., Tan, A. R., Nur, S., Roesley, A. and Sarcevic, B.** (2012). Protein Monoubiquitination and Polyubiquitination Generate Structural Diversity to Control Distinct Biological Processes. *IUBMB Life* **64**, 136–142.

**Sangodkar, J., Ohlmeyer, M., Narla, G., Sangodkar, J., Perl, A., Tohme, R., Kiselar, J., Kastrinsky, D. B., Zaware, N., Izadmehr, S., et al.** (2017). Activation of tumor suppressor protein PP2A inhibits KRAS-driven tumor growth. *J. Clin. Invest.* **127**, 2081–2090.

**Santamaria, D. and Ortega, S.** (2006). Cyclins and CDKS in development and cancer: lessons from genetically modified mice. *Front. Biosci.* **11**, 1164–1188.

**Santamaria, D., Barriere, C., Cerqueira, A., Hunt, S., Tardy, C., Newton, K., Caceres, J. F., Dubus, P., Malumbres, M. and Barbacid, M.** (2007). Cdk1 is sufficient to drive the mammalian cell cycle. *Nature* **448**, 811–818.

**Sasi, N. K., Tiwari, K., Soon, F. F., Bonte, D., Wang, T., Melcher, K., Xu, H. E. and Weinreich, M.** (2014). The potent Cdc7-Dbf4 (DDK) kinase inhibitor XL413 has limited activity in many cancer cell lines and discovery of potential new DDK inhibitor scaffolds. *PLoS One* **9**, 1–13.

**Saunders, D. N., Hird, S. L., Withington, S. L., Dunwoodie, S. L., Henderson, M. J., Biben, C., Sutherland, R. L., Ormandy, C. J., Colin, K., Watts, W., et al.** (2004).

Edd, the Murine Hyperplastic Disc Gene , Is Essential for Yolk Sac Vascularization and Chorioallantoic Fusion. *Mol. Cell. Biochem.* **24**, 7225–7234.

**Schenone, M., Wagner, B. K., Clemons, P. A. and Program, B.** (2013). Target identification and mechanism of action in chemical biology and drug discovery. *Nat. Chem. Biol.* **9**, 232–240.

**Schneider-Poetsch, T., Ju, J., Eyler, D. E., Dang, Y., Bhat, S., Merrick, W. C., Green, R., Shen, B. and Liu, J. O.** (2010). Inhibition of eukaryotic translation elongation by cycloheximide and lactimidomycin. *Nat. Chem. Biol.* **6**, 209–217.

**Schulman, B. A. and Wade Harper, J.** (2009). Ubiquitin-like protein activation by E1 enzymes: The apex for downstream signalling pathways. *Nat. Rev. Mol. Cell Biol.* **10**, 319–331.

**Shah, N. P., Tran, C., Francis, Y., Chen, P., Norris, D. and Charles, L.** (2004). Overriding Imatinib Resistance with a Novel ABL Kinase Inhibitor. **305**, 399–402.

**Shakhnovich, V.** (2018). It's Time to Reverse our Thinking : The Reverse Translation Research Paradigm. *Clin. Transl. Sci.* **11**, 98–99.

**Shearer, R. F., Iconomou, M., Watts, C. K. W. and Saunders, D. N.** (2015). Functional Roles of the E3 Ubiquitin Ligase UBR5 in Cancer. *Mol. Cancer Res.* **13**, 1523–1532.

**Shen, W. H., Yin, Y., Broussard, S. R., McCusker, R. H., Freund, G. G., Dantzer, R. and Kelley, K. W.** (2004). Tumor Necrosis Factor  $\alpha$  Inhibits Cyclin A Expression and Retinoblastoma Hyperphosphorylation Triggered by Insulin-like Growth Factor-I Induction of New E2F-1 Synthesis. *J. Biol. Chem.* **279**, 7438–7446.

- Siddiqui, K., On, K. F. and Diffley, J. F. X.** (2013). Regulating DNA Replication in Eukarya. *Cold Spring Harb Perspect Biol* **5**, 1–20.
- Simpson-Lavy, K. J., Zenvirth, D. and Brandeis, M.** (2015). Phosphorylation and dephosphorylation regulate APC/Ccdh1 substrate degradation. *Cell Cycle* **14**, 3138–3145.
- Skaar, J. R. and Pagano, M.** (2009). Control of cell growth by the SCF and APC / C ubiquitin ligases. *Curr. Opin. Cell Biol.* **21**, 816–824.
- Skaar, J. R., Pagan, J. K. and Pagano, M.** (2013). Mechanisms and function of substrate recruitment by F-box proteins. *Nat. Rev. Mol. Cell Biol.* **14**, 1–28.
- Skowyra, D., Craig, K. L., Tyers, M., Elledge, S. J. and Harper, J. W.** (1997). F-Box Proteins Are Receptors that Recruit Phosphorylated Substrates to the SCF Ubiquitin-Ligase Complex. *Cell* **91**, 209–219.
- Song, J., Yang, D., Xu, J., Zhu, T., Chen, Y. E. and Zhang, J.** (2016). RS-1 enhances CRISPR/Cas9- and TALEN-mediated knock-in efficiency. *Nat. Commun.* **7**, 1–7.
- Spence, J., Sadis, S. and Haas, A. L.** (1995). A Ubiquitin Mutant with Specific Defects in DNA Repair and Multiubiquitination. *Mol. Cell. Biol.* **15**, 1265–1273.
- Spencer, S. L., Cappell, S. D., Tsai, F., Overton, K. W., Wang, L. and Meyer, T.** (2013). The Proliferation-Quiescence Decision Is Controlled by a Bifurcation in CDK2 Activity at Mitotic Exit. *Cell* **155**, 369–383.
- Stewart, M. D., Ritterhoff, T., Klevit, R. E. and Brzovic, P. S.** (2016). E2 enzymes: More than just middle men. *Cell Res.* **26**, 423–440.

- Stewart, E. R., Turner, R. M. L., Newling, K., Ridings-figueroa, R., Scott, V., Ashton, P. D., Ainscough, J. F. X. and Coverley, D.** (2019). Maintenance of epigenetic landscape requires CIZ1 and is corrupted in differentiated fibroblasts in long-term culture. *Nat. Commun.* **10**, 1–13.
- Sun, Y.** (2003). Targeting E3 Ubiquitin Ligases for Cancer Therapy. *Cancer Biol. Ther.* **2**, 623–629.
- Sun, Y.** (2006). E3 Ubiquitin Ligases as Cancer Targets and Biomarkers. *Neoplasia* **8**, 645–654.
- Sun, X. and Kaufman, P. D.** (2018). Ki-67: more than a proliferation marker. *Chromosoma* **127**, 175–186.
- Sun, X., Bao, J., You, Z., Chen, X. and Cui, J.** (2016). Modeling of signaling crosstalk-mediated drug resistance and its implications on drug combination. *Oncotarget* **7**, 63995–64006.
- Sunwoo, H., Colognori, D., Froberg, J. E., Jeon, Y. and Lee, J. T.** (2017). Repeat E anchors Xist RNA to the inactive X chromosomal compartment through CDKN1A-interacting protein (CIZ1). *Proc. Natl. Acad. Sci.* **114**, 10654–10659.
- Swarts, D. R. A., Stewart, E. R., Higgins, G. S. and Coverley, D.** (2018). CIZ1-F, an alternatively spliced variant of the DNA replication protein CIZ1 with distinct expression and localisation, is overrepresented in early stage common solid tumours. *Cell Cycle* **17**, 2268–2283.
- Swatek, K. N. and Komander, D.** (2016). Ubiquitin modifications. *Cell Res.* **26**, 399–422.

**Tai, S., Sun, Y., Squires, J. M., Zhang, H., Oh, W. K., Liang, C. Z. and Huang, J.** (2011).

PC3 is a cell line characteristic of prostatic small cell carcinoma. *Prostate* **71**, 1668–1679.

**Takeda, D. Y. and Dutta, A.** (2005). DNA replication and progression through S phase.

*Oncogene* **24**, 2827–2843.

**Tanaka, S. and Araki, H.** (2013). Helicase Activation and Establishment of Replication

Forks at Chromosomal Origins of Replication. *Cold Spring Harb Perspect Biol* **5**, 1–14.

**Tasaki, T., Zakrzewska, A., Dudgeon, D. D., Jiang, Y., Lazo, J. S. and Kwon, Y. T.**

(2009). The substrate recognition domains of the N-end rule pathway. *J. Biol. Chem.* **284**, 1884–1895.

**Thacker, U.** (2017). Analysis of cyclin-CDK mediated regulation of the G1 / S

transition in post quiescent murine fibroblasts.

**Ticau, S., Friedman, L. J., Ivica, N. A., Gelles, J. and Bell, S. P.** (2015). Single-molecule

studies of origin licensing reveal mechanisms ensuring bidirectional helicase loading. *Cell* **161**, 513–525.

**Ticau, S., Friedman, L. J., Champasa, K., Corrêa, I. R., Gelles, J. and Bell, S. P.** (2017).

Mechanism and timing of Mcm2-7 ring closure during DNA replication origin licensing. *Nat. Struct. Mol. Biol.* **24**, 309–315.

**Tokunaga, F., Sakata, S., Saeki, Y., Satomi, Y., Kirisako, T., Kamei, K., Nakagawa, T.,**

**Kato, M., Murata, S., Yamaoka, S., et al.** (2009). Involvement of linear

polyubiquitylation of NEMO in NF -  $\kappa$  B activation. *Nat. Cell Biol.* **11**, 123–132.

**Toledo, L., Neelsen, K. J. and Lukas, J.** (2017). Perspective Replication Catastrophe :

When a Checkpoint Fails because of Exhaustion. *Mol. Cell* **66**, 735–749.

**Topacio, B. R., Zatulovskiy, E., Cristea, S., Xie, S., Tambo, C. S., Rubin, S. M., Sage, J.,**

**Koivomagi, M. and Skotheim, J. M.** . (2018). Cyclin D-Cdk4,6 drives cell cycle progression via the retinoblastoma protein's C-terminal helix. *bioRxiv* 1–55.

**Trovesi, C., Manfrini, N., Falcettoni, M. and Longhese, M. P.** (2013). Regulation of

the DNA damage response by cyclin-dependent kinases. *J. Mol. Biol.* **425**, 4756–4766.

**Truong, L. N. and Wu, X.** (2011). Prevention of DNA re-replication in eukaryotic cells.

*J. Mol. Cell Biol.* **3**, 13–22.

**Tsuji, T., Ficarro, S. and Jiang, W.** (2006). Essential Role of Phosphorylation of MCM2

by Cdc7/Dbf4 in the Initiation of DNA Replication in Mammalian Cells. *Mol. Biol.* **17**, 4459–4472.

**Ullah, K., Zubia, E., Narayan, M., Yang, J. and Xu, G.** (2018). Diverse roles of the

E2/E3 hybrid enzyme UBE2O in the regulation of protein ubiquitination, cellular functions, and disease onset. *FEBS J.*

**Van Wijk, S. J. L., De Vries, S. J., Kemmeren, P., Huang, A., Boelens, R., Bonvin, A.**

**M. J. J. and Timmers, H. T. M.** (2009). A comprehensive framework of E2-RING E3 interactions of the human ubiquitin-proteasome system. *Mol. Syst. Biol.* **5**, 1–16.

- VanArsdale, T., Boshoff, C., Arndt, K. T. and Abraham, R. T. (2015).** Molecular pathways: Targeting the cyclin D-CDK4/6 axis for cancer treatment. *Clin. Cancer Res.* **21**, 2905–2910.
- Vanotti, E., Amici, R., Bargiotti, A., Berthelsen, J., Bosotti, R., Ciavolella, A., Cirila, A., Cristiani, C., D'Alessio, R., Forte, B., et al. (2008).** Cdc7 kinase inhibitors: Pyrrolopyridinones as potential antitumor agents. 1. Synthesis and structure-activity relationships. *J. Med. Chem.* **51**, 487–501.
- Vijayaraghavan, S., Moulder, S., Keyomarsi, K. and Layman, R. M. (2018).** Inhibiting CDK in Cancer Therapy: Current Evidence and Future Directions. *Target. Oncol.* **13**, 21–38.
- Vila, I. K., Yao, Y., Kim, G., Xia, W., Kim, H., Kim, S., Park, K., Hwang, J. P., Billalabeitia, E. G. and Hung, M. (2017).** A UBE2O-AMPK $\alpha$ 2 Axis That Promotes Tumor Initiation and Progression Offers Opportunities for Therapy. *Cancer Cell* **31**, 208–224.
- Vodermaier, H. C. (2004).** APC/C and SCF: Controlling each other and the cell cycle. *Curr. Biol.* **14**, 787–796.
- Wagner, S. A., Beli, P., Weinert, B. T., Nielsen, M. L., Cox, J., Mann, M. and Choudhary, C. (2011).** A Proteome-wide, Quantitative Survey of In Vivo Ubiquitylation Sites Reveals Widespread Regulatory Roles. *Mol. Cell. Proteomics* **10**, M111.013284.
- Wallace, M. and Ball, K. L. (2004).** Docking-Dependent Regulation of the Rb Tumor Suppressor Protein by Cdk4. *Mol. Cell. Biol.* **24**, 5606–5619.

- Wan, L., Niu, H., Futcher, B., Zhang, C., Shokat, K. M., Boulton, S. J. and Hollingsworth, N. M.** (2008). Cdc28-Clb5 (CDK-S) and Cdc7-Dbf4 (DDK) collaborate to initiate meiotic recombination in yeast. *Genes Dev.* **22**, 386–397.
- Wang, C., Deng, L., Hong, M. and Akkaraju, G. R.** (2001). TAK1 is a ubiquitin-dependent kinase of MKK and IKK. *Nature* **412**, 346–351.
- Wang, J., Zhou, J. Y. and Gen, S. W.** (2007). ERK-dependent MKP-1-mediated cisplatin resistance in human ovarian cancer cells. *Cancer Res.* **67**, 11933–11941.
- Wang, J., Han, F., Wu, J., Lee, S. W., Chan, C. H., Wu, C. Y., Yang, W. L., Gao, Y., Zhang, X., Jeong, Y. S., et al.** (2011). The role of Skp2 in hematopoietic stem cell quiescence, pool size, and self-renewal. *Blood* **118**, 5429–5438.
- Wang, D. qing, Wang, K., Yan, D. wang, Liu, J., Wang, B., Li, M. xue, Wang, X. wei, Liu, J., Peng, Z. hai, Li, G. xin, et al.** (2014). Ciz1 is a novel predictor of survival in human colon cancer. *Exp. Biol. Med.* **239**, 862–870.
- Wang, L., Zhang, J., Wan, L., Zhou, X., Wang, Z. and Wei, W.** (2015). Targeting Cdc20 as a novel cancer therapeutic strategy. *Pharmacol. Ther.* **151**, 141–151.
- Wang, Y., Li, D., Zhang, S. and Wang, Y.** (2018). CIZ1 expression is increased in hemangioma of the tongue. *Pathol. Oncol. Res.*
- Warder, D. E. and Keherly, M. J.** (2003). Ciz1, Cip1 interacting zinc finger protein 1 binds the consensus DNA sequence ARYSR(0-2)YYAC. *J. Biomed. Sci.* **10**, 406–417.
- Weathington, N. M. and Mallampallii, R. K.** (2014). Emerging therapies targeting the

ubiquitin proteasome system in cancer. *J. Clin. Invest.* **124**, 6–12.

**Weber, P. L., Brown, S. C. and Mueller, L.** (1987). Sequential <sup>1</sup>H NMR Assignments and Secondary Structure Identification of Human Ubiquitin. *Biochemistry* **26**, 7282–7290.

**Weber, S., Meyer-Roxlau, S., Wagner, M., Dobrev, D. and El-Armouche, A.** (2015). Counteracting protein kinase activity in the heart: The multiple roles of protein phosphatases. *Front. Pharmacol.* **6**, 1–19.

**Weinberg, R. A.** (1995). The retinoblastoma protein and cell cycle control. *Cell* **81**, 323–330.

**Welcker, M. and Clurman, B. E.** (2008). FBW7 ubiquitin ligase: a tumour suppressor at the crossroads of cell division, growth and differentiation. *Nat. Rev. Cancer* **8**, 83–94.

**Wilson, R. H. C. and Coverley, D.** (2013). Relationship between DNA replication and the nuclear matrix. *Genes to Cells* **18**, 17–31.

**Winkler, C., Munter, S. De, Dessel, N. Van, Lesage, B., Heroes, E., Boens, S., Beullens, M., Eynde, A. Van and Bollen, M.** (2015). The selective inhibition of protein phosphatase-1 results in mitotic catastrophe and impaired tumor growth. *J. Cell Sci.* **128**, 4526–4537.

**Wlodarchak, N. and Xing, Y.** (2016). PP2A as a master regulator of the cell cycle. *Crit. Rev. Biochem. Mol. Biol.* **51**, 162–184.

**Wood, D. J. and Endicott, J. A.** (2018). Structural insights into the functional diversity

of the CDK–cyclin family. *Open Biol.* **8**, 1–26.

**Wu, J., Lei, L., Gu, D., Liu, H. and Wang, S.** (2016). CIZ1 is upregulated in hepatocellular carcinoma and promotes the growth and migration of the cancer cells. *Tumor Biol.* **37**, 4735–4742.

**Wynn, M. L., Ventura, A. C., Sepulchre, J. A., García, H. J. and Merajver, S. D.** (2011). Kinase inhibitors can produce off-target effects and activate linked pathways by retroactivity. *BMC Syst. Biol.* **5**, 156.

**Xiao, J., Vemula, S., Xue, Y., Khan, M., Kuruvilla, K., Marquez-Lona, E., Cobb, M. and LeDoux, M.** (2016). Motor phenotypes and molecular networks associated with germline deficiency of Ciz1. *Exp. Neurol.* **283**, 110–120.

**Xiao, J., Khan, M. M., Vemula, S., Tian, J. and LeDoux, M. S.** (2018). Consequences of Cre-mediated deletion of Ciz1 exon 5 in mice. *FEBS Lett.* **592**, 3101–3110.

**Yamada, M., Sato, N., Taniyama, C., Ohtani, K., Arai, K. I. and Masai, H.** (2002). A 63-base pair DNA segment containing an Sp1 site but not a canonical E2F site can confer growth-dependent and E2F-mediated transcriptional stimulation of the human ASK gene encoding the regulatory subunit for human Cdc7-related kinase. *J. Biol. Chem.* **277**, 27668–27681.

**Yamada, N., Hasegawa, Y., Yue, M., Hamada, T., Nakagawa, S., Ogawa, Y., Simon, M. D., Pinter, S. F., Fang, R., Sarma, K., et al.** (2015). A system for imaging the regulatory noncoding Xist RNA in living mouse embryonic stem cells. *Cell* **8**, 2634–2645.

**Yanagitani, K., Juszkievicz, S. and Hegde, R. S.** (2017). UBE2O is a quality control

- factor for orphans of multiprotein complexes. *Science (80-. )*. **357**, 472–475.
- Yao, G.** (2014). Modelling mammalian cellular quiescence. *Interface Focus* **4**, 1–10.
- Yau, R. and Rape, M.** (2016). The increasing complexity of the ubiquitin code. *Nat. Cell Biol.* **18**, 579–586.
- Yau, R. G., Doerner, K., Castellanos, E. R., Matsumoto, M. L., Dixit, V. M., Yau, R. G., Doerner, K., Castellanos, E. R., Haakonsen, D. L., Werner, A., et al.** (2017). Assembly and Function of Heterotypic Ubiquitin Chains in Cell-Cycle and Protein Quality Control Article Assembly and Function of Heterotypic Ubiquitin Chains in Cell-Cycle and Protein Quality Control. *Cell* **171**, 918–933.e20.
- Yeeles, J. T. P., Deegan, T. D., Janska, A., Early, A. and Diffley, J. F. X.** (2015). Regulated eukaryotic DNA replication origin firing with purified proteins. *Nature* **519**, 431–435.
- Yeeles, J. T. P., Janska, A., Early, A. and Diffley, J. F. X.** (2017). How the Eukaryotic Replisome Achieves Rapid and Efficient DNA Replication. *Mol. Cell* **65**, 105–116.
- Yin, J., Wang, C., Tang, X., Sun, H., Shao, Q., Yang, X. and Qu, X.** (2013). CIZ1 regulates the proliferation, cycle distribution and colony formation of RKO human colorectal cancer cells. *Mol. Med. Rep.* **8**, 1630–1634.
- Yokota, T., Nagai, H., Harada, H., Mine, N., Terada, Y., Fujiwara, H., Yabe, A., Miyazaki, K. and Emi, M.** (2001). Identification, tissue expression, and chromosomal position of a novel gene encoding human ubiquitin-conjugating enzyme E2-230k. *Gene* **267**, 95–100.

- Yoo, B., Billig, A.-M. and Medarova, Z.** (2017). Guidelines for Rational Cancer Therapeutics. *Front. Oncol.* **7**, 1–8.
- Zeman, M. and Cimprich, K.** (2014). Causes and consequences of replication stress. *Nat. Cell Biol.* **16**, 1–10.
- Zetterberg, A. and Larsson, O.** (1985). Kinetic analysis of regulatory events in G1 leading to proliferation or quiescence of Swiss 3T3 cells. *Proc. Natl. Acad. Sci.* **82**, 5365–5369.
- Zhang, J., Yang, P. L. and Gray, N. S.** (2009). Targeting cancer with small molecule kinase inhibitors. *Nat. Rev. Cancer* **9**, 28–39.
- Zhang, T., Cronshaw, J., Kanu, N., Snijders, A. P. and Behrens, A.** (2014). UBR5-mediated ubiquitination of ATMIN is required for ionizing radiation-induced ATM signaling and function. *Proc. Natl. Acad. Sci.* **111**, 12091–12096.
- Zhang, D., Wang, Y., Dai, Y., Wang, J., Suo, T., Pan, H., Liu, H., Shen, S. and Liu, H.** (2015). CIZ1 promoted the growth and migration of gallbladder cancer cells. *Tumor Biol.* **36**, 2583–2591.
- Zhang, Y., Chen, X., Gueydan, C. and Han, J.** (2018). Plasma membrane changes during programmed cell deaths. *Cell Res.* **28**, 9–21.
- Zheng, L. and Lee, W. H.** (2001). The retinoblastoma gene: A prototypic and multifunctional tumor suppressor. *Exp. Cell Res.* **264**, 2–18.
- Zheng, N., Wang, Z. and Wei, W.** (2016). Ubiquitination-mediated degradation of cell cycle-related proteins by F-box proteins. *Int. J. Biochem. Cell Biol.* **73**, 99–110.

**Zhou, X., Liu, Q., Wada, Y., Liao, L. and Liu, J.** (2018). CDKN1A-interacting zinc finger protein 1 is a novel biomarker for lung squamous cell carcinoma. *Oncol. Lett.* **15**, 183–188.

**Zhu, H. and Mao, Y.** (2015). Robustness of cell cycle control and flexible orders of signaling events. *Sci. Rep.* **5**, 1–13.

# Appendices

Appendices

**A**

2 1	CGA Arg	GCT Ala	CAG Gln	CTT Leu	CGA Arg	ATT Ile	CTG Leu	CAG Gln	TCG Ser	ACG Thr	ATG Met	CTG Leu	CAA Gln	AGA Arg	GCT Ala	46 15
47 16	TTG Leu	CTC Leu	CTA Leu	CAG Gln	CAG Gln	TTG Leu	CAA Gln	GGA Gly	CTG Leu	GAC Asp	CAG Gln	TTT Phe	GCA Ala	ATG Met	CCA Pro	91 30
92 31	CCA Pro	GCC Ala	ACG Thr	TAT Tyr	GAC Asp	GGT Gly	GCC Ala	AGC Ser	CTC Leu	ACC Thr	ATG Met	CCT Pro	ACG Thr	GCA Ala	ACA Thr	136 45
137 46	CTG Leu	GGT Gly	AAC Asn	CTC Leu	CGT Arg	GCT Ala	TTC Phe	AAT Asn	GTG Val	ACA Thr	GCC Ala	CCA Pro	AGC Ser	CTA Leu	GCA Ala	181 60
182 61	GCT Ala	CCC Pro	AGC Ser	CTT Leu	ACA Thr	CCA Pro	CCC Pro	CAG Gln	ATG Met	GTC Val	GCC Ala	CCA Pro	AAT Asn	CTG Leu	CAG Gln	226 75
227 76	CAG Gln	TTC Phe	TTT Phe	CCC Pro	CAG Gln	GCT Ala	ACT Thr	CGA Arg	CAG Gln	TCT Ser	CTG Leu	CTG Leu	GGG Gly	CCT Pro	CCT Pro	271 90
272 91	CCT Pro	GTT Val	GGG Gly	GTC Val	CCA Pro	ATA Ile	AAC Asn	CCT Pro	TCT Ser	CAG Gln	CTC Leu	AAC Asn	CAC His	TCA Ser	GGG Gly	316 105
317 106	AGG Arg	AAC Asn	ACC Thr	CAG Gln	AAA Lys	CAG Gln	GCC Ala	AGA Arg	ACC Thr	CCC Pro	TCT Ser	TCC Ser	ACC Thr	GCC Ala	CCC Pro	361 120
362 121	AAT Asn	CGC Arg	AAG Lys	ACG Thr	GTG Val	CCT Pro	CTG Leu	GAA Glu	GAC Asp	AGG Arg	GAA Glu	GAC Asp	CCC Pro	ACA Thr	GAG Glu	406 135
407 136	GGG Gly	TCT Ser	GAG Glu	GAA Glu	GCC Ala	ACG Thr	GAG Glu	CTC Leu	CAG Gln	ATG Met	GAC Asp	ACA Thr	TGT Cys	GAA Glu	GAC Asp	451 150
452 151	CAA Gln	GAT Asp	TCA Ser	CTA Leu	GTC Val	GGT Gly	CCA Pro	GAT Asp	AGC Ser	ATG Met	CTG Leu	AGT Ser	GAG Glu	CCC Pro	CAA Gln	496 165
497 166	GTG Val	CCT Pro	GAG Glu	CCT Pro	GAG Glu	CCC Pro	TTT Phe	GAG Glu	ACA Thr	TTG Leu	GAA Glu	CCA Pro	CCA Pro	GCC Ala	AAG Lys	541 180
542 181	AGG Arg	TGC Cys	AGG Arg	AGC Ser	TCA Ser	GAG Glu	GAG Glu	TCC Ser	ACC Thr	GAG Glu	AAA Lys	GGC Gly	CCT Pro	ACA Thr	GGG Gly	586 195
587 196	CAG Gln	CCA Pro	CAA Gln	GCA Ala	AGG Arg	GTC Val	CAG Gln	CCT Pro	CAG Gln	ACC Thr	CAG Gln	ATG Met	ACA Thr	GCA Ala	CCA Pro	631 210
632 211	AAG Lys	CAG Gln	ACA Thr	CAG Gln	GCC Ala	CCG Pro	GAT Asp	CGG Arg	CTG Leu	CCT Pro	GAG Glu	CCA Pro	CCA Pro	GAA Glu	GTC Val	676 225
677 226	CAA Gln	ATG Met	CTG Leu	CCG Pro	CGT Arg	ATC Ile	CAG Gln	CCA Pro	CAG Gln	GCA Ala	CTG Leu	CAG Gln	ATC Ile	CAG Gln	ACC Thr	721 240
722 241	CAG Gln	CCA Pro	AAG Lys	CTG Leu	CTG Leu	AGG Arg	CAG Gln	GCA Ala	CAG Gln	ACA Thr	CAG Gln	ACC Thr	GCT Ala	CCA Pro	GAG Glu	766 255
767 256	CAC His	TTA Leu	GCG Ala	AGG Arg	CAC His	AGA Arg	CAC His	AGA Arg	CCG Pro	CTC Leu	CAG Gln	AGC Ser	ACT Thr	TAG End	CGC Arg	811 270
812 271	AGG Arg	CAC His	AGA Arg	CAC His	AGA Arg	CCG Pro	CTC Leu	CAG Gln	AGC Ser	ACT Thr	TAG End	CGC Arg	CCC Pro	AGC Ser	AGG Arg	856 285
857 286	ATC Ile	AGG Arg	TAC Tyr	CCA Pro	CCC Pro	AAG Lys	CAC His	AGT Ser	CAC His	AGG Arg	AGC Ser	AGA Arg	CTT Leu	CAG Gln	--- XXX	901 299

Appendices

**B**

1	CTT	CGA	ATT	CTG	CAG	TCG	ACG	ATG	CTG	CAA	AGA	GCT	TTG	CTC	CTA	45
1	Leu	Arg	Ile	Leu	Gln	Ser	Thr	Met	Leu	Gln	Arg	Ala	Leu	Leu	Leu	15
46	CAG	CAG	TTG	CAA	GGA	CTG	GAC	CAG	TTT	GCA	ATG	CCA	CCA	GCC	ACG	90
16	Gln	Gln	Leu	Gln	Gly	Leu	Asp	Gln	Phe	Ala	Met	Pro	Pro	Ala	Thr	30
91	TAT	GAC	GGT	GCC	AGC	CTC	ACC	ATG	CCT	ACG	GCA	ACA	CTG	GGT	AAC	135
31	Tyr	Asp	Gly	Ala	Ser	Leu	Thr	Met	Pro	Thr	Ala	Thr	Leu	Gly	Asn	45
136	CTC	CGT	GCT	TTC	AAT	GTG	ACA	GCC	CCA	AGC	CTA	GCA	GCT	CCC	AGC	180
46	Leu	Arg	Ala	Phe	Asn	Val	Thr	Ala	Pro	Ser	Leu	Ala	Ala	Pro	Ser	60
181	CTT	ACA	CCA	CCC	CAG	ATG	GTA	GAT	CCA	AAT	CTG	CAG	CAG	TTC	TTT	225
61	Leu	Thr	Pro	Pro	Gln	Met	Val	Asp	Pro	Asn	Leu	Gln	Gln	Phe	Phe	75
226	CCC	CAG	GCT	ACT	CGA	CAG	TCT	CTG	CTG	GGG	CCT	CCT	CCT	GTT	GGG	270
76	Pro	Gln	Ala	Thr	Arg	Gln	Ser	Leu	Leu	Gly	Pro	Pro	Pro	Val	Gly	90
271	GTC	CCA	ATA	AAC	CCT	TCT	CAG	CTC	AAC	CAC	TCA	GGG	AGG	AAC	ACC	315
91	Val	Pro	Ile	Asn	Pro	Ser	Gln	Leu	Asn	His	Ser	Gly	Arg	Asn	Thr	105
316	CAG	AAA	CAG	GCC	AGA	ACC	CCC	TCT	TCC	ACC	GAC	CCC	AAT	CGC	AAG	360
106	Gln	Lys	Gln	Ala	Arg	Thr	Pro	Ser	Ser	Thr	Asp	Pro	Asn	Arg	Lys	120
361	ACG	GTG	CCT	CTG	GAA	GAC	AGG	GAA	GAC	CCC	ACA	GAG	GGG	TCT	GAG	405
121	Thr	Val	Pro	Leu	Glu	Asp	Arg	Glu	Asp	Pro	Thr	Glu	Gly	Ser	Glu	135
406	GAA	GCC	ACG	GAG	CTC	CAG	ATG	GAC	ACA	TGT	GAA	GAC	CAA	GAT	TCA	450
136	Glu	Ala	Thr	Glu	Leu	Gln	Met	Asp	Thr	Cys	Glu	Asp	Gln	Asp	Ser	150
451	CTA	GTC	GGT	CCA	GAT	AGC	ATG	CTG	AGT	GAG	CCC	CAA	GTG	CCT	GAG	495
151	Leu	Val	Gly	Pro	Asp	Ser	Met	Leu	Ser	Glu	Pro	Gln	Val	Pro	Glu	165
496	CCT	GAG	CCC	TTT	GAG	ACA	TTG	GAA	CCA	CCA	GCC	AAG	AGG	TGC	AGG	540
166	Pro	Glu	Pro	Phe	Glu	Thr	Leu	Glu	Pro	Pro	Ala	Lys	Arg	Cys	Arg	180
541	AGC	TCA	GAG	GAG	TCC	ACC	GAG	AAA	GGC	CCT	ACA	GGG	CAG	CCA	CAA	585
181	Ser	Ser	Glu	Glu	Ser	Thr	Glu	Lys	Gly	Pro	Thr	Gly	Gln	Pro	Gln	195
586	GCA	AGG	GTC	CAG	CCT	CAG	ACC	CAG	ATG	ACA	GCA	CCA	AAG	CAG	ACA	630
196	Ala	Arg	Val	Gln	Pro	Gln	Thr	Gln	Met	Thr	Ala	Pro	Lys	Gln	Thr	210
631	CAG	GAC	CCG	GAT	CGG	CTG	CCT	GAG	CCA	CCA	GAA	GTC	CAA	ATG	CTG	675
211	Gln	Asp	Pro	Asp	Arg	Leu	Pro	Glu	Pro	Pro	Glu	Val	Gln	Met	Leu	225
676	CCG	CGT	ATC	CAG	CCA	CAG	GCA	CTG	CAG	ATC	CAG	ACC	CAG	CCA	AAG	720
226	Pro	Arg	Ile	Gln	Pro	Gln	Ala	Leu	Gln	Ile	Gln	Thr	Gln	Pro	Lys	240
721	CTG	CTG	AGG	CAG	GCA	CAG	ACA	CAG	ACC	GAT	CCA	GAG	CAC	TTA	GCG	765
241	Leu	Leu	Arg	Gln	Ala	Gln	Thr	Gln	Thr	Asp	Pro	Glu	His	Leu	Ala	255
766	CCC	CAG	CAG	GAT	CAG	GTA	CCC	ACC	CAA	ACA	CAG	TCA	CAG	GAG	CAG	810
256	Pro	Gln	Gln	Asp	Gln	Val	Pro	Thr	Gln	Thr	Gln	Ser	Gln	Glu	Gln	270
811	ACA	TCA	GAG	AAG	ACC	CAG	GAC	CAG	CCT	CAG	ACC	TGG	CCA	CAG	GGG	855
271	Thr	Ser	Glu	Lys	Thr	Gln	Asp	Gln	Pro	Gln	Thr	Trp	Pro	Gln	Gly	285
856	TCA	GTA	CCC	CCA	CCA	GAA	CAA	GCG	TCA	GGT	CCA	GCC	TGT	GCC	ACG	900
286	Ser	Val	Pro	Pro	Pro	Glu	Gln	Ala	Ser	Gly	Pro	Ala	Cys	Ala	Thr	300
901	GAA	CCA	CAG	CTA	TCC	TCT	CAC	GCT	GCA	GAA	GCT	GGG	AGT	GAC	CCA	945
301	Glu	Pro	Gln	Leu	Ser	Ser	His	Ala	Ala	Glu	Ala	Gly	Ser	Asp	Pro	315
946	GAC	AAG	GCC	TTG	CCA	GAA	CCA	GTA	AGT	GCC	CAA	A--	981			
316	Asp	Lys	Ala	Leu	Pro	Glu	Pro	Val	Ser	Ala	Gln	XXX	326			

**Appendix 1. Site directed mutagenesis in T144, T192, T293, and S331 Ciz1 phospho-sites. A)** The sequencing results for GFP - ECiz1 AAAA (T144A, T192A, T293A, and S331A) were translated using ExPASy Translate. Mutated residues are highlighted in yellow. **B)** Sequencing results for GFP - ECiz1 DDDD (T144D, T192D, T293D, and S331D).